

ANALYTICAL AND EXPERIMENTAL INVESTIGATIONS
OF THE TRANSIENT PROPERTIES OF
DENSE ALUMINUM PLASMAS

By

HAROLD WAYNE WILLIS

II

Bachelor of Science
Lamar State College of Technology
Beaumont, Texas
1966

Master of Science
Oklahoma State University
Stillwater, Oklahoma
1969

Submitted to the Faculty of the Graduate College
of the Oklahoma State University
in partial fulfillment of the requirements
for the Degree of
DOCTOR OF PHILOSOPHY
May, 1971

OKLAHOMA
STATE UNIVERSITY
LIBRARY
AUG 12 1971

ANALYTICAL AND EXPERIMENTAL INVESTIGATIONS
OF THE TRANSIENT PROPERTIES OF
DENSE ALUMINUM PLASMAS

Thesis Approved:

William J. Lewis

Thesis Adviser

Leon W. Schneider

Tom E. Moore

D. D. Durhan

Dean of the Graduate College

788828

PREFACE

The research reported in this work is based on the continuing study of the transient properties of dense plasmas by Dr. F. C. Todd and his dense plasma group, of which this author is a member. A quadrupole mass filter was employed to investigate properties of a vacuum spark plasma. In addition, an electrostatic lens system was constructed to study the velocity distributions of ionic species which are emitted from such a plasma. In addition to the preceding two phases, an expanded study was made of two mathematical models which represent respectively, a laser impact plasma and an expanding plasma sphere. The former model is a continuation of the doctoral research by Dr. L. J. Peery and the latter represents a revised approach to the modeling technique of Dr. R. E. Bruce. Both of these men were members of the Research Group supervised by Dr. Todd who acted as major advisor to this student.

The initial phases of this work were completed at the Oklahoma State University and the current phase was concluded at the Research Institute of The University of Alabama in Huntsville.

This author is particularly grateful for the opportunity to continue his education in this rapidly expanding field and for the experience of having worked with the plasma group. He also shares with the previous and current members of this group a sincere appreciation for the lasting benefits which have accrued to those who have participated in the work and for the unique talents of Dr. Todd, who

afforded us this opportunity to contribute.

Appreciation is also expressed for the persons who comprise the Physics Departments of both Oklahoma State University and The University of Alabama in Huntsville, and for the staff of the Research Institute. Mr. Richard Rodkin was responsible for much of the electronic work on the redesigned quadrupole power supply and the electrostatic lens system. Mrs. Sylvia Heard is gratefully acknowledged for her assistance with the computer programming.

The professional satisfaction, which befalls those who cooperate on any scientific endeavor toward a successful end, is in itself a giant reward; and the author is especially thankful for the many pleasurable hours of enlightening discussions and the many sessions of mutual cooperation on the theoretical phases of this work with his good friend, Dr. Larry J. Peery.

The patience, assistance and constant encouragement of my wonderful wife, Eva, during the completion of this work have been the necessary ingredients which have contributed, as much as any other factors, to its success.

The author is indebted to the National Aeronautics and Space Administration which has provided the support for his research through NASA Contract numbers NASr-7 and NAS8-21391 administered through the Research Foundation, Oklahoma State University and NAS8-25055 administered through the Research Institute, The University of Alabama in Huntsville.

TABLE OF CONTENTS

Chapter	Page
I. INTRODUCTION	1
II. GENERAL AREA OF STUDY	9
Experimental Phase	9
Quadrupole Mass Filter	11
Electrostatic Lens System.	12
Theoretical Phase.	13
Laser Impact Plasma Model.	14
Expanding Plasma Sphere Model.	15
Summary.	15
III. QUADRUPOLE MASS FILTER.	17
Introduction	17
Ion Source	18
Mass Analyzer.	19
Detector	19
Quadrupole Theory.	22
Quadrupole Assembly.	29
IV. ELECTROSTATIC LENS SYSTEM	40
Introduction	40
Theory and Design.	41
Lens Power Supply.	48
Lens Vacuum System	50
Operating Procedure.	50
V. LASER IMPACT PLASMA	55
Introduction	55
Background Discussion.	56
Theory	57
Computer Model	62
Summary.	66

TABLE OF CONTENTS (Continued)

Chapter	Page
VI. EXPANDING PLASMA SPHERE.	69
Introduction.	69
General	70
Theoretical Discussion.	72
Computer Model.	77
Evolution of the Flow Variables	81
Program Condensation.	89
Numerical Methods	90
Data Reduction.	94
Summary	96
VII. DISCUSSION OF RESULTS.	99
Introduction.	99
Quadrupole Mass Filter Data	99
Electrostatic Lens Data	114
Laser Impact Plasma Data.	135
Expanding Plasma Sphere Data.	146
VIII. SUMMARY AND CONCLUSIONS.	156
General Summary	156
Recommendation for Future Improvements.	158
Experimental Research	158
Theoretical Research.	159
SELECTED BIBLIOGRAPHY.	161
APPENDIX A - DERIVATION OF VISCOUS TERMS	165
APPENDIX B - PLASMA OSCILLATIONS	170
APPENDIX C - PROGRAM CONSTRUCTION FOR SPHERICAL MODEL.	180

LIST OF TABLES

Table	Page
I. Stability Parameters for AL +1.	30
II. Stability Parameters for AL +2.	31
III. Stability Parameters for AL +3.	32
IV. Stability Parameters for AL +4.	33
V. Stability Parameters for AL +5.	34
VI. Voltage Values and Potential Gradients.	49
VII. Machine Listing of Main Program	185
VIII. Subroutine CKOT	201
IX. Subroutine HYDRO1	208
X. Subroutine ICOND	211
XI. Subroutine OPTR	214
XII. Subroutine PRTOT1	218
XIII. Subroutine QUAT	220
XIV. Subroutine REDBL.	225
XV. Subroutine REMESH	228
XVI. Subroutine XOV.	231
XVII. Statement Functions	233
XVIII. Program Data.	234

LIST OF FIGURES

Figure	Page
1. Quadrupole Electrode Geometry.	20
2. Diagram of Quadrupole Electrode Arrangement.	21
3. Mathieu Stability Ranges	26
4. Mass Filter Operating Point.	28
5. Block Diagram of Quadrupole Mass Filter and Support Equipment.	35
6. Quadrupole Field Electrode Mounting.	36
7. Basic Power Supply Section for Quadrupole.	37
8. R.F. Section for Quadrupole Power Supply	38
9. Electrostatic Lens	43
10. Electrostatic Lens in Operational Configuration	47
11. Pulse Amplifier and Voltage Divider for Lens System.	51
12. Diagram of Electrostatic Lens System with Support Equipment.	53
13. Region of Validity of Equation of State (After Peery).	60
14. Laser-Target Geometry.	63
15. Computer Grid for Laser Impact Plasma Model.	65
16. Basic Geometry for Expanding Plasma Sphere Model	78
17. Space - Time Geometry for Remesh Procedure	82
18. Remesh Geometry for Interior Mesh Point.	84
19. Remesh Geometry for End Mesh Point	86
20. Remesh Geometry for First Mesh Point	88

LIST OF FIGURES (Continued)

Figure	Page
21. Geometry for Redouble Procedure Showing Old and New Mesh Coordinates.	91
22. Simplified Computer Geometry for Single Mesh Cell.	93
23. Simplified Flow Diagram.	95
24. Al ⁺¹ Ions, Metastable Atoms and Light from Vacuum Spark - Quadrupole System.	102
25. Al ⁺¹ Ions, Metastable Atoms and Light from Vacuum Spark - Quadrupole System.	103
26. Al ⁺² Ions, Metastable Atoms and Light from Vacuum Spark - Quadrupole System.	104
27. Al ⁺² Ions, Metastable Atoms and Light from Vacuum Spark - Quadrupole System.	105
28. Al ⁺³ Ions, Metastable Atoms and Light from Vacuum Spark - Quadrupole System.	106
29. Al ⁺³ Ions, Metastable Atoms and Light from Vacuum Spark - Quadrupole System.	107
30. Al ⁺⁴ Ions, Metastable Atoms and Light from Vacuum Spark - Quadrupole System.	108
31. Al ⁺⁴ Ions, Metastable Atoms and Light from Vacuum Spark - Quadrupole System.	109
32. Al ⁺⁵ Ions, Metastable Atoms and Light from Vacuum Spark - Quadrupole System.	110
33. Al ⁺⁵ Ions, Metastable Atoms and Light from Vacuum Spark - Quadrupole System.	111
34. Time-of-Flight Curve for Al ⁺¹ Ions from Vacuum Spark - Electrostatic Lens System.	117
35. Time-of-Flight Curve for Al ⁺¹ Ions from Vacuum Spark - Electrostatic Lens System.	118
36. Time-of-Flight Curve for Al ⁺¹ Ions from Vacuum Spark - Electrostatic Lens System.	119
37. Time-of-Flight Curve for Al ⁺² Ions from Vacuum Spark - Electrostatic Lens System.	120

LIST OF FIGURES (Continued)

Figure	Page
38. Time-of-Flight Curve for Al ⁺² Ions from Vacuum Spark - Electrostatic Lens System.	121
39. Time-of-Flight Curve for Al ⁺² Ions from Vacuum Spark - Electrostatic Lens System.	122
40. Time-of-Flight Curve for Al ⁺³ Ions from Vacuum Spark - Electrostatic Lens System.	123
41. Time-of-Flight Curve for Al ⁺³ Ions from Vacuum Spark - Electrostatic Lens System.	124
42. Time-of-Flight Curve for Al ⁺³ Ions from Vacuum Spark - Electrostatic Lens System.	125
43. Time-of-Flight Curve for Al ⁺⁴ Ions from Vacuum Spark - Electrostatic Lens System.	126
44. Time-of-Flight Curve for Al ⁺⁴ Ions from Vacuum Spark - Electrostatic Lens System.	127
45. Time-of-Flight Curve for Al ⁺⁴ Ions from Vacuum Spark - Electrostatic Lens System.	128
46. Time-of-Flight Curve for Al ⁺⁵ Ions from Vacuum Spark - Electrostatic Lens System.	129
47. Time-of-Flight Curve for Al ⁺⁵ Ions from Vacuum Spark - Electrostatic Lens System.	130
48. Time-of-Flight Curve for Al ⁺⁵ Ions from Vacuum Spark - Electrostatic Lens System.	131
49. Maxwellian Velocity Distribution (Arbitrary Scale)	133
50. Variation of Mass Density and Internal Energy Density along Radiation Axis	136
51. Variation of Pressure and Temperature along Radiation Axis	138
52. Variation of Mass Density and Internal Energy Density along Radiation Axis	139
53. Variation of Pressure and Temperature along Radiation Axis	140

LIST OF FIGURES (Continued)

Figure	Page
54. Fluctuations of Laser Beam Reflection Over Time Intervals at Start and End of Run.	141
55. Laser Impact Plasma - Quadrupole Geometry.	143
56. Al ⁺³ Ions, Metastable Atoms and U.V. Light Emission from Laser Induced Plasma	144
57. Variation of Mass Density along the Plasma Sphere Radius (Cycles 1-3)	149
58. Variation of Mass Density along the Plasma Sphere Radius (Cycles 4-6)	150
59. Variation of Mass Density along the Plasma Sphere Radius (Cycles 7-9)	151
60. Variation of Mass Density along the Plasma Sphere Radius (Cycles 10-11)	152
61. Variation of Mass Density along the Plasma Sphere Radius (Cycles 12-13)	153
62. Variation of Mass Density along the Plasma Sphere Radius (Cycles 14-15)	154
63. Relative Motion of Ion and Electron in an External Pressure Gradient.	172
64. Displacement of Electron Gas in Ion Background	175

CHAPTER I

INTRODUCTION

It is now well known that, from a scientific viewpoint, man must describe natural phenomena in terms of the behavior of at least four states of matter: solid, liquid, gaseous and plasma. While the transitions of matter through the first three phases are fairly well understood, the transition into the plasma state is still the subject of considerable interest and scientific study. Indeed, it was not until 1928 that this additional state of matter received a name. It was Langmuir (1929) who is generally credited with first using the word plasma to describe the inner region of an electrical discharge. Previously, Sir William Crookes had described this new state as simply the "fourth state of matter." Of course, the plasma state has always existed and occurs naturally in many forms. It has intrigued the scientist for many years, perhaps for no other reason than that it eludes his quantitative description. Some of the more common forms of this fourth state of matter include solar flares, the aurorae and lightning. In fact, at least 99% of the matter in our universe is in the plasma state and this alone should be sufficient justification for the study of plasma physics. Probably the most common of the forms listed above is the lightning stroke and it is now known that a transient plasma exists in the earth's atmosphere each time this phenomenon occurs. These naturally occurring plasmas, however,

while being interesting and the subject of intense investigations, do not lend themselves to the systematic and controlled environment of the laboratory. It is here that the detailed mechanisms of plasma creation, evolution and decay must undergo the scrutiny of carefully monitored, diagnostic instruments. In many cases these laboratory plasmas are able to closely simulate the naturally occurring types. Some examples of these include electrical discharges in gases, a simple spark gap in air or vacuum, hypervelocity impact of a particle on a plate, an exploding wire and the incidence of a focused laser beam on a target. While these experiments cannot duplicate the magnitude of natural plasmas, many of the essential properties are present for an analysis.

The importance of this rapidly expanding field may be readily appreciated when one contemplates the possible benefits to be derived by a better understanding in this area. One of the most exciting proposed application currently being considered is energy conversion by means of thermonuclear reactions. Many of the ideas being advanced at present include the use of focused laser radiation to heat small fuel pellets. As one of the proponents of this idea, Lubin (1970) proposes to provide the high temperatures and particle densities by this method to achieve laser-induced fusion. The advent of high-peak-power, pulsed laser systems appears to be advancing the realization of this method of power generation. The rapid technological development in the area of plasma containment is of equal importance as is evidenced by the tremendous efforts being expended by a wide variety of researchers. Many of the problems peculiar to plasma containment may only be solved through a knowledge of the intricate mechanisms of the

plasma during its early stages of development.

There are, of course, many other possible applications of plasmas: magnetohydrodynamic power generation; the plasma diode, a form of thermionic energy converter; the glow discharge which is common to every fluorescent lamp; and the voltage regulator gas tubes that are widely used in electronic circuits. Other major applications in this area are long distance radio communications, which require an understanding of the refraction properties of the ionosphere, and the special transmission properties that must be understood, for example, when communicating with a space vehicle during reentry. Another example of plasma application is found in the propulsion field. The plasma jet is a device which may produce a very high temperature gas flow suitable for the propulsion of space craft.

The above list represents only a few of the most publicized research efforts and they serve to illustrate typical accomplishments, as well as the need for continued research.

In many cases, the study of plasma physics cannot be avoided. One prominent example of this is in the study of hypervelocity impact. This study, originating primarily from the need to protect space craft from high energy micrometeoroids, has grown to include the investigation of the complex phenomena at the impact zone. At the instant of impact, a brief but intense light flash is emitted and the pressures created by the impacting particles are sufficient to convert the target material into a hot, dense plasma.

In describing the plasma as a fourth state of matter, many authors have submitted several definitions. Solomon (1964) presents the description as a conductor consisting of an electrically charged

gas with ions and electrons. Holt and Haskell (1965) have used the term, ionized gaseous state, synonymously with plasma. Pai (1962), also, prefers the more liberalized definition that a plasma is simply an ionized gas. It is important to realize that, at first, the designation plasma represented a fully ionized gas in which the excess electric charge was zero. This case is of course an idealization. Most laboratory plasmas are partially ionized and may even contain mixtures of neutral gas atoms, in addition to singly and doubly ionized atoms.

The temperature and density of plasmas at one atmosphere may vary somewhat depending on the material to be ionized. In general, number densities are of the order of 10^{18} charged particles per cubic centimeter and temperatures are of the order of 10^4 °K. This would be classified as a relatively cool, gaseous plasma. One must exercise care in setting limits for the definition of plasmas, however, since the liberalized use of the term includes at least two classes of solids: metals and semiconductors. These satisfy the conditions at room temperature, to be called plasmas. The conditions are that the charged particle concentrations are high enough and consist of approximately equal numbers of positive and negative charges.

For a dense plasma, these requirements may vary considerably. Laboratory plasmas are produced that are many times as dense as the solid state. The most striking example of such a natural plasma is, of course, the sun.

Throughout the text of this thesis, the term "dense plasma" will be reserved for the case in which a correction to the ideal gas equation of state is essential for an adequate description of its evolu-

tion. This type of plasma has been among the subjects of investigation by our dense plasma group for several years. This group consists mainly of the previous and current graduate students of Dr. F. C. Todd, who serves as Principal Investigator for this project.

Some of the more recent work by this group is cited to establish the extent of the foundation for the program of studies that follows. This work will be documented by giving the date of the thesis of each individual responsible for a particular phase of the work. For the study of dense plasmas, there are essentially five methods which have been available for plasma production:

1. A Q-switched, twin ruby laser (Peery, 1967; Robinson, 1970)
2. An exploding wire facility (Yoder, 1970; Hamby, 1970)
3. A vacuum spark gap (Brown, 1968)
4. The hypervelocity impact of sphere (Hardage, 1967)
5. A co-axial plasma gun (Shriver, 1970)

A brief description of the above methods will illustrate the several techniques which are used and any advantage one may have compared to another. This description is deferred until Chapter II. The experimental methods for analyzing the properties of these dense, transient plasmas that have been employed for taking measurements may be summarized by the following:

1. A vacuum spectrograph for the far ultraviolet (Payne, 1966; Carpenter, 1970)
2. A pulsed, high gain photomultiplier (Brown, 1968)
3. An electrical probe system to measure plasma expansion velocity (Robinson, 1970)

4. A quadrupole mass filter (Willis, 1969)
5. An electrostatic lens system used as a velocity analyzer (Willis, 1969)

These diagnostic tools have been used separately and as coupled units in several experiments to determine some of the properties of the plasmas produced by the methods outlined above.

In addition to the experimental phase of the dense plasma work, substantial progress has been made in the theoretical area. Some of the more recent work in this area include the following:

1. A computer model for hypervelocity impact (Sodek, 1965; Hardage, 1967)
2. A computer model for an expanding plasma sphere (Ables, 1963; Bruce, 1966)
3. A computer model for a laser induced plasma (Peery, 1970)

The general purpose of this thesis is to describe the work which has been accomplished on four of the phases that are currently in progress. These may be roughly categorized into two experimental and two theoretical parts, although they are interrelated. The experimental work includes measurements on vacuum spark plasmas with an improved quadrupole mass filter. This device has been used, also, to investigate the degree of ionization, the variation of ultraviolet light intensity with time, and the expansion velocity of the laser induced aluminum plasmas. This work was carried out at Oklahoma State University in a joint effort with Robinson (1970) and some of the initial results were included by the author in his Masters thesis (1969). A further evaluation of this work has been performed and is presented. In addition, considerable more data has been compiled and

reduced in conjunction with the aluminum spark gap in vacuum. The details of the modifications on the quadrupole system will be given in Chapter III. The electrostatic lens which was designed earlier has been constructed and is currently in use as a velocity analyzer. The initial results indicate its usefulness as a device which is capable of yielding direct measurements of ion velocity distributions. A description of this experimental device is given in Chapter IV.

The two phases of theoretical work include an improved model for laser induced plasmas. Major credit for this phase of the work is due to Dr. L. J. Peery, who designed the original computer model and has continued to be responsible for most of the implementation. The author's contribution to this effort lies mainly in the area of converting the program to a form compatible with the Univac 1108 computer system, revising and debugging the program elements, devising a computerized method of data output and reduction, and coordinating a production run. Some of the results of this production run formed the basis of a paper which was presented at the November 1970 meeting of the South Eastern Section of the American Physical Society, and was co-authored with Drs. L. J. Peery and F. C. Todd. A brief review of this model and some of the preliminary results of the production run are presented in Chapter V.

The other theoretical phase included in this work is the improved computer model of an expanding plasma sphere. This work has provided an improvement to the modeling techniques of Ables (1963) and Bruce (1966). The essential features of this model and a discussion of the revisions and improvements will be outlined in Chapter VI. The results and conclusions are presented in Chapter VII. Suggestions for

for future investigators concerning refinements which may be made to both the experimental and theoretical phases of the work are presented in Chapter VIII.

CHAPTER II

GENERAL AREA OF STUDY

The primary purpose of this section is to outline the four general areas of research and then to show their interrelation. As with most scientific research in which experimental and theoretical data are compared, the procedure is somewhat arbitrary. In one approach, one may predict theoretical results using a mathematical model and then take the experimental measurements necessary to either verify or refute those results. Another approach is to obtain experimental data and use these results to provide boundary conditions for the mathematical models. The experimental results may then be validated depending on whether or not the model produces a solution which converges on a known, correct result.

Actually, both of these approaches have been taken in this work, so that the relationships between the experimental and theoretical phases should become readily apparent.

Experimental Phase

The experimental projects which have been undertaken will be better understood after a brief description of the methods which were used to produce the dense, transient plasmas under consideration. The Q-switched, twin ruby laser, designed and constructed by Peery (1967) and Robinson (1970) produces such a plasma. By impacting a focused

laser pulse onto the surface of an aluminum target, a dense, rapidly expanding plasma is produced and is allowed to decay into a vacuum. The laser gives a giant pulse with 15 joules of energy in 30 nanoseconds, so the average power is 500 megawatts.

An exploding wire facility has been designed and is currently being made operational. This device is capable of producing an approximately spherical plasma in a very short time. It is expected that the energy input to the aluminum wire will require a time interval of the order of one microsecond. This experiment should provide the results necessary to compare with the computer model of an expanding plasma sphere. This model is discussed in detail in Chapter VI.

The vacuum spark gap is a very simple device for the production of dense, transient plasmas. It employs spectroscopically pure aluminum electrodes to which a high voltage is applied and the gap is allowed to breakdown in a vacuum. A major advantage of this method of producing plasmas is the relatively short turn-around-time between shots. It, therefore, has provided an excellent calibration facility for several of the diagnostic instruments.

Some of the previous diagnostic work on plasmas that were produced by the above methods include the spectral analysis by Carpenter (1970) and the variation of the u.v. and visible light emission by Brown (1968). The work by Carpenter includes the use of the vacuum spectrograph to record characteristic radiation emitted from the spark gap plasmas. This instrument employs a section of a Rowland circle with a range of 100 to 1,400 angstroms. The resolution at 320 angstroms is approximately 3 angstroms per centimeter in the second order.

Brown recorded the variation with time of the ultraviolet and visible light with a pulsed, high gain photomultiplier. These measurements were also made on the vacuum spark plasmas. The resolution of the pulsed photomultiplier and recorder was determined by the 519 Tek-tronic oscilloscope and was found to be approximately one nanosecond.

Other previous work includes the probe measurements of Robinson (1970) on the laser induced plasmas. The data with the Langmuir probes indicates that the plasma expands with velocities of the order of 1.6×10^7 cm/sec. The quadrupole mass filter was also employed to analyze the laser induced plasma. The presence of several ionic species was experimentally verified and a qualitative analysis was made of the relative velocity distributions. Some of these initial results were presented by Willis (1969) and Robinson (1970). These results include photographs of the output current from an electron multiplier which was the detector for the quadrupole system. These results give an indication of the ultraviolet light, metastable atoms and the ions which are present in the plasma.

With this discussion of the previous work in mind, the specific areas of the present work are presented.

Quadrupole Mass Filter

After the preliminary results of the diagnostic work with the quadrupole were analyzed, it was decided to redesign the power supply for the system. The continuation of this experimental project was justified by the encouraging quality of the initial data. Data was compiled for both types of plasmas which were described above, viz., the vacuum spark and laser induced plasmas.

The present work includes additional measurements taken with the quadrupole on the vacuum spark plasmas. The major refinements that have been made to the system include a regulated power supply, which supplies a constant voltage, and a crystal control for the frequency. With these modifications, the uncertainty, with which the measurements are taken, has been reduced considerably. In addition, a better data-taking procedure was developed which has enhanced the reproducibility of the results. A more detailed description is provided in Chapter III. Briefly, aluminum ions Al^{+1} through Al^{+5} were investigated with the improved system and some typical results are presented in Chapter VII.

Electrostatic Lens System

One of the more interesting projects on which this author has participated, has been the basic research involved with an attempt to directly measure the individual velocity distributions of several ionic species. This work was originated at the suggestion of Dr. Todd as the initial phase of the quadrupole study was nearing completion. The design and construction are presented in the work covered by this author's Masters thesis (Willis, 1969). The original idea precipitated from the necessity to isolate the ionized aluminum atoms from the metastables and the ultraviolet light. The electron multiplier, which was used as the detector for the quadrupole system, is sensitive to all three of the above signals. The particular difficulty in separating the final output signal into signals from the respective sources will be realized by those familiar with this type of detector. There are, of course, several different approaches to the solution

of this difficulty and most of them include the use of some combination of electric and magnetic fields.

Since the aim of the proposed device was not only to separate the ions from the metastable atoms and light, but to allow a determination of velocity distributions as well, many of the well known focusing ideas were discarded. A pulsed device was finally chosen after the investigation of several possible methods. This relatively new diagnostic device and its method of operation is presented in Chapter IV. Typical results are provided for measurements made for ionic species Al^{+1} through Al^{+5} . The quadrupole mass filter system was used as the detector for the lens, so that double filtering was achieved. This novel method is also described in Chapter IV.

Theoretical Phase

Along with the experimental projects undertaken by this group, several theoretical programs have been in progress. The theoretical studies have consisted mainly of mathematical models of the plasmas that are produced by the varied methods which are available. Although these models have not been limited to plasma models per se, most are either directly or indirectly related to the central problem of plasma production and evolution. The work of Sodek (1965) and Hardage (1967) which pertains to hypervelocity impact is only indirectly related to the work presented in this thesis and therefore no detailed discussion of it will be presented. Their work has, however, been of great value to this program. The computer techniques and methods for solving flow equations which were developed in their work has contributed considerably to the current phases of the work.

The modeling techniques of Ables (1963) and Bruce (1966) have been used as a foundation on which to build. Many refinements have been made and new techniques were added by Peery (1970). The work of Ables and Bruce included a mathematical model of an expanding sphere of plasma. The work of Peery involved a model and calculations on a laser induced, aluminum plasma. In general, these theoretical efforts have been correlated with the experimental work.

Laser Impact Plasma Model

This model was proposed and investigated in conjunction with the experimental laser facility, which was designed and constructed by the plasma group. The primary goal of this research was to develop and apply a mathematical model for the plasma which is created by a Q-switched laser beam impacting on the surface of an aluminum target. The plasma is assumed to expand in such a manner that cylindrical coordinates are more applicable than the spherical coordinates for the earlier models. A cylindrical system of coordinates is required to follow the emitted plasma as it continues to receive energy from the incident laser beam. The basis for this model was the macroscopic equations which determine the evolution of the plasma. A modified, single fluid theory has been developed and the latest modification was presented by Peery (1970). Additional improvements to this model of the laser beam impact have been made and are discussed in Chapter V. Briefly, some of the refinements include the revision of several of the program elements, improved digital techniques and a computerized method of data output and reduction.

Expanding Plasma Sphere Model

The complex problems inherent in plasma evolution may be reduced by a variety of simplifying assumption. Probably, the most obvious, and more easily justified, is the reduction to spherical geometry. The basic assumption in this case, of course, is that the expanding plasma exhibits a spherical symmetry. The extensive work done on this model by Ables and Bruce has provided an excellent foundation.

The work of Bruce represented an improvement on the previous work of Ables, significantly in the development of an improved equation of state for aluminum. The model, developed as a boundary-value problem, proved to be most reliable at relatively low densities and high temperatures. Some of the successes of this model include the development of an equation of state for a wider range of temperatures and pressures and of a qualitative description of the plasma expansion for several initial conditions. The qualitative description predicts that the plasma expands with a hot, low density core, surrounded by a relatively cold, high density shell.

Because of the relative simplicity of this type of model and since many of the properties, basic to the experimentally produced plasmas, may be investigated, it was highly desirable to continue this study. An evaluation of this model and the refinements which have been made to it are the subject of Chapter VI. Some of the results of the improved model are discussed in Chapter VII.

Summary

The work presented in this thesis may be summarized in the follow-

ing manner. The experimental work with the quadrupole mass filter and electrostatic lens provides an analysis of some of the properties of the dense, transient plasmas produced by the vacuum spark gap. The most significant results are the determinations of velocity distributions for several ionic species. The theoretical work illustrates the progress that has been made toward a better understanding of the intricate physical processes which determine the evolution of this type of plasma. The discussion of the laser impact model has been introduced, primarily to illustrate the significant progress that has been made in the art of mathematical plasma models and to provide a background for the discussion of the spherical plasma model.

CHAPTER III

QUADRUPOLE MASS FILTER

Introduction

In the study of transient, dense plasmas, the number of parameters, which must be monitored in order to attain a degree of understanding, is quite large. The more basic ones, which must be directly determined by theory and/or experiment, include the degree of ionization, the relative abundance of particular ionic species and the rate of plasma expansion. The velocity distribution of the plasma ions is basic in determining if calculations may be made on the basis of local thermodynamic calculations, or not. With a knowledge of these parameters, predictions may then be made regarding the variation of the plasma density, pressure and temperature. Although these represent only a few of the interesting variables, they are some of the more basic ones which must be followed to acquire an understanding of plasma evolution. The quadrupole mass filter is a device which exhibits considerable flexibility as a diagnostic tool for determining some of these parameters.

Since its conception, this revolutionary measuring device has commanded the interest of many researchers. Paul and Steinwendel (1953) introduced the mass filter. Its theory and application to many scientific areas is well documented, (Paul and Raether, 1955;

Woodward and Crawford, 1963; Brubaker and Tuul, 1964; Dawson and Whetten, 1968; Willis, 1969).

As with any type of mass spectrometer, the quadrupole system consists of three major parts whose functions are distinctly unique. These parts include the source, mass analyzer and detector. A description of each of these components will be given.

Ion Source

For much of the work involving analysis with the quadrupole, a continuous thermal source is used. This type is common for the study of ionized gases. For partial pressure analysis, ionizing fields or electron beams provide the ion source. For the study of heavier masses, such as aluminum, practical continuous sources present many difficulties. Because of this, much of the previous analytical work with the quadrupole has been with light masses.

In the scope of the present work, two sources were provided. These were the transient aluminum plasmas created by the vacuum spark gap and the pulsed laser. The vacuum spark plasmas provide a comparatively easily obtainable source and therefore has been used extensively in the present work. Not only has the vacuum spark produced the dense, transient plasmas for investigation, but it has also provided a reliable calibration source for many of the diagnostic instruments. This source consists of a vacuum chamber into which spectroscopically pure aluminum electrodes are inserted via mechanical feed-throughs. These electrodes are spaced so that a gap of approximately one millimeter exists at the tapered tips.

A power supply is used to charge a condenser, which is then

allowed to discharge through the electrodes. The subsequent voltage breakdown at the electrode gap produces an aluminum plasma of very short duration. The intensity of the spark is controlled by the voltage applied to the condenser. For most of the present work, voltages of order of 8.0-10.0 KV were used. The capacitor was rated at 1.0 microfarad.

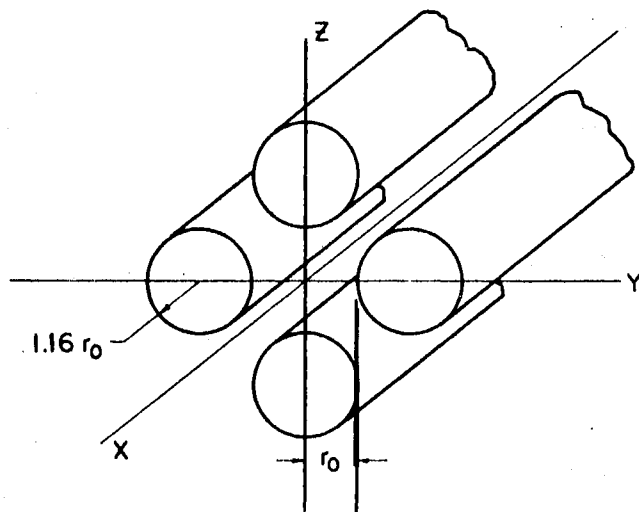
Mass Analyzer

The quadrupole analyzer consists of four cylindrical electrodes which are spaced so that a hyperbolic geometry is simulated. This spacing is shown in Figure 1. Hyperbolic geometry is simulated to one percent with the quadrupole rod radius at 1.16 that of the field radius. A diagram of the quadrupole electrode arrangement with the basic power supply is shown in Figure 2.

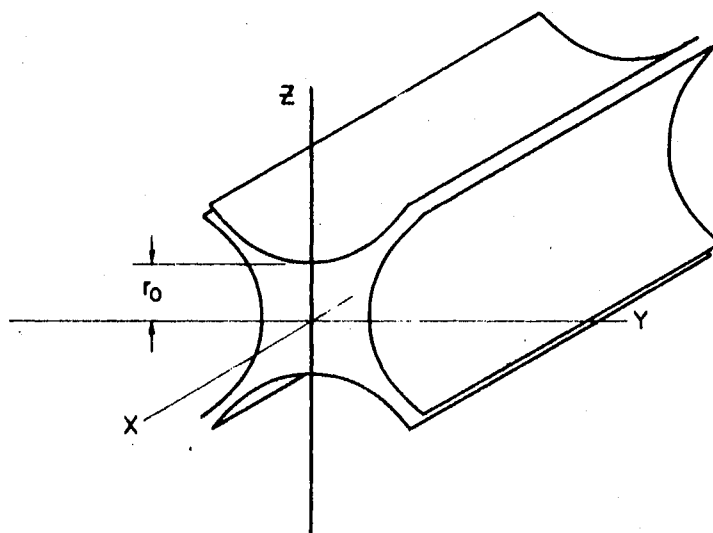
Mass filtering is achieved by applying a superposed radio frequency and dc voltage to the opposing sets of cylindrical electrodes. The theory of the quadrupole is available in the literature cited previously and the details of the specific application to the present work has been presented earlier (Willis, 1969). For the convenience of the reader, a brief summary of the operating principle and the adaptation to the present work is given after the discussion of the quadrupole system detector.

Detector

The detector is a device which responds to the transmission of the aluminum ions through the quadrupole field. A secondary emission detector was chosen for the system which consists of a twenty stage



Actual Cylindrical Surfaces



Ideal Hyperbolic Surfaces

Figure 1. Quadrupole Electrode Geometry

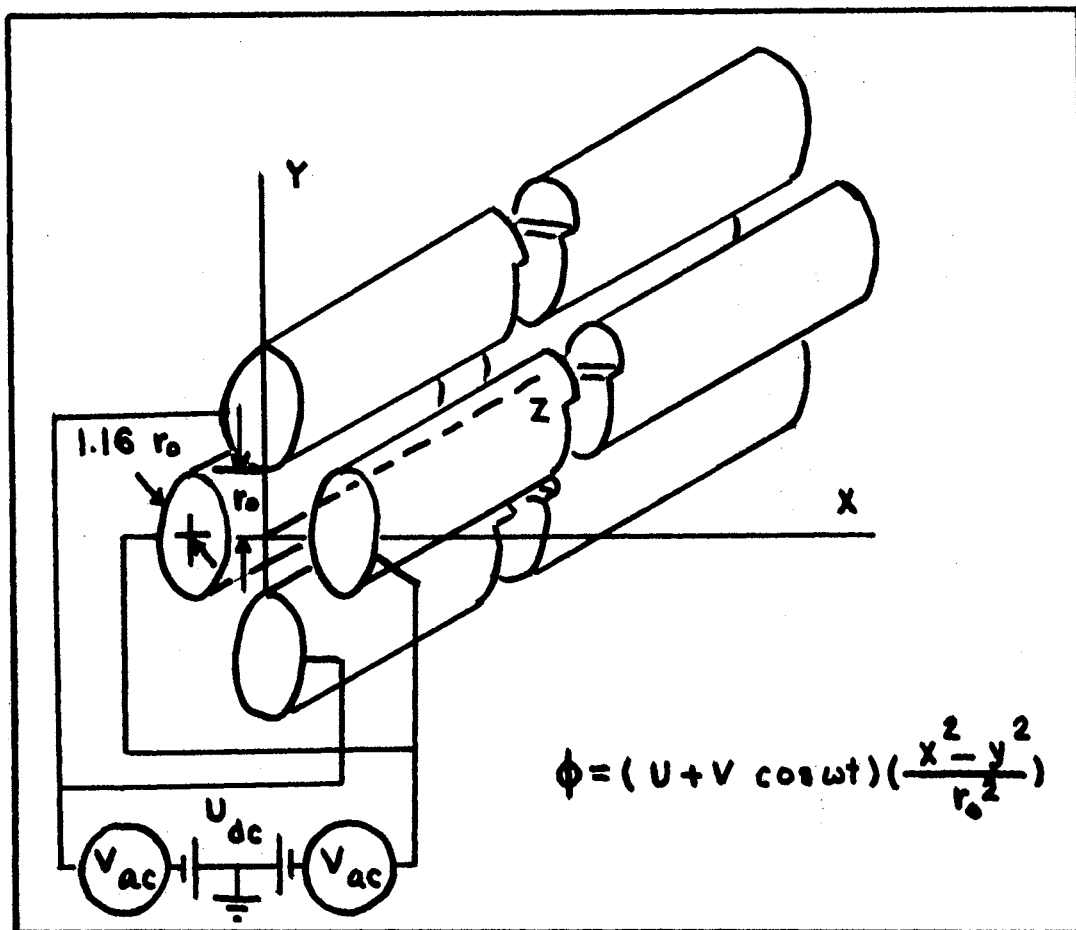


Figure 2. Diagram of Quadrupole Electrode Arrangement

copper-beryllium electron multiplier. The electrons for input to the electron multiplier are obtained, primarily, from the neutralization of the Al^{+1} , Al^{+2} , etc. ions at the cathode of the electron multiplier. The multiplier current was monitored on the vertical input of a 585 Tektronic oscilloscope. The accelerating voltage between successive dynodes was maintained at a constant 50 volts. The gain was estimated at approximately 1.0 million. The detailed theory of this secondary emission device is presented by Allen (1939) and many others.

This device is sensitive to ions, metastable atoms and ultraviolet photons. All of these agents eject electrons from the cathode of the electron multiplier and produce an output signal to the oscilloscope.

A type 86 (Tektronic) plug-in unit was used with the 585 oscilloscope. This plug-in unit has a high gain and a rise time of the order of 4.0 nanoseconds, with constant deflection factors from 0.01 volts per centimeter to 50.0 volts per centimeter. Variable sweep speeds of from 2.0 seconds per centimeter to 50.0 nanoseconds per centimeter are provided. The features of single and delayed sweep were used in the data collecting procedures.

The data was recorded with a Tektronic, type C-12 camera to photograph the oscilloscope trace that is produced by the multiplier current. Type 410 Polaroid film was used because of its high recording speed, which is 10,000 ASA. The photographs may then be enlarged, or the data may be reduced directly from the film.

Quadrupole Theory

Although the quadrupole mass filter may be adapted to several

applications, for example, partial pressure analyzer (Gunther, 1960) and residual gas detector, the present discussion is limited to its use as an "ion filter." Any mass that can be filtered with the device must be ionized, but in this case, only a single mass, viz., that of aluminum is considered. The filtering is achieved by resolving charge to mass ratios for the single mass 27 amu and the electronic charges of from 1 to 13.

The filter employs electric fields which permit only those ions which have a particular charge-to-mass ratio to pass through it. In theory, all other ions are rejected. The filtering action is based on the behavior of the solutions to the equations of motion of the charged particles which pass through the quadrupole field.

The application of a voltage ($U + V \cos \omega t$) to the properly spaced cylindrical electrodes will result in a potential distribution within the quadrupole field region. Neglecting end effects, this distribution, which is the solution to the Laplace equation of hyperbolic fields, is given below.

$$\Phi = (U + V \cos \omega t) \frac{x^2 - y^2}{r_0^2} \quad (3.1)$$

where: Φ = electric potential

U = dc voltage

V = rf voltage

ω = driving frequency

r_0 = quadrupole field radius

The electric fields and equation of motion for the ions which traverse this field are then presented.

$$\vec{E} = - \vec{\nabla} \Phi \quad (3.2)$$

$$E_x = - \frac{\partial \Phi}{\partial x} = - 2(U + V \cos \omega t) \frac{x}{r_o^2} \quad (3.3)$$

$$E_y = - \frac{\partial \Phi}{\partial y} = - 2(U + V \cos \omega t) \frac{y}{r_o^2} \quad (3.4)$$

and

$$E_z = 0 \quad (3.5)$$

The force exerted on the ions determine their trajectory.

$$\vec{F} = m\vec{\ddot{u}} = Ze\vec{E} \quad (3.6)$$

and

$$m\ddot{x} = ZeE_x = - 2Ze(U + V \cos \omega t) \frac{x}{r_o^2} \quad (3.7)$$

$$m\ddot{y} = ZeE_y = 2Ze(U + V \cos \omega t) \frac{y}{r_o^2} \quad (3.8)$$

$$m\ddot{z} = 0 \quad (3.9)$$

The solutions to Equations (3.7) and (3.8) require a change of variables,

$$\xi = \frac{\omega t}{2} \quad (3.10)$$

so that

$$\frac{dx}{dt} = \frac{\omega}{2} \frac{dx}{d\xi} \quad (3.11)$$

and

$$\frac{d^2x}{dt^2} = \frac{\omega}{2} \frac{d}{d\xi} \left(\frac{\omega}{2} \frac{dx}{d\xi} \right) = \frac{\omega^2}{4} \frac{d^2x}{d\xi^2} \quad (3.12)$$

The equations of motion for the ions in the quadrupole field become:

$$\frac{d^2 x}{d\xi^2} = - \frac{8Ze}{m\omega^2 r_o^2} [U + V \cos 2\xi]x \quad (3.13)$$

and

$$\frac{d^2 y}{d\xi^2} = + \frac{8Ze}{m\omega^2 r_o^2} [U + V \cos 2\xi]y \quad (3.14)$$

Rewriting Equations (3.13) and (3.14),

$$\frac{d^2 x}{d\xi^2} + (a + 2q \cos 2\xi)x = 0 \quad (3.15)$$

$$\frac{d^2 y}{d\xi^2} - (a + 2q \cos 2\xi)y = 0 \quad (3.16)$$

where:

$$a = \pm \frac{8ZeU}{m\omega^2 r_o^2} \quad (3.17)$$

and

$$q = \pm \frac{4ZeV}{m\omega^2 r_o^2}, \quad (3.18)$$

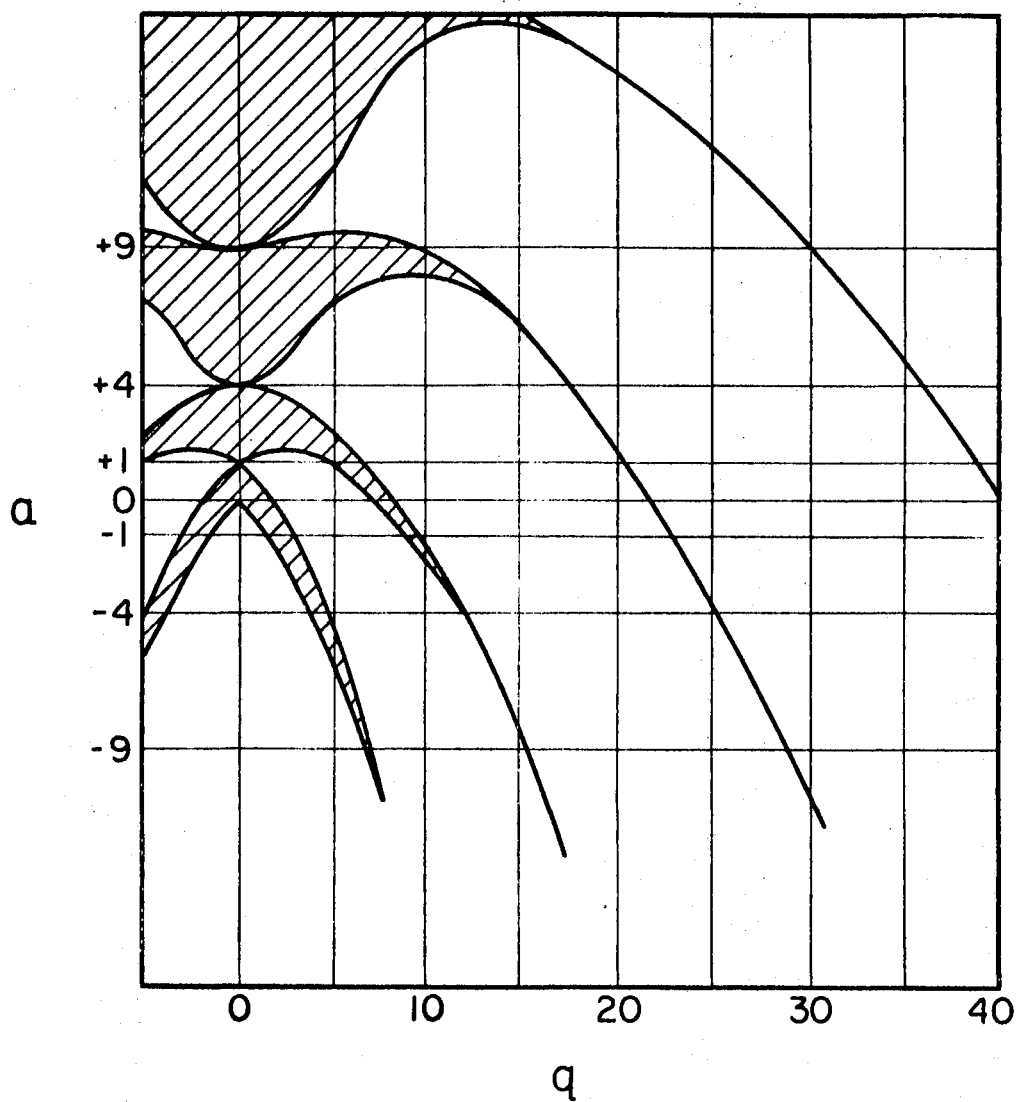
the general form of the Mathieu equation is obtained:

$$\frac{d^2 u}{d\xi^2} + (a - 2q \cos 2\xi)u = 0 \quad (3.19)$$

The solution has the general form:

$$u = Ae^{\mu\xi} \sum_{n=-\infty}^{\infty} C_n e^{in\xi} + Be^{-\mu\xi} \sum_{n=-\infty}^{\infty} C_n e^{-in\xi} \quad (3.20)$$

The solution is bounded for imaginary values of (μ) and will oscillate in some stable range, depending on parameters "a" and "q". The ranges of stability are shown in Figure 3 and the first stability



RANGES OF STABILITY FOR
SOLUTIONS OF MATHIEU EQUATIONS

Figure 3. Mathieu Stability Ranges

region is given in Figure 4. The operating point was chosen to be $a = 0.2$, $q = 0.7$.

The values of the dc and rf voltages were determined using this operating point as a basis.

$$U = \pm \frac{m\omega^2 r_o^2}{8Ze} \quad (3.21)$$

and

$$V = \pm \frac{m\omega^2 r_o^2}{4Ze} \quad (3.22)$$

With the variables evaluated below, these voltages assume the following values:

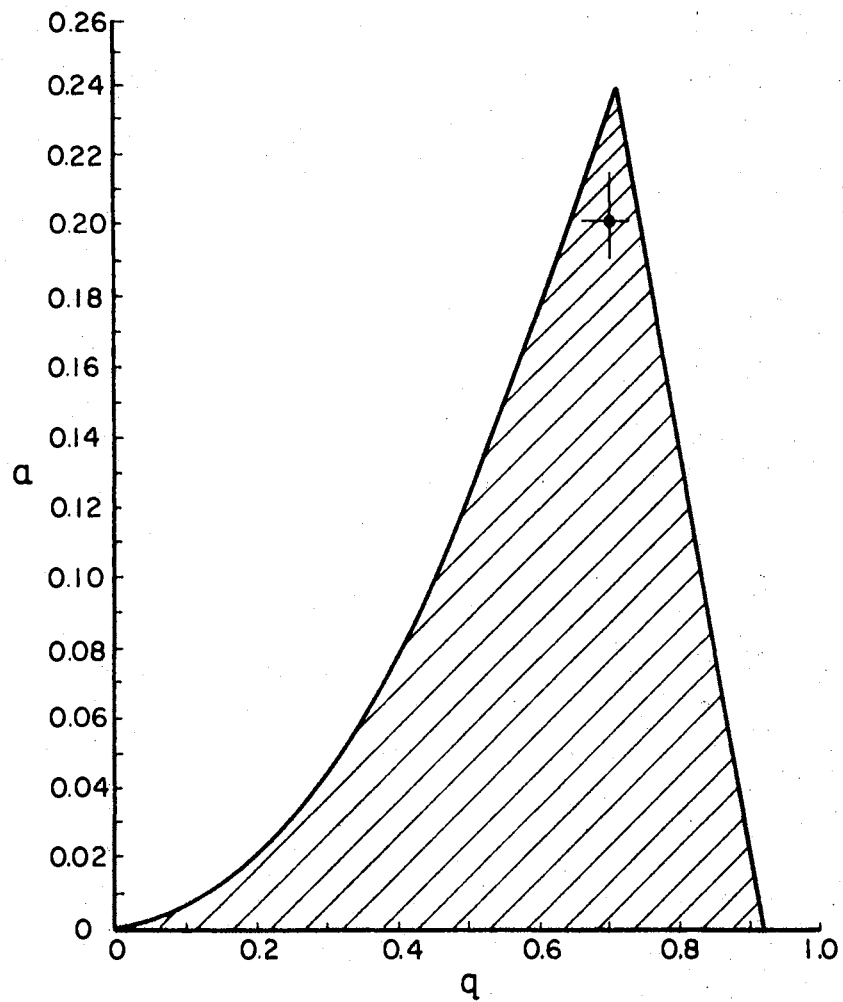
$$\begin{aligned} m &= 27 \text{ amu} = 4.48 \times 10^{-26} \text{ kg} \\ \omega^2 &= (2\pi f)^2 \\ f &= 3.2 \times 10^6 \text{ Hz} \\ \omega^2 &= 4.04 \times 10^{14} \text{ (rad/sec)}^2 \\ r_o^2 &= 3.31 \times 10^{-5} \text{ (meters)}^2 \\ a &= 0.2 \\ q &= 0.7 \\ e &= 1.602 \times 10^{-19} \text{ Coulombs} \\ Z &= \text{degree of ionization (1-13)} \end{aligned} \quad (3.23)$$

Therefore:

$$U = \pm \frac{93.63}{Z} \text{ volts (dc)} \quad (3.24)$$

$$V = \pm \frac{655.4}{Z} \text{ volts (ac)} \quad (3.25)$$

The work reported here is limited to aluminum ionic species Al^{+1}



FIRST STABILITY RANGE
FOR MATHIEU SOLUTIONS

Figure 4. Mass Filter Operating Point

through Al^{+5} , so that the following tables illustrate the voltage requirements for ion acceptance for $Z = 1$ to $Z = 5$. Note that only ions with the appropriate Z -value are accepted, i.e., transmitted through the quadrupole field.

Quadrupole Assembly

The quadrupole unit itself was designed and constructed as part of the work reported on previously (Willis, 1969). A block diagram of the unit and the support equipment is shown in Figure 5. The basic specifications for the field rods and power supply are given below:

1. Quadrupole electrode length - 30 cm. (four rods with diameter 13.23 mm and separation 11.50 mm).
2. The radio frequency generator operates at 3.2 mhz from 0 to 3,000 VAC, peak-to-peak.
3. The dc power supply operates in the range 0 to 150 volts.

The mounting arrangement for the electrodes themselves is shown in Figure 6.

The power supply for the quadrupole electrodes has been modified to provide a regulated, constant voltage and a crystal control for the frequency. These modifications are included in the schematics shown below. The basic power supply section is given in Figure 7, and the rf section is presented in Figure 8. The improvements reduced considerably the fluctuations in the voltage settings and eliminated the frequency drift, which were the major difficulties with the earlier design.

The operating procedure was improved so that the reproducibility of the data is better than that of the previous results. The rf and

TABLE I
STABILITY PARAMETERS FOR AL +1

$$Z = 1$$

$$U = \pm 93.63 \text{ volts}$$

$$V = \pm 655.4 \text{ volts}$$

Z	a	q	Classification
1	0.20	0.70	accepted
2	0.40	1.40	rejected
3	0.60	2.10	rejected
4	0.80	2.80	rejected
5	1.00	3.50	rejected
6	1.20	4.20	rejected
7	1.40	4.90	rejected
8	1.60	5.60	rejected
9	1.80	6.30	rejected
10	2.00	7.00	rejected
11	2.20	7.70	rejected
12	2.40	8.40	rejected
13	2.60	9.10	rejected

TABLE II
STABILITY PARAMETERS FOR AL +2

$$Z = 2$$

$$U = \pm 46.82 \text{ volts}$$

$$V = \pm 327.7 \text{ volts}$$

Z	a	q	Classification
1	0.10	0.35	rejected
2	0.20	0.70	accepted
3	0.30	1.05	rejected
4	0.40	1.40	rejected
5	0.50	1.75	rejected
6	0.60	2.10	rejected
7	0.70	2.45	rejected
8	0.80	2.80	rejected
9	0.90	3.15	rejected
10	1.00	3.50	rejected
11	1.10	3.85	rejected
12	1.20	4.20	rejected
13	1.30	4.55	rejected

TABLE III
STABILITY PARAMETERS FOR AL +3

$$Z = 3$$

$$U = \pm 31.21 \text{ volts}$$

$$V = \pm 218.5 \text{ volts}$$

Z	a	q	Classification
1	0.07	0.23	rejected
2	0.13	0.47	rejected
3	0.20	0.70	accepted
4	0.27	0.93	rejected
5	0.33	1.17	rejected
6	0.40	1.40	rejected
7	0.47	1.63	rejected
8	0.53	1.87	rejected
9	0.60	2.10	rejected
10	0.67	2.33	rejected
11	0.73	2.57	rejected
12	0.80	2.80	rejected
13	0.87	3.03	rejected

TABLE IV
STABILITY PARAMETERS FOR AL +4

$$Z = 4$$

$$U = \pm 23.41 \text{ volts}$$

$$V = \pm 163.85 \text{ volts}$$

Z	a	q	Classification
1	0.05	0.18	rejected
2	0.10	0.35	rejected
3	0.15	0.53	rejected
4	0.20	0.70	accepted
5	0.25	0.88	rejected
6	0.30	1.05	rejected
7	0.35	1.23	rejected
8	0.40	1.40	rejected
9	0.45	1.58	rejected
10	0.50	1.76	rejected
11	0.55	1.93	rejected
12	0.60	2.11	rejected
13	0.65	2.28	rejected

TABLE V
STABILITY PARAMETERS FOR AL +5

$$Z = 5$$

$$U = \pm 18.73 \text{ volts}$$

$$V = \pm 131.1 \text{ volts}$$

Z	a	q	Classification
1	0.04	0.14	rejected
2	0.08	0.28	rejected
3	0.12	0.42	rejected
4	0.16	0.56	rejected
5	0.20	0.70	accepted
6	0.24	0.84	rejected
7	0.28	0.98	rejected
8	0.32	1.12	rejected
9	0.36	1.26	rejected
10	0.40	1.40	rejected
11	0.44	1.54	rejected
12	0.48	1.68	rejected
13	0.52	1.82	rejected

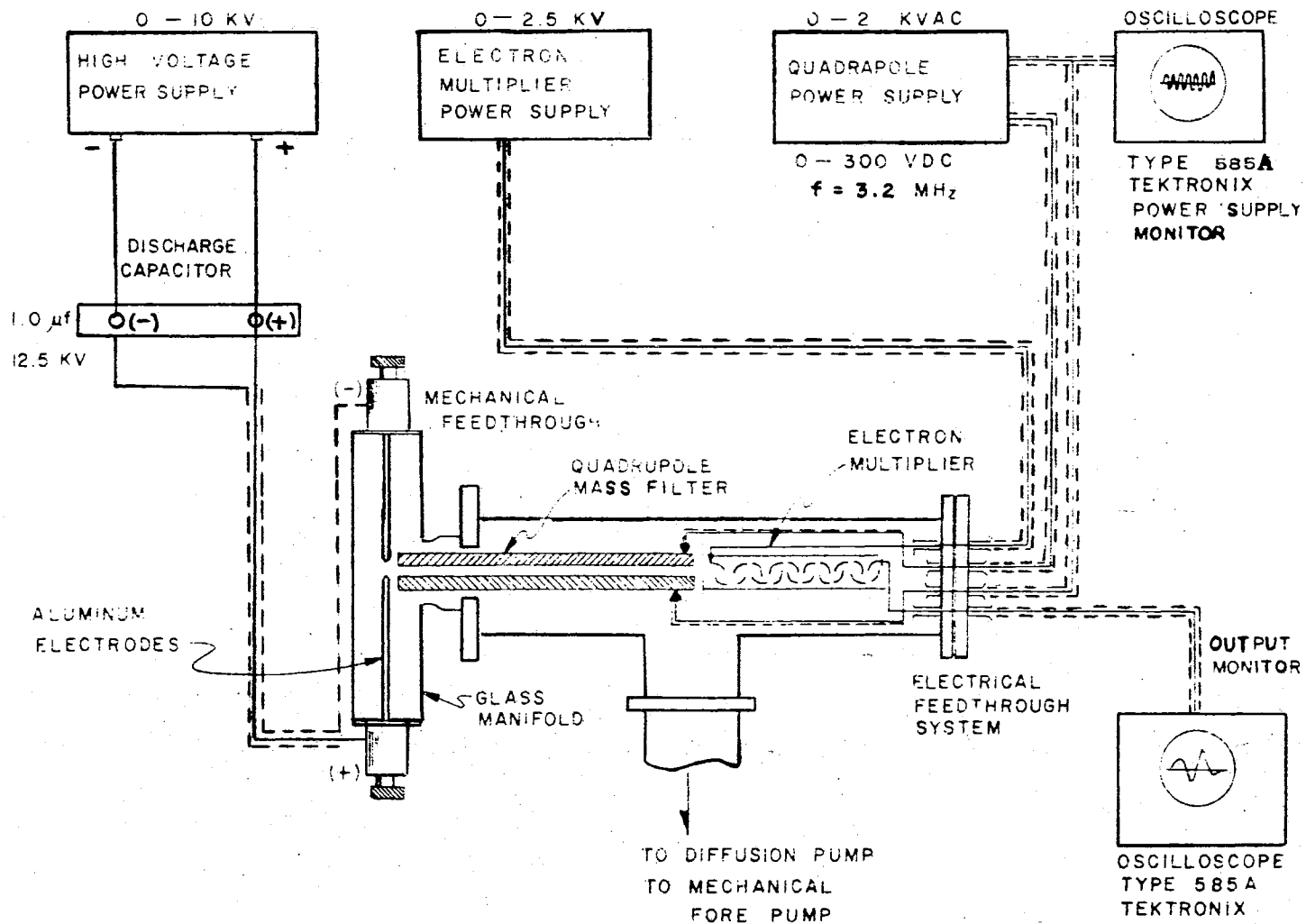
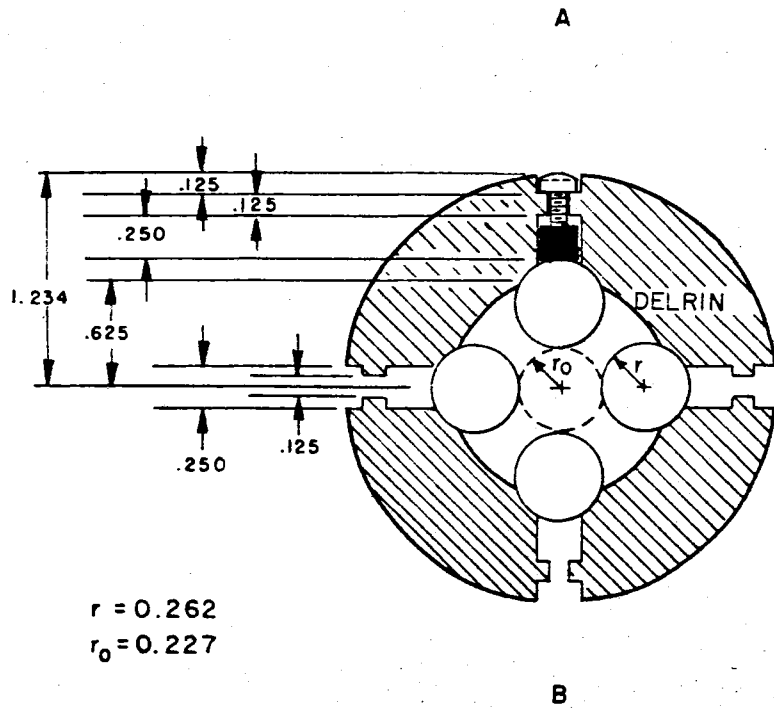
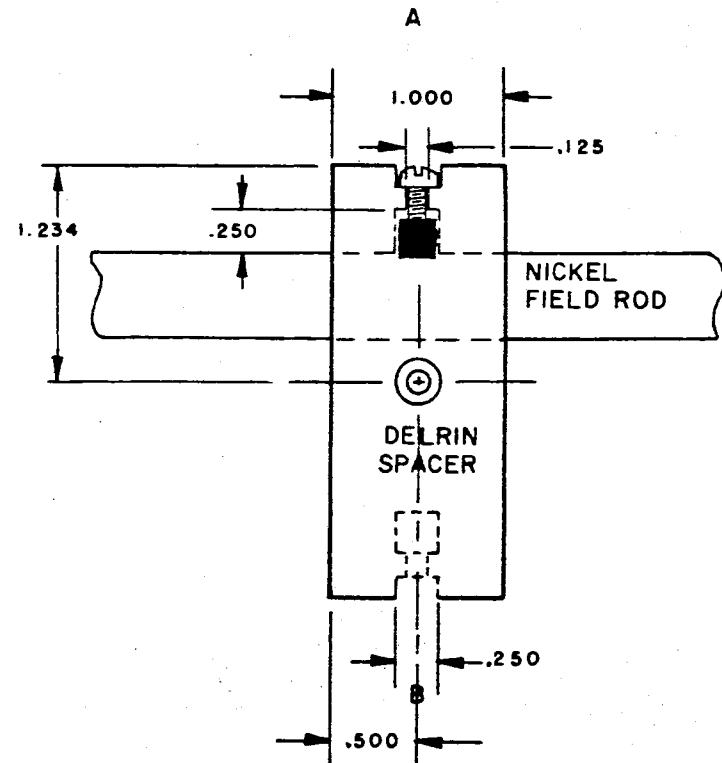


Figure 5. Block Diagram of Quadrupole Mass Filter and Support Equipment

CROSS SECTION VIEW



SIDE VIEW



1 inch
full scale

Figure 6. Quadrupole Field Electrode Mounting

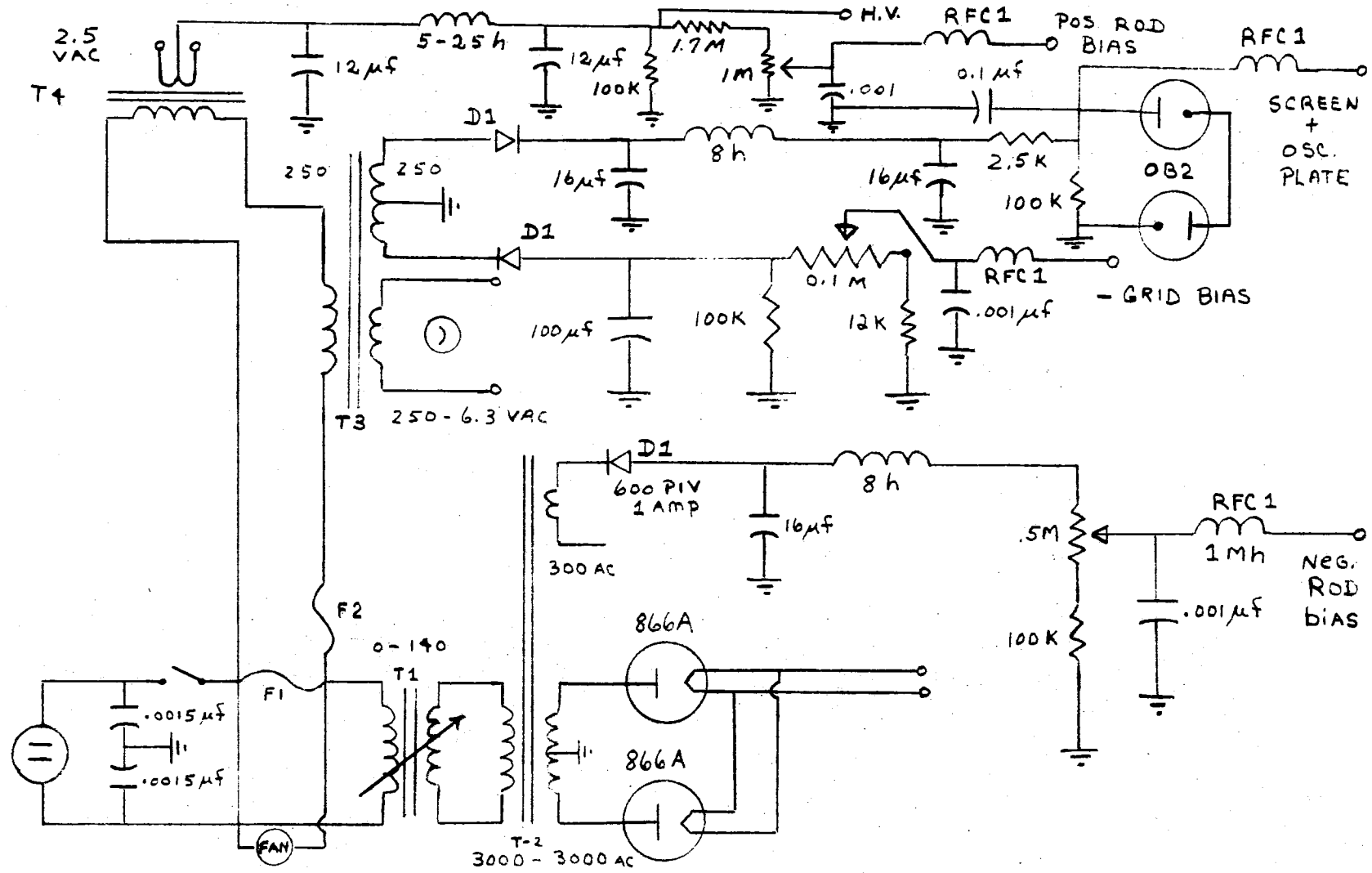


Figure 7. Basic Power Supply Section for Quadrupole

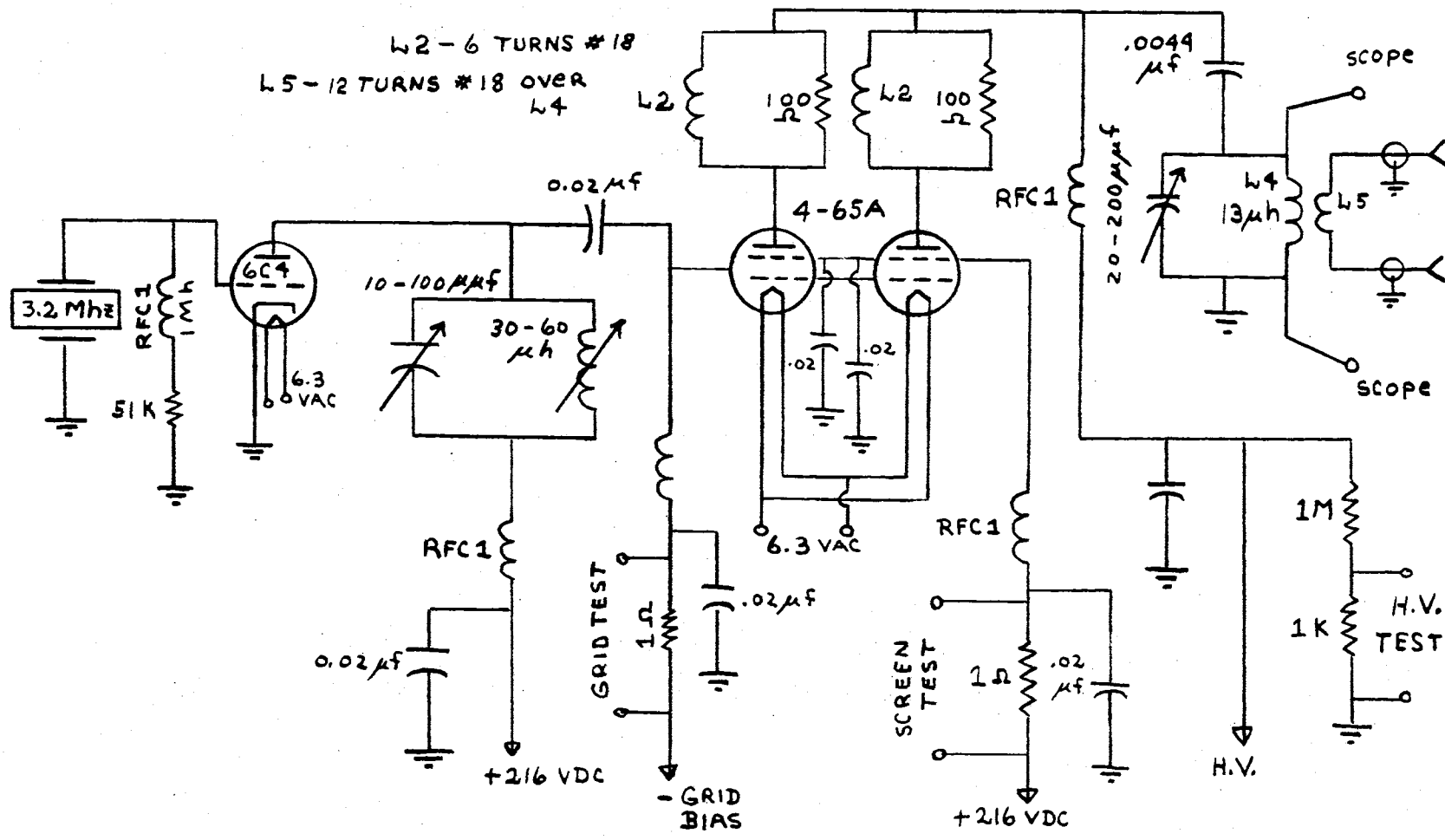


Figure 8. R.F.-Section for Quadrupole Power Supply

dc voltages were monitored with a Tektronic 585A dual trace oscilloscope. Better shielding was added to the capacitor discharge leads so that much of the transient signal due to inductive coupling was eliminated.

The electron multiplier detector was also shielded within the vacuum chamber. This also helped to decrease the transients. In addition, the discharge capacitor itself was housed inside a grounded metal cabinet. The vacuum chamber was maintained at a pressure between 10^{-5} - 10^{-6} torr.

Some of the typical results which were obtained with the improved quadrupole will be shown in Chapter VII. The curves presented there were reduced directly from the pictures taken of the oscilloscope trace. They show the output current of the electron multiplier which is a composite signal representing the aluminum ions, metastable atoms and ultraviolet photons. A discussion of the interpretation of these results accompanies the curves.

CHAPTER IV

ELECTROSTATIC LENS SYSTEM

Introduction

In the work with the quadrupole mass filter, the electron multiplier detector yields a signal which is a superposition of the ions, neutral atoms and u.v. photons. The considerable difficulty in reducing the data led to an attempt to separate these component particles before they reach the collector dynode of the detector. The metastable atoms are uncharged and are, therefore, not affected by the alternating quadrupole fields. The photon beam which emanates from the ionizing region of the source is also unaffected. These photons travel through the quadrupole field, releasing electrons at the end of their paths at the multiplier cathode. Photon-ejected electrons from the detector produce the electrical signals from the electron multiplier which are indistinguishable from signals that are produced by electrons from the neutralization of incident ions and by the electrons from the impact of high energy, metastable atoms. Impressed fields may be used, for example, to suppress photo-ejected electrons in a Faraday cup, but this cannot be done with a secondary emission multiplier, since the electrons constitute the signal. The neutrals, of course, may not be suppressed by fields in any case.

The electrostatic lens was designed to deflect the ions from the

constituent beam of ions, neutrals and light. In the early stages of the study on the project, several geometric configurations were studied. One of the fundamental requirements which was selected for the design was that all ions, regardless of their velocity, should leave the lens at approximately the same angle, and should converge onto a single point. This requirement precludes the use of a continuous device on account of the wide range of ionic velocities. The use of magnetic fields was undesirable, since the required magnitude of the field would introduce shielding problems. It would be possible, in theory, to use an asymmetrical electrode geometry to accomplish ion beam deflection, but the difficulties with construction and the problems with fringing discourage this design.

While the lens was still in the design stage, another requirement was added which prompted a broader study. This requirement was that the ions be deflected from the emission beam with the least possible variation in their velocity in the direction of initial travel. The reason for this requirement is that the velocity distributions of the ions thus deflected will be unaltered. The ultimate goal of this new device was then two-fold: (1) to separate the ions from the plasma emission beam and (2) to provide a direct determination of the velocity distribution of ions of one specie at a time.

Theory and Design

The objective of the lens is to act on a beam of ions, photons, excited atoms and neutrals from an ion source. From this beam, it is desired to extract a group of ions of a preselected specie, such as Al^{+2} or Al^{+4} . The general method of application is to collimate a

beam of ions that escape from the source with slits and without electrostatic fields to extract the ions from the source, or to form the beam. The collimated beam still contains photons, atoms, excited atoms and a mixture of species.

Several computer studies were made of the lens system and the final design was determined. The details of this design are given by Willis (1969). A brief summary of the design and operating principle is given below.

The geometry which more closely satisfies the requirements stated above is a parallel plate capacitor configuration, with two important modifications. The unseparated beam passes midway between the plates. First, the ground base plate of the lens is a solid plate, while the positive "plate" is made up of several discrete electrodes. The closely spaced, individual electrodes allow a much larger electric field gradient than would be possible with a solid positive plate of any practical geometry. Second, the voltage is applied to the lens in a pulse, rather than a steady electric field. The basic mechanical design for the lens electrodes is shown in Figure 9.

The operating principle of the lens has, for a basis, the equations of motion for the ions which traverse the pulsed field. Consider an ion of charge Ze and mass m which is directed into the region of the electric field, produced by the electrostatic lens, where Z is a small whole number, such as 1, 2, 3, etc. Since the voltage supplied to the electrodes of the lens increases in the direction of ion travel, the electric field is an increasing function of (x) , depending on the gradient of the voltage between successive electrodes. There are two forces which are exerted on the ion, both of which are directed at

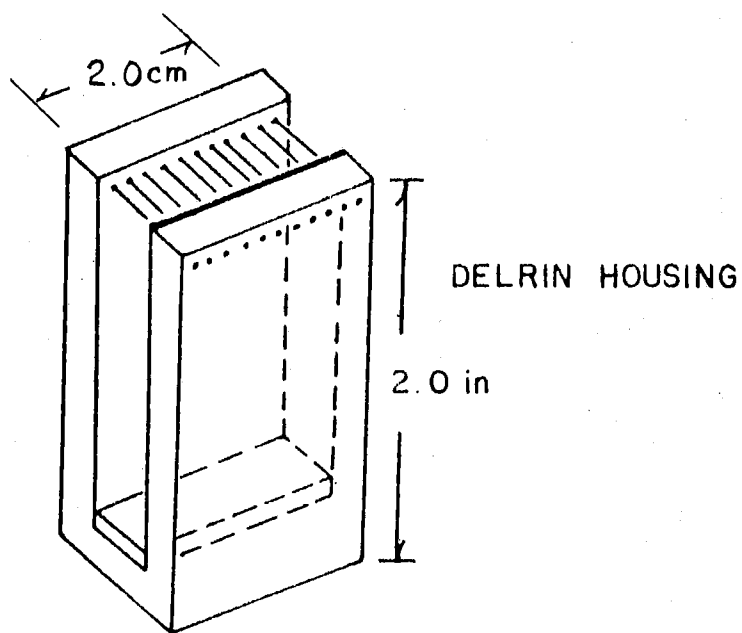
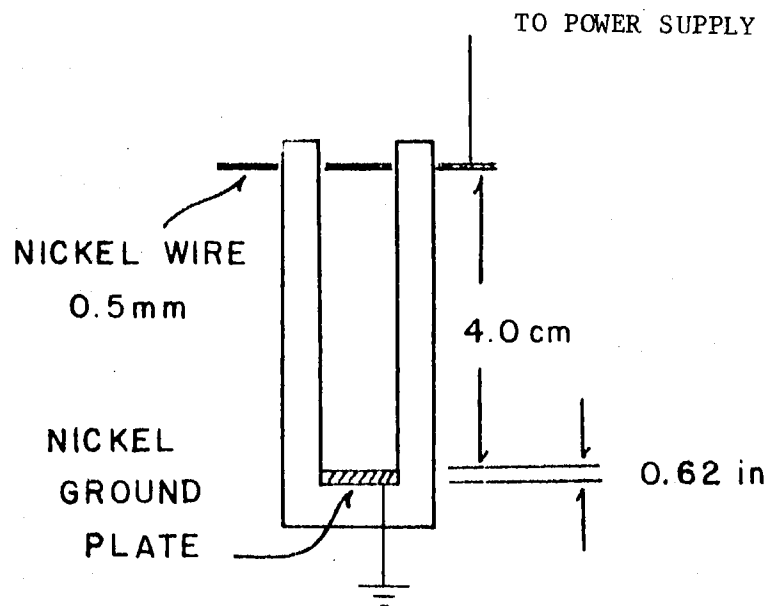


Figure 9. Electrostatic Lens

right angles to the direction of initial travel. In the region immediately below an electrode, the electric field is approximately constant.

$$\vec{F} = Ze\vec{E} = ZeE_y \vec{j} \quad (4.1)$$

$$E_x \vec{i} = 0 \quad (4.2)$$

The equation of motion for this region is given

$$\ddot{y} = \frac{ZeE}{m} \quad (4.3)$$

or

$$y = \frac{ZeEt^2}{2m} + (\dot{y})_0 t + y_0 \quad (4.4)$$

where: y = vertical ion deflection

Z = degree of ionization

E = constant electric field (V/d)

V = accelerating potential

d = vertical extent of field

t = time

m = ionic mass

\dot{y}_0 = initial vertical velocity

y_0 = initial vertical displacement

The slope of the ion trajectory is determined for any horizontal displacement.

$$v = \frac{(x - x_0)}{t} \quad (4.5)$$

v = velocity in x-direction

Now substitute Equation (4.5) into Equation (4.4) to obtain the slope.

$$\frac{dy}{dx} = \frac{ZeE}{2m} \frac{2(x - x_0)}{v^2} + \frac{\dot{y}_0}{v} \quad (4.6)$$

or

$$\theta = \text{TAN}^{-1} \left[\frac{dy}{dx} \right] \quad (4.7)$$

The trajectory of the ion in the constant field region is then completely specified with Equations (4.4) and (4.7).

As the ions pass through the region between successive electrodes, they experience the effect of an electric field which is an increasing function of (x). The equation of motion for the ion in this region differs from that derived above, to the extent that $E = E(x)$.

Rewriting Equation (4.4),

$$y(t) = \frac{ZeV(x)t^2}{2md} + \dot{y}_0 t + y_0 \quad (4.8)$$

where: $V(x) = V_0 + \alpha x$

$$\alpha = \frac{\partial V}{\partial x}$$

and making the change of variables, Equation (4.5), the vertical deflection of the ion for this region is given.

$$y(x) = \frac{Ze}{md} \left[\frac{V_0(x - x_0)^2}{2v^2} + \frac{\alpha(x - x_0)^3}{6v^2} \right] + \frac{\dot{y}_0(x - x_0)}{v} + y_0 \quad (4.9)$$

The slope of the trajectory for the ion in this region is then derived according to Equation (4.6) and is given.

$$\theta = \text{TAN}^{-1} \left\{ \frac{Ze}{md} \left[\frac{V_o(x - x_o)}{v^2} + \frac{\alpha(x - x_o)^2}{2v^2} \right] + \frac{\dot{y}_o}{v} \right\} \quad (4.10)$$

The trajectory of the ion is then known at any point, as it traverses the lens by the appropriate application of Equations (4.4), (4.7), (4.9) and (4.10).

A computer model of the lens was developed to determine the mechanical design as well as the electric field values required to properly separate one specie of ion from the mixture of ions, metastables, photons, etc. in the beam from the plasma. The model was also used to predict the geometry required to monitor the ion beam with the quadrupole mass filter. This geometry is depicted in Figure 10. It will be noted from this figure that the angular separation of the ions of one specie from the mixed beam was designed to be 15.0 degrees.

The calculations were made for aluminum ions in the velocity range from 700 m/sec to 5×10^4 m/sec. The final, vertical deflection and slope of the ion trajectories were determined for ionic species $Z = 1$ through $Z = 5$; and the optimum voltages, that are required to maintain an exit slope of 15° , were calculated. These voltages were applied to the five central electrodes of the lens. Additional electrodes at the entrance and exit of the lens were employed to counteract fringing. These electrodes are situated so that the field separa-

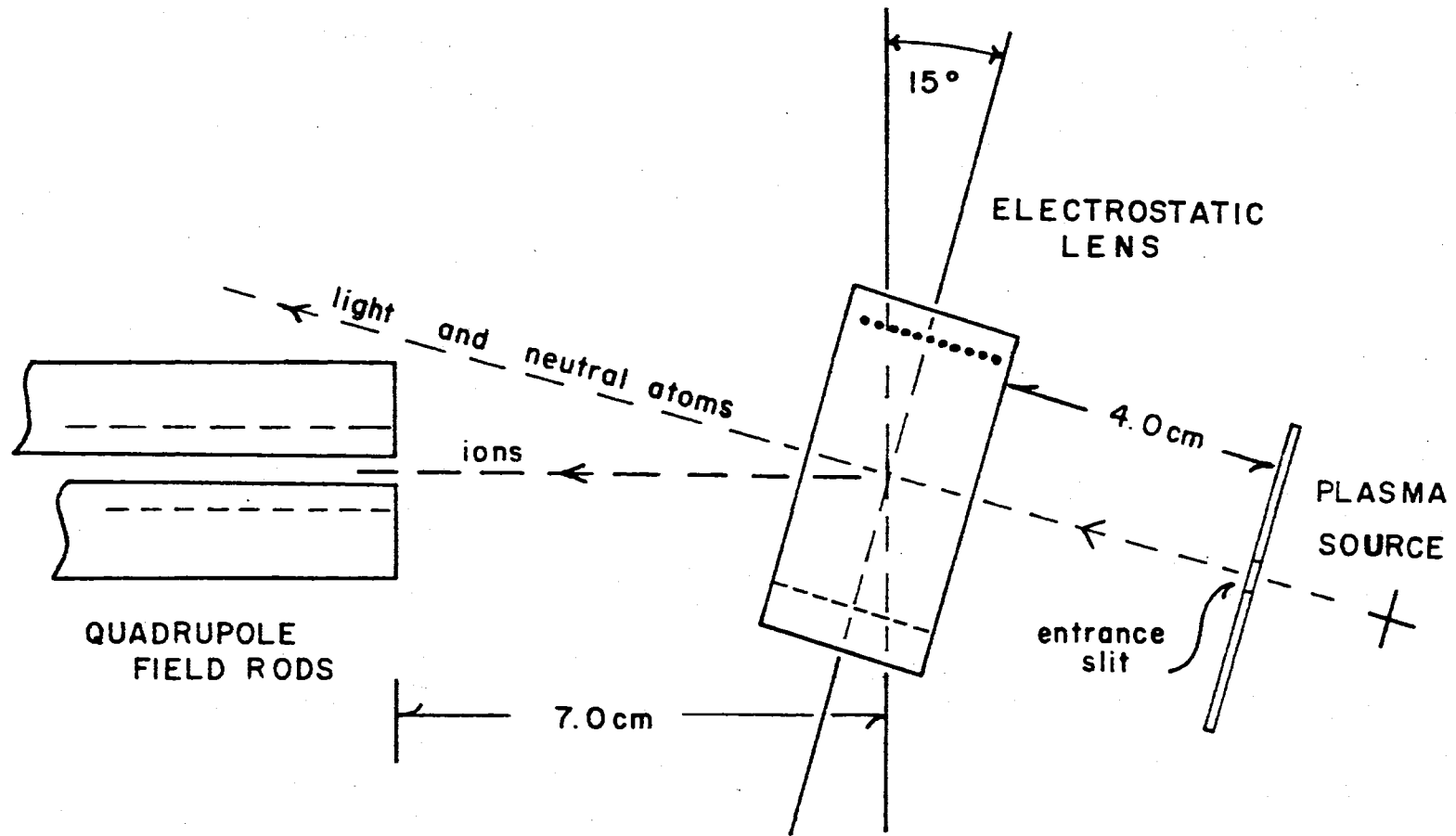


Figure 10. Electrostatic Lens in Operational Configuration

tion between them and the base ground plate is a constant 4.0 cm. The electrodes themselves are 0.5 mm in diameter and the center-to-center separation between successive electrodes is 2.0 mm. They were constructed of high purity nickel (Ni #200, 99%). The entrance slit and ground base plate are also constructed of nickel.

Lens Power Supply

The values of the voltage which are calculated from the computer model are presented in Table VI. The potential gradients are also shown. In this table, electrode number 1 corresponds to the wire electrode which is nearest to the entrance of the lens. ALPHA I is the potential gradient in the direction of ion travel for values of displacement into the field of from 0.0 to 2.5 mm. ALPHA II is for values in the 2.5 to 8.0 mm range.

From this table, it is apparent that there are a unique set of voltage values for each specie of ion. It should be emphasized that the lens deflects only the ions of a single, preselected Z-value from the emission beam. This deflected beam is allowed to enter the quadrupole field which is set to transmit this same specie to the detector. The ultraviolet photons and metastable atoms pass through the electrostatic lens, unaffected by the pulsed field, and thereby are not allowed to enter the quadrupole.

The ions which reach the detector have then been doubly filtered; first by the lens itself and then by the quadrupole field. The output signal from the detector must then be a measure of only ions of a particular charge.

For the initial experiments with the lens system, pulse duration

TABLE VI
VOLTAGE VALUES AND POTENTIAL GRADIENTS

ION	ELECTRODE #1 volts	ELECTRODE #2 volts	ELECTRODE #3 volts	ELECTRODE #4 volts	ELECTRODE #5 volts	ALPHA I & II	
						volts/mm	
1	3.00	20.00	55.00	90.00	125.00	8.947	18.420
2	1.50	10.00	27.50	45.00	62.50	4.474	9.210
3	1.00	6.67	18.33	30.00	41.67	2.982	6.140
4	0.75	5.00	13.75	22.50	31.25	2.237	4.605
5	0.60	4.00	11.00	18.00	25.00	1.789	3.684

of 1.0 microsecond was used. The values for the voltages on the electrodes for the lens are obtained from a commercial, unit pulse generator. The generator was a type 1217-B generator which is manufactured by the General Radio Company. This unit was externally triggered to produce a one microsecond, 40 volt square wave in the single pulse mode. This signal was then amplified to provide the higher voltages which are required by the lens. A schematic of the pulse amplifier is shown in Figure 11. This amplifier is a high speed device capable of amplifying a low level, square wave, input signal. Due to the fast switching time of the Motorola 2N5345 transistor, only an additional 25-35 nanoseconds are added to the rise time of the input signal. Coupled with the pulse amplifier, the voltage divider network provides five different output voltages which range from 0 to 200 volts.

Lens Vacuum System

The vacuum system for the original quadrupole and detector was modified to provide the additional capacity to house the lens. The major modification was the addition of a glass envelope which is commercially available from Owens-Illinois. This envelope consists of a modified reducer cross #6250 with conical end type connectors. The diameter of the main section is 4.0 inches and the diameter of the right angle extensions is 2.0 inches. A diagram of the vacuum system is provided in Figure 12. The system was maintained at a pressure ranging between 10^{-5} and 10^{-6} torr for the experiments with the lens.

Operating Procedure

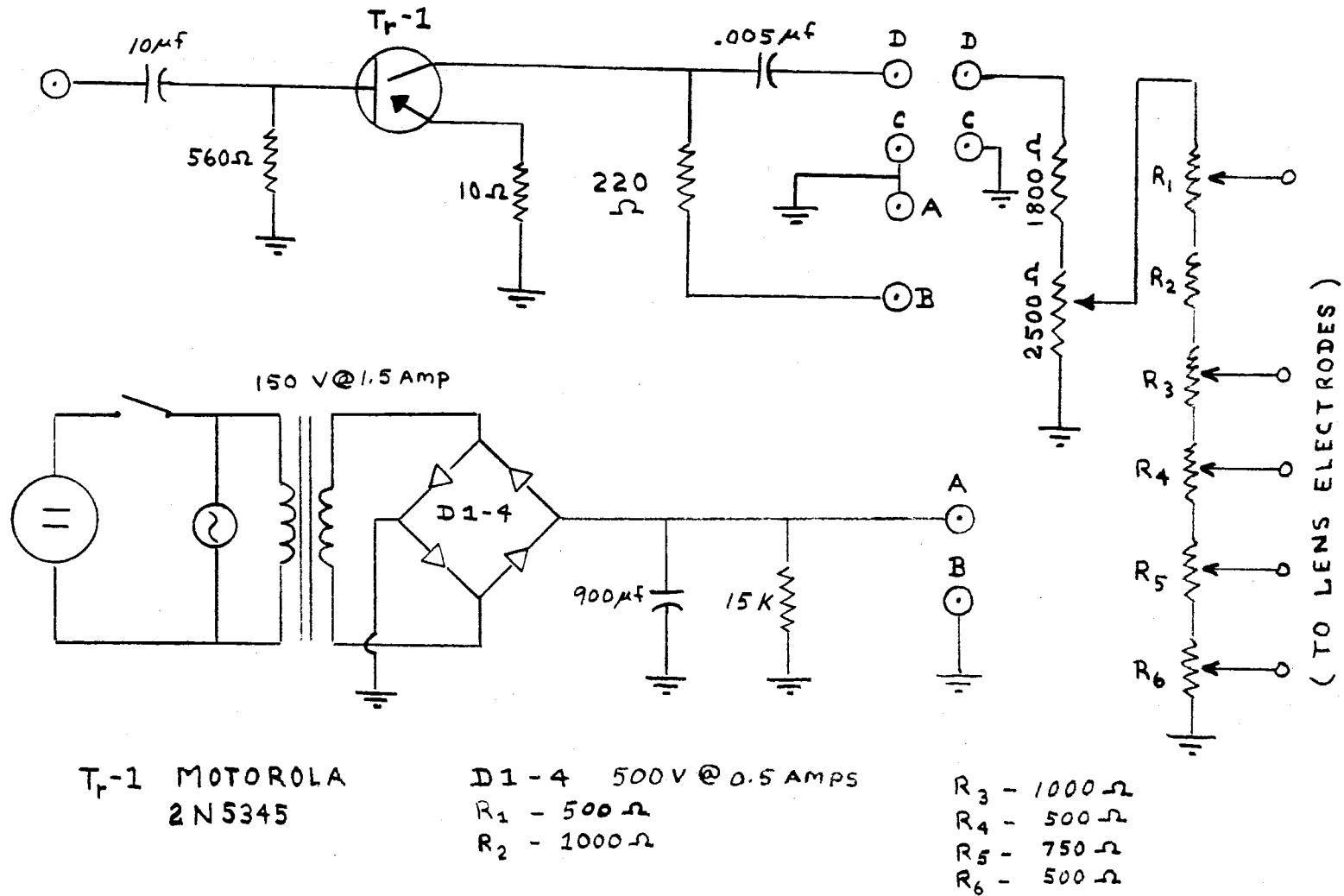


Figure 11. Pulse Amplifier and Voltage Divider for Lens System

The diagram in Figure 12 shows essentially the same support equipment for the system as was shown in Figure 5. The major additions to the system include the enlarged vacuum system, unit pulse generator, pulse amplifier with voltage divider network, and a time delay for synchronizing the electrostatic lens pulse. The variable time delay available on the 585A Tektronic oscilloscope was used to turn on the field of the lens at the instant that the ions arrive at the lens from the vacuum spark plasma.

The procedure for obtaining the plasma source is the same as for the initial quadrupole work. A large condenser is charged to 8.0-10.0 KV and allowed to discharge through the spark between the aluminum electrodes. The proper rf and dc voltage values are set for the quadrupole field. The voltages for the electrostatic lens electrodes are selected from the pulse amplifier. The dual trace 585A oscilloscope is used to monitor these values to insure that they are set properly and are stabilized. The time delay for the lens pulse is set to coincide with the position of the ions that are to be observed. The output oscilloscope, a 585A single trace type, is set for the external trigger, single sweep mode. This scope is triggered by the breakdown of the vacuum spark gap, so that reference to zero time is established. The C-12 camera records the output of the detector so that the oscilloscope traces may be analyzed.

Some of the typical results for ionic species Al^{+1} through Al^{+5} are presented in Chapter VII. One of the most interesting results obtained in this experiment is the indication of the ionic velocity distributions. A discussion of the initial results and some of their implications is provided in the section of Chapter VII that deals

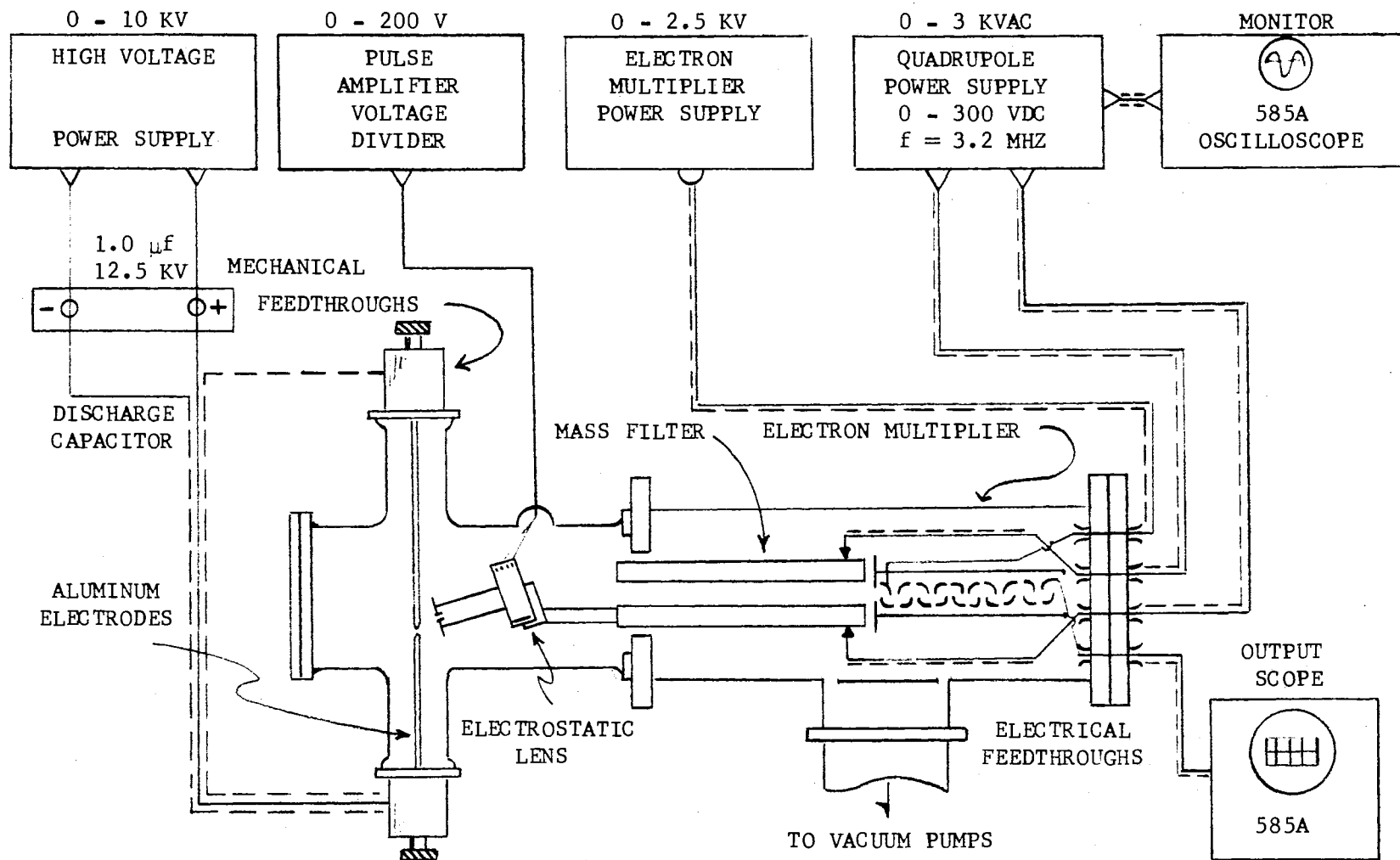


Figure 12. Diagram of Electrostatic Lens System with Support Equipment

with the electrostatic lens. A brief summary of improvements, which may be made to this experimental device, is included in Chapter VIII.

CHAPTER V

LASER IMPACT PLASMA

Introduction

The dense, transient plasma which is produced by laser impact on a solid aluminum target has been investigated. The type of plasma was employed as one of the sources for the quadrupole mass filter. In this study, the emission of ions and u.v. light was studied. As mentioned earlier in this report, Langmuir probes were also employed for an approximate determination of the plasma expansion velocity (Robinson, 1970). The interpretation of these experimental results have provided guidelines for the theoretical phase of the work with laser impact plasmas. The continuing theoretical study of dense, transient plasmas includes a mathematical model for the plasma which is produced by the laser. The original computer program for this model was designed earlier by Peery (1970) and has been used as a basis for the continuing work in this area. The model has been implemented with improved computer techniques as well as with a revision of some of the program elements. A method for computerized data output and reduction has been developed and will be described in the text. This program was prepared for a production run and some of the initial results from this run are presented and discussed in Chapter VII.

Background Discussion

The laser impact model was developed to simulate the creation and subsequent expansion into vacuum of a plasma that is produced by the incidence of a Q-switched, twin-ruby laser beam onto an aluminum plate at room temperature. The plasma induced by the laser beam is defined as a modified, single fluid type. In this type of plasma, the ions are treated as the single fluid and the electrons are held in the fluid by charge and by viscous forces. This plasma may be represented analytically in this manner and the plasma interactions are governed by the usual macroscopic equations of flow. The equations which constitute this set include the electromagnetic and hydrodynamic relations which determine the plasma creation and decay. The detailed derivation of these equations may be reviewed in the work by Peery, and will not be repeated here. This set of equations are solved to obtain values for the plasma properties as a function of spatial coordinates and time. Two of the significant improvements that the laser impact model contain over the previous analytical work, are the extension to cylindrical geometry and an improved equation of state for aluminum. This equation of state has an extended region of applicability to include a somewhat lower temperature and high density region, which was considered inadequate in the equation that was developed and employed by Bruce (1966).

To solve the set of equations, values for the thermal and electrical conductivity, viscosity, and the optical properties were also calculated by the program. The method of solution was by numerical procedures which are devised to obtain a computer solution of the

flow equations.

These flow equations are listed below:

1. Mass continuity equation
2. Equation of motion
3. Conservation of energy equation
4. Equation defining heat conduction
5. Equation of state for aluminum
6. Maxwell electromagnetic equations

Theory

The analytical form of the macroscopic equations in the previous section are now presented with a brief discussion. For a more detailed analysis of the plasma variables, the derivation of the flow equations and the more subtle feature of the equation of state, the reader is urged to consult the references given in Chapter I.

The conservation of mass is

$$\frac{\partial \rho}{\partial t} + \vec{\nabla} \cdot (\rho \vec{u}) = 0. \quad (5.1)$$

The equation of motion is given, as usual by the conservation of momentum.

$$\rho \left\{ \frac{\partial \vec{u}}{\partial t} + (\vec{u} \cdot \vec{\nabla}) \vec{u} \right\} = - \vec{\nabla} P + \vec{F}_{vis} + \vec{F}_{las} + \rho_q [\vec{E} + \mu (\vec{J} \times \vec{H})] \quad (5.2)$$

where: ρ = mass density
 \vec{u} = plasma flow velocity
 P = total pressure
 \vec{F}_{vis} = viscous force term

$$\begin{aligned}
\vec{F}_{\text{las}} &= \text{laser source term} \\
\rho_q &= \text{total charge density} \\
\vec{E} &= \text{electric field strength} \\
\mu &= \mu_o \\
\vec{J} &= \text{current density} \\
\vec{H} &= \text{magnetic field strength}
\end{aligned}$$

The viscous force term is approximated by the Navier-Stokes relation (Pai, 1962).

$$F^i = \frac{\partial \pi^{ij}}{\partial x^j} = (\vec{\nabla} \cdot \pi^{ij}) \quad (5.3)$$

where:

$$\pi^{ij} = \mu \left(\frac{\partial u^i}{\partial x^j} + \frac{\partial u^j}{\partial x^i} \right) - \frac{2}{3} \mu \frac{\partial u^k}{\partial x^k} \delta^{ij} \quad (5.4)$$

μ = coefficient of viscosity

The laser source term is given approximately by the following.

$$\vec{F}_{\text{las}} = \frac{\text{Photon momentum absorbed in } \Delta t}{\Delta t} \quad (5.5)$$

The conservation of energy equation is given as the scalar relation:

$$\begin{aligned}
\frac{\partial \xi}{\partial t} + \vec{\nabla} \cdot (\xi \vec{u}) &= - \vec{\nabla} \cdot (\vec{u} P) + \chi_{\text{vis}} \\
&\quad + \vec{E} \cdot \vec{J} + \vec{\nabla} \cdot (\kappa T) + \chi_{\text{las}}
\end{aligned} \quad (5.6)$$

where: ξ = total energy density

χ_{vis} = viscous energy term

κ = coefficient of thermal conductivity

T = temperature

χ_{las} = laser energy term

δ^{ij} = Kronecker delta function

The viscous energy term may be expressed as

$$\chi_{\text{vis}} = (\vec{\nabla} \cdot \vec{u})_{\pi}{}^{ij} = \frac{\partial u^i \pi^{ij}}{\partial x^j} \quad (5.7)$$

with the viscous stress tensor defined as in Equation (5.4).

The laser energy term is calculated by the program and is a measure of the energy absorbed in a mesh cell in time Δt . This term will vary with the type of energy pulse. A gaussian shaped pulse is currently employed by the computer model.

The equation defining heat conduction may be expressed with the relation for heat flux.

$$\vec{Q} = \kappa \vec{\nabla} T \quad (5.8)$$

The equation of state for aluminum is entered in the computer program in tabular form. This equation has been developed in previous research for specific use in mathematical models of the type presented here. The tabular forms of this equation is presented in detail in the work by Peery. Values for the temperature, pressure and ionization are calculated as functions of the plasma mass density and specific internal energy. The values were derived, using essentially three models for the plasma in different mass density and temperature regions. These regions are shown in Figure 13.

The specific internal energy is written

$$\xi_{\text{int}} = \xi_{\text{tot}} - \frac{1}{2} \rho v^2 - \xi_{\text{oscillational}} \quad (5.9)$$

This expression for the internal energy represents a recent improvement in that a term for the oscillational energy has been added. A more detailed discussion of the oscillational energy term is given in Chapter VI. The equation of state may be briefly summarized with the

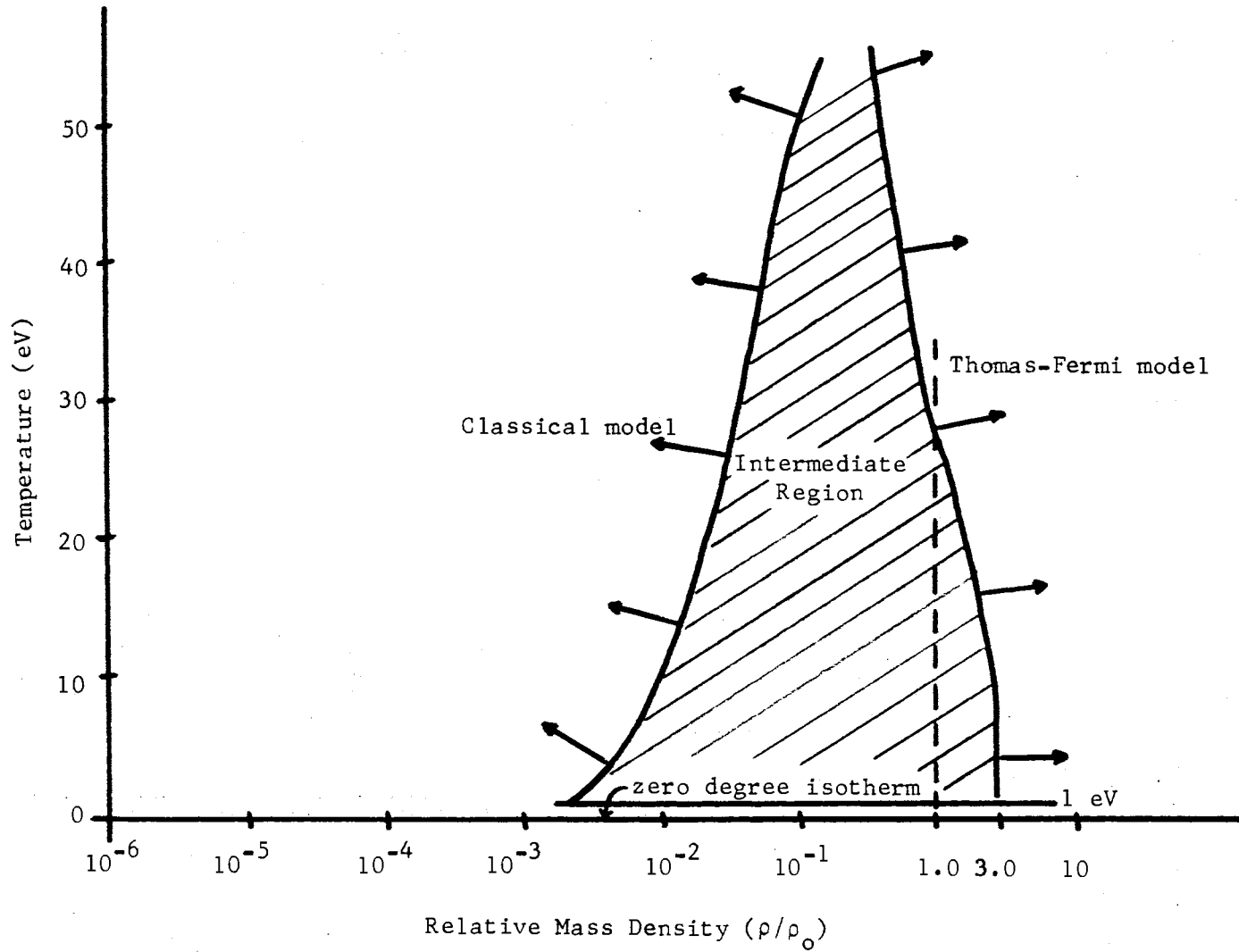


Figure 13. Regions of Validity for Equation of State (After Peery)

following general relations for the pressure, temperature and ionization:

$$P = P(\rho/\rho_0, \xi_{int}) \quad (5.10)$$

$$T = T(\rho/\rho_0, \xi_{int}) \quad (5.11)$$

$$\alpha = \alpha(\rho/\rho_0, \xi_{int}) \quad (5.12)$$

where: α = degree of ionization

ρ/ρ_0 = relative mass density

The Maxwell electromagnetic equations, as they apply to the laser impact model, are listed below.

$$\vec{\nabla} \times \vec{H} = \vec{J} \quad (5.13)$$

$$\vec{\nabla} \times \vec{E} = -\mu_0 \frac{\partial \vec{H}}{\partial t} \quad (5.14)$$

$$\frac{\partial \rho_q}{\partial t} + \vec{\nabla} \cdot \vec{J} = 0 \quad (5.15)$$

The electric current density is given by

$$\vec{J} = \sigma [\vec{E} + \mu_0 (\vec{u} \times \vec{H})] + \rho_q \vec{u} + \text{Source Term} \quad (5.16)$$

where: σ = electrical conductivity

The source term for the current density may be given:

$$\text{Source Term} = \frac{-e\nu P_e}{m\omega_p^2 t}$$

where: $\omega_p^2 = \frac{4\pi n_e e^2}{m}$

and

e = electronic charge

P_e = electron pressure

m = electronic mass

ω_p = plasma frequency

n_e = electron number density

t = time

Computer Model

The model was formulated to describe the creation and evolution of the aluminum plasma that is formed by the incidence of the laser pulse on a plane target. The basic geometry for the model is shown in Figure 14. The laser pulse is assumed to be focused onto an area of 1.0 mm^2 of the aluminum target. For the present model, the pulse was taken to be gaussian in form with an energy of 20 joules and duration of 20 nanoseconds. The above flow equations were reduced to finite difference form and coded for the Univac 1108 computer in FORTRAN IV.

The model is based on two primary assumptions, which have been stated previously. First, the model exhibits a cylindrical symmetry and is therefore a two dimensional problem in cylindrical coordinates. The laser pulse is incident along the z-direction, normal to the target surface which lies in the r, θ plane. This is shown in Figure 14. The second assumption is that the aluminum plasma, formed by the laser pulse, may be described by modified single fluid equations. A prerequisite to this type of description is that one must assume that the plasma exists in local thermodynamic equilibrium.

There is also a provision in the program for separating the high frequency events, such as plasma oscillations from the slower plasma

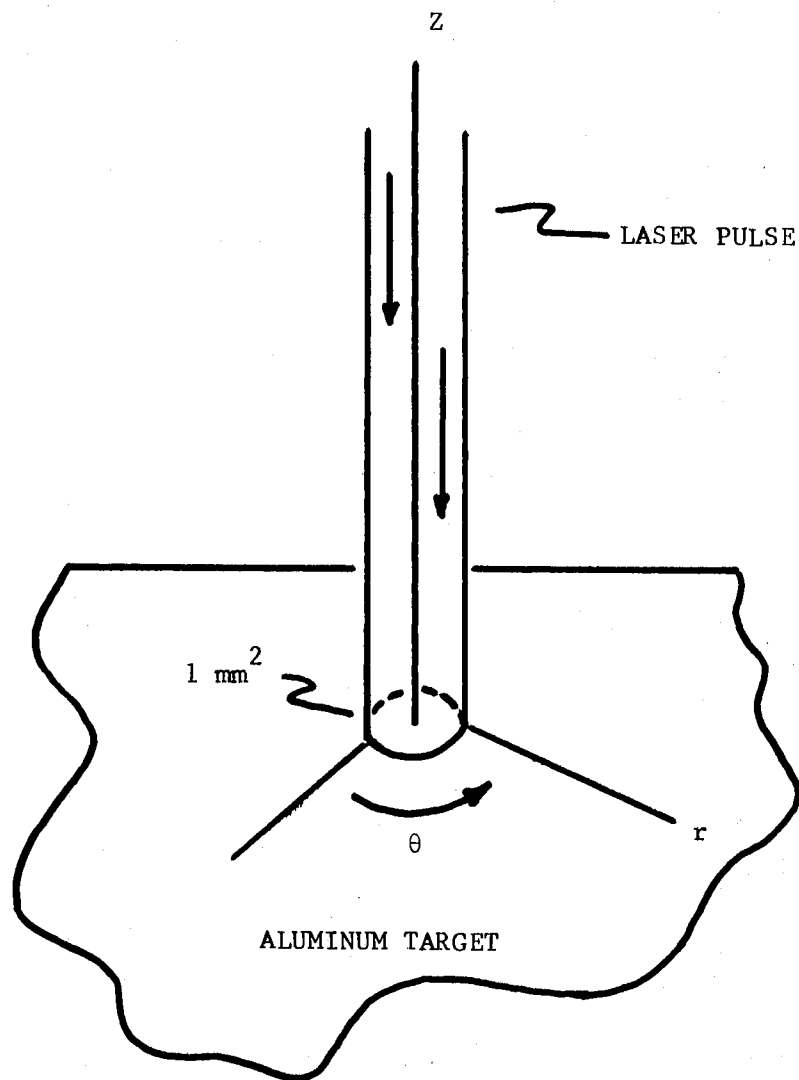


Figure 14. Laser-Target Geometry

flow characteristics. In order to accomplish this, the displacement currents have been neglected in the Maxwell equations and the oscillational character of the problem is separately calculated. The electrons are allowed greater mobility in the pressure gradients and this is seen in the source term for the electrical current density. From plasmon theory, the ions provide a restoring force to the electrons influenced by the pressure gradient. The result of this restoring force is that the electrons oscillate about a displaced position and are therefore inhibited from contributing to abnormally high currents in the plasma.

The actual grid for the model consists of 20 cells radially and 30 vertically. This grid is shown in Figure 15. The initial vertical cell thickness was calculated to be 4.06×10^{-7} cm. This is the skin depth for aluminum at the laser wavelength of 6943 Å. This initial cell size was set in order to follow the attenuation of the laser pulse as it interacts with the target material. One of the subprograms of the computer model is designed, specifically, to cope with the rapidly expanding nature of the plasma. This subroutine allows part of the mesh to expand as the cells are filled when the problem progresses. The details of this type of expanding mesh are outlined in Chapter VI in the discussion of the spherical model.

The absorption and reflectance are calculated at each interface between cell layers and part of the incident radiation is reflected. The nonreflected radiation is attenuated until reaching the next interface, etc. The reflected radiation is also attenuated if it passes through cells filled with plasma on its way back to the vacuum. The radiation absorbed in this manner contributes to the total energy of

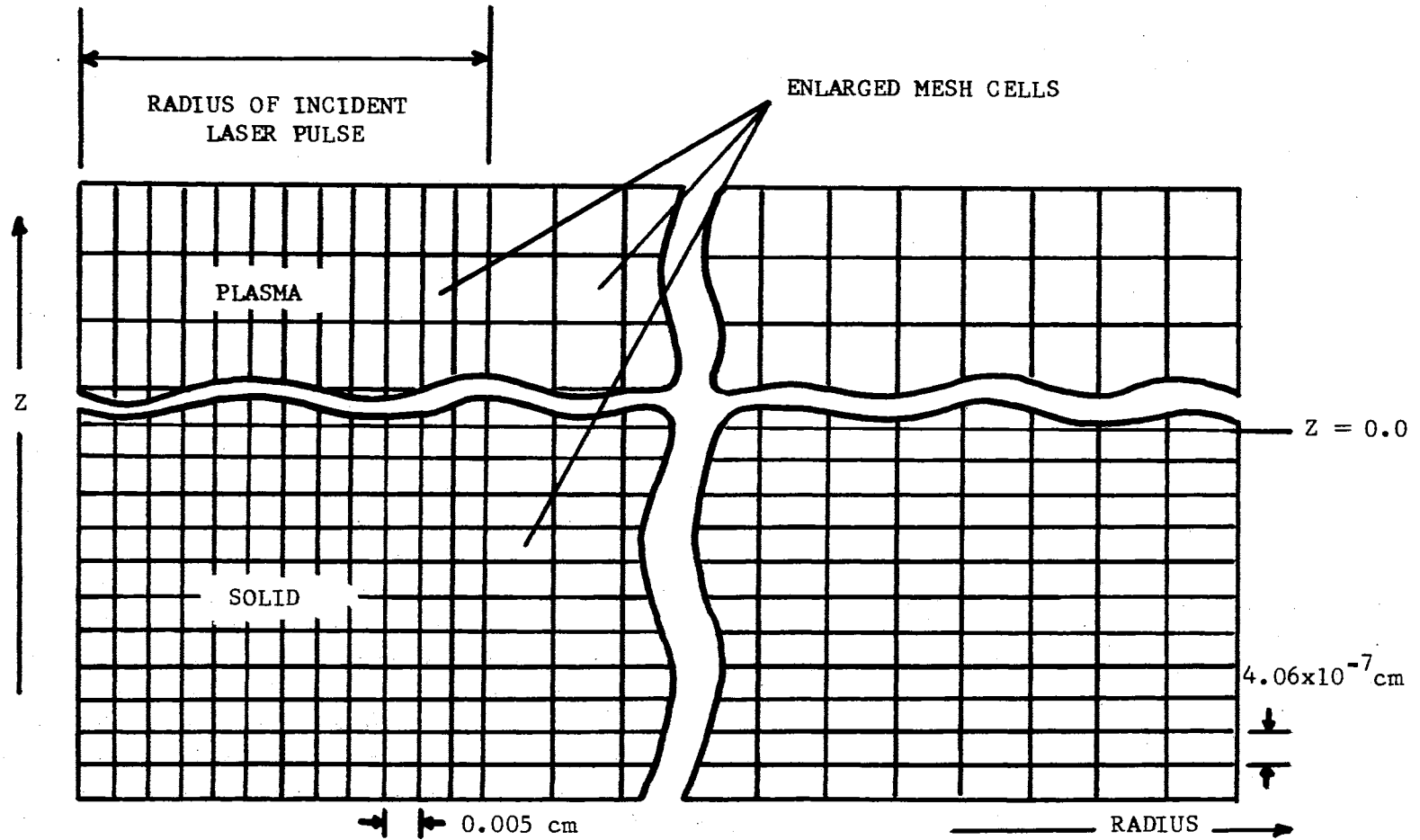


Figure 15. Computer Grid for Laser Impact Plasma Model

the plasma.

Summary

The preceding model has proven to be a flexible method for investigating several facets of this type of plasma. The model is not limited with respect to the initial energy input, target material or computer mesh size. The pulse from the laser is gaussian in shape for the present problem, but may be altered to practically any shape.

After the main program and subroutine elements are debugged, the procedure for a production run is as follows. Values for all of the flow variables are initially specified. Time is increased from $t = 0$ to $t = \Delta t$. The initial time increment is chosen to satisfy the Courant condition. The Courant time is determined by the maximum flow velocity, and by the initial grid size. It is always calculated by the program. As the program is incremented in time, the laser pulse is absorbed and the flow equations are solved for new values of the flow variables at the grid cell centers.

From these, new values at the mesh points are generated and the space grid is adjusted, if necessary. The program is then incremented for another step in time, and the calculations are repeated. This process is continued until a predetermined point in time is reached. Values of any or all of the flow variables may be printed out for any point in time that is desired. The large size of the program presents a major difficulty. The cylindrical geometry, the small size of the mesh cells, the large number of variables which must be monitored and the very small time increments which are used to satisfy the Courant condition result in a computer time that is

very large. An example of the time that is required for a production run on a computer for this model is given by the last production run on the program. A one and one-half hour production run on the Univac 1108 produced only 180 time increments. While this represents a considerable amount of data to be reduced, it represents an evolution in time of only 2.6 nanoseconds.

A technique for reducing the large data output was devised for the expanding plasma sphere and is described in the section on data reduction of Chapter VI. A similar scheme was developed by the author for the laser impact model. The vast quantities of data which are produced by this computer model can be appreciated from the following illustration. For the production run of 180 cycles, the computerized graphs of the plasma variables require a total of approximately 60,000. Many of these graphs were reduced by the computer to 35 mm film. If the total number of graphs were projected at the standard rate of 24 frames per second, the result would be a movie which would require 45 minutes to project.

Some of these computer-drawn graphs are presented in Chapter VII to illustrate typical, initial results which are produced from this model.

In concluding this section, the major revisions to the model are summarized. (1) The separation of the high and low frequency events in the plasma have produced two significant improvements. These are: (a) the plasma oscillations are more adequately followed and (b) the pressure induced currents are restrained within justifiable bounds. (2) The logarithmic mesh, previously used in the vertical cell dimension, has been changed to a linear mesh. (3) An

entirely new subroutine has been added to the program which provides a check on the variables to insure that they remain within reasonable limits. This check-out routine guards against oscillations in the variables of flow which would cause the computer program to overflow and has contributed immensely to the increased stability of the overall program. (4) Another feature, which has been added, is the provision in the main program for the Courant condition to be forced, i.e., this condition may be overridden at carefully, computer-selected intervals to achieve a more practical total elapsed time for the program. (5) The final revision that should be noted here has been mentioned previously and is the addition of a computerized data reduction scheme.

CHAPTER VI

EXPANDING PLASMA SPHERE

Introduction

A new mathematical model has been formulated for the expansion of a sphere of plasma. The present model uses the same spherical geometry which was employed, previously, by other investigators (Ables, 1963; Bruce, 1966; Mulser and Witkowski, 1968). The work of Ables and Bruce, who were previously members of this group, is employed extensively as a foundation for the development of the new model, which is being developed in order to bring this earlier work up to the present status of our knowledge of plasma theory. The work of Mulser and Witkowski is cited as an example of similar work by experts who are not members of our group. The model by Mulser and Witkowski is for a spherically expanding hydrogen plasma that results from laser impact.

The exploding-plasma, spherical model of Bruce contributed significantly in several areas. These include the development of a fairly wide ranging equation of state for aluminum. The present work represents a considerable advance in this area with an equation of state that extends down to a density of one and lower, in contrast to the Bruce equation, which had large deviations at a density of one-tenth solid density. The qualitative analysis by

Bruce presents profiles of the density and temperature, under the assumption of local thermodynamic equilibrium. These profiles are obtained in order to follow the spherical expansion of a plasma into a vacuum. Along with the successes of the Bruce model, there are several recognized defects. These range from failure to fully correct for the mathematical singular point at the center of the sphere to the use of an equation of state which is now rejected. This equation was found to be inadequate for the region of low temperatures and high densities (Peery, 1970). Bruce's equation of state for aluminum is replaced by the equation of state that was briefly discussed in Chapter V. In resolving the problem, improvements were made in the numerical techniques and computer methods which are basic to this type of modeling. These have been developed in the last six to seven years.

With the solution for a laser impact plasma model, an up-to-date recalculation for the expanding plasma sphere is extremely desirable. The usefulness and flexibility of this model will be discussed and the construction and applicability to our work is described.

General

The general features of the solution by Bruce are now considered to be proved by information from several experiments. The measured emission of light from a vacuum spark by Brown (1968) verified the existence of a relatively cold, dense plasma shell shortly after the plasma begins to expand. This shell was predicted by Bruce's model. The rapid decrease in radiation from the vacuum spark, measured with the quadrupole mass filter, also seems to verify that the plasma

expands with a hot, low density core surrounded by a relatively cold, high density shell. Other researchers have also observed this phenomenon. Notably, photographs of a vacuum spark indicate the formation and subsequent breakup of such a cold dense shell. Some of the photographs may be seen in a paper by Heinz Fisher of the Cambridge Air Force Base (1966).

The usefulness of the spherical model for plasma expansion was mentioned, previously, in this thesis. The plasma which is formed by the vacuum spark expands in a nearly spherical geometry for very short, electrode gap widths. The exploding wire experiment produces a plasma which exhibits an even better spherical symmetry. The work of Basov (1967) indicates that the plasma "flare," which is produced by a giant laser pulse, expands in a nearly hemispherical geometry. This is shown by the shadowgraphs from the work by Basov and his co-workers. From their analysis of the flare that is produced at a metal target, at least the dense, central region of the plasma exhibits a spherical symmetry. There is, of course, other evidence which requires cylindrical geometry. Indeed, some the experimental work has indicated the requirement for elliptical geometry. This work includes the analysis by Robinson (1970) which shows the craters that are formed by the laser impact on solid targets to be elliptical.

Since the spherical model requires a one-dimensional solution, and there are several plasmas which may be simulated with this model, it has received considerable attention. There appears to be significant outside interest as well.

Possibly the most interesting comparison between the experimental and theoretical phases of the work is provided by the explod-

ing wire experiment. The initial energy input to the wire may be carefully controlled and the plasma expansion may be analyzed by the several diagnostic instruments available in the laboratory. Since the expanding plasma sphere model is a boundary value problem, the relationship between these two phases is readily seen. One of the most flexible features of the model is that an unlimited set of initial conditions may be specified to meet whatever physical arrangement exists.

Theoretical Discussion

The problem may be stated as follows: at $t = 0$, consider an isolated sphere of aluminum which has an initial radius, $r = R_0$. The sphere is situated in a vacuum and is given a uniform, initial energy density. This energy density, E_0 , is constant throughout the sphere and is sufficient in magnitude to cause the aluminum to be a hot plasma at solid density. This initial energy may be expressed in terms of the energy per atom of aluminum at solid state. The corresponding values of pressure and temperature are determined by the equation of state. Local thermodynamic equilibrium is assumed to exist initially and during the subsequent expansion.

The immediate objective of the model is to provide values for the plasma variables, at strategic times in the evolution, which may be compared with those provided by experiment.

The physical laws which govern the expansion of the spherical plasma and relate the many variables of interest are expressed in mathematical form and may be roughly grouped into three categories: (1) gas dynamic equations, (2) the equation of state and (3) Maxwell's

equations. These equations along with the relations for thermal conductivity constitute a complete set which may be solved numerically on the computer. The gas dynamic equations and Maxwell's equations are presented. The equation of state was discussed in Chapter V and only the general form is given here.

To solve the differential equations for the spherically symmetric model, one must consider the following differential operators:

$$\frac{\partial}{\partial \theta} = \frac{\partial}{\partial \varphi} = 0 \quad (6.1)$$

This requires that the θ and φ components of the velocity be zero so that only a radial velocity is considered.

The vector relations for the spherical case are given.

$$\vec{\nabla} \mathbf{A} = \frac{\partial \mathbf{A}}{\partial r} \hat{r} \quad (6.2)$$

$$\vec{\nabla} \cdot \vec{\mathbf{A}} = \frac{1}{r^2} \frac{\partial}{\partial r} (r^2 \mathbf{A}) \quad (6.3)$$

$$\vec{\nabla} \times \vec{\mathbf{A}} = 0 \quad (6.4)$$

and

$$\nabla^2 \mathbf{A} = \frac{1}{r^2} \frac{\partial}{\partial r} \left(r^2 \frac{\partial \mathbf{A}}{\partial r} \right) \quad (6.5)$$

The conservation equations are now presented. Mass continuity is expressed by the following relation.

$$\frac{\partial \rho}{\partial t} + \vec{\nabla} \cdot (\rho \vec{\mathbf{u}}) = 0 \quad (6.6)$$

where: ρ = plasma mass density
 $\vec{\mathbf{u}}$ = plasma flow velocity

The conservation of momentum is given.

$$\rho \left[\frac{\partial \vec{\mathbf{u}}}{\partial t} + (\vec{\mathbf{u}} \cdot \vec{\nabla}) \vec{\mathbf{u}} \right] = - \nabla P + (\vec{\nabla} \cdot \pi^{ij}) + \rho_q \vec{\mathbf{E}} \quad (6.7)$$

where: P = pressure
 π^{ij} = viscous stress tensor
 ρ_q = total charge density
 \vec{E} = electric field strength

The term $\vec{\nabla} \cdot \pi^{ij}$ is the viscous force term and is derived in Appendix A. Equation (6.7) may also be termed the equation of motion.

The equation expressing the conservation of energy assumes the following form.

$$\frac{\partial(\rho\xi)}{\partial t} + \vec{\nabla} \cdot (\rho\xi\vec{u}) = -\vec{\nabla} \cdot (P\vec{u}) + \frac{\partial(u^i\pi^{ij})}{\partial x_j} + \vec{\nabla} \cdot (\kappa\vec{\nabla}T) + \vec{E} \cdot \vec{J} \quad (6.8)$$

where: ξ = total specific energy
 κ = coefficient of thermal conductivity
 T = temperature
 \vec{J} = electric current density
 $\xi_{vis} = \frac{\partial(u^i\pi^{ij})}{\partial x_j}$, viscous energy term (see Appendix A)

The internal energy may then be given.

$$\xi_{int} = \xi - \frac{1}{2}\rho u^2 - \xi_{osc} \quad (6.9)$$

where: ξ_{int} = internal energy
 ξ_{osc} = oscillational energy

These equations must now be converted to spherical form. Using the relations of Equations (6.2) through (6.5), the conservation expressions of Equations (6.6) through (6.8) become, respectively:

$$\frac{\partial \rho}{\partial t} + \frac{u\rho}{r} + \frac{\partial(\rho u)}{\partial r} = 0 \quad (6.10)$$

$$\rho \frac{\partial u}{\partial t} + \rho u \frac{\partial u}{\partial r} = - \frac{\partial P}{\partial r} + \frac{4}{3} \mu \left[\frac{\partial^2 u}{\partial r^2} + \frac{2}{r} \frac{\partial u}{\partial r} - \frac{2u}{r^2} \right] + \rho_q E \quad (6.11)$$

and,

$$\begin{aligned} \frac{\partial(\rho \xi)}{\partial t} + \frac{\rho \xi u}{r} + \frac{\partial(\rho \xi u)}{\partial r} = & - \frac{Pu}{r} - \frac{\partial(Pu)}{\partial r} + \frac{4}{3} \mu \left[\left(\frac{\partial u}{\partial r} \right)^2 + \left(\frac{u}{r} \right)^2 \right] \\ & + \frac{\kappa}{r} \frac{\partial T}{\partial r} + \frac{\partial \kappa}{\partial r} \frac{\partial T}{\partial r} + \kappa \frac{\partial^2 T}{\partial r^2} + EJ \end{aligned} \quad (6.12)$$

where: μ = coefficient of viscosity

The electromagnetic character of the problem is followed by the Maxwell equations. These equations are first given in general form and then in the symmetry form as they are incorporated into the model.

$$\vec{\nabla} \times \vec{H} = \vec{J} + \frac{\partial \epsilon \vec{E}}{\partial t} \quad (6.13)$$

$$\vec{\nabla} \times \vec{E} = - \frac{\partial \mu \vec{H}}{\partial t} \quad (6.14)$$

$$\frac{\partial \rho_q}{\partial t} + \vec{\nabla} \cdot \vec{J} = 0 \quad (6.15)$$

The current density is expressed in the generalized Ohm's law.

$$\vec{J} = \sigma \vec{E} + \rho_q \vec{u} + PIT \quad (6.16)$$

The terms in these equations are defined below:

\vec{H} = magnetic field strength

ϵ = permittivity constant

μ = permeability constant

σ = electrical conductivity

PIT = pressure induced term

The pressure induced term in Ohm's law is discussed in Appendix B in the section on plasma oscillations and may be given by

$$\text{PIT} = \frac{-e\nabla P_e}{m\omega_p^2 \Delta t} \quad (6.17)$$

where: e = electronic charge

P_e = electron pressure

m = electronic mass

ω_p = plasma frequency

t = time

Equations (6.13) through (6.16) are reduced to spherical form.

$$\epsilon_0 \frac{\partial E}{\partial t} + J = 0 \quad (6.18)$$

$$\nabla \times \vec{H} = 0 \quad (6.19)$$

$$\frac{\partial(\mu H)}{\partial t} = 0 \quad (6.20)$$

$$\frac{\partial \rho_q}{\partial t} + \frac{J}{r} + \frac{\partial J}{\partial r} = 0 \quad (6.21)$$

and

$$J = \sigma E + \rho_q u - \frac{e}{m\omega_p^2 \Delta t} \frac{\partial P_e}{\partial r} \quad (6.22)$$

The improved equation of state was developed by Peery (1970) for use in the laser impact model. Since the regions of applicability for the present problem are similar to those of the laser problem, and because the equation is tabulated without regard to geometric considerations, it has been easily adapted to the spherical model. The

general form is repeated below and expresses the pressure, temperature and ionization as functions of the internal energy and mass density.

$$P = P(\xi_{\text{int}}, \rho/\rho_0) \quad (6.23)$$

$$T = T(\xi_{\text{int}}, \rho/\rho_0) \quad (6.24)$$

and
$$\alpha = \alpha(\xi_{\text{int}}, \rho/\rho_0) \quad (6.25)$$

The equations presented in this section constitute the complete set required to specify the flow properties of the expanding sphere. The optical properties of the plasma are followed with a special subroutine tailored for the laser model. This routine has also been adapted to the spherical model. The details of the methods employed in this routine have been given by Peery (1970).

The equations were coded for the Univac 1108 computer in FORTRAN V. Some of the details of the program construction are provided in the next section.

Computer Model

In order to construct the actual computer program, a basic geometry was chosen and is illustrated in Figure 16. The physical arrangement is shown as well as the geometry the computer actually "sees". For the initial phase of the problem, a total of 50 cells were chosen to be monitored. As can be seen from Figure 16 twenty-five of the cells are initially filled with solid aluminum and the remaining twenty-five cells are empty, i.e., they are given vacuum values. With origin defined as mesh point number 1, there are a total of 51

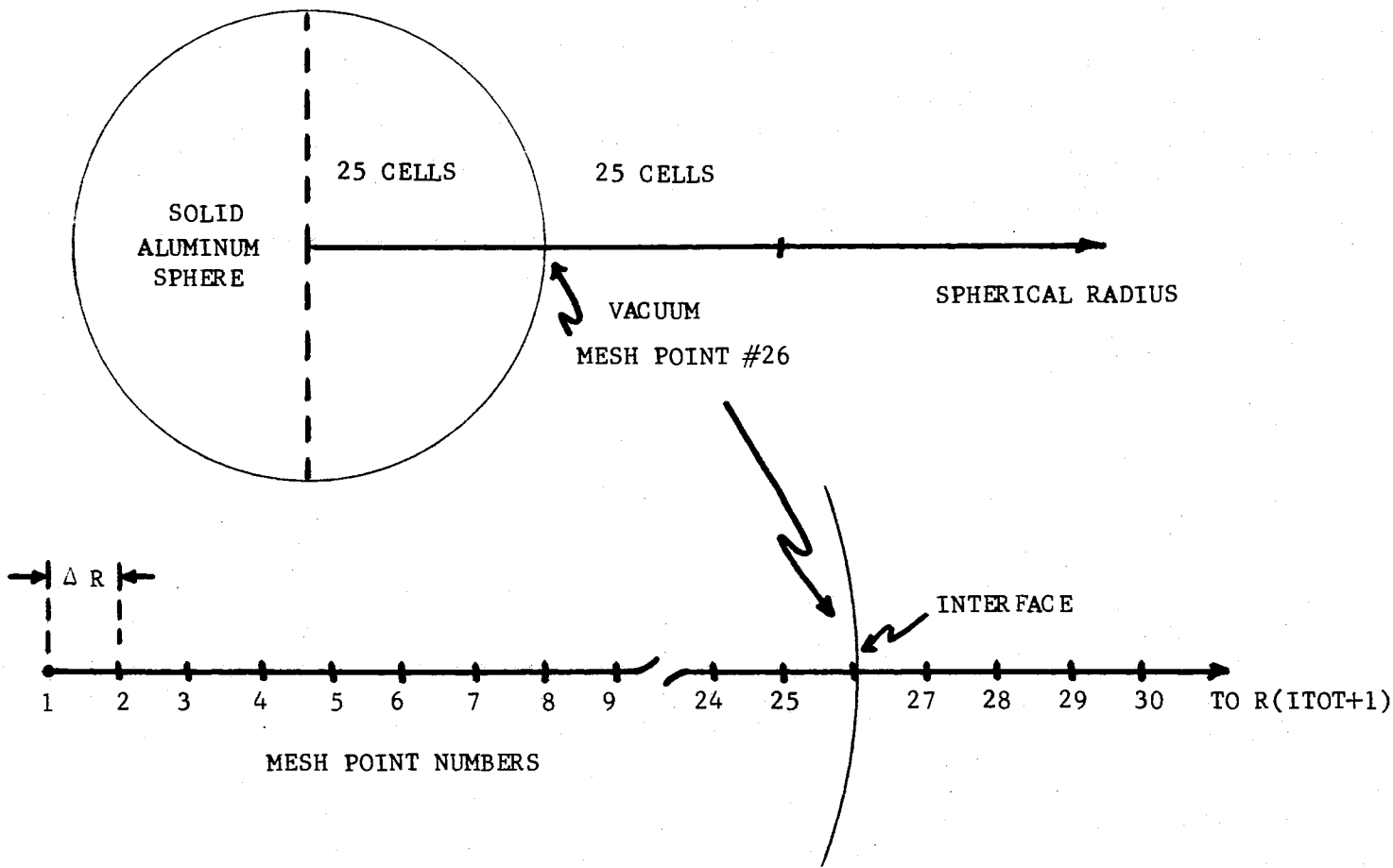


Figure 16. Basic Geometry for Expanding Plasma Sphere Model

mesh points and 50 cell centers, with the interface defined by mesh point number 26.

The flow variables can now be defined as the model begins to be formed. To keep track of the radius in the problem, consider the following definition:

$$R(I) = \text{RADIUS}; I = 1, \text{ITOT} + 1 \quad (6.26)$$

where: ITOT = total number of cells

ITOT + 1 = total number of mesh points

The initial conditions for the problem are now specified. These may be generally summarized below.

1. DR = initial mesh size (ΔR)
2. ITOT = total number of initial cells
3. Initial values for the flow variables at $t = 0$
4. DT = initial time increment (Δt)

The flow variables, which were defined by the relations in the previous section, may now be defined for the computer. The units of each variable are also shown.

1. AOSC = amplitude of oscillations (cm)
2. DENQ = net charge density (coul/m^2)
3. EGRM = energy per unit mass (erg/gm)
4. EOSC = oscillational energy per unit mass (erg/gm)
5. POSC = period of oscillation (sec^{-1})
6. PRES = pressure (dyne/cm^2)
7. RELC = radial electric field ($\text{volt}/\text{m} = \text{nt}/\text{coul}$)
8. RHOM = mass density (gm/cm^3)
9. RJDE = radial current density (amp/m^2)
10. RVEL = plasma flow velocity (cm/sec)

11. TEMP = temperature (eV)

12. XION = degree of ionization (no. free electrons/atom)

From the definitions above, it can be seen that most of the flow variables are defined in C.G.S. units. The exceptions are the electromagnetic variables which are given in M.K.S. and the temperature which is expressed as electron volts.

It will be helpful, for the remainder of this section, to define a general parameter which represents any one of the flow variables. Let this parameter be called FLOVAR. This representation, however, is not sufficient to completely follow the evolution of the problem, since one must specify the value of the flow variables at both the mesh points and at the cell centers. In addition, the time rate of change of the flow variables must be followed. Let these quantities be further defined as follows:

1. FLOVAR 1(I) = value of the flow variables at the mesh points at time t.
2. FLOVAR 2(I) = value of the flow variables at the cell centers at time t.
3. FLOVAR 3(I) = the time rate of change of the flow variables at the cell centers.

The construction of the model begins with the generation of the mesh. This is accomplished by the allocation of 51 spaces in the computer memory. These spaces are reserved for defining the initial mesh points and cell centers. The initial conditions subroutine is then written to provide the initial values. For the first 26 mesh points, FLOVAR 1(I) is given values which correspond to the initial conditions inside the target sphere. Likewise, FLOVAR 2(I) is given

interior values for the first 25 cell centers. Mesh points 27 through 51 and cell centers 26 through 50 are the positions of FLOVAR 1(I) and FLOVAR 2(I) which are assigned vacuum values. At $t = 0$, the time rate of change of the variables is specified, FLOVAR 3(I) = 0.

After the initial values are specified, the program is allowed to evolve in time. The calculations involved with each time step are the subject of the next section.

Evolution of the Flow Variables

From the boundary conditions, FLOVAR 1(I) and FLOVAR 2(I) are specified at (r_0, t_0) . New values are calculated for the cell centers, i.e., FLOVAR 2(I) at time $t = t + \Delta t$. A remeshing operation then interpolates values for all the mesh points, i.e., FLOVAR 1(I), still at $t = t + \Delta t$. After the initial time step, Δt is determined by the Courant condition. This condition is given below.

$$\Delta t_c = k \frac{\Delta r}{u_{\max}} \quad (6.27)$$

where: t_c = Courant time
 k = Courant coefficient
 Δr = mesh size
 u_{\max} = maximum flow velocity

For the current model, a Courant coefficient of 0.9 has been used in an attempt to maintain stability. A graphic illustration of the remesh procedure is provided in Figure 17. This remesh operation is handled as a separate subroutine in the computer program. It is very important to note that for this operation there are two special cases. The interior cells may be routinely taken care of, but there

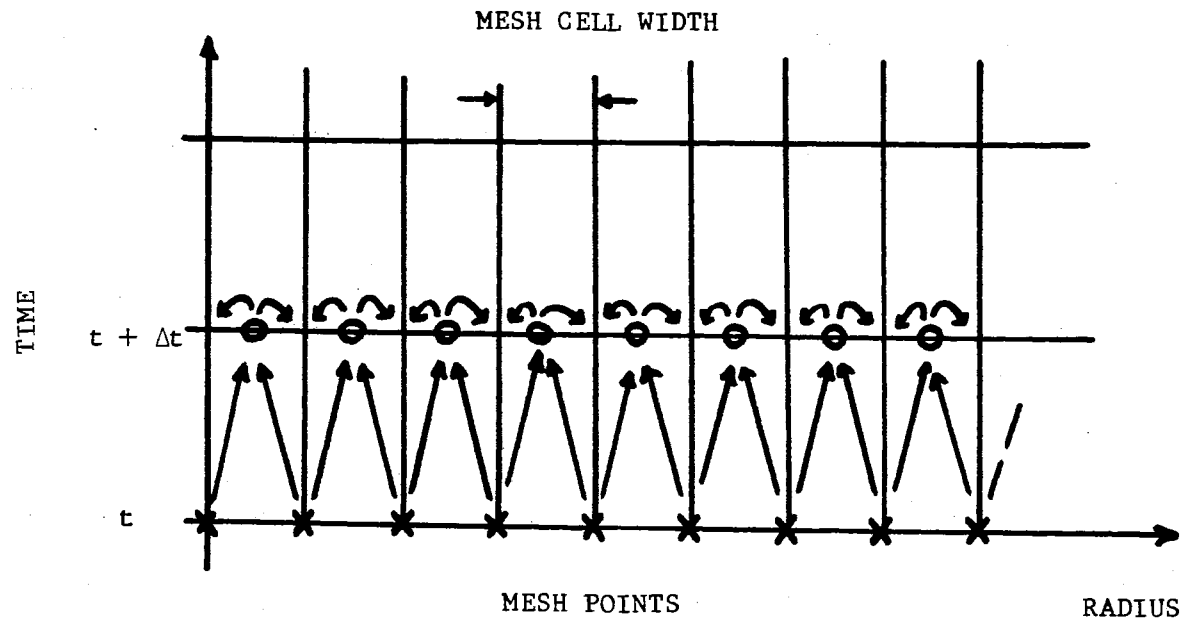


Figure 17. Space - Time Geometry for Remesh Procedure

are two edge cells. These cells may be labeled FLOVAR 1(1) and FLOVAR 1(ITOT + 1).

First consider the interior cells. A physical picture for this case is given in the diagram of Figure 18. For any of the interior cells, the remesh operation will be executed via a statement function which is labeled RESET. The arguments for this function are derived from the diagram in Figure 18. A value may be defined for a mesh point at $t + \Delta t$, based on the value of the mesh point at time t and the values of the time rate of change of the cell centers on either side of the mesh point in question. This value may be given below.

$$\begin{aligned} FV1(I) = & FV1(I) + DELT[FV3(I - 1) \\ & + DEL/DEL1 (FV3(I) - FV3(I-1))] \end{aligned} \quad (6.28)$$

where: $FV = \text{FLOVAR}$

$$DELT = \Delta t$$

$$\text{and } DEL = \Delta = \frac{R(I) - R(I - 1)}{2.0} \quad (6.29)$$

$$DEL1 = \Delta 1 = \frac{R(I + 1) - R(I - 1)}{2.0} \quad (6.30)$$

Now in terms of the above parameters, the statement function may be written in general terms.

$$\begin{aligned} \text{RESET } (A_1, A_2, A_3, A_4, A_5, A_6) = & A_1 + A_2 * \\ & (A_3 + ((A_4/A_5) * (A_6 - A_3))) \end{aligned} \quad (6.31)$$

The arguments of this general function are given below.

$$A_1 = FV1(I); I = 2, \text{ ITOT}$$

$$A_2 = DELT$$

$$A_3 = FV3(I - 1)$$

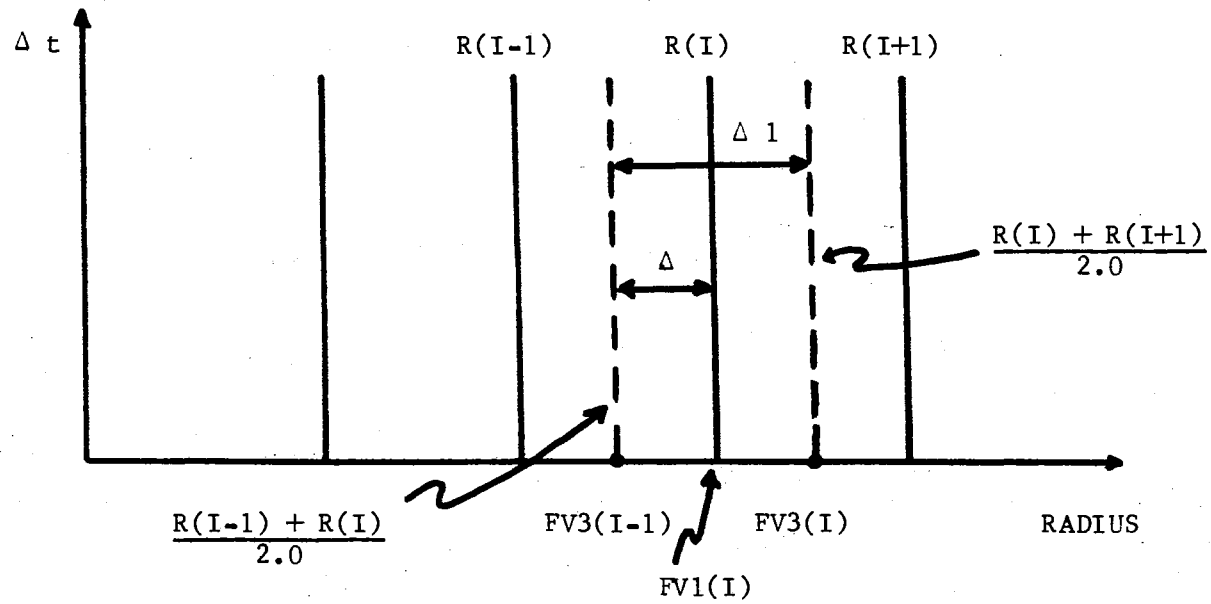


Figure 18. Remesh Geometry for Interior Mesh Points

$$A_4 = \text{DEL}$$

$$A_5 = \text{DEL1}$$

$$A_6 = \text{FV3(I)}$$

An example of the program flow for remeshing the interior cells is given for the temperature. It is very important to note that the identical order of the variable components must be maintained as defined by the statement function.

```

SUBROUTINE REMESH
COMMON STATEMENTS
C  REMESH INTERIOR CELLS
DO 7  I = 2, 50      (NOTE: ITOT = 50)
DEL = ( R(I) - R(I-1) ) / 2.0
DEL1 = ( R(I+1) - R(I-1) ) / 2.0
C  AN EXAMPLE OF FV1(I) TO BE FOLLOWED BY ALL OTHER FLOW VARIABLES
TEMP1(I) = RESET ( TEMP1(I), DELT, TEMP3(I-1), DEL, DEL1,
                  TEMP3(I) )
7  CONTINUE

```

Now the two special edge cell cases must be considered. For these cases a new statement function must be defined. Let this function be called REEDG. A diagram is presented in Figure 19 which illustrates the remeshing operation for the last mesh point. From the figure, the value of FV1(I) may be derived.

$$\begin{aligned}
 \text{FV1(ITOT + 1)} &= \text{FV1(ITOT + 1)} + \text{DELT} [\text{FV3(ITOT)} \\
 &\quad + \text{DEL/DEL1(FV3(ITOT)} \\
 &\quad - \text{FV3(ITOT - 1))}] \qquad (6.32)
 \end{aligned}$$

$$\text{where: } \text{DEL} = \Delta = \frac{\text{R(ITOT + 1)} - \text{R(ITOT)}}{2.0} \qquad (6.33)$$

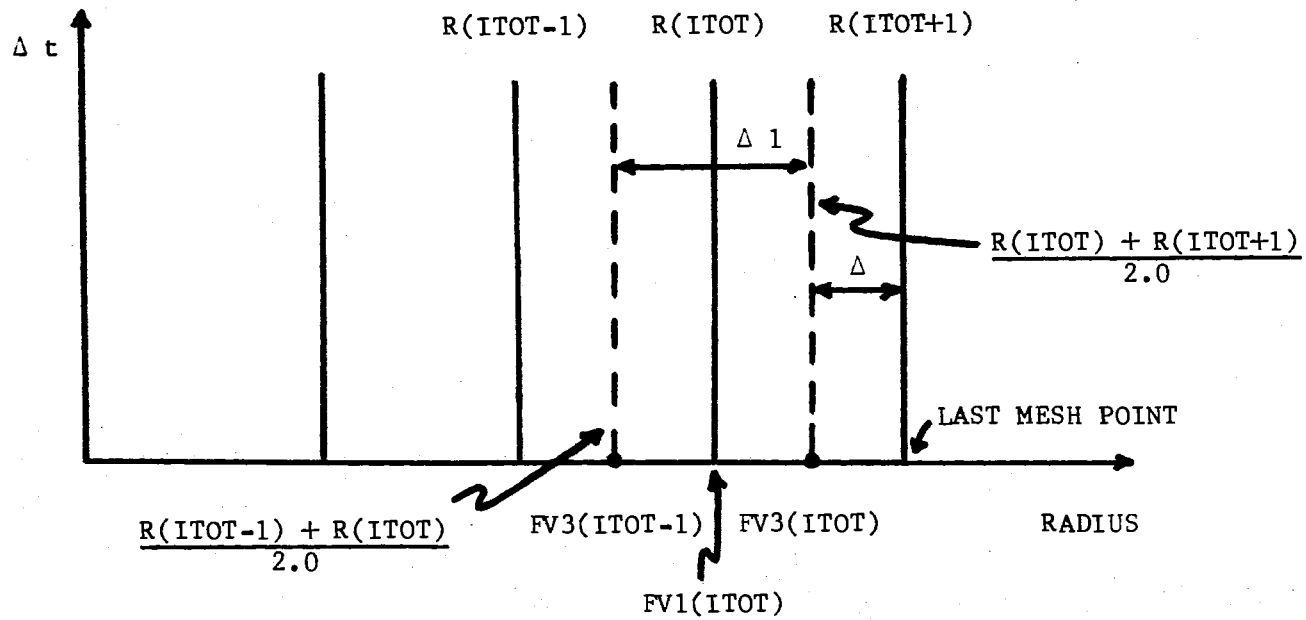


Figure 19. Remesh Geometry for End Mesh Point

$$\text{DEL1} = \Delta 1 = \frac{R(\text{ITOT} + 1) - R(\text{ITOT} - 1)}{2.0} \quad (6.34)$$

Rewriting Equation (6.32) in general form, one obtains

$$\begin{aligned} \text{REEDG}(A_1, A_2, A_3, A_4, A_5, A_6) = \\ A_1 + A_2 * (A_3 + ((A_4/A_5) * (A_3 - A_6))) \end{aligned} \quad (6.35)$$

with the arguments defined as follows

$$A_1 = \text{FV1}(\text{ITOT} + 1)$$

$$A_2 = \text{DELT}$$

$$A_3 = \text{FV3}(\text{ITOT})$$

$$A_4 = \text{DEL}$$

$$A_5 = \text{DEL1}$$

$$A_6 = \text{FV3}(\text{ITOT} - 1)$$

An example of the remeshing operation for the flow variables at the last mesh point is given.

$$\begin{aligned} \text{TEMP1}(\text{ITOT} + 1) = \text{REEDG}(\text{TEMP1}(\text{ITOT} + 1), \\ \text{DELT}, \text{TEMP3}(\text{ITOT}), \text{DEL}, \text{DEL1}, \\ \text{TEMP3}(\text{ITOT} - 1)) \end{aligned} \quad (6.36)$$

The zero-point edge, or the first cell may be handled with the same general statement function given in Equation (6.35), but with the arguments rearranged. The geometry of the first cell is presented in Figure 20. From this diagram, FV1(1) is defined.

$$\begin{aligned} \text{FV1}(1) = \text{FV1}(1) + \text{DELT} [\text{FV3}(1) + \text{DEL}/\text{DEL1} \\ (\text{FV3}(2) - \text{FV3}(1))] \end{aligned} \quad (6.37)$$

$$\text{where: } \text{DEL} = \Delta = - \left[\frac{R(2) - R(1)}{2.0} \right] \quad (6.38)$$

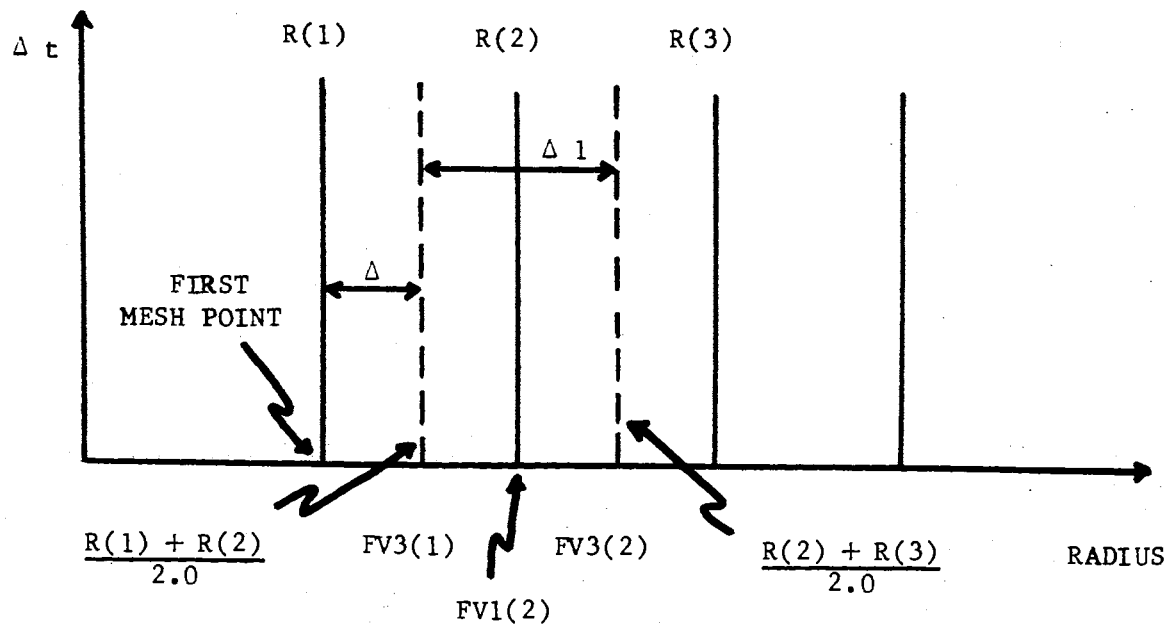


Figure 20. Remesh Geometry for First Mesh Point

$$\text{DEL1} = \Delta 1 = \frac{R(3) - R(1)}{2.0} \quad (6.39)$$

The arguments are then given for Equation (6.35).

$$A_1 = \text{FV1}(1)$$

$$A_2 = \text{DELT}$$

$$A_3 = \text{FV3}(2)$$

$$A_4 = \text{DEL}$$

$$A_5 = \text{DEL1}$$

$$A_6 = \text{FV3}(1)$$

The temperature is used again to illustrate remeshing the first cell.

$$\begin{aligned} \text{TEMP1}(1) = \text{REEDG}(\text{TEMP1}(1), \text{DELT}, \text{TEMP3}(1), \\ \text{DEL}, \text{DEL1}, \text{TEMP3}(2)) \end{aligned} \quad (6.40)$$

This concludes the discussion of the remesh operation. To summarize, a routine has been constructed for calculating the values of the flow variables and reassigning them to the mesh points at any time $t + \Delta t$. In doing so, all three possible cases which might arise have been considered.

1. RESET --- for the interior mesh points
2. REEDG --- for the end mesh point
3. REEDG --- for the zero-point mesh point

Program Condensation

As the computer program progress in time, it becomes necessary to allow that the expanding plasma has filled all the existing cells. This means that the program must provide additional "space" into which the plasma may expand. The operation which provides for this is

called SUBROUTINE REDOUBLE. Essentially, this subroutine allows the program to keep the total number of cells constant, while doubling the size of each cell. This enlarged the grid, while keeping the physical dimensions of the plasma consistent with the initial mesh size. The geometry for this operation is given in Figure 21. From this figure, it can be seen that the indexing scheme remains the same for the linear mesh.

It should be pointed out that there is no time evolution during the process of condensing, or redoubling the mesh. The details of this procedure may be seen in Appendix C where a listing of the program is given. It should be emphasized again that the physical dimensions of the plasma remains the same, while the mesh points receive a new index value, i.e., $R(3)$ assumes the new index $R(2)$, $R(5) \rightarrow R(3)$, $R(7) \rightarrow R(4)$, etc. After this process is completed, the program continues in the new, expanded mesh.

Numerical Methods

In the theoretical discussion, the set of equations which govern the plasma expansion were derived for spherical coordinates. These equations must be reduced to finite difference form so they may be "digested" by the computer. The final form of these equations may be seen in the actual computer listing, available in Appendix C. An example of the technique used to approximate the flow equations is given.

Consider the conservation of mass expression given by Equations (6.6) and (6.10).

$$\frac{\partial \rho}{\partial t} + \frac{u\rho}{r} + \frac{\partial(\rho u)}{\partial r} = 0 \quad (6.41)$$

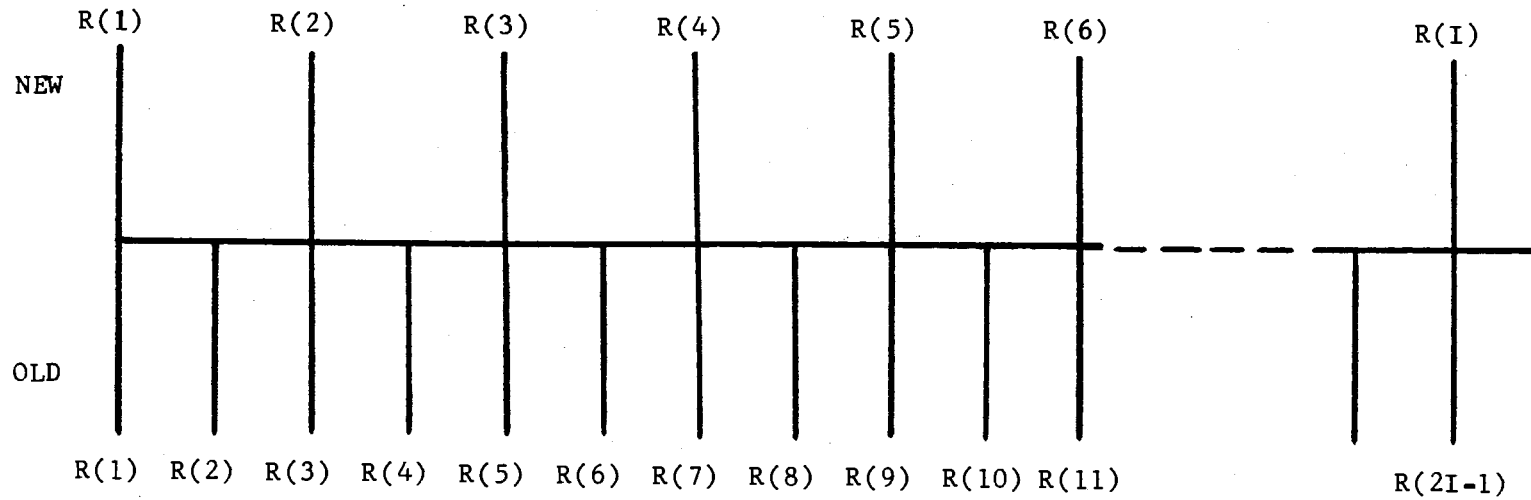


Figure 21. Geometry for Redouble Procedure Showing Old and New Mesh Coordinates

The computer geometry for a single grid cell is represented in Figure 22. Based on this geometry, note that since all calculations are from values given at the mesh points, and the final result will be the value at the cell center, then the average of the mesh point values are used. Equation (6.41) is then written in the following approximate form for the general cell number (I).

$$\frac{\Delta \rho}{\Delta t}_{cc} = - \left(\frac{u\rho}{r} \right)_{cc} - \left\{ \frac{(u\rho)_+ - (u\rho)_-}{\Delta r} \right\} \quad (6.42)$$

where: cc = cell center

Recall that FV3(I) expresses the time rate of change at the center of cell (I).

In computer language, Equation (6.42) becomes

$$\begin{aligned} \text{RHOM3(I)} = & - \frac{1}{2} \left[\frac{\text{RVEL1(I)} * \text{RHOM1(I)}}{\text{R(I)}} \right. \\ & + \frac{\text{RVEL1(I+1)} * \text{RHOM1(I+1)}}{\text{R(I+1)}} \left. \right] \\ & - \left[\frac{\text{RHOM1(I+1)} * \text{RVEL1(I+1)}}{\text{R(I+1)} - \text{R(I)}} \right. \\ & \left. - \frac{\text{RHOM1(I)} * \text{RVEL1(I)}}{\text{R(I+1)} - \text{R(I)}} \right] \end{aligned} \quad (6.43)$$

Now in order to obtain a new value for the mass density at the cell center (I), the following expression is given.

$$\text{RHOM2(I)} = \text{RHOM2(I)} + \text{DELT} * \text{RHOM3(I)} \quad (6.44)$$

It is pointed out here that the first argument on the right-hand side of Equation (6.44) represents the old value for the mass density

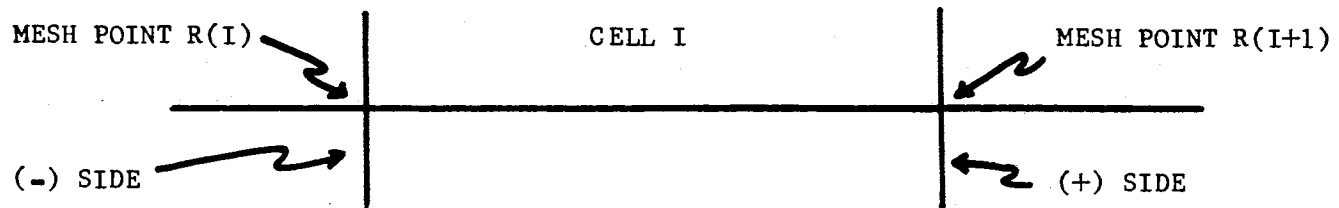


Figure 22. Simplified Computer Geometry for Single Mesh Cell

at the center of cell (I).

The remaining flow equations are reduced to finite difference form by similar methods and are included in the program. A simplified flow diagram is shown in Figure 23. The program elements, including the main program and the subroutines are discussed in Appendix C where a listing of the entire program is also presented.

Data Reduction

The variables defined in the computer model section were monitored and printed out by special, separate subroutine. After the flow equations were coded and the program construction was completed, several trial runs were made on the computer. At each increment of time, this subroutine collects all of the variable values at each of the 50 grid cells and prints them out for analysis. For the twelve flow variables, there are then 600 values printed after each program cycle. The print out subroutine is written so that in addition to the paper print out, a record is made on magnetic tape of each of the variable values for each cycle. This tape record is then used to eventually make a graphical display of the data. The procedure for obtaining the computer-drawn curves is briefly discussed.

A separate program was written to arrange the raw data for submission to the SC 4020 plotter which was available at the Computation Laboratory of the Marshall Space Flight Center. This program takes the raw data tape and establishes upper and lower limits for each of the variables which are to be plotted versus the radial coordinate of the plasma sphere for each time cycle. The program also provides the labels for the graphs and provides other information such as the

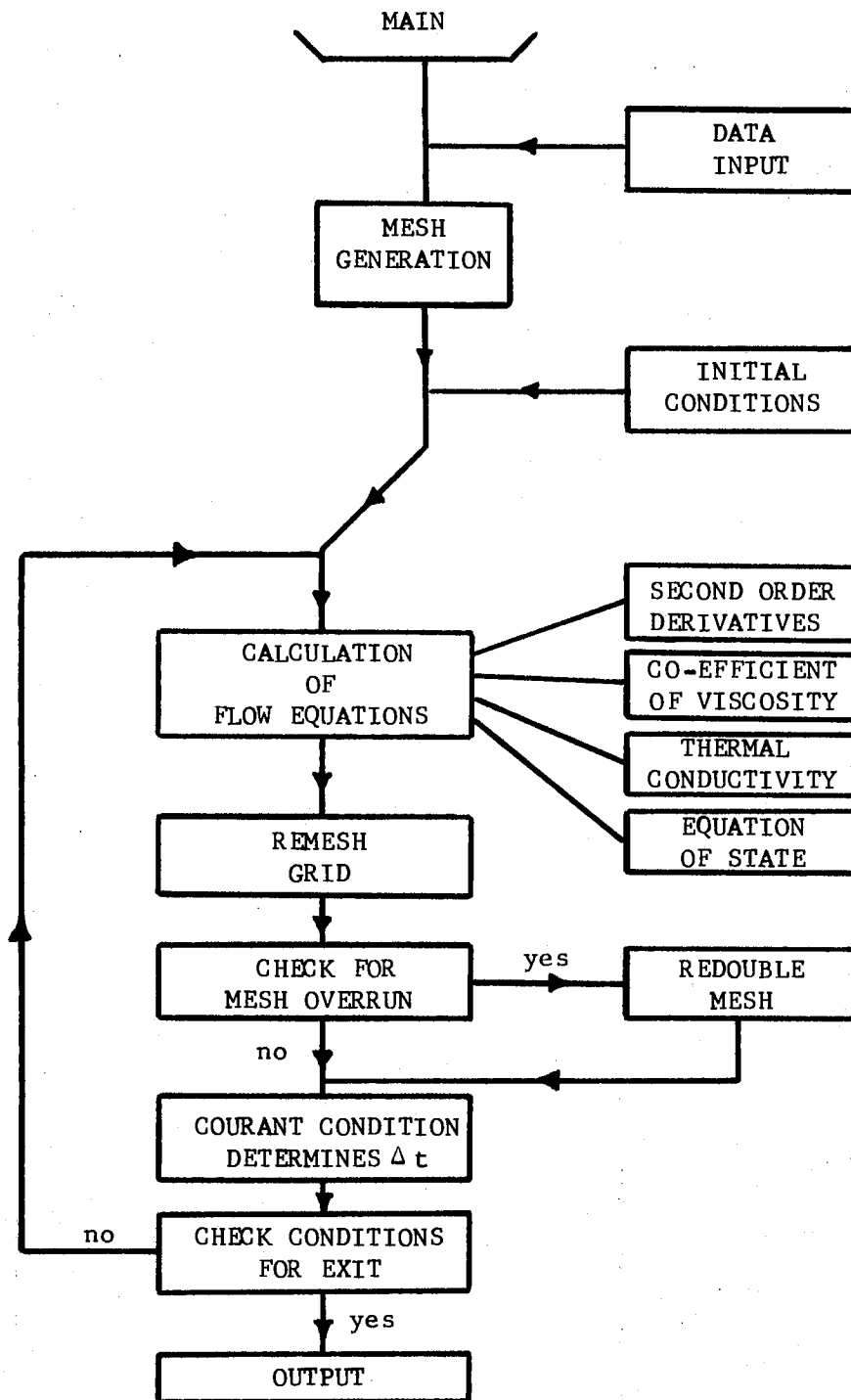


Figure 23. Simplified Flow Diagram

time and cycle number in addition to establishing the coordinate axes. The raw data tape and this program produces a final plot tape which is then used as the input tape to the SC 4020 unit. The resulting graphs are then the final product of the program run. These curves for the desired variables may then be studied to determine the consequences of the model for a given set of initial conditions.

Several of the computer-drawn curves are presented in Chapter VII in the section on the expanding plasma sphere, for the initial trial executions.

Summary

In the preceding sections, an improved model for an expanding sphere of plasma has been discussed. The general approach has been based on the equations which govern the plasma flow. The model has been constructed to describe the nature of the expanding aluminum plasma from a variety of initial boundary conditions. The author has drawn extensively from the earlier work done in the area of mathematical modeling and has profited considerably from the experience gained in computer techniques by the previous members of the group (Bruce, 1966; Peery, 1970). Many of the finer details involved with the derivation of some of the flow equations were worked out in this previous work. The terms for the thermal and electrical conductivity were presented in this earlier work and need not be repeated here. The term for the electrical conductivity has been incorporated into the subroutine dealing with the optical properties and the thermal conductivity is derived, based on the assumption that the expression for heat flux, $\vec{Q} = \kappa \nabla T$, may be applied to the problem. The viscous terms

for the conservation equations for momentum and energy are derived in Appendix A. The general format of the program has been outlined in this chapter and the detailed form is shown in Appendix C. All of the flow variables, for the equations governing the plasma expansion, may be summarized by the single variable $FLOVAR_i(I)$, where $i = 1, 2, 3$. For $i = 1$, the value at the mesh point (I) is given; for $i = 2$, the value at the cell center (I) is given; for $i = 3$, the time rate of change of the variable at the cell center (I) is given.

To conclude this section, the significant improvements which have been made to the previous model by Bruce are discussed. One of the major refinements has been the complete reformulation of the model to incorporate the extended equation of state for aluminum. The validity of this new equation has been shown by the production run of the laser impact plasma model (Peery, Willis and Todd, 1970). The mechanism of energy transfer that is associated with plasma oscillations was completely neglected in the Bruce model and has been incorporated into the present model. The computer techniques have been significantly improved with the addition of a special check out subroutine which helps to maintain program stability by insuring that variable values remain within physical feasible limits. This routine also remedies one of the previous difficulties which was program overflow. The check out program constantly monitors all the plasma variables and guards against any value which would cause a machine overflow. The final improvement which should be given here is the computerized method of data reduction. Many man-hours of tedious manual reduction will be saved by this new system of data collection and analysis. With this method applied to the work, much more of

the computer results can be analyzed in a shorter time. This is a particularly helpful feature when a new application for a model is being debugged.

Some of the initial results are presented in the next chapter and some of the areas for improvement on the current model are discussed in Chapter VIII.

CHAPTER VII

DISCUSSION OF RESULTS

Introduction

The results of the four major areas of study are presented in this chapter. The discussion of the data is divided into four sections which correspond to these areas. The experimental results include the data taken with the quadrupole mass filter and the electrostatic lens system. The theoretical data includes the computer solutions for the laser impact plasma model and some of the initial results of the computer model for the expanding plasma sphere. Because of the large amount of data, produced by both the experimental and theoretical work, only typical examples of the data are presented.

Quadrupole Mass Filter Data

The theory and operating procedure for the quadrupole mass filter were presented in Chapter III. The curves which are presented in this section were produced by the output current of the electron multiplier, which was the detector for the quadrupole system. The drift space from the spark gap source to the detector was approximately 34.0 cm. The variables which are considered in analyzing the curves, which are shown in this section, are given below:

1. Ultraviolet light emitted from the spark source

2. Neutral aluminum atoms
3. Aluminum atoms which are excited to a metastable state
4. Aluminum ions ($\text{Al}^{+1} - \text{Al}^{+5}$)

The initial response of the quadrupole detector is to the ultraviolet light. This provides an indication of time zero. The detector is electrically biased to receive no electrons. The resultant curves are then a superposition of the ions of a preselected specie, metastable atoms and u.v. photons. Two curves are presented for each specie of ion so that the diversity of data for similar operating conditions may be illustrated. The differences in the data are attributed to the spark source. Any two consecutive plasmas, produced by the spark source, are rarely even similar. The tapered electrodes are eventually worn by repeated breakdowns so that, actually the initial conditions for all the shots are slightly different. For example, a very strong breakdown may be followed by a weak one, etc., so that many shots must be taken in order that a general trend in the data can be seen. The curves shown here were selected to show typical examples of the data that appear most often for each specie of ion.

The data presented here were taken with the vacuum system maintained at $10^{-5} - 10^{-6}$ torr. The voltage to the aluminum spark gap electrodes was 8.5 - 10.0 KV. The total accelerating voltage to the electron multiplier detector was 1.0 KV and the load resistor used throughout the experiment had a value of 1,000 ohms. The 585A Tektronic oscilloscope, which was employed to monitor the detector output signal, was set to be triggered internally, in the single sweep mode. The sensitivity of the oscilloscope was set at 0.2 volts/cm

and the time scale was set at 5.0 microseconds/cm. The data was reduced directly from the polaroid film.

The curves which are presented in Figure 24 and Figure 25 give an indication of the Al^{+1} ions, metastables and light. The type of curve for Al^{+1} , shown in Figure 24, occurred most frequently, and indicated the arrival of most of the ions and/or neutral atoms at approximately 13 microseconds after the initial breakdown. An indication of the Al^{+2} ions is presented in Figure 26 and Figure 27. In these curves, as in most of the other curves obtained with the quadrupole, the first 3 to 5 microseconds were masked with noise and no interpretation of this region was attempted. The majority of the curves for Al^{+2} were of the type shown in Figure 26. Several curves of the type shown in Figure 27 were obtained under similar conditions. The smaller amplitude of this curve, relative to the one shown in Figure 26, is possibly due to a lower intensity of the spark source for this shot. The first peak in Figure 26 is centered about a velocity of approximately 1.5×10^6 cm/sec.

The curves presented in Figure 28 and Figure 29 were obtained with the quadrupole mass filter set to receive the Al^{+3} ions. The curves in these two figures represent the type most frequently obtained for Al^{+3} ions. The reproducibility, with respect to the arrival time, of the first major peaks of these curves is reasonably good. Indications of the Al^{+4} ion are given in Figure 30 and Figure 31. Two typical curves for the Al^{+5} ions are given in Figure 32 and Figure 33.

Occasionally, the type of curve for Al^{+1} , shown in Figure 25, was produced. The higher velocities of the ions and metastables,

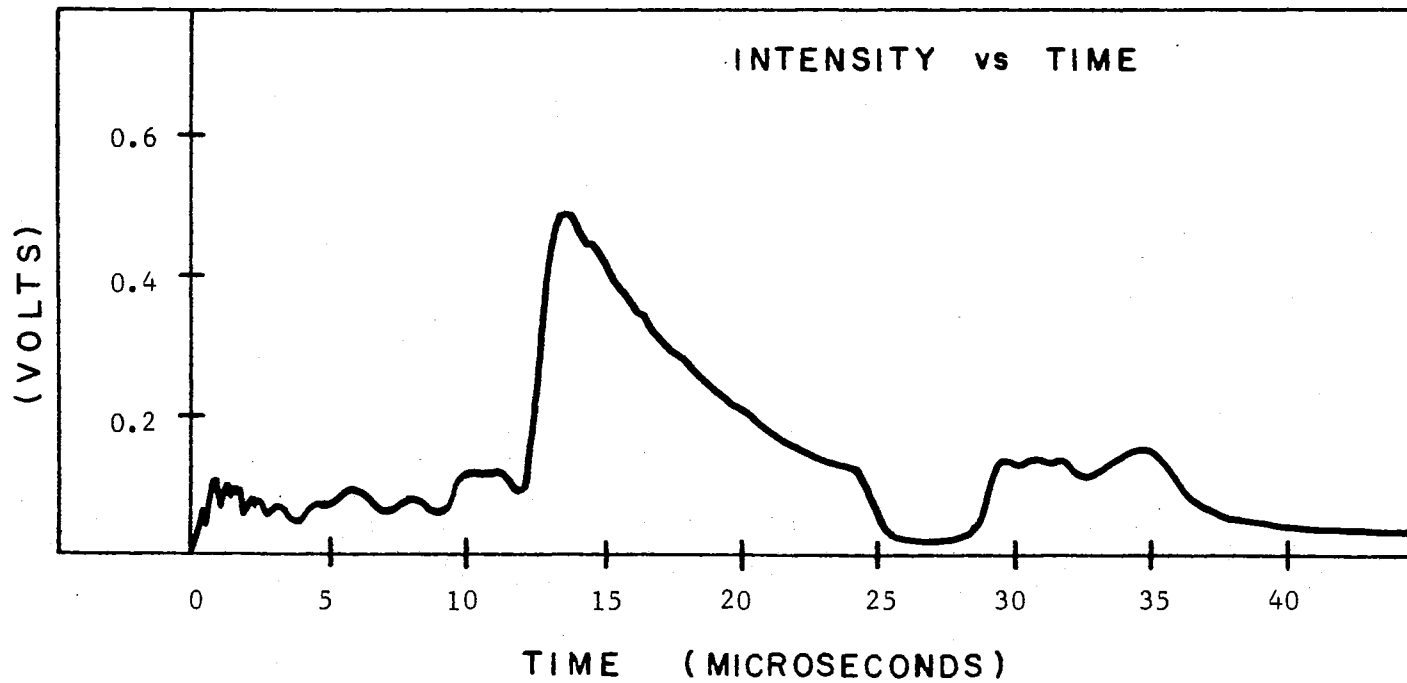


Figure 24. Al^{+1} Ions, Metastable Atoms and Light from Vacuum Spark - Quadrupole System

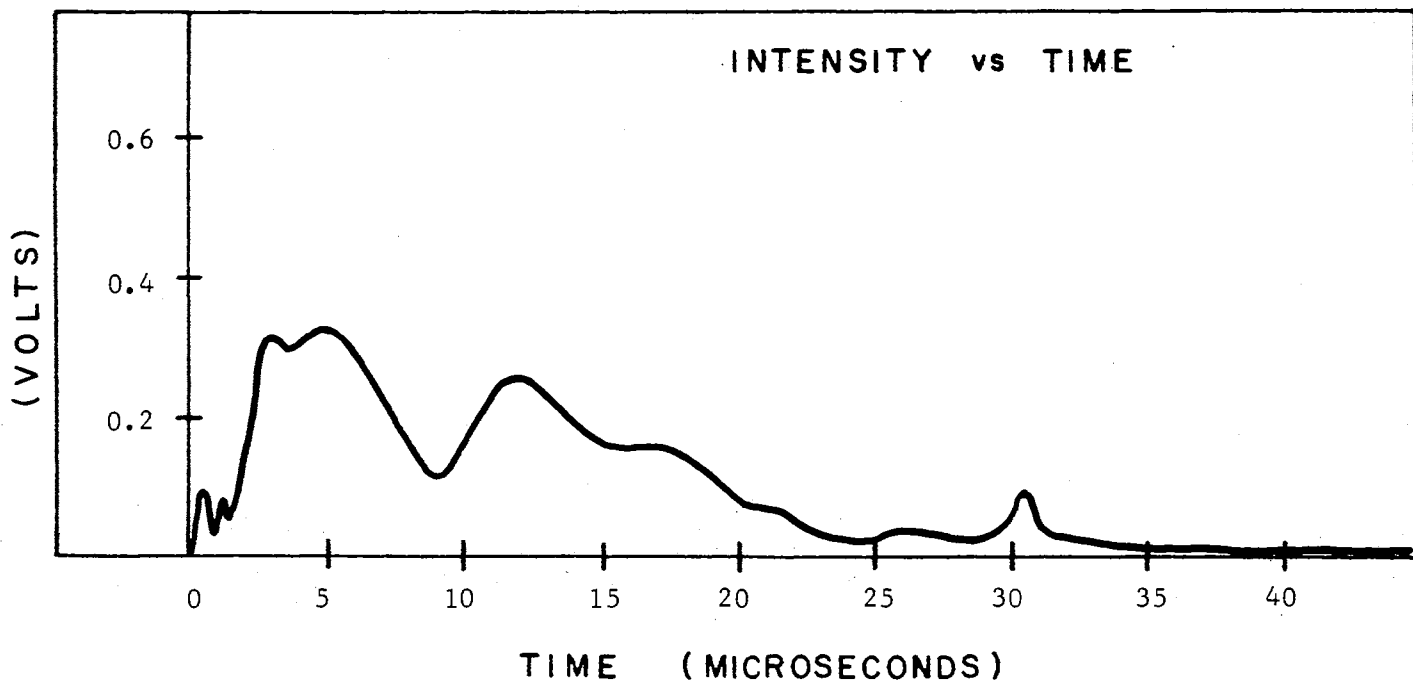


Figure 25. Al^{+1} Ions, Metastable Atoms and Light from Vacuum Spark - Quadrupole System

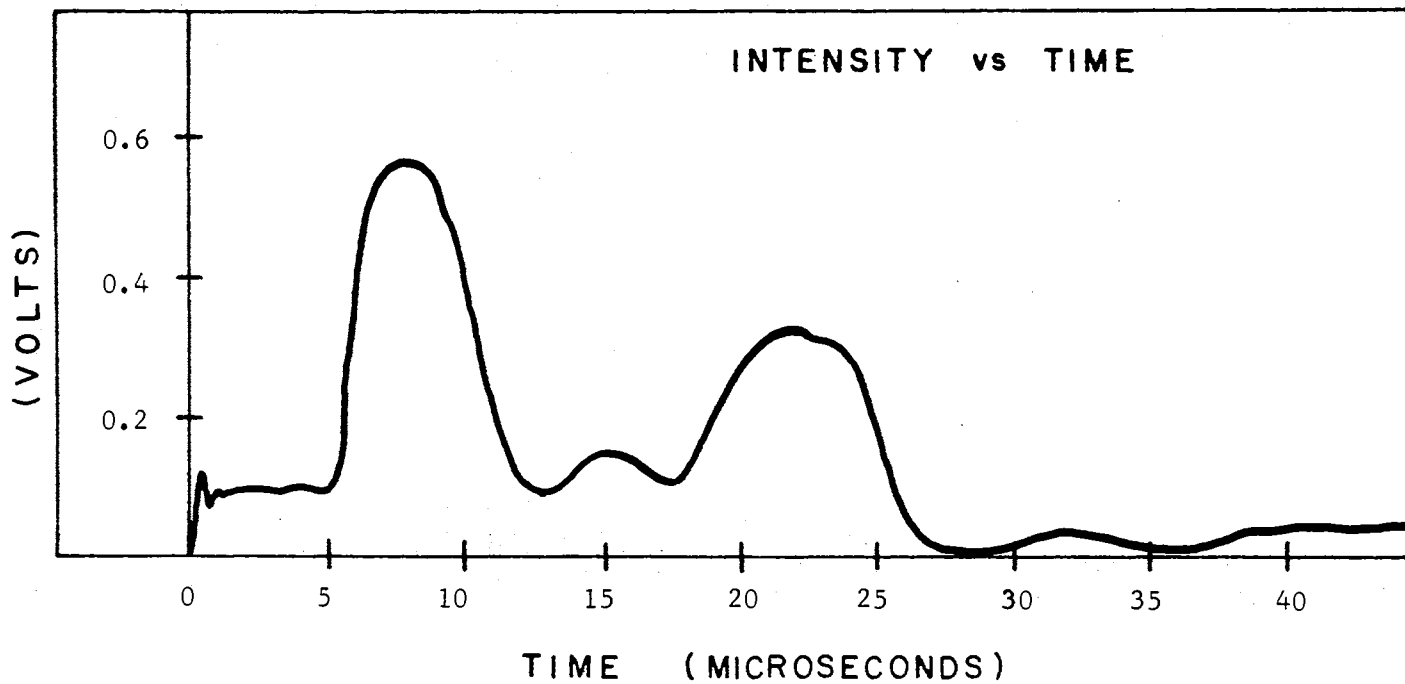


Figure 26. Al^{+2} Ions, Metastable Atoms and Light from Vacuum Spark - Quadrupole System

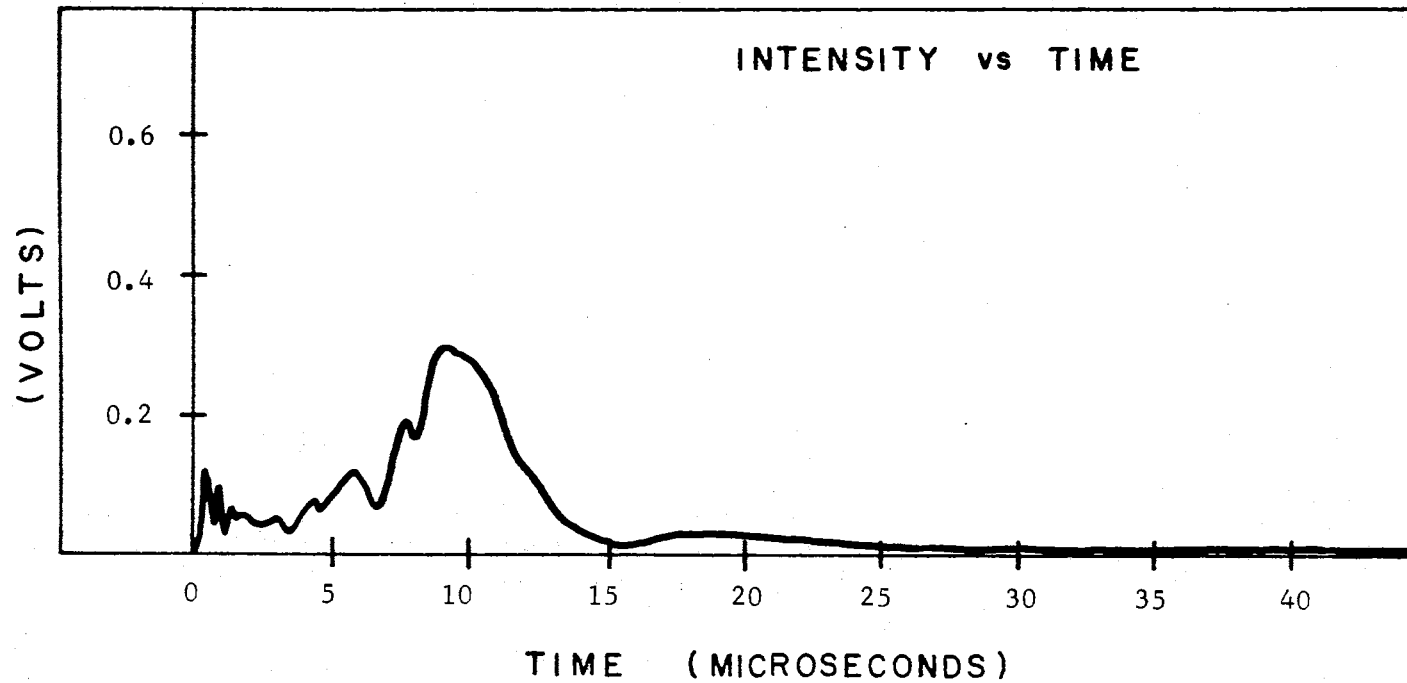


Figure 27. Al^{+2} Ions, Metastable Atoms and Light from Vacuum Spark - Quadrupole System

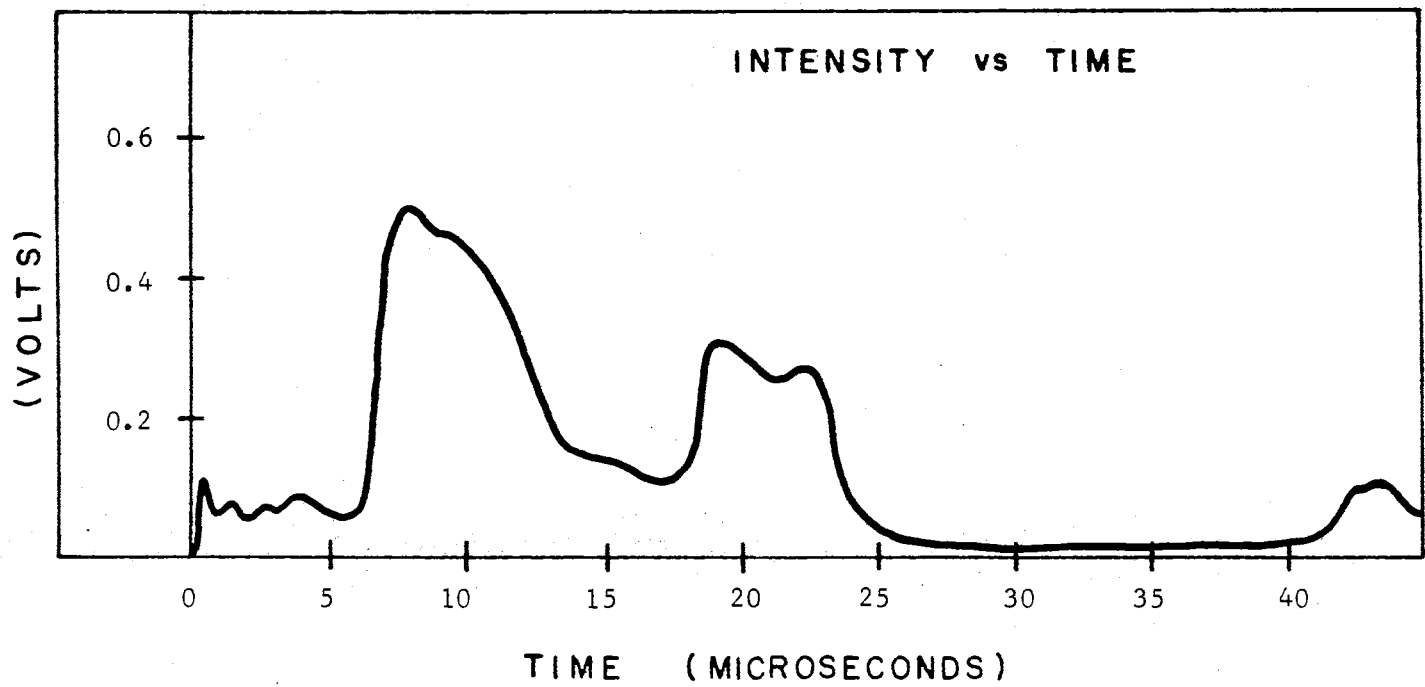


Figure 28. Al^{+3} Ions, Metastable Atoms and Light from Vacuum Spark - Quadrupole System

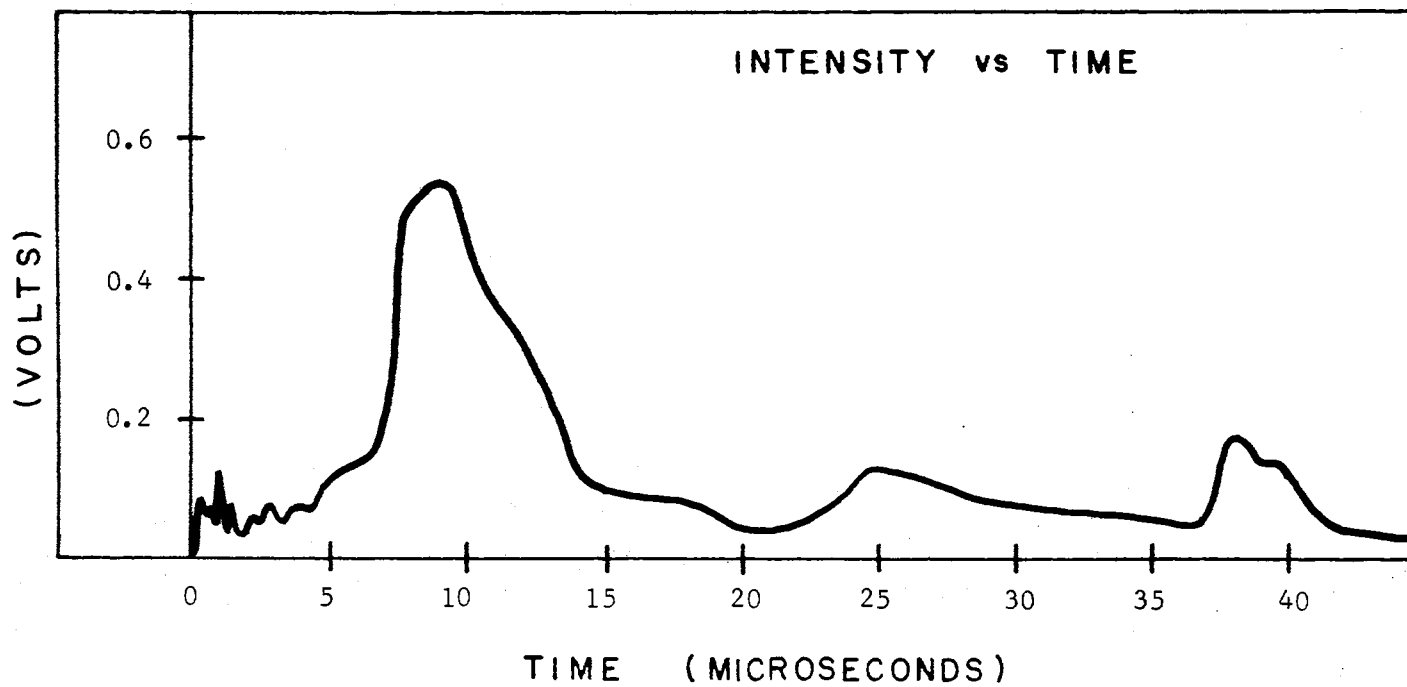


Figure 29. Al^{+3} Ions, Metastable Atoms and Light from Vacuum Spark - Quadrupole System

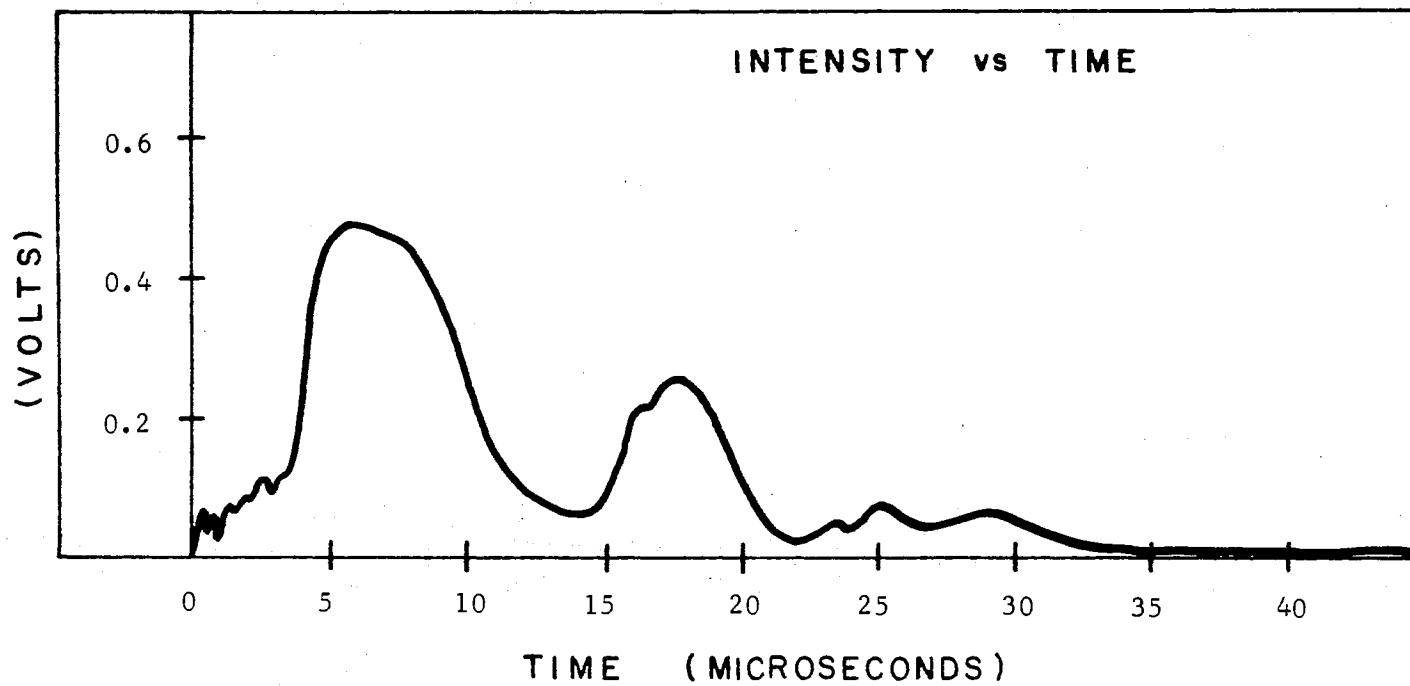


Figure 30. Al^{+4} Ions, Metastable Atoms and Light from Vacuum Spark - Quadrupole System

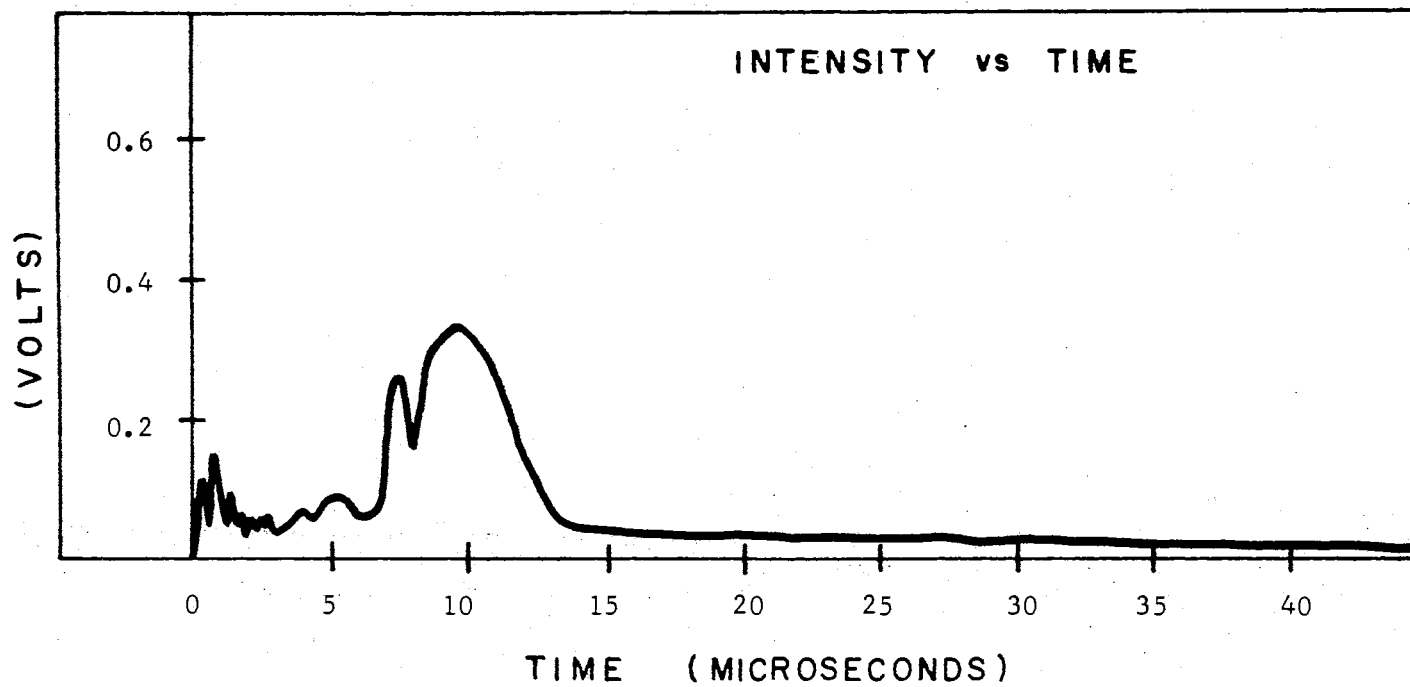


Figure 31. Al^{+4} Ions, Metastable Atoms and Light from Vacuum Spark - Quadrupole System

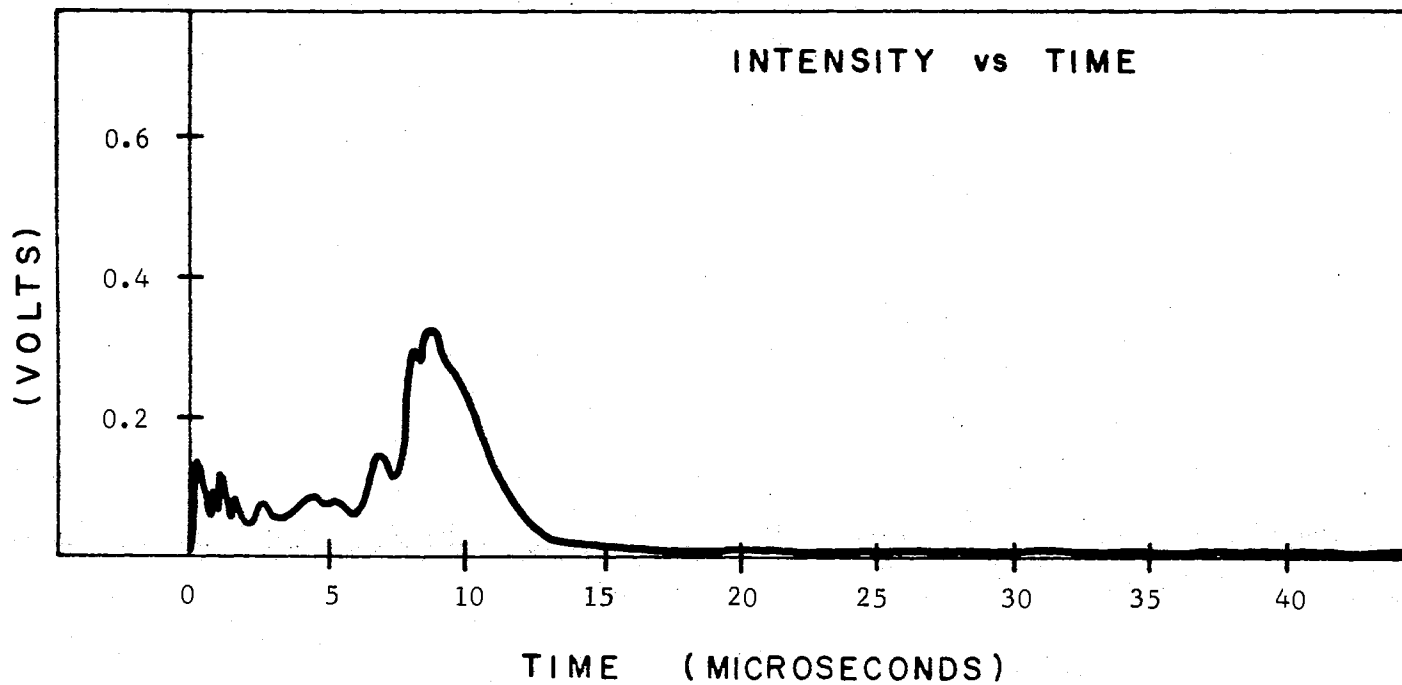


Figure 32. Al^{+5} Ions, Metastable Atoms and Light from Vacuum Spark - Quadrupole System

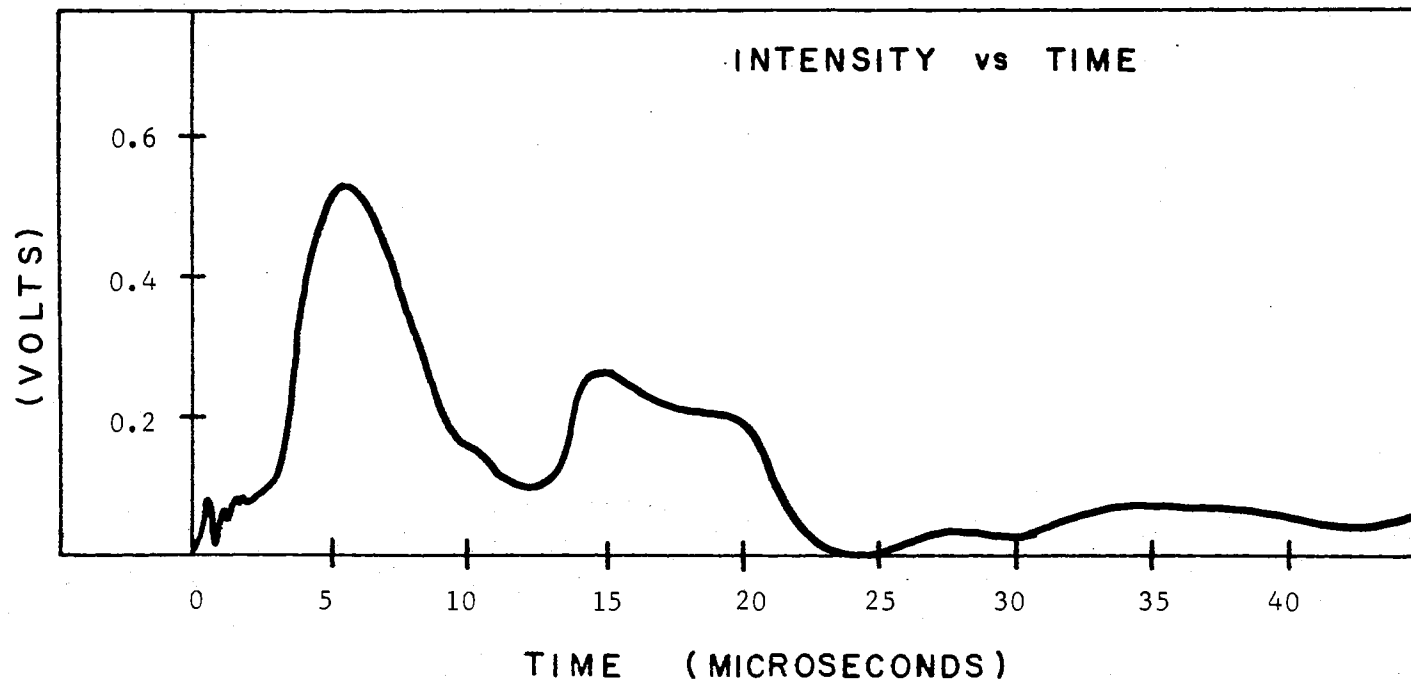


Figure 33. Al⁺⁵ Ions, Metastable Atoms and Light from Vacuum Spark - Quadrupole System

shown in this curve, should be briefly discussed. One possible mechanism, which could be responsible for these higher velocities, is included with the discussion below. Consider the breakdown between the aluminum electrodes. As the electrodes become worn, the smooth, tapered points become rough, ragged surfaces. The pits and corona points, which exist on the uneven surfaces of the electrodes, greatly influence the manner in which the breakdown occurs. In the first few nanoseconds of the breakdown, the spark begins in the region where the electric field gradient and current density is greater. Corona points, which protrude from each electrode, would be the most likely region for the initiation of the breakdown. As the plasma gas is formed between the electrodes, the spark will then migrate to other regions of the electrodes. As the spark migrates across the uneven surfaces, the intensity of the spark will vary according with the current density, which is a function of the varying gap width. The energy density of the plasma, formed by the method described above, is a varying function of time. The frequency of the capacitor discharge is known to be in the kilocycle range, so that multiple velocity peaks in the data shown here cannot be attributed to multiple sparks. Since these velocity peaks are separated by only a few microseconds, the particles, which reach the detector, must have originated from a single spark plasma with an intensity that varies with time. This interpretation is consistent with the data for all the aluminum ionic specie shown in this section. It should be noted that the intensity of the spark will not decay to zero until the end of the first half-cycle of the capacitor discharge. Since none of the curves show a decrease in intensity to zero be-

tween major peaks, and since the separation between peaks is of the order of a few microseconds, it must be assumed that the entire phenomenon shown by each curve occurs in the first half-cycle of a single breakdown.

The relatively fast Al^{+1} ions and metastables which are shown in Figure 25 are thought to have originated outside the central breakdown region. These ions are produced by the cascading electrons from the negative electrode to the anode. These Al^{+1} ions could not exist in equilibrium with the hot plasma which is formed in the central region of the breakdown, but may be accelerated by the very high pressure gradient produced by the expanding and migrating plasma. No temperature determination can be made from the curve shown in Figure 25, which occurs only infrequently, since the velocities of the particles shown by this curve, must be attributed to kinetic, rather than thermal, energy.

At least one other possible mechanism should be discussed, which may affect the velocity of the ionic specie, which reach the detector. If the aluminum electrodes are slightly misaligned, the ions which escape the plasma, may be slightly accelerated. This small accelerations would be positive if the spark plasma is formed between the anode and the quadrupole entrance. If the anode of the spark gap electrodes is misaligned so that it lies between the cathode and the quadrupole entrance, then the ions which escape the plasma may receive a small negative acceleration. Any additional velocity, or any decrease in velocity of the ionic specie, which is attributed to such an acceleration, must be considered before a temperature determination is made from the curves.

It is possible that the spark gap electrodes may be occasionally, misaligned so that the electrode points lie on a line which is normal to the axis of the quadrupole lens. In this case, no acceleration would be given to the ions along the direction toward the quadrupole aperture.

The neutral aluminum atoms and the metastable atoms are not affected by the mechanism discussed above, but are affected by the pressure gradients which exist in the expanding plasma. The effects of the mechanisms, which were discussed above, are difficult to analyze quantitatively. One of the major difficulties, in this regard, is the non-reproducibility of the spark source.

The velocity curves, which were presented in this section, give a qualitative indication of the aluminum ionic specie, metastable atoms and light, which escape the plasma, which is produced by the vacuum spark. From the interpretation of these curves, an insight has been gained, regarding the manner in which the plasma is formed.

Electrostatic Lens Data

The design features and the operating principle of the electrostatic lens system were discussed in Chapter IV. Several of the initial results obtained with the lens system are presented in this section. One of the major advantages that the lens system exhibits over the original quadrupole system is the capability to eliminate the metastable atoms and light from the detector output signal. This feature allows the ions of a single specie to be monitored separately. The quadrupole detector system was employed with the electrostatic lens so that double filtering was achieved. The lens, itself, was

designed so that only ions of a predetermined charge will be directed into the quadrupole aperture. The quadrupole is set to receive this same charge in the conventional manner. Therefore, only ions of the desired charge may reach the electron multiplier detector. Since the aluminum ions of a particular charge constitute the entire beam to the quadrupole, the output current of the detector to the oscilloscope is proportional to the time-of-flight of the ions only. The drift space from the spark source to the detector is constant, in this case approximately 46 cm, so that the curve actually represents a distribution of ion velocities.

The curves which are presented in this section were obtained with the system vacuum maintained at 10^{-5} - 10^{-6} torr. The spark gap voltage was 8.5 - 10.0 KV and the high voltage to the electron multiplier was 1.0 KV. The oscilloscope was triggered externally by the vacuum spark, in the single sweep mode. The sensitivity of the scope was set at 0.1 volts/cm and the time scale was set at 10.0 microseconds/cm. The load resistor value was 1,000 ohms. The electrostatic lens was set to deflect a particular ionic specie and the quadrupole mass filter was set to pass this same specie. The time delay to the lens was determined by several trials for each specie. The delay time which produced the strongest signal was used in each case. The electrostatic lens was operated in a pulsed model. The lens field was actuated to correspond with the arrival of the ions at the lens electrodes. The oscilloscope used to monitor the output signal began its sweep, simultaneously with the breakdown of the spark gap, so that zero time was established for the data curves. The variables which are considered in the curves presented here are

the aluminum ions Al^{+1} through Al^{+5} , the drift space and the time-of-flight. From these variables the velocity of the ions are determined. Three typical examples of the data are presented for each ionic specie.

Curves for the Al^{+1} ions are presented in Figure 34, Figure 35 and Figure 36. The Al^{+2} ions are shown in Figure 37, Figure 38 and Figure 39. It should be noted that the time-of-flight data for the Al^{+2} ions, presented in Figure 37, was produced with an expanded time scale. It can be seen from this curve that no significant presence of ions appears after about 80 microseconds. Al^{+3} ions are shown in Figure 40, Figure 41 and Figure 42. The reproducibility with respect to the arrival time for the first major peak for these curves is quite good. Curves for the Al^{+4} ions are presented in Figure 43, Figure 44 and Figure 45. Al^{+5} ions are shown in Figure 46, Figure 47 and Figure 48.

In all of the curves presented here, the first 10-15 microseconds is masked by noise and no interpretation was attempted for this region. The noise probably originated from the breakdown of the spark gap itself, which was used as the triggering source. The major peak for all the ions, except the Al^{+1} ions, is approximately centered about the arrival time of 20 microseconds. With the drift space given as 46 centimeters, this time corresponds to a velocity of the order of 2.3×10^6 cm/sec.

The curves for the aluminum ionic specie presented in Figure 34 through 48 may be interpreted as ion velocity distributions. The distribution is in the reverse order from conventional velocity distribution curves, since the velocities are shown in decreasing order,

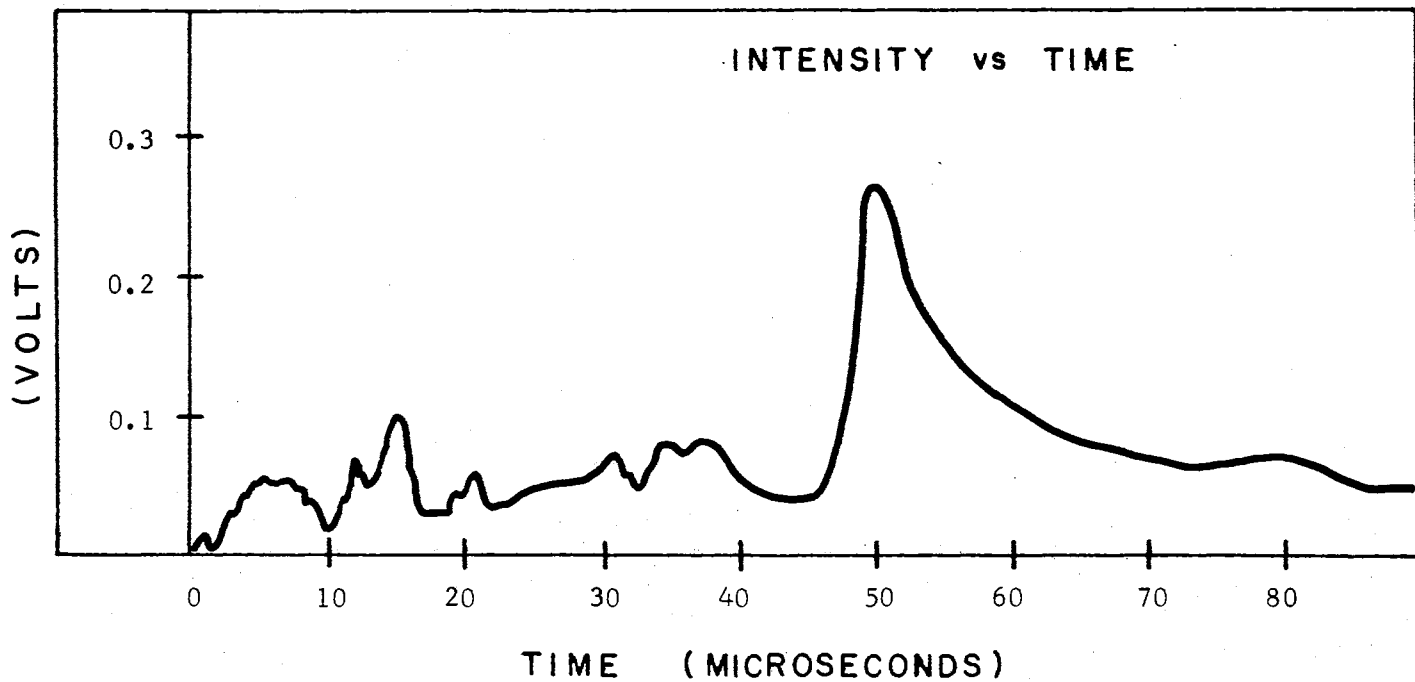


Figure 34. Time-of-Flight Curve for Al⁺¹ Ions from Vacuum Spark - Electrostatic Lens System

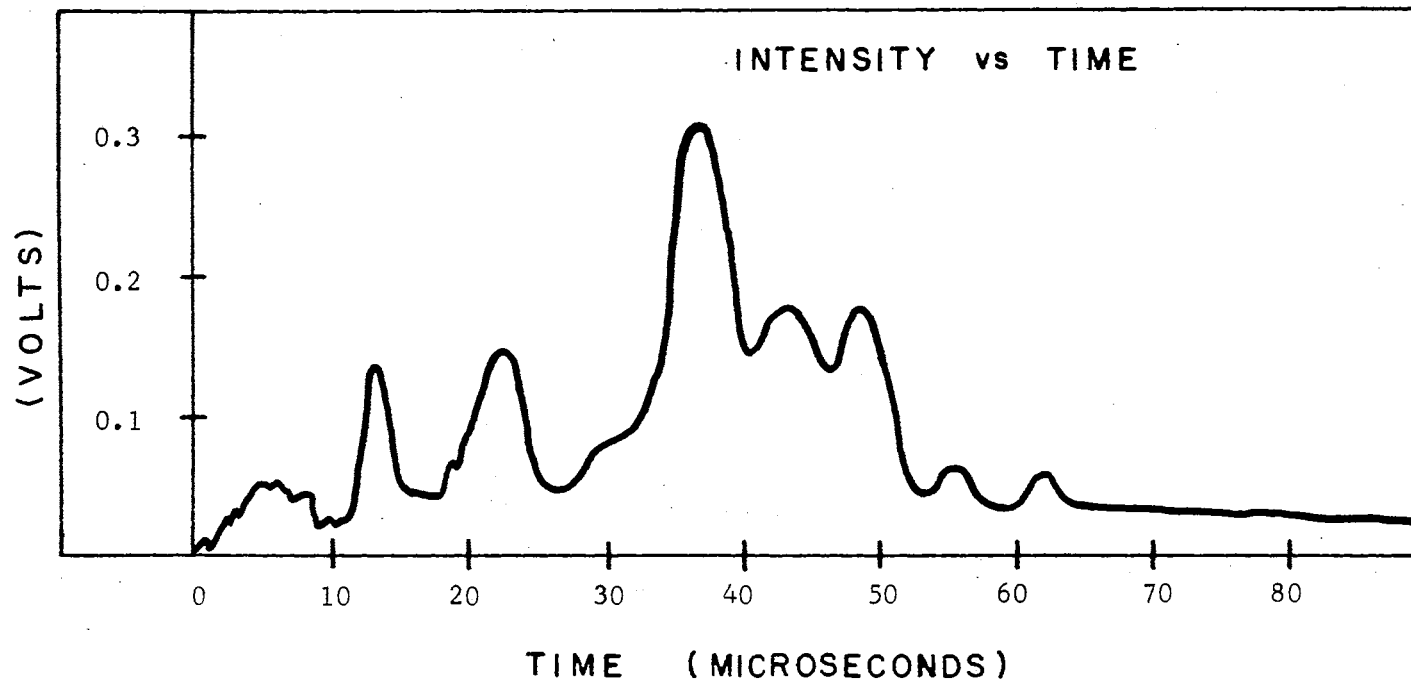


Figure 35. Time-of-Flight Curve for Al⁺¹ Ions from Vacuum Spark - Electrostatic Lens System

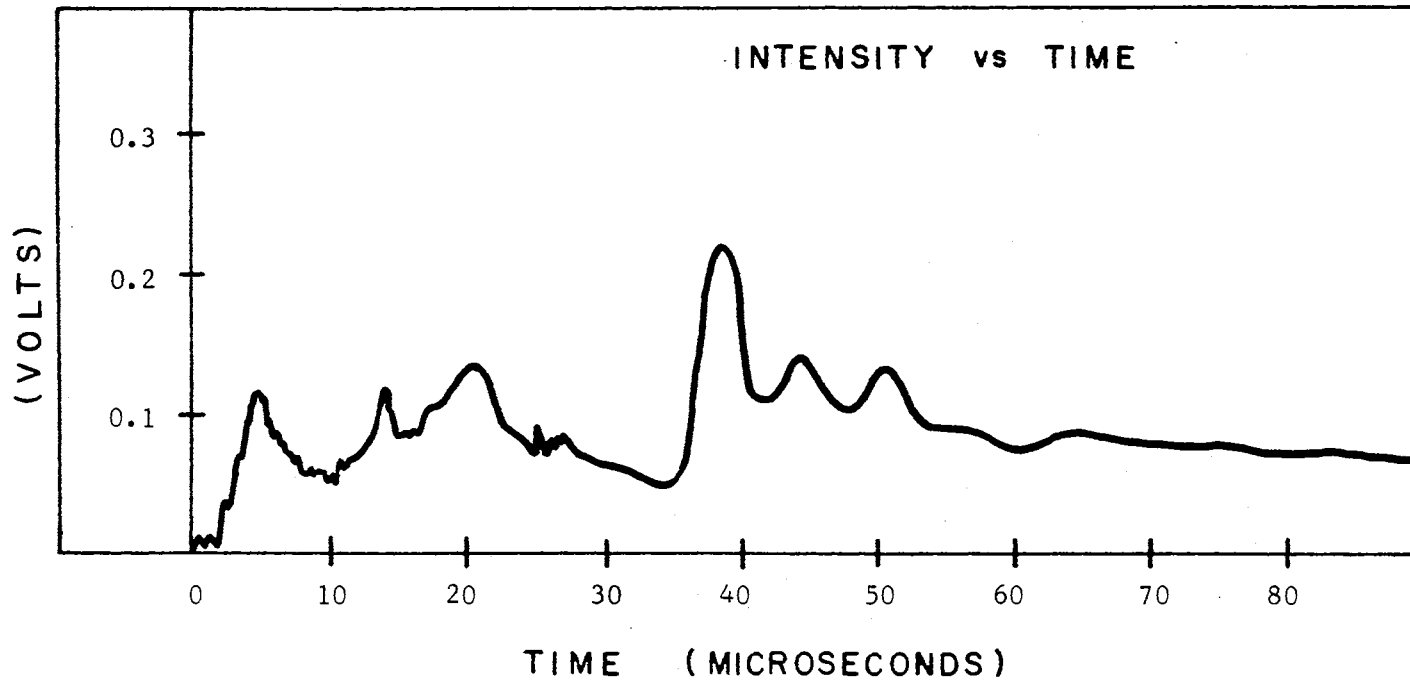


Figure 36. Time-of-Flight Curve for Al^{+1} Ions from Vacuum Spark - Electrostatic Lens System

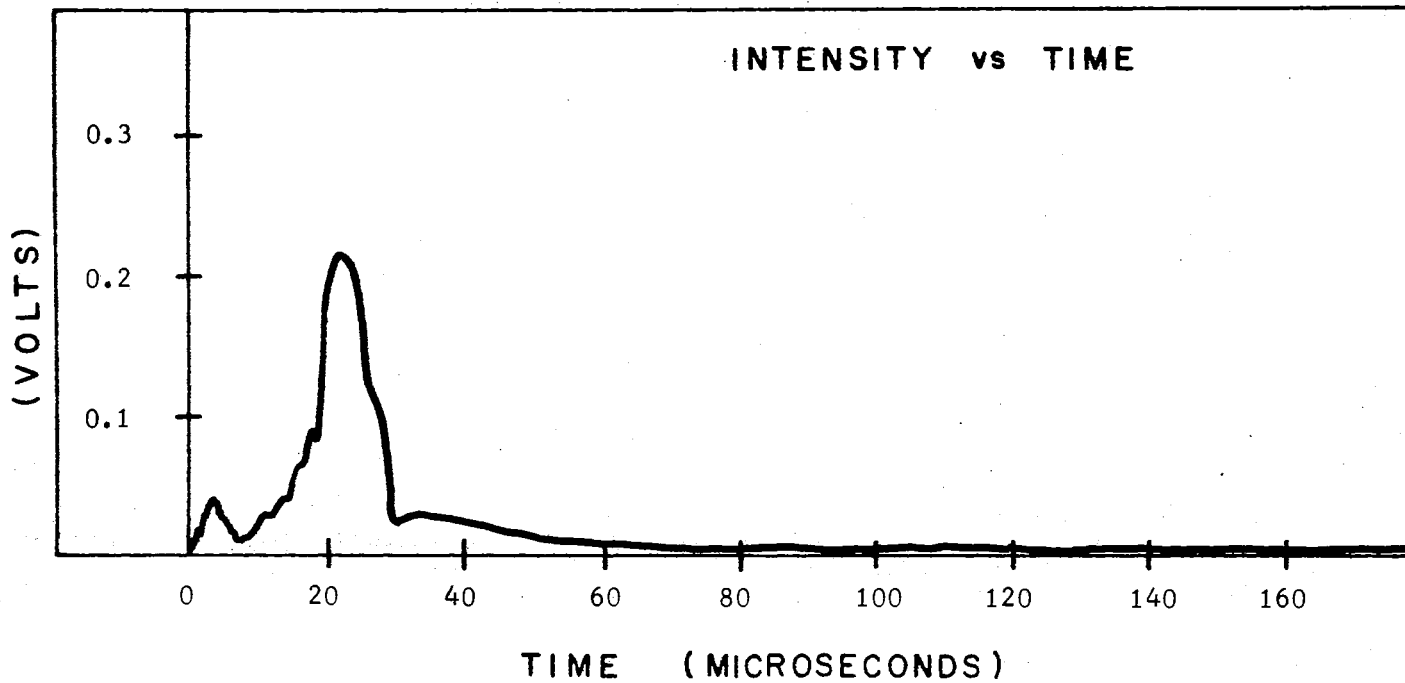


Figure 37. Time-of-Flight Curve for Al⁺² Ions from Vacuum Spark - Electrostatic Lens System

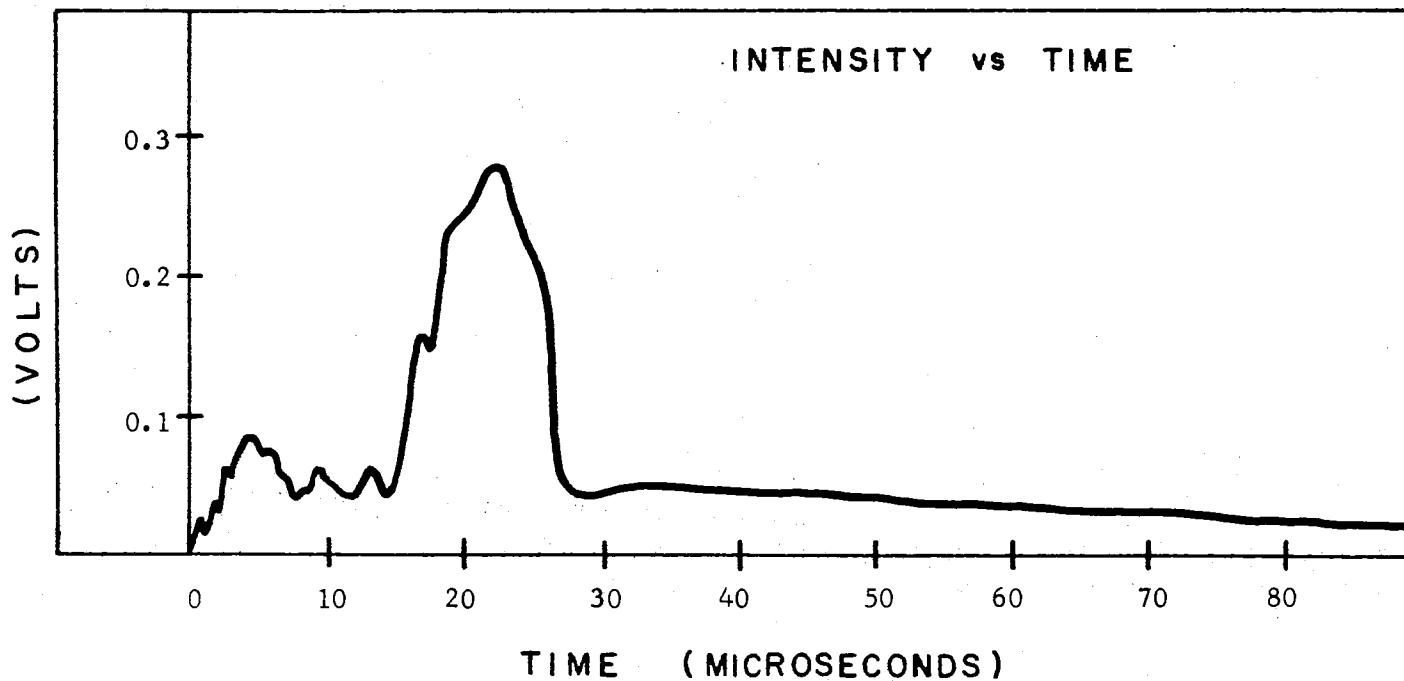


Figure 38. Time-of-Flight Curve for Al^{+2} Ions from Vacuum Spark - Electrostatic Lens System

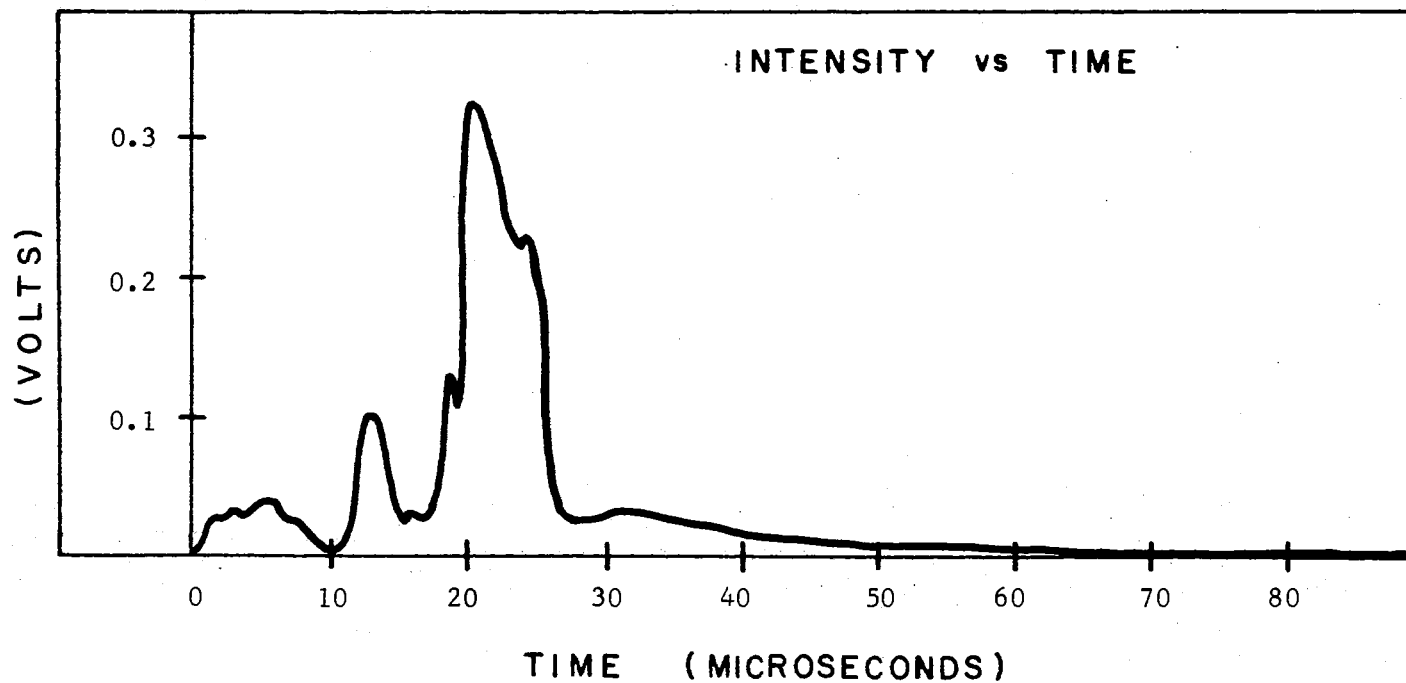


Figure 39. Time-of-Flight Curve for Al^{+2} Ions from Vacuum Spark - Electrostatic Lens System

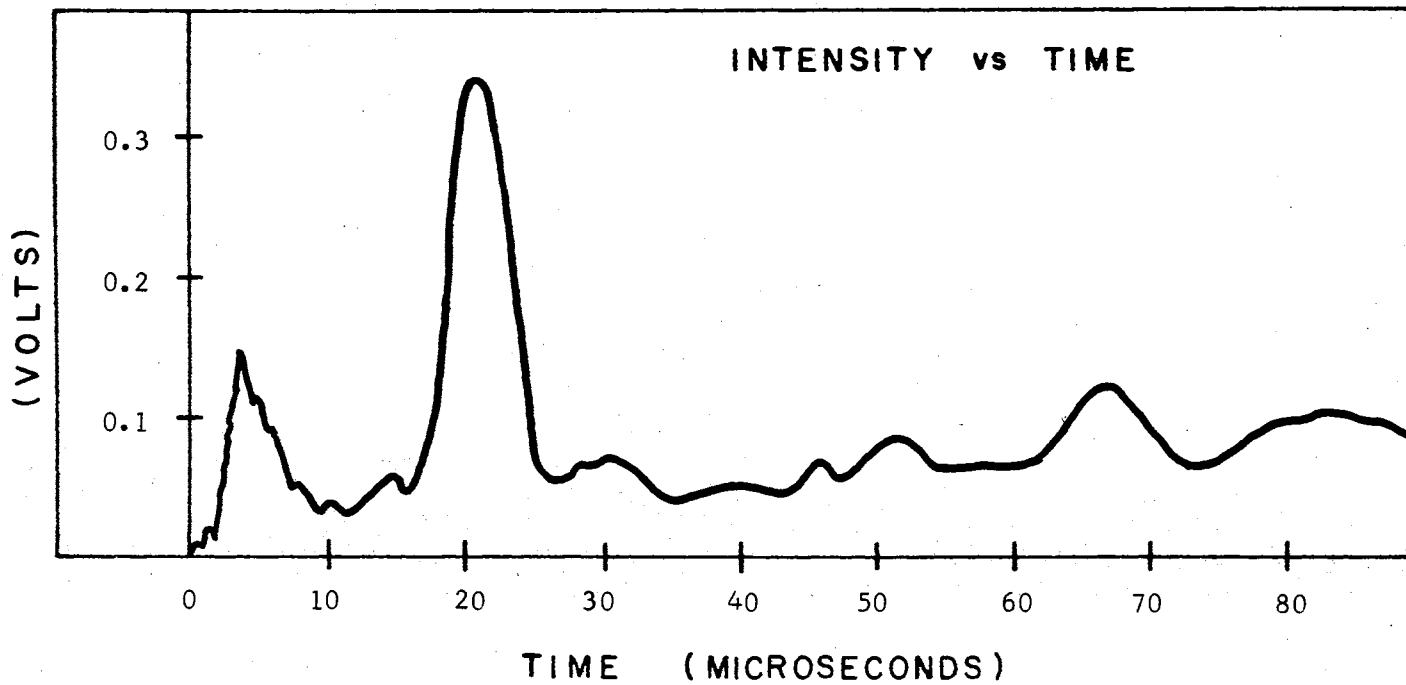


Figure 40. Time-of-Flight Curve for Al⁺³ Ions from Vacuum Spark - Electrostatic Lens System

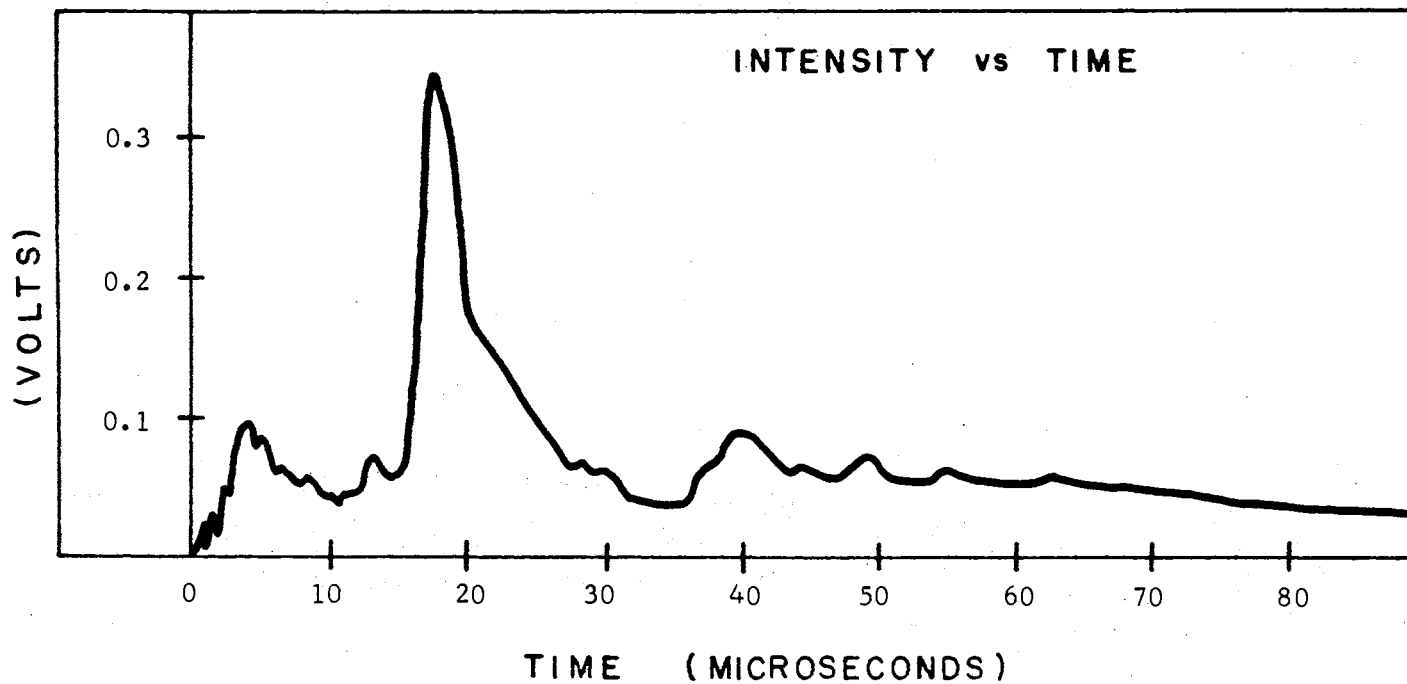


Figure 41. Time-of-Flight Curve for Al⁺³ Ions from Vacuum Spark - Electrostatic Lens System

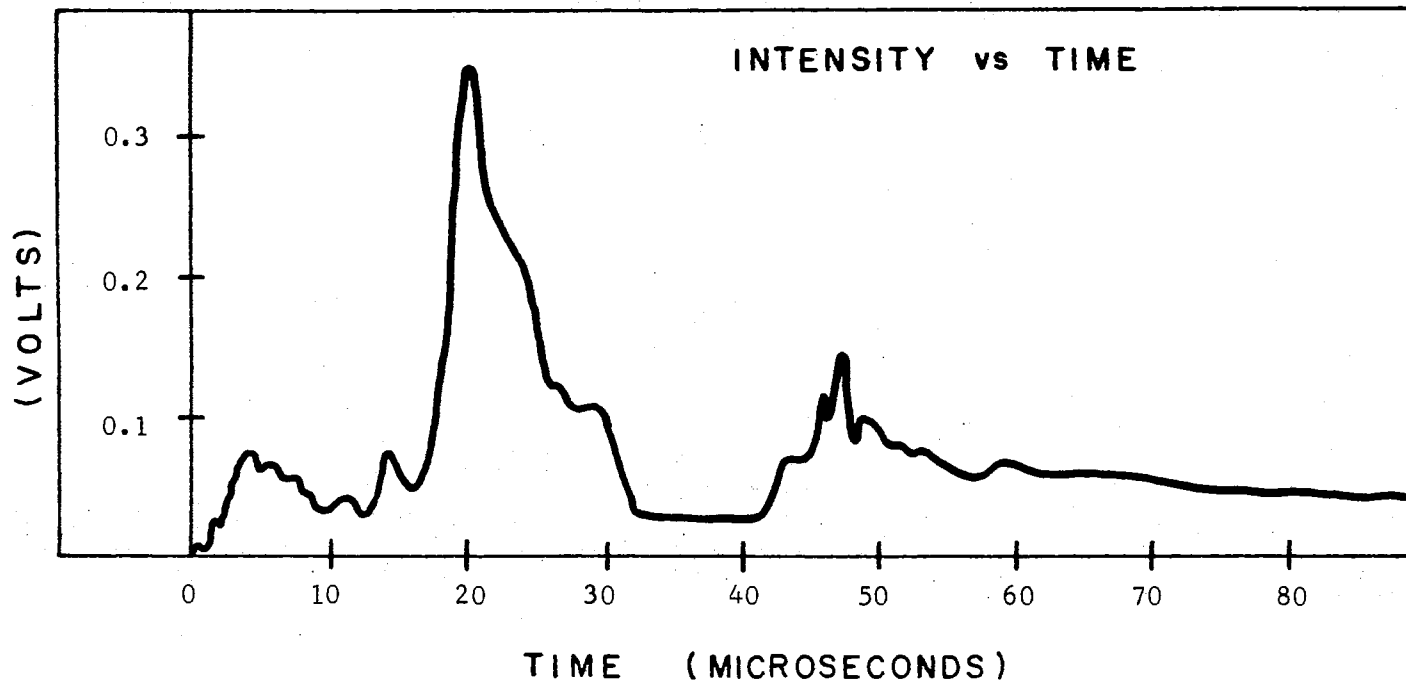


Figure 42. Time-of-Flight Curve for Al⁺³ Ions from Vacuum Spark - Electrostatic Lens System

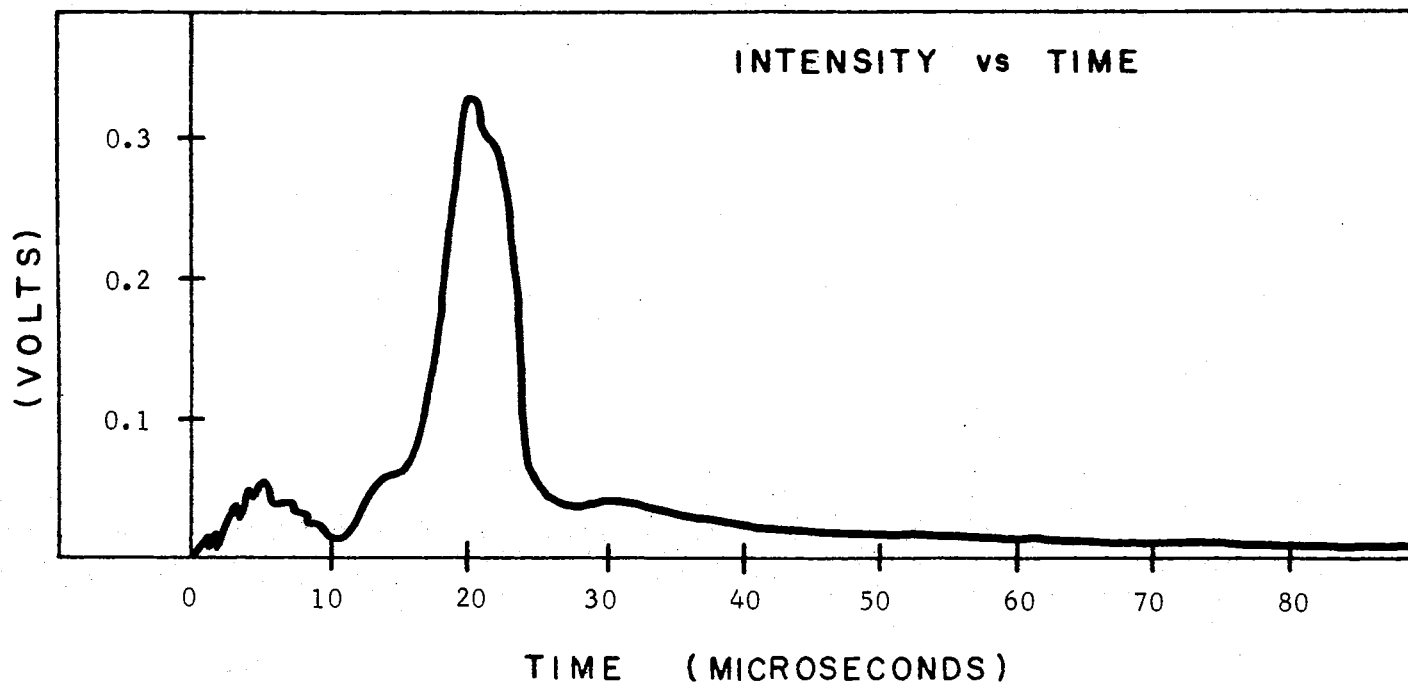


Figure 43. Time-of-Flight Curve for Al^{+4} Ions from Vacuum Spark - Electrostatic Lens System

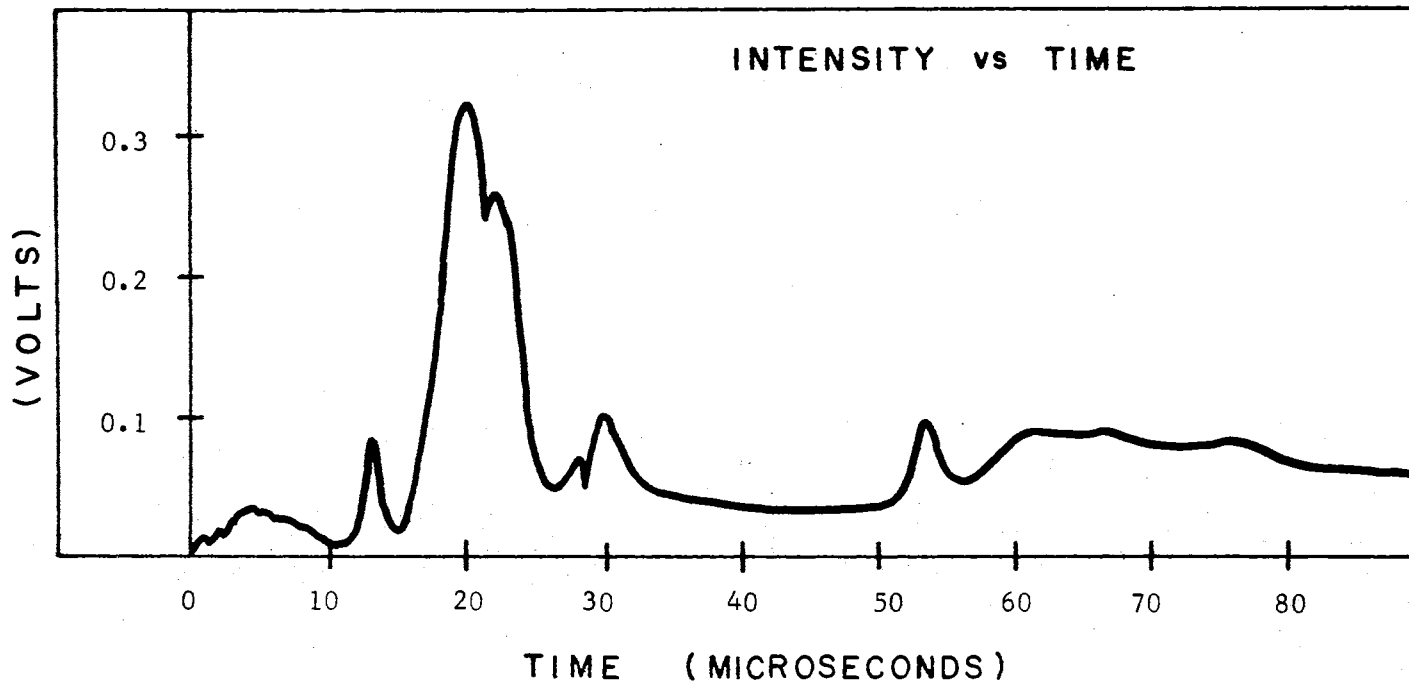


Figure 44. Time-of-Flight Curve for Al^{+4} Ions from Vacuum Spark - Electrostatic Lens System

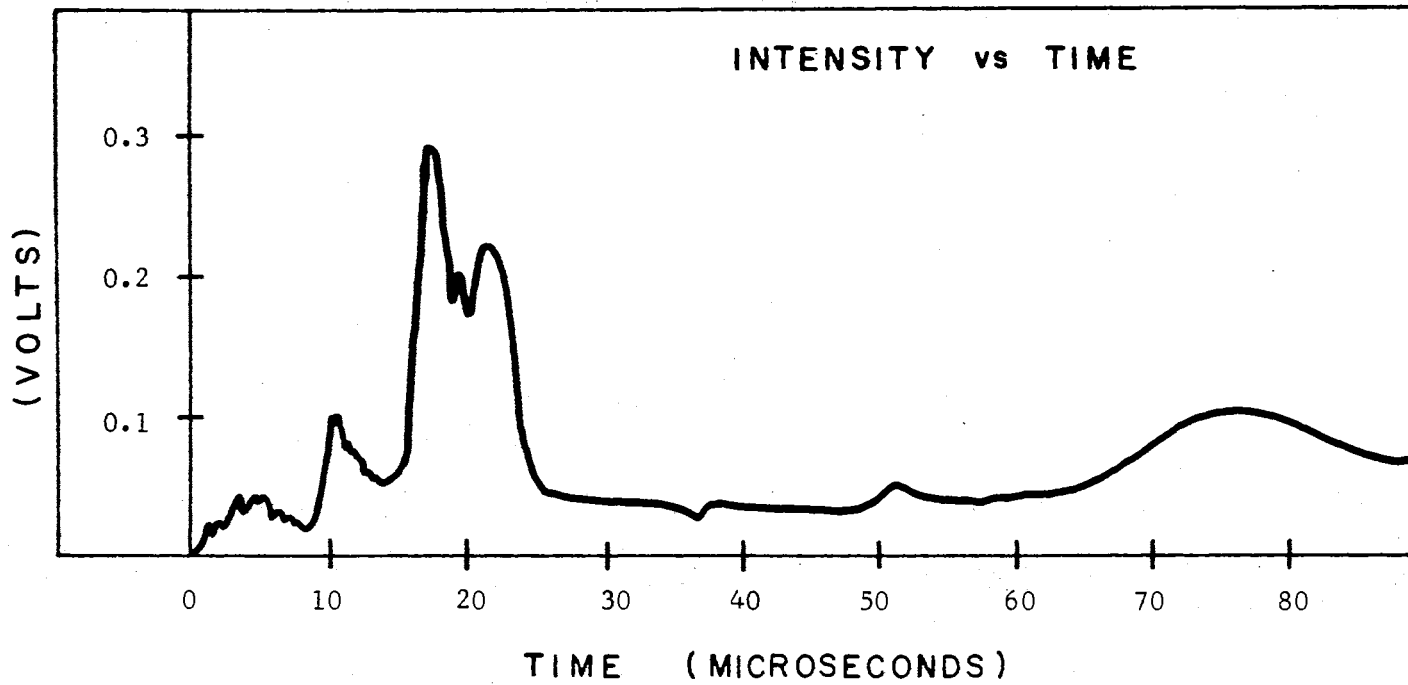


Figure 45. Time-of-Flight Curve for Al⁺⁴ Ions from Vacuum Spark - Electrostatic Lens System

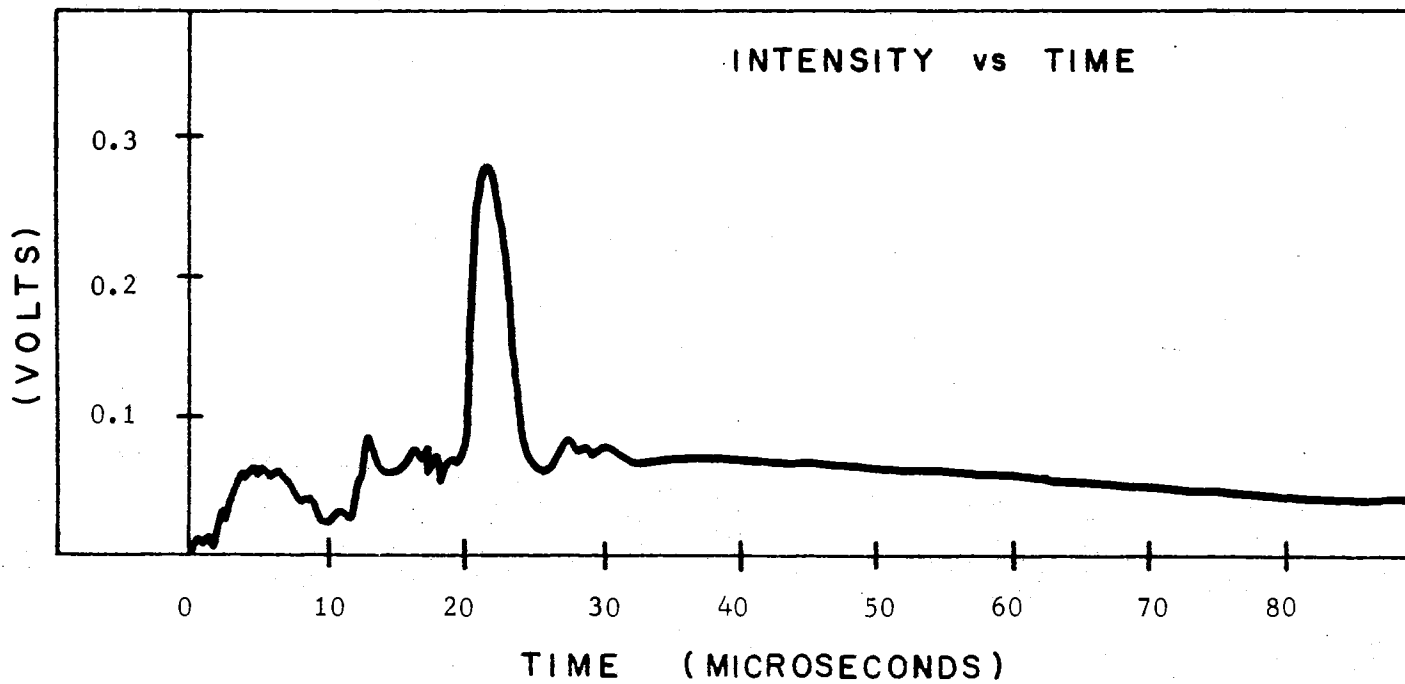


Figure 46. Time-of-Flight Curve for Al^{+5} Ions from Vacuum Spark - Electrostatic Lens System

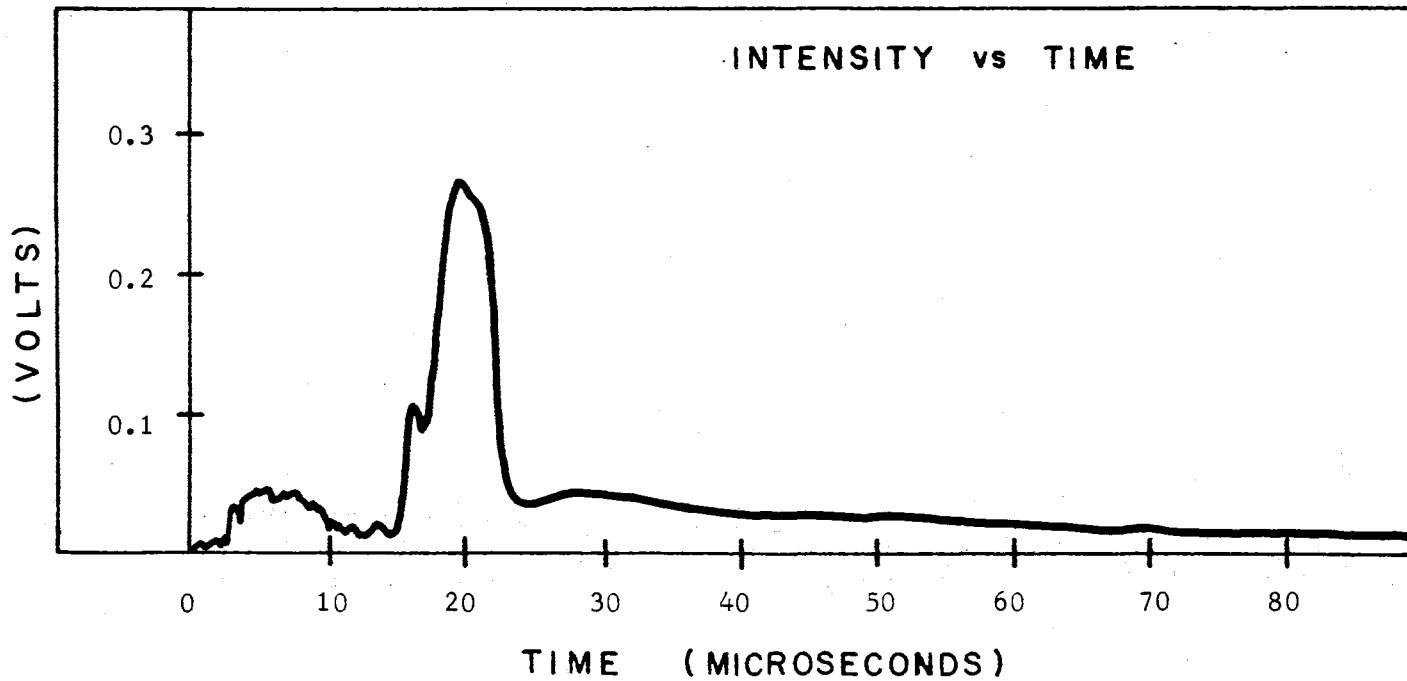


Figure 47. Time-of-Flight Curve for Al⁺⁵ Ions from Vacuum Spark - Electrostatic Lens System

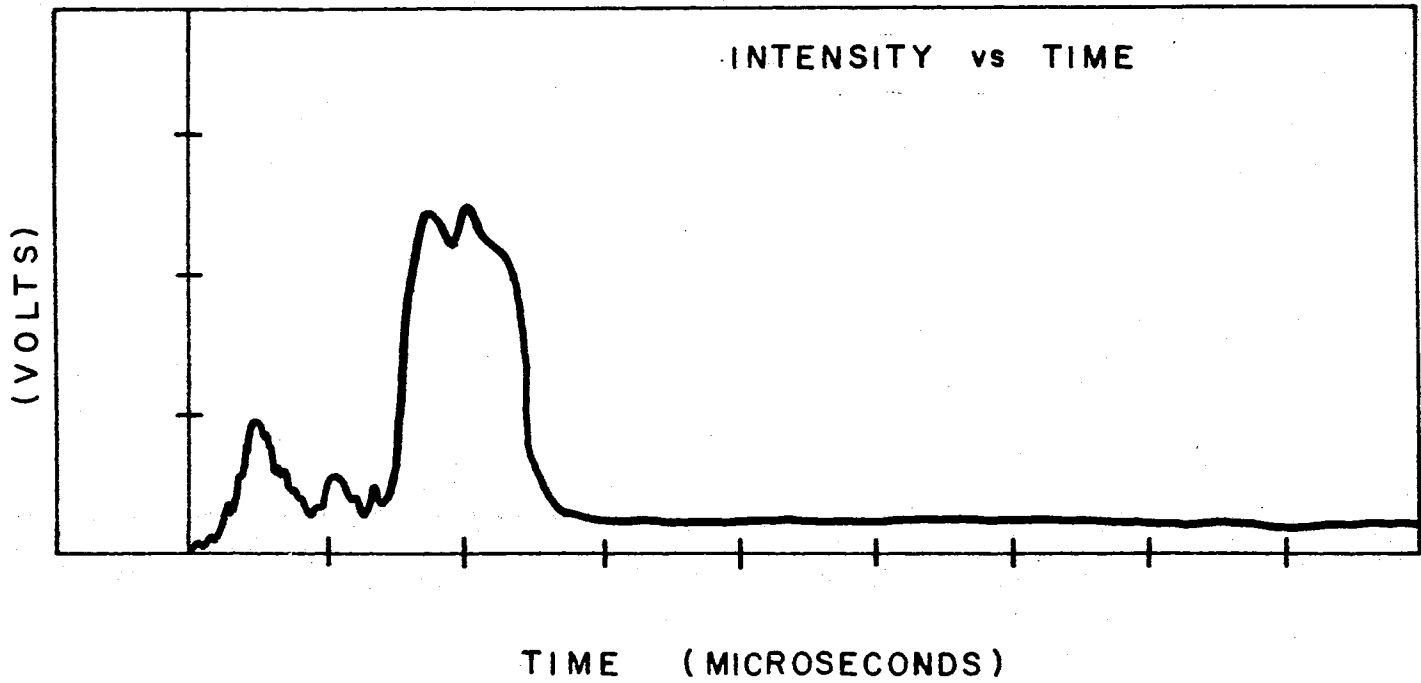


Figure 48. Time-of-Flight Curve for Al⁺⁵ Ions from Vacuum Spark - Electrostatic Lens System

from left to right on the graphs. The lower velocities appear at the extreme right of the curves and increase back toward the origin. The range of velocities which are shown, correspond to the flight times of 10-80 microseconds. The velocity corresponding to 80 microseconds is of the order of 0.58×10^6 cm/sec. The velocity corresponding to 10 microseconds is of the order of 4.6×10^6 cm/sec.

One of the assumptions which is made, in the theoretical work with plasma creation and evolution, is that the plasma exists in a state of local thermodynamic equilibrium. The thermal equilibrium state of a plasma is described in kinetic theory terms by stating that each single particle velocity distribution function has a Maxwell-Boltzmann form. The validity of the assumption of local thermodynamic equilibrium may then be checked by observing the velocity distributions of the ions which escape the plasma which is under study. The classical theory of the Maxwellian distribution is well known and may be reviewed in most any elementary text on thermodynamics. The shape of the Maxwellian curve is shown in Figure 49. The experimental curves for the ionic specie may be compared with the Maxwellian curve for a qualitative insight as to their relative form. In making these comparisons, it must be remembered that the experimental curves are velocity distributions in reverse. It is also important to note that the curves originate from approximately a one microsecond pulse of ions, which are ejected from the collimated beam of ions, metastable atoms and u.v. photons, which is emitted from the plasma.

The initial results presented here give an indication of the form of the distribution of ion velocities. These results must be

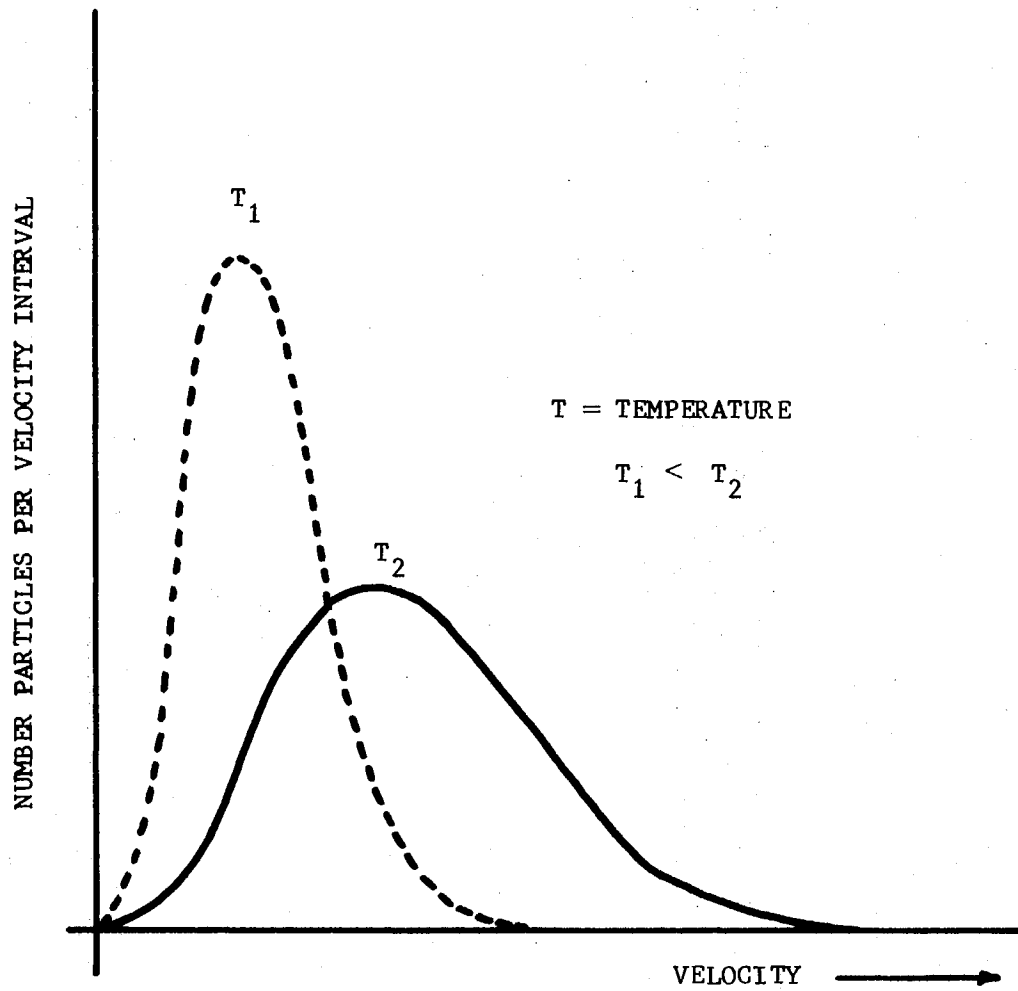


Figure 49. Maxwellian Velocity Distribution
(Arbitrary Scale)

viewed qualitatively because of the many variables yet to be determined. The amplitudes of curves should not be compared from one ionic specie to another. The output current from the detector is not necessarily a linear response to ion charge. The output current of the detector depends, not only on the number and charge of the ions reaching the cathode of the detector, but also it depends on the velocity of the individual ions. However, the amplitudes of the curves for any single specie may be compared.

The velocities of a Maxwellian distribution are randomized, i.e., they are isotropic. The most probable speed of this distribution will then yield a value for the temperature through the relation: $v_p = 1.4 (kT/m)^{\frac{1}{2}}$. If the assumption is made that the ion velocities, shown in the data curves present here, are random, i.e., they are thermal velocities, then a most probable speed of 2.3×10^6 cm/sec corresponds to a plasma temperature of the order of 8.7×10^5 °K. This qualitative determination of the temperature of the plasma is valid, only to the extent that only thermal ions reach the detector. For a quantitative determination, additional data will be necessary.

The multiple, velocity peaks, which are present in several of the curves, which were presented in this section, may be attributed to the same mechanism, that was discussed in the previous section on the quadrupole data. This mechanism of spark migration at the spark gap electrodes, in the first half-cycle of the capacitor discharge, could be responsible for the variation in the amplitudes of the time-of-flight curves, which were presented above for the electrostatic lens.

The major advantage, that the lens system contains over the

original quadrupole data, is that no neutral, aluminum atoms, metastable atoms or light are present in the beam, which reaches the detector. These initial results serve to illustrate the effectiveness, of the electrostatic lens system, for analyzing the individual ionic specie, which escape from a plasma.

Laser Impact Plasma Data

The computer model for a plasma, produced by the incidence of a giant laser pulse onto an aluminum plate, was discussed in Chapter V. A production run was made on the Univac 1108 computer and the evolution of the plasma was followed for a period of 2.6 nanoseconds. This run required approximately one hour of time in the computer central processing unit. For this run, a gaussian laser pulse with an energy of 20 joules was assumed. The duration of the pulse was taken to be 20 nanoseconds. An initial time increment of 1.0×10^{-12} seconds was chosen. A total of 180 time cycles were produced.

In this section, several of the flow variables are shown, at the beginning and end of the production run, to illustrate the type of solution which may be achieved with this model.

The evolution in time of the plasma mass density, internal energy density, temperature and pressure are presented. It must be noted that the plasma is in a creation state for all of the curves presented here, i.e., the laser pulse continues to be incident on the aluminum target for 20 nanoseconds. The first set of curves show the variation of the plasma mass density and the internal energy density at a time, 0.50207 nanoseconds, after the incidence of the laser pulse. These are presented in Figure 50. The absissca for

$T = 0.50207$ nanoseconds

MASS DENSITY —————

INTERNAL ENERGY DENSITY - - - - -

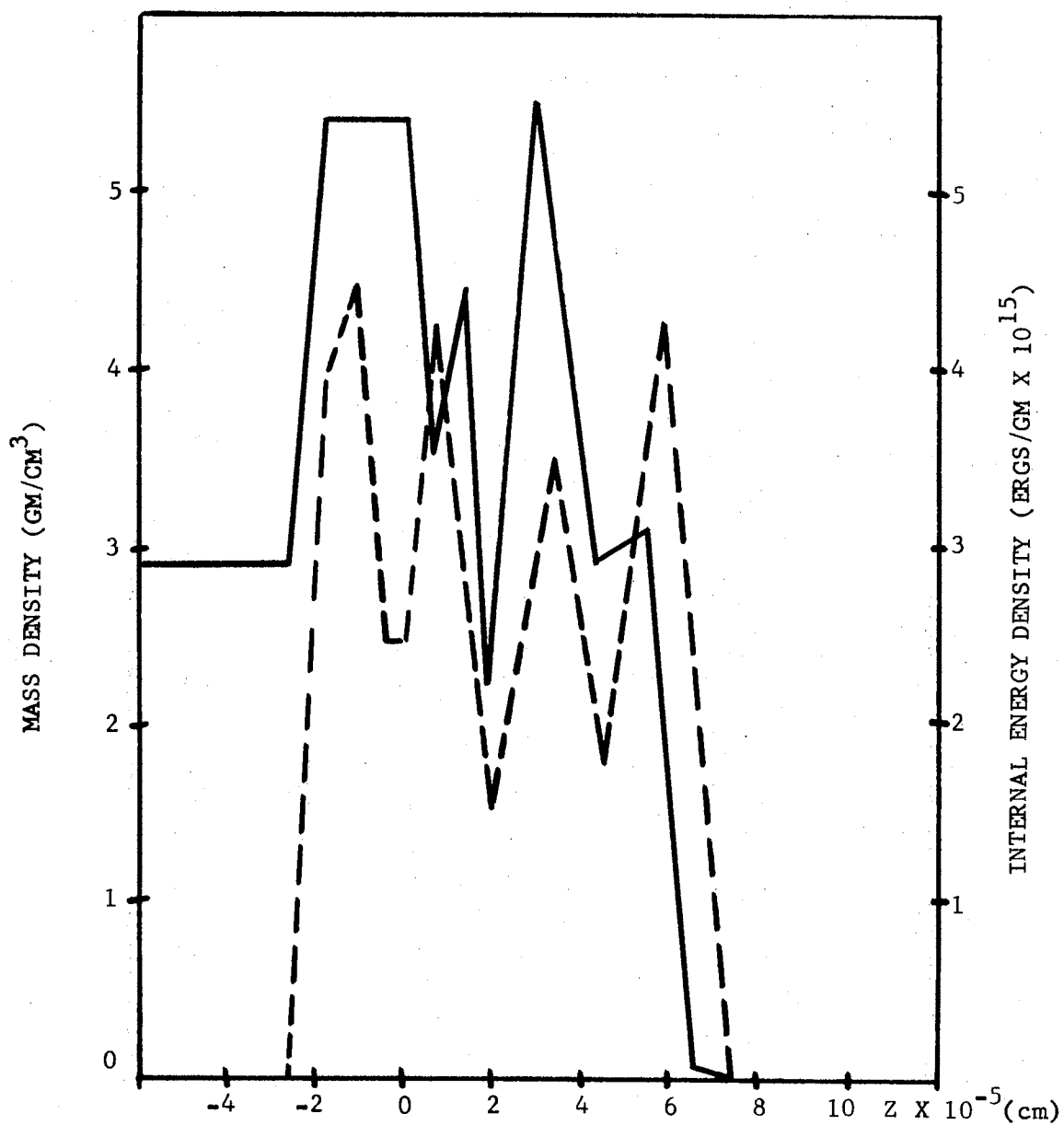


Figure 50. Variation of Mass Density and Interval Energy Density along Radiation Axis

this figure represents the Z-direction, along which the laser pulse travels. The laser pulse is incident from right to left. The point, 0, on the graph, along Z, represents the aluminum target-vacuum interface. The normal, solid density of 2.7 gm/cm is shown at the left of the figure.

The plasma temperature and pressure are presented in Figure 51, for the same point in time. The laser pulse is incident from the right, along the Z-direction. These graphs were produced by a separate computer program, which was used to reduce the data from the laser program. Graphs for each cycle were produced, but are not presented here because of their large number. The two figures above were extracted from the 37th cycle of the run.

The next two sets of curves are presented to illustrate the evolution of the plasma towards the end of the run. These curves were extracted from cycle 173, at a time 2.4821 nanoseconds from zero time.

The mass density and internal energy density are presented in Figure 52. The plasma temperature and pressure are presented in Figure 53, for this later time. In both of these figures, the interface is shown shifted back to the origin. As in the previous, figures, the laser beam is still incident from the right.

Figure 54 is presented to illustrate the fluctuations of the laser beam reflection over several time intervals, at the beginning and at the end of the computer run. The significant factor to note from this figure is the rate at which the laser beam is being absorbed by the plasma. The intervals, shown in Figure 54, are divided into equal parts, covering the entire run from 1.0×10^{-12} seconds to 2.6

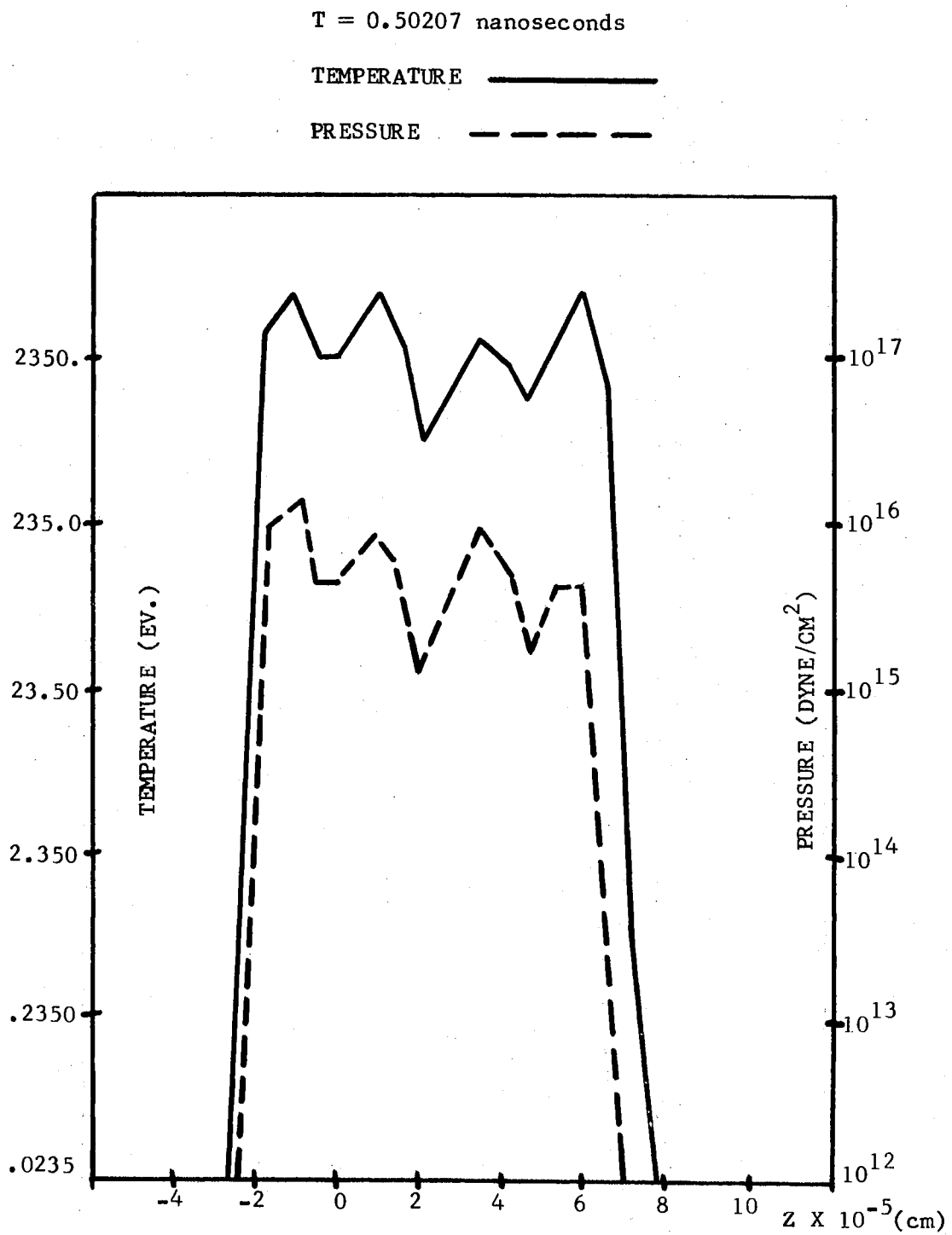


Figure 51. Variation of Pressure and Temperature along Radiation Axis

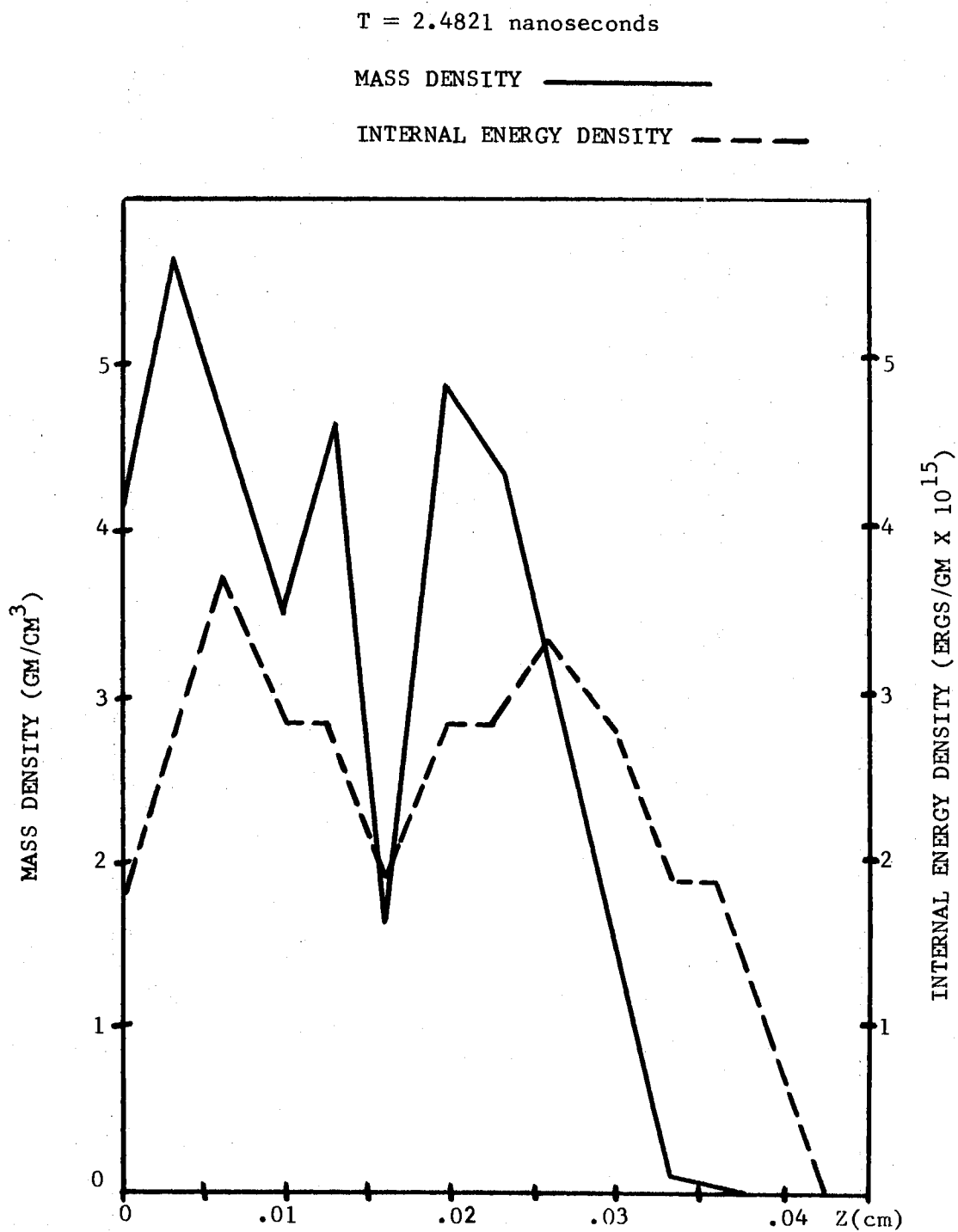


Figure 52. Variation of Mass Density and Internal Energy Density along Radiation Axis

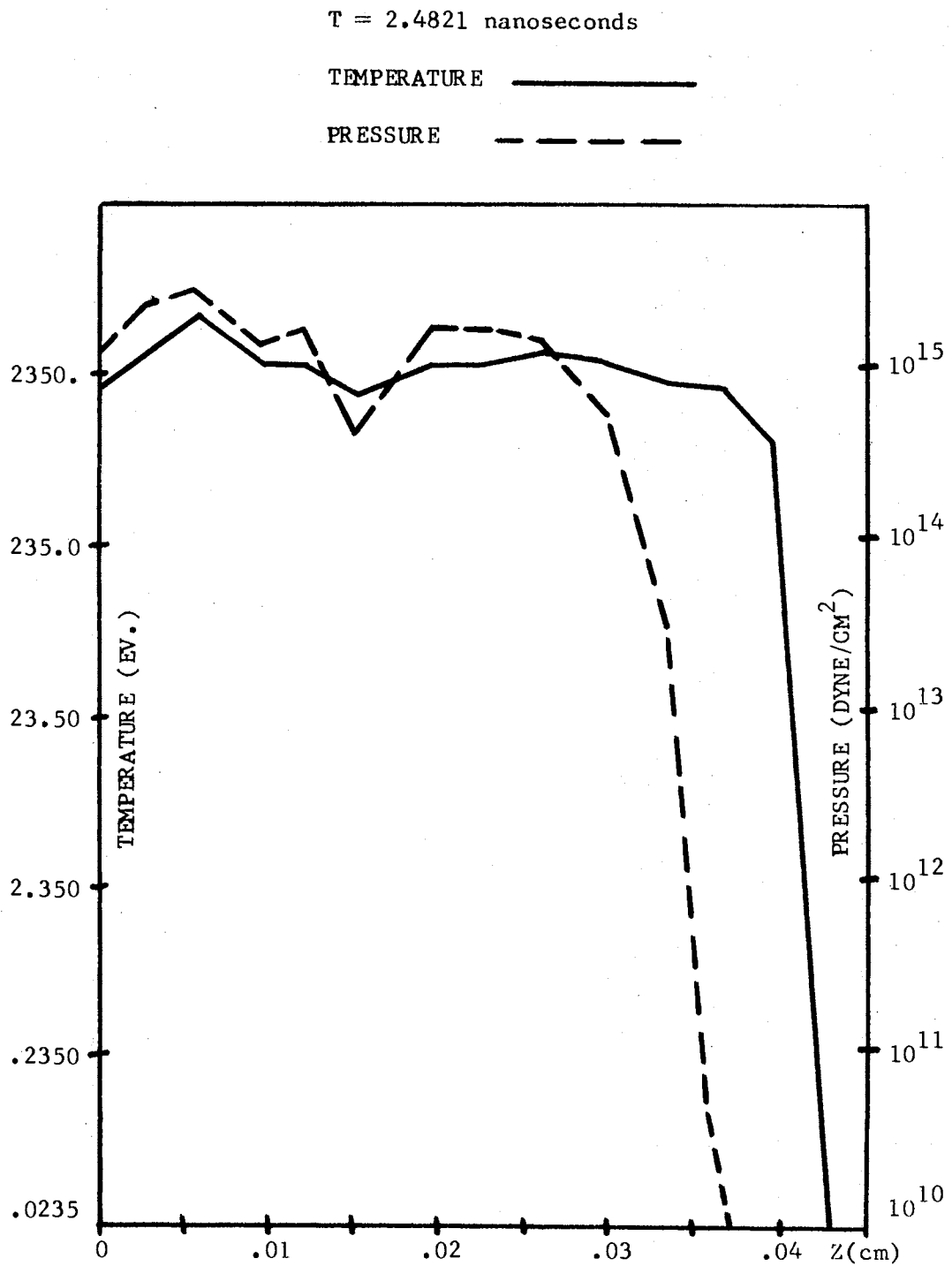


Figure 53. Variation of Pressure and Temperature along Radiation Axis

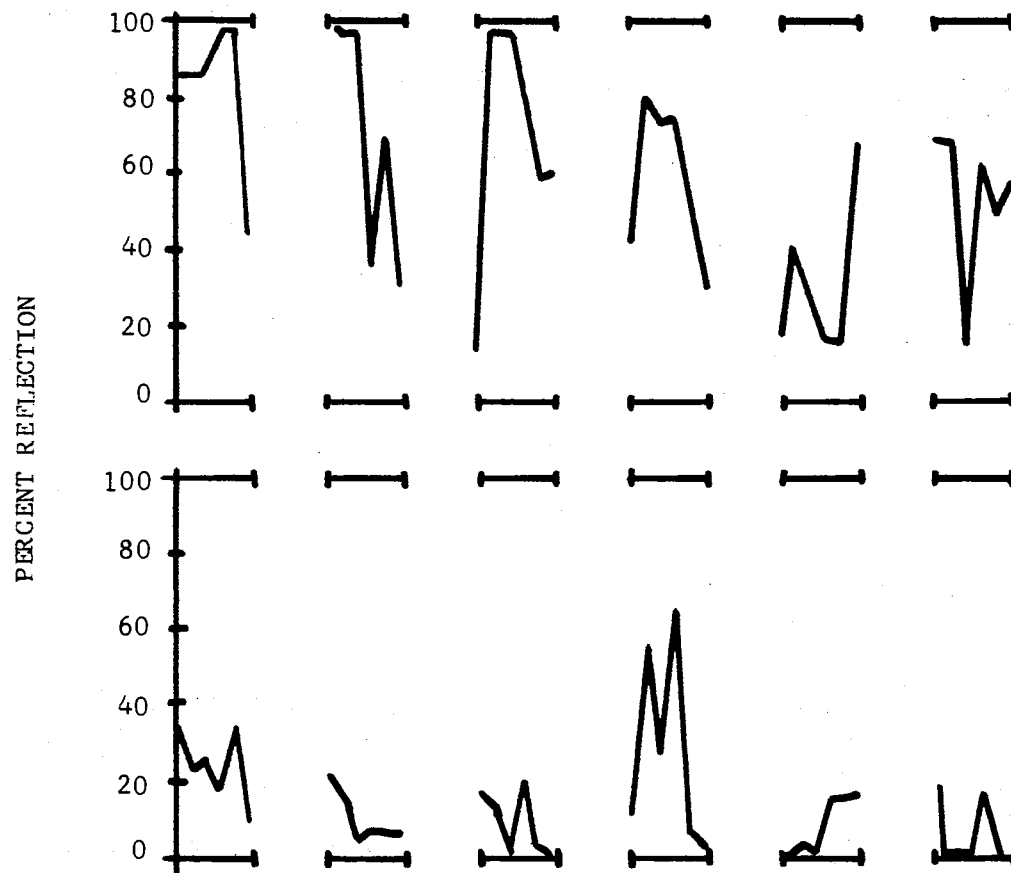


Figure 54. Fluctuations of Laser Beam Reflection Over Time Intervals at Start and End of Run

nanoseconds.

One of the interesting features of the curves, shown in Figure 50 and Figure 52, is seen in the behavior of the mass density. As the laser beam is absorbed by the aluminum target material, the mass begins to vaporize from the target surface. The mass density, rather than decreasing continuously to a gaseous state, indicates that the aluminum atoms and ions leave the surface in fairly dense pulses. The breaks in the mass density curve indicate that the particles are ejected from the surface in groups of varying density.

This phenomenon has been observed in the laboratory experiments. Several of the data taken with the quadrupole mass filter on the laser induced plasmas exhibit this same type of mass density variation. The twin ruby laser was employed to produce an aluminum plasma, in the configuration shown in Figure 55. The aluminum ions, metastable atoms and u.v. photons were monitored with the mass filter, as shown. An example of the data produced by this system is presented in Figure 56. The curve in this figure represents the electron multiplier detector output signal in response to Al^{+3} ions, metastable atoms and light. The dotted curve represents the trace which was photographed directly from the oscilloscope screen. The solid curves represent the resolved peaks of the original curve. The relatively steep decrease in amplitude at the extreme left of Figure 56 is interpreted to be the decay of the u.v. light emission from the laser impact plasma. For this data, the detector response to the u.v. light was taken to establish zero time. From the resolved peaks of Figure 56, it is evident that the Al^{+3} ions and metastable atoms reach the detector in discrete velocity groups. It is interesting to consider the mechanism respons-

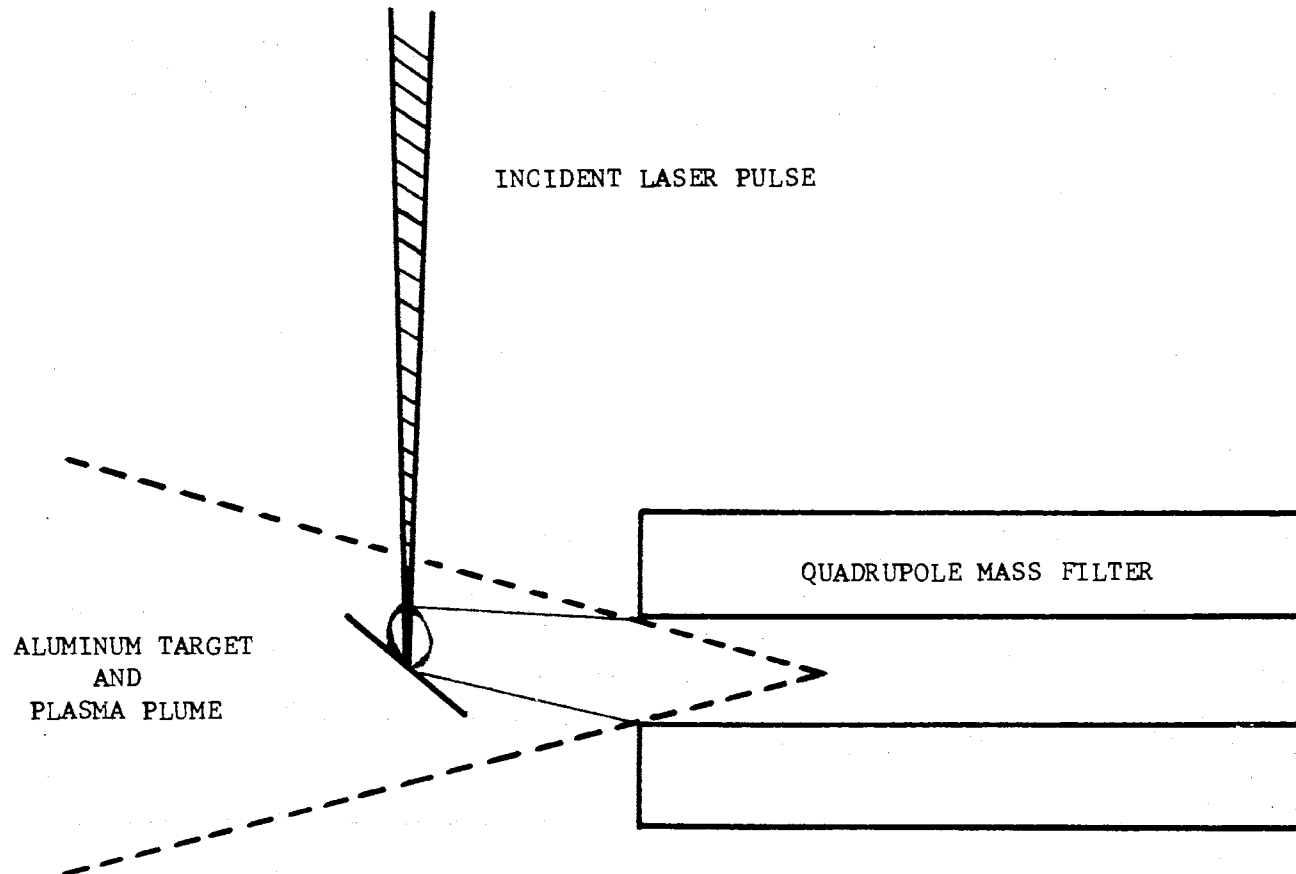


Figure 55. Laser Impact Plasma - Quadrupole Geometry

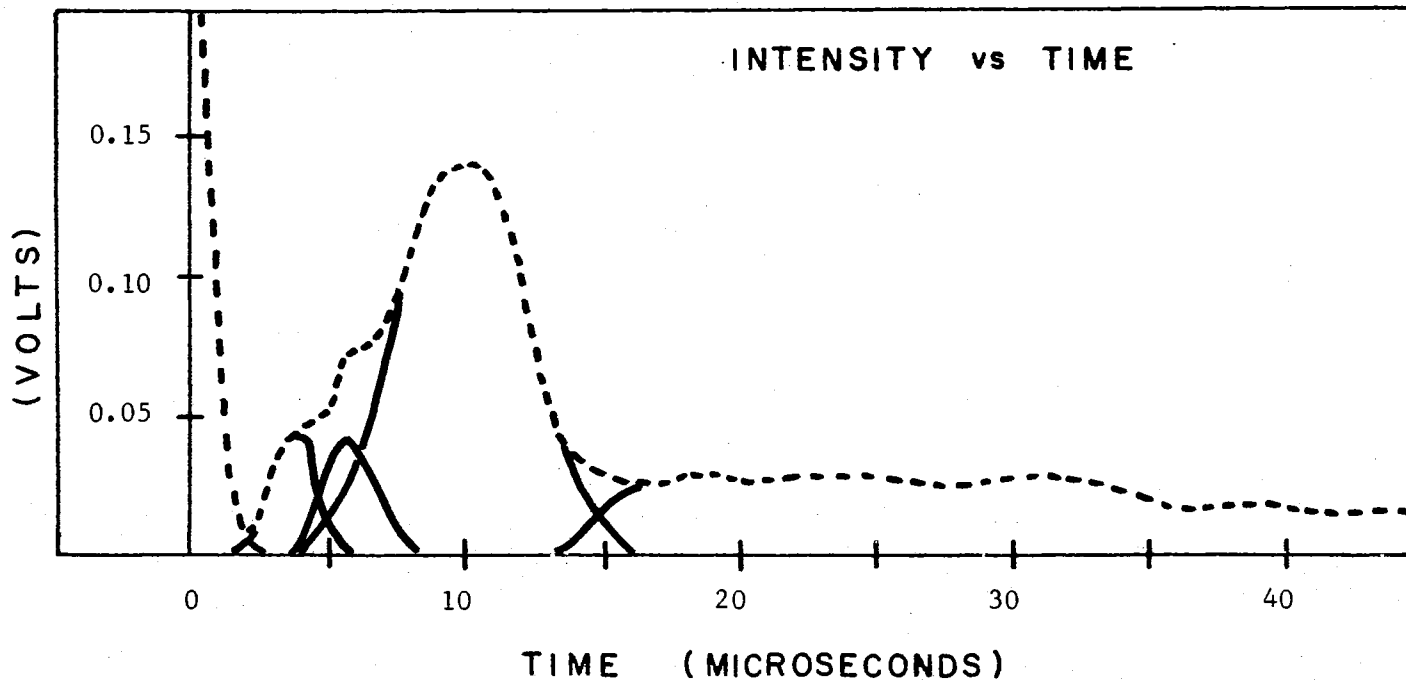


Figure 56. Al^{+3} Ions, Metastable Atoms and U.V. Light Emission from Laser Induced Plasma

ible for this phenomenon. One tentative explanation for the discrete nature of the velocity distributions is now offered.

Consider the following possibility when the incident laser pulse first reaches the target interface, sufficient energy is absorbed by the surface layer atoms to escape in the form of a gaseous shock front. This phenomenon must occur in the first few nanoseconds. Much of the subsequent laser radiation is absorbed exponentially by the expanding plasma. In this manner, additional energy is gained by the vanguard of the shock front which is propagating into vacuum. This would result in some of the ions moving ahead of the initial shock front, depending on the energy increase due to absorption. This process, of course, must conform with momentum conservation, so that the group of ions which move out with additional velocity, must necessarily be less massive than the group that remains behind in the break up. This means that there are fewer ions in the leading group. If the laser radiation continues to be incident on the target area, it might be assumed that it is not unfeasible for the faster velocity group to absorb more energy and break up into still smaller groups. Here again the forefront group of ions, having gained additional velocity, is less massive, i.e., there are fewer ions in the group.

The resolved peaks presented in Figure 56 illustrate the faster, smaller peaks and the slower, larger peaks. While several of the data seems to bear out the hypothesis discussed above, other data shows irregularities which need to be investigated further, in light of target geometry, turbulence and the possible effects of material defects in the aluminum target plate.

The encouraging similarity between the theoretical predictions

and the experimental data illustrates the effectiveness of the computer model for this one case.

Expanding Plasma Sphere Data

The computer model for an expanding plasma sphere was discussed in Chapter VI. The flow equations and the basic computer techniques, which are employed to solve these equations, were presented. A description of the program elements is provided in Appendix C, along with a machine listing of a typical program. The data which is presented in this section were obtained from a very short, trial computer run. Although a production run has not yet been made with this model, the results of the trial runs will serve to illustrate the type of solutions which can be expected from the model.

For the trial run, which is discussed in this section, the initial conditions of the model are now given. A total of 50 radial mesh cells was chosen, with 25 of the cells filled with aluminum at solid density. The remaining 25 cells were assigned vacuum values. The initial size of each cell was chosen to be 1.0×10^{-4} centimeters. This corresponds to an initial volume of 6.54×10^{-8} cubic centimeters and a total mass of 1.77×10^{-7} grams. The initial, internal energy density was chosen to be 1.81×10^{11} ergs/gram, which is equivalent to an energy of 5.07 eV. per atom. The total initial, internal energy of the aluminum sphere is then, 3.20×10^4 ergs. This corresponds to an initial temperature of 2.0 eV.

From the equation of state for aluminum, the initial relative ionization was determined to be 3 electrons per atom and the initial pressure was given, 2.57×10^{12} dynes per cubic centimeter. An

initial time increment of 1.0×10^{-10} seconds was chosen to begin the plasma evolution.

The curves which are presented here illustrate the variation with time of the mass density, as the plasma expands. Although, all of the flow variables are monitored each cycle, the mass density variation gives a good indication of whether or not the program is proceeding correctly.

This variable may be compared with the evolution of the other plasma variables to give an indication that their values are reasonable and that they do not violate the conservation laws. For example, a high value for the temperature at a point in the grid where the mass is known to be zero, would indicate that the calculations for the temperature need revisions. There are, of course, many other comparisons with the other flow variables which provide a check on the feasibility of the computer solution.

A special subroutine was designed and incorporated into the program to provide a real-time check on all the variables. This check-out routine not only monitors the variables to note any improper values, but is programmed to actually reset a variable value which has reached an unreasonable limit. An example of the function of this routine is given. Suppose the flow velocity is calculated at a point in time, to be a value which exceeds the speed of light. The check-out routine will notice this unreasonable value, and reset it to a value which is consistent with the values of the other variables at that point. Provision is also made in this routine to monitor the values of such variables as the temperature, pressure, internal energy, etc. to insure that they are maintained at values




which are consistent with the equation of state.

The model may be programmed to abort, if unfeasible limits are reached for which no real-time correction can be made.

With the above discussion in mind, the first 15 cycles of a trial run are presented. The curves in Figure 57 show the evolution of the plasma mass density for the first 3 time increments. The initial time increment was given above as 1.0×10^{-10} seconds. The subsequent time intervals, which are shown on each graph, were calculated by the computer to be consistent with the Courant condition.

The curves in Figure 58 and Figure 59 represent the variation in mass density for the next six time cycles. The curves in Figure 60 through Figure 62 show the remaining time cycles of the total of 15 presented here. The significant feature of this trial run, as depicted by the curves which have been presented, is that the computer model "flows" in a manner which is expected. The nature of the density variations at the interface is in good agreement with the previous work on this type of model.

Since no production run has yet been attempted with the model, no quantitative conclusions are presented at this time. However, the qualitative agreement, of the preliminary computer solutions for this model, with solutions from previous models, and with experiment, indicate that the basic framework of the model is sound. This model is presented here as a basic theoretical tool, and not an end result, in itself. It provides a boundary value program which, with some modification and implementations, may be employed to investigate a large variety of plasma expansion problems. The equation of state for the model was developed for aluminum, but the model is suf-

$T_1 = 1.0000 \times 10^{-10}$ seconds 
 $T_2 = 1.0008 \times 10^{-10}$ seconds 
 $T_3 = 1.0016 \times 10^{-10}$ seconds 

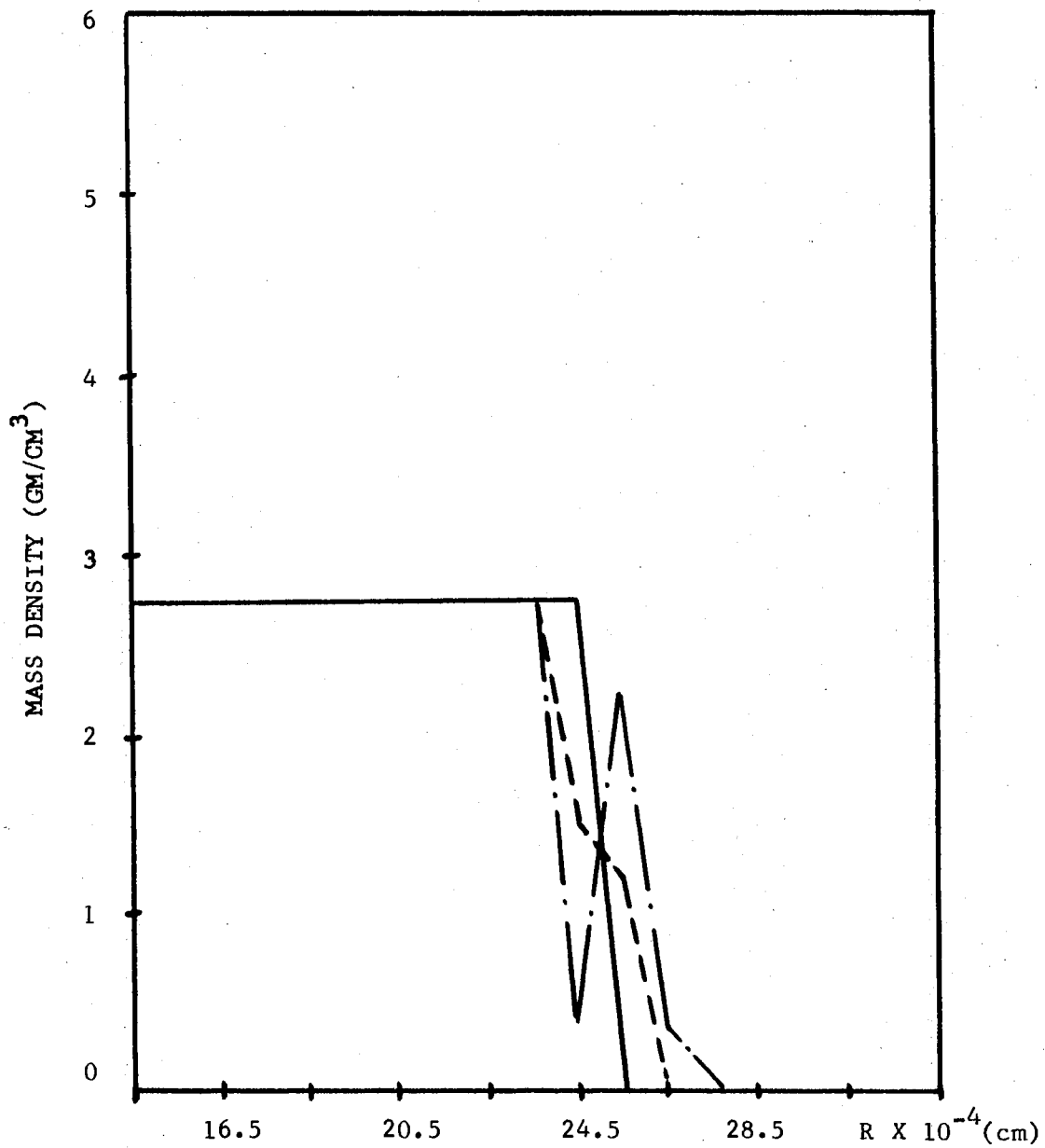


Figure 57. Variation of Mass Density along the Plasma Sphere Radius (Cycles 1-3)

$$T_4 = 1.0025 \times 10^{-10} \text{ seconds} \quad \text{—————}$$

$$T_5 = 1.0033 \times 10^{-10} \text{ seconds} \quad \text{- - - - -}$$

$$T_6 = 1.0041 \times 10^{-10} \text{ seconds} \quad \text{- . - . - .}$$

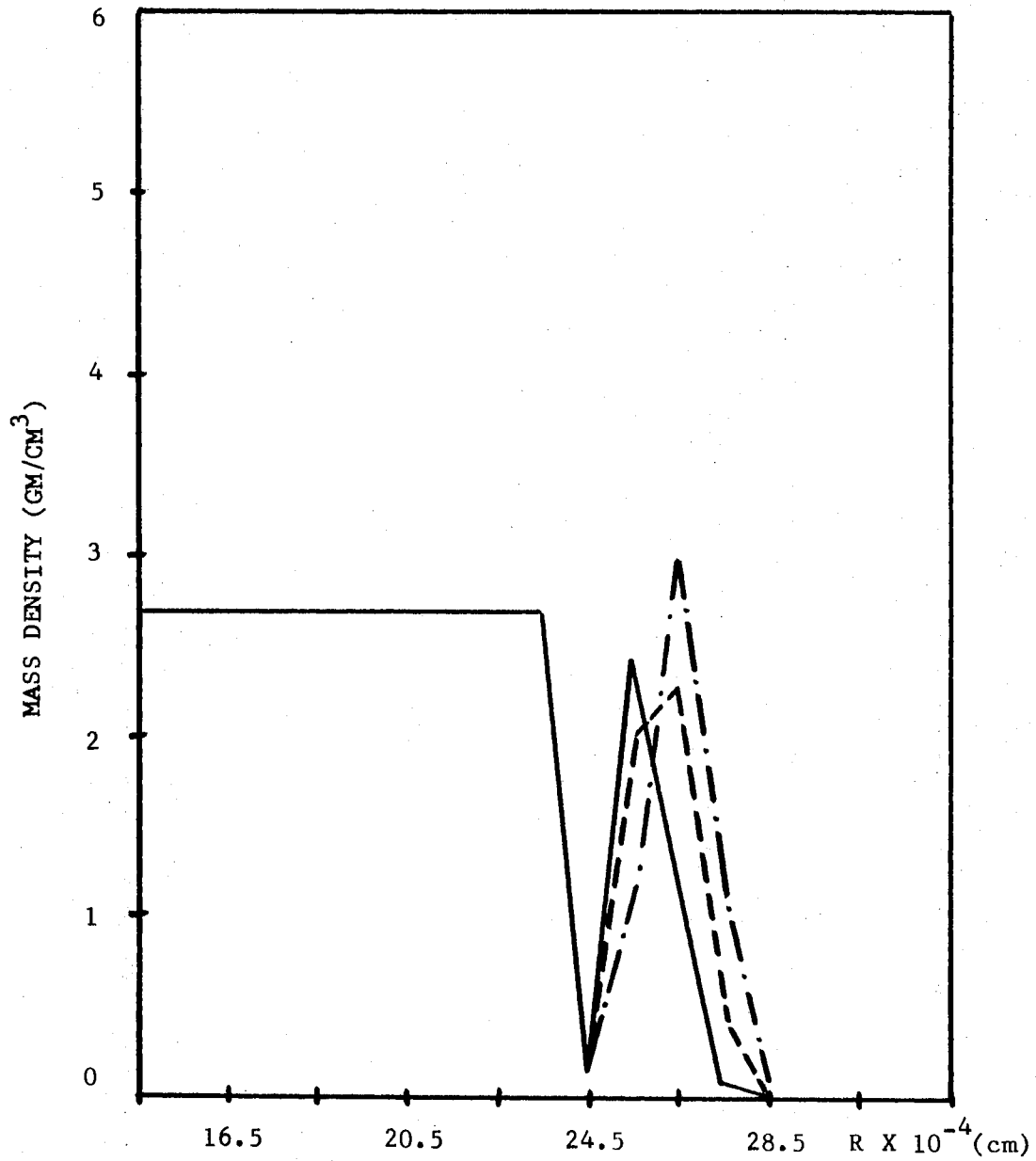





Figure 58. Variation of Mass Density along the Plasma Sphere Radius (Cycles 4-6)

$T_7 = 1.0049 \times 10^{-10}$ seconds 
 $T_8 = 1.0057 \times 10^{-10}$ seconds 
 $T_9 = 1.0065 \times 10^{-10}$ seconds 

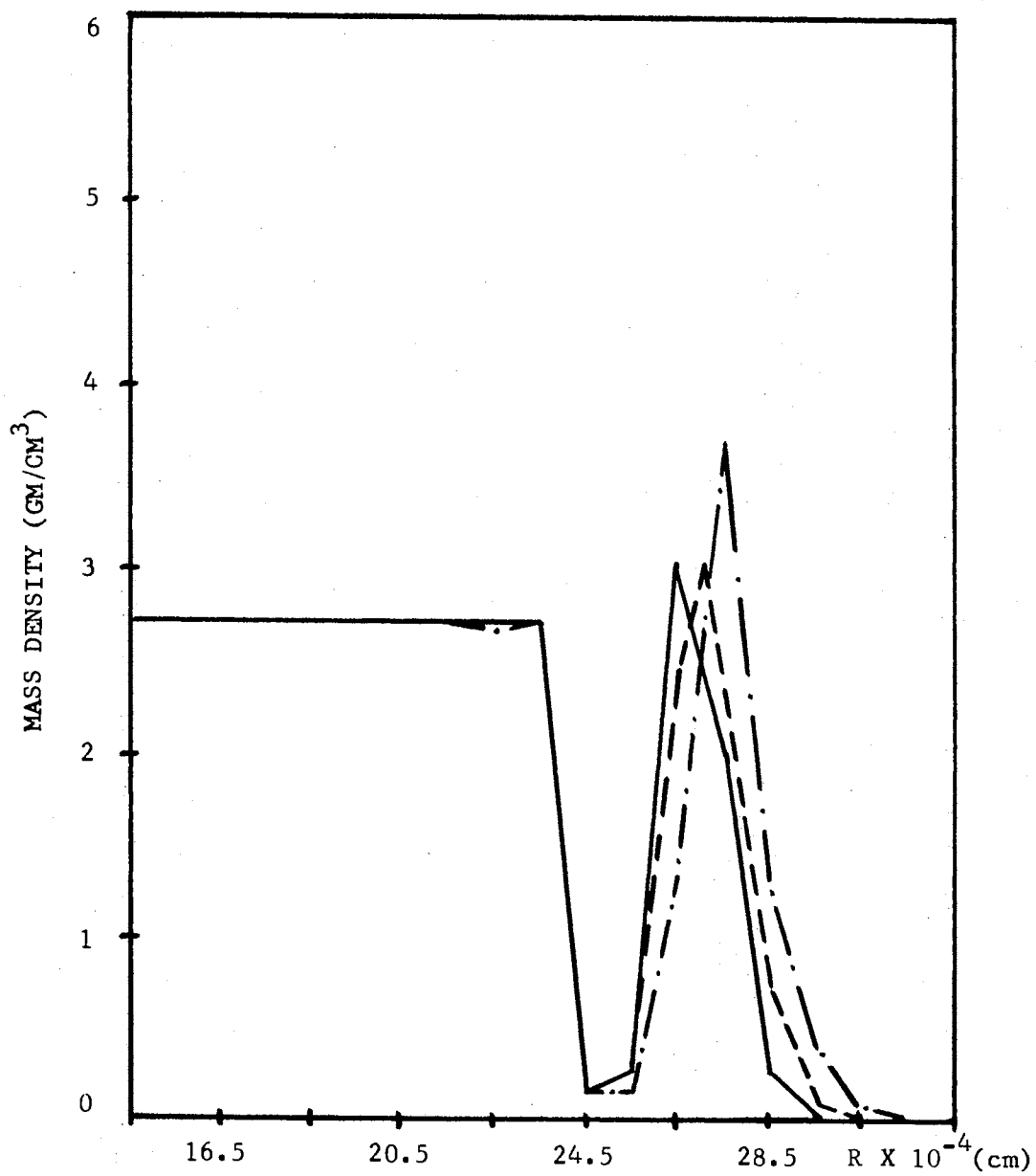


Figure 59. Variation of Mass Density along the Plasma Sphere Radius (Cycles 7-9)

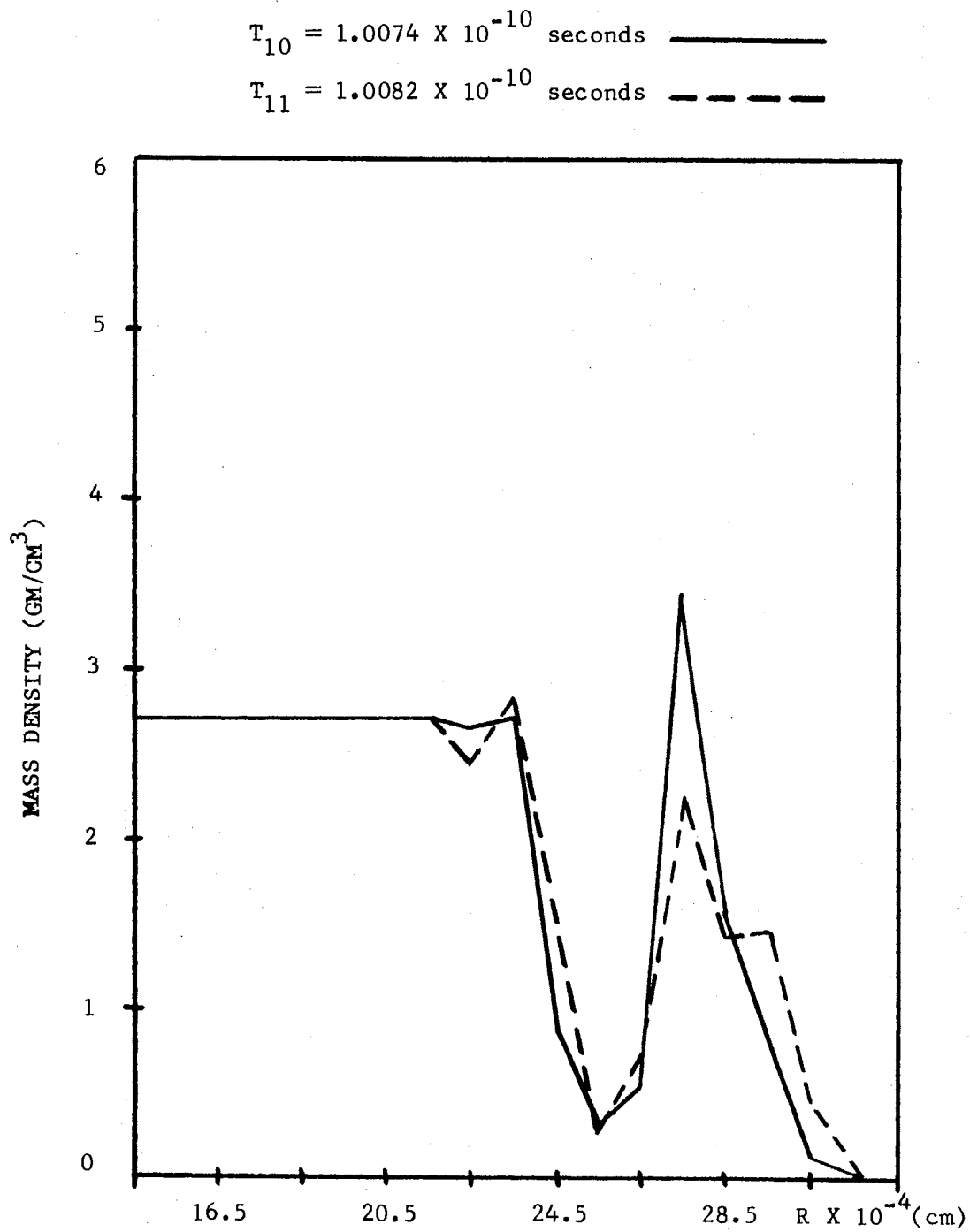


Figure 60. Variation of Mass Density along the Plasma Sphere Radius (Cycles 10-11)

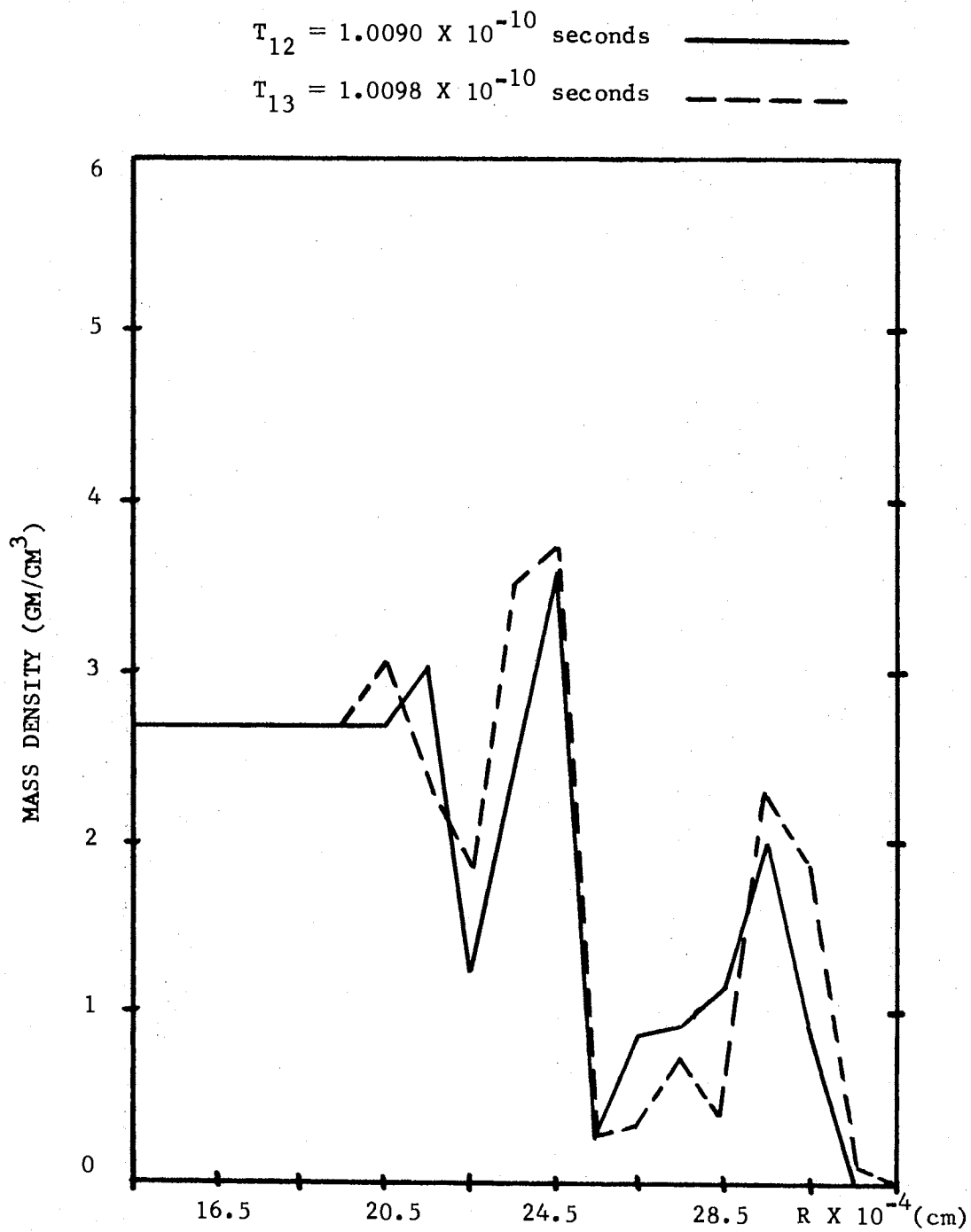


Figure 61. Variation of Mass Density along the Plasma Sphere Radius (Cycles 12-13)

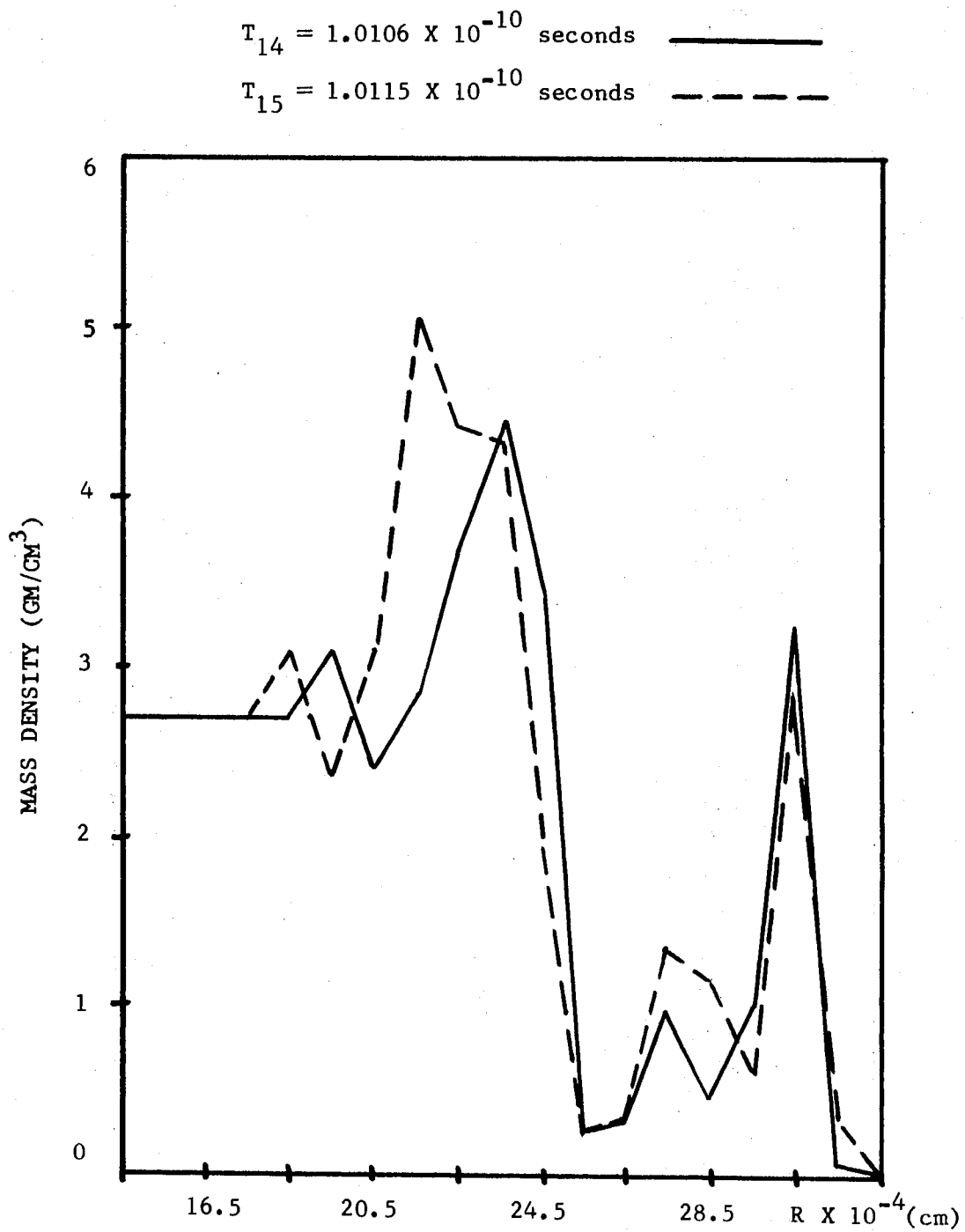


Figure 62. Variation of Mass Density along the Plasma Sphere Radius (Cycles 14-15)

ficiently flexible to accommodate equations of state for other materials. The variety of initial conditions, which may be set for the boundary values of the computer model, are limited only by the restriction that they be consistent with the equation of state for the model.

CHAPTER VIII

SUMMARY AND CONCLUSIONS

Introduction

The purpose of this chapter is to briefly summarize the areas of research, which were presented in the previous chapters. The results of the four major areas of study were presented in Chapter VII. A general summary of the overall program of research is presented below.

General Summary

For the study of dense, transient aluminum plasmas, two experimental devices were developed. These are the quadrupole mass filter and the electrostatic lens. The quadrupole mass filter was employed to monitor the emission of aluminum ions, metastable atoms and u.v. light from the plasma, which is produced by the vacuum spark. The quadrupole data, which was presented in the previous chapter, was obtained with an improved quadrupole system. The major modifications, which were discussed in Chapter III, include the addition of a regulated power supply and a crystal to control the frequency of the r.f. voltage, which is applied to the quadrupole rods.

The electrostatic lens was designed and constructed to eliminate the neutral atoms and u.v. light from the beam of particles, which

emanates from the vacuum spark plasma, and is detected by the electron multiplier of the quadrupole system. One of the most significant results of the experiments with the electrostatic lens is the indication of individual ionic velocity distributions. From an analysis of the data, obtained with both the quadrupole and the electrostatic lens, a better understanding, of the method in which the vacuum spark plasma is produced, was achieved.

The initial results of a trial production run were presented, in Chapter VII, for the laser impact plasma model. Typical examples of the data were presented to illustrate the evolution of the plasma variables. The plasma, which is produced by the incidence of a giant laser pulse, is simulated by the computer model. The creation and subsequent expansion of the laser induced plasma were illustrated by the curves, which were presented for two different times in the production run.

The expanding plasma sphere model, which was discussed in Chapter VI, was developed as a boundary value model. This theoretical approach to the problem of transient plasmas was employed by previous members of this research group. The present model, which is described in this thesis, was developed to include an improved equation of state for aluminum. Other basic advantages, which the present model contains over the previous models, include the addition of program elements, such as the check-out routine, and the incorporation of a computerized method of data output and reduction. The oscillational energy, which was neglected in the previous spherical model, was included in the present model. In addition, a provision was included, in the present computer model, for the calculation of

pressure induced currents in the plasma. These calculations are based on plasmon theory and are discussed in Appendix B. One of the most interesting research areas, in which the spherical plasma model should prove to be useful, is the experimental work with the exploding wire.

Recommendations for future Improvements

This section is divided into two parts. In the first part of this section suggestions are offered for improvements which could be made in the experimental research. The second part is devoted to possible improvements in the theoretical research.

Experimental Research

One improvement to the quadrupole mass filter experiment would be the calibration of the electron multiplier detector. A prerequisite to such a calibration, is the availability of a reproducible, ion source. With a calibrated detector, a quantitative analysis could be made for the relative abundance of each ionic specie. The multiple velocity peaks, which were shown in both the quadrupole data and electrostatic lens data, were attributed to a possible mechanism by which the breakdown of the spark gap occurs. Briefly, it is thought that the multiple peaks result from spark migration, when the electrodes have become worn. An experiment could be made to determine if multiple velocity peaks still exist in the data, immediately after the aluminum electrodes have been ground to a point, and polished.

Improvements, which may be made to the electrostatic lens

system, include the use of a calibrated detector, a modified spacing arrangement for the lens electrodes, and a more reliable time delay. The need for a calibrated detector was discussed above. The vertical separation, between the positive lens electrodes and the ground plate, is 4.0 cm. If this separation were decreased to 2.0 cm, for example, then the voltages, required for the lens electrodes to maintain the same electric field strength, would be decreased by a factor of two. This would decrease the problem with electric field fringing, and would possibly eliminate the need for a pulse amplifier, which contributes several nanoseconds to the rise time of the pulse.

Theoretical Research

The number of refinements which could be made to most any theoretical research is practically unlimited. The computer models for both the laser impact plasma and the expanding plasma sphere are in a constant state of revision. As additional experimental evidence is obtained for the properties of the plasmas, which are produced in the laboratory, the computer models are revised to be consistent with the experimental data.

There are a few general areas in which basic improvements could be made to the existing models. These are briefly discussed below. The mechanism of radiative transfer has been neglected and should be included in both models. A better technique could possibly be developed to overcome the difficulty involved with the small mesh size and the Courant condition. For very small cell dimensions, the time intervals which satisfy the Courant condition, are too small to be

practical. One final improvement is suggested. There should be a provision in the computer programs to check the conservation of mass. The procedure for redoubling the mesh for both of the models could be modified to provide this check. With the current redouble procedure, it is possible that additional mass is introduced into the problem, each time the redouble procedure is used. A subroutine could be written which will monitor the mass density in each mesh cell, so that no violation of the conservation of mass can occur.

SELECTED BIBLIOGRAPHY

- Ables, J. G. "A computer Solution for a Spherically Exploding Plasma." (unpublished M. S. thesis, Oklahoma State University, 1963).
- Allen, James S. "The Detection of Single Positive Ions, Electrons and Photons by a Secondary Electron Multiplier." Physical Review, Vol. 55 (1939) pp. 966-971.
- Basov, N. G. et. al. "Heating and Decay of Plasma Produced by a Giant Laser Pulse Focused on a Solid Target." Soviet Physics JETP, Vol. 24, No. 4 (1967) p. 659.
- Brown, Vernon D. and F. C. Todd. "Use of a Pulsed Photomultiplier to Measure the Light Intensity versus Time for a Spark Discharge Between Aluminum Electrodes." (unpublished Ph.D. dissertation, Oklahoma State University, 1968).
- Brubaker, W. M. and J. Tuul. "Performance Studies of a Quadrupole Mass Filter." Rev. Sci. Inst., Vol. 35 (1964) pp. 1007-1010.
- Bruce, R. E. "A Model and Calculations for the Properties of an Exploding Plasma Sphere." (unpublished Ph.D. dissertation, Oklahoma State University, 1966).
- Bykovski, Y. A. et. al. "Mass Spectrometer Investigation of Ions Formed by Interaction Between Laser Radiation and Matter." Soviet Physics - Technical Physics, Vol. 13, No. 7 (1969) p. 986.
- Carpenter, T. M. "Calibration of a Far Ultraviolet Spectrograph and a Study of Vacuum Spark Breakdown." (unpublished M. S. report, Oklahoma State University, 1970).
- Compton, K. T. and Irving Langmuir. "Electrical Discharges in Gases." Review of Modern Physics, Vol. II (April, 1930).
- David, C. et. al. "7A9-Density and Temperature of a Laser Induced Plasma." IEEE Journal of Quantum Electronics, Vol. qe-2, No. 9 (1966) p. 493.
- Dawson, P. H. and N. R. Whetten. "Quadrupoles, Monopoles and Ion Traps." Research and Development, (February, 1968) pp. 46-50.

- Ehler, A. W. "Plasma formed by a Laser Pulse on a Tungsten Target." Journal of Applied Physics, Vol. 37, No. 13 (1966) p. 4962.
- Fenner, N. C. "Ion Energies in the Plasma Produced by a High Power Laser." Physics Letters, Vol. 22, No. 4 (1966) p. 421.
- Fisher, H. "Erosion Jets: Newly Observed Phenomenon." Research Review, Vol IV, No. 11 (1966) p. 7.
- Gartenhaus, Solomon. Elements of Plasma Physics. New York: Holt, Rinehart and Winston, 1964.
- Gunther, Karl-Georg. "A Partial Pressure Vacuum Gauge Working According to the Principle of the Electrical Mass Filter." Vacuum, Vol. 10 (1960) pp. 293-308.
- Hamby, H. G. (Private Communication, 1970).
- Hardage, B. A. "Hypervelocity Impact with Flow and Shock Penetration Through Fluid, Plastic and Elastic Zones." (unpublished Ph.D. dissertation, Oklahoma State University, 1967).
- Hastie, J. W. and D. L. Swingler. "Use of the Quadrupole Mass Filter for High Temperature Studies." High Temperature Science, Vol. 1 (1969) p. 46.
- Hellund, E. J. The Plasma State. New York: Reinhold Publishing Corporation, 1961.
- Holt, E. H. and R. E. Haskell. Foundations of Plasma Dynamics. New York: The Macmillan Company, 1965.
- Honig, R. E. and J. R. Woolston. "Laser-Induced Emission of Electrons, Ions, and Neutral Atoms from Solid Surfaces." Applied Physics Letters, Vol. 2, No. 7 (1963) p. 138.
- Jackson, J. D. Classical Electrodynamics. New York: John Wiley and Sons, Inc., 1962.
- Jones, D. S. The Theory of Electromagnetism. New York: Pergamon Press, 1964.
- Kittel, C. Introduction to Solid State Physics. New York: John Wiley and Sons, Inc., 1968.
- Kramer, N. D. and H. J. King. "Extraction of Dense Ion Beams from Plasmas." Journal of Applied Physics, Vol. 38, No. 10 (1967) p. 4019.
- Langer, P. et. al. "Laser Induced Emission of Electrons, Ions, and X-Rays from Solid Targets." IEEE Journal of Quantum Electronics, Vol. qe-2, No. 9 (1966) p. 499.

- Langmuir, I. and L. Tonks. Physical Review, Vol. 33 (1929) pp. 195, 990.
- Linlor, W. I. "Some Properties of Plasma Produced by Laser Giant Pulse." Physics Review Letters, Vol. 12 No. 14 (1964) p. 383.
- Linlor, W. I. "Ion Energies Produced by Laser Giant Pulse." Applied Physics Letters, Vol. 3, No. 11 (1963) p. 210.
- Lubin, M. J. "Laser-Induced Plasmas for Power Generation and Space Propulsion." Astronautics and Aeronautics, Vol. 8, No. 11 (1970) pp. 42-48.
- McCormick, J. M. and M. G. Salvadori. Numerical Methods in Fortran. New Jersey: Prentice-Hall, Inc., 1965.
- McCracken, D. D. and W. S. Dorn. Numerical Methods and Fortran Programming. New York: John Wiley and Sons, Inc., 1964.
- McLachlan, N. W. Theory and Application of Mathieu Functions. New York: Dover Publications, Inc., 1964.
- Malmstadt, H. V. and C. G. Enke. Electronics for Scientist. New York: W. A. Benjamin, Inc., 1962.
- Mosharrafa, M. and H. J. Oskam. "Design and Construction of a Mass-Spectrometer for the Study of Basic Processes in Plasma Physics." (Tech. Rep. No. 2, AD-274249, University of Minnesota, 1961).
- Mulser, P. and S. Witkowski. "Numerical Computation of the Production of a Dense Plasma by Irradiation of a Solid by a Laser." (Report IPP 3/74, Institut fur Plasmaphysik, 1968).
- Norgren, Carl T. et. al. Colloid Thrustor Beam Analysis; Design and Operation of a Suitable Quadrupole Mass Filter. Lewis Research Center, NASA TN D-3036, Cleveland, Ohio, 1965.
- Paul, W. and M. Raether. "Das Electriche Massenfilter." Zeit. fur Phys., Vol. 140 (1955) pp. 262-273.
- Paul, W. and H. Steinwendel. "Ein Neues Massenspektrometer ohne Magnetfeld." Zeit. Naturforschg, Vol. 82 (1953).
- Payne, R. D. and F. C. Todd. "A Spectrograph for the Far Ultraviolet," Proc. Okla. Acad. Sci., Vol. 46 (1966) pp. 115-121.
- Peery, L. J. "A Model and Calculations for Laser Induced Plasmas." (unpublished Ph.D. dissertation, Oklahoma State University, 1970).
- Peery, L. J. "Design and Construction of a Twin Ruby Laser." (unpublished M. S. thesis, Oklahoma State University, 1967).

- Ready, J. F. "Development of a Plume of Material Vaporized by a Giant Pulse Laser." Applied Physics Letters, Vol. 3, No. 1 (1963) p. 11.
- Ready, J. F. "Effects Due to Absorption of Laser Radiation," Journal of Applied Physics, Vol. 36, No. 2 (1965) p. 462.
- Robinson, W. G. "Modification and Design of a Twin Ruby, Q-switched Laser for Plasma Production." (unpublished M. S. thesis, Oklahoma State University, 1970).
- Sauter, G. F., R. A. Gerber and H. J. Oskam. "Technique for Simultaneously Measuring Ion Densities, Metastable Atom Densities, and Light Emission in Decaying Gaseous Plasmas." Rev. of Sci. Instr., Vol. 37, No. 5 (1966) p 572.
- Schmidt, C. "A Quadrupole Energy Filter." Rev. of Sci. Instr., Vol. 41 (1970) p. 117.
- Shriver, E. L. (Private Communication, 1970).
- Sodek, B. A. "A Hydrodynamic Model of Micrometeroid Impact." (unpublished Ph.D. dissertation, Oklahoma State University, 1965).
- Willis, H. W. "Quadrupole Mass Filter Design and Construction for Plasma Ion Analysis." (unpublished M. S. thesis, Oklahoma State University, 1969).
- Woodward, C. E. and C. K. Crawford. "Design of a Quadrupole Mass Spectrometer." (Tech. Rep. No. 176, NP-12543, Mass. Inst. of Tech., 1963).
- Yoder, J. A. "Theory, Design and Performance of a Coaxial, Exploding Wire System." (unpublished M. S. thesis, Oklahoma State University, 1970).

APPENDIX A

DERIVATION OF VISCOUS TERMS

In this section, the viscous terms for the flow equations are derived. These terms were included in the conservation of momentum and energy equations for the expanding plasma sphere model in Chapter VI. The viscous effects are defined in cartesian coordinates and are then transformed to the spherical geometry required by the model. The derivation begins with the viscous stress tensor which was defined in Equation (5.4) and is employed in Equations (6.7) and (6.8).

$$\pi^{ij} = \mu \left(\frac{\partial u^i}{\partial x^j} + \frac{\partial u^j}{\partial x^i} \right) - \frac{2}{3} \mu \frac{\partial u^k}{\partial x^k} \delta^{ij} \quad (\text{A-1})$$

The terms of this tensor may then be written in cartesian form.

$$\pi^{11} = \mu \left(2 \frac{\partial u_x}{\partial x} \right) - \frac{2}{3} \mu (\vec{\nabla} \cdot \vec{u}) \quad (\text{A-2})$$

$$\pi^{12} = \mu \left(\frac{\partial u_x}{\partial y} + \frac{\partial u_y}{\partial x} \right) \quad (\text{A-3})$$

$$\pi^{13} = \mu \left(\frac{\partial u_x}{\partial z} + \frac{\partial u_z}{\partial x} \right) \quad (\text{A-4})$$

$$\pi^{21} = \mu \left(\frac{\partial u_y}{\partial x} + \frac{\partial u_x}{\partial y} \right) \quad (\text{A-5})$$

$$\pi^{22} = \mu \left(2 \frac{\partial u_y}{\partial y} \right) - \frac{2}{3} \mu (\vec{\nabla} \cdot \vec{u}) \quad (\text{A-6})$$

$$\pi^{23} = \mu \left(\frac{\partial u_y}{\partial z} + \frac{\partial u_z}{\partial y} \right) \quad (\text{A-7})$$

$$\pi^{31} = \mu \left(\frac{\partial u_z}{\partial x} + \frac{\partial u_x}{\partial z} \right) \quad (\text{A-8})$$

$$\pi^{32} = \mu \left(\frac{\partial u_z}{\partial y} + \frac{\partial u_y}{\partial z} \right) \quad (\text{A-9})$$

$$\pi^{33} = \mu \left(2 \frac{\partial u_z}{\partial z} \right) - \frac{2}{3} \mu (\vec{\nabla} \cdot \vec{u}) \quad (\text{A-10})$$

The equations above must now be transformed to spherical coordinates. The components of the flow velocity, u^i , are given below.

$$\begin{aligned} u_x &= u_r \sin \theta \cos \varphi \\ u_y &= u_r \sin \theta \sin \varphi \\ u_z &= u_r \cos \theta \end{aligned} \quad (\text{A-11})$$

The differential operators for spherical coordinates are given.

$$\frac{\partial}{\partial x} = \frac{\partial r}{\partial x} \frac{\partial}{\partial r} + \frac{\partial \theta}{\partial x} \frac{\partial}{\partial \theta} + \frac{\partial \varphi}{\partial x} \frac{\partial}{\partial \varphi} \quad (\text{A-12})$$

$$\frac{\partial}{\partial y} = \frac{\partial r}{\partial y} \frac{\partial}{\partial r} + \frac{\partial \theta}{\partial y} \frac{\partial}{\partial \theta} + \frac{\partial \varphi}{\partial y} \frac{\partial}{\partial \varphi} \quad (\text{A-13})$$

and

$$\frac{\partial}{\partial z} = \frac{\partial r}{\partial z} \frac{\partial}{\partial r} + \frac{\partial \theta}{\partial z} \frac{\partial}{\partial \theta} + \frac{\partial \varphi}{\partial z} \frac{\partial}{\partial \varphi} \quad (\text{A-14})$$

These operators are simplified to the following forms because of the assumption of spherical symmetry.

$$\frac{\partial}{\partial x} = \sin \theta \cos \varphi \frac{\partial}{\partial r} + \cos \theta \cos \varphi \frac{1}{r} \frac{\partial}{\partial \theta} - \frac{\sin \varphi}{\sin \theta} \frac{1}{r} \frac{\partial}{\partial \varphi} \quad (\text{A-15})$$

$$\begin{aligned} \frac{\partial}{\partial y} &= \sin \theta \sin \varphi \frac{\partial}{\partial r} + \cos \theta \sin \varphi \frac{1}{r} \frac{\partial}{\partial \theta} \\ &\quad - \sin \theta \frac{1}{r^2} \frac{\partial}{\partial \varphi} \end{aligned} \quad (\text{A-16})$$

$$\frac{\partial}{\partial z} = \cos \theta \frac{\partial}{\partial r} - \sin \theta \frac{1}{r} \frac{\partial}{\partial \theta} \quad (\text{A-17})$$

and

$$\vec{\nabla} \cdot \vec{u} = \frac{1}{r^2} \frac{\partial}{\partial r} (r^2 u_r) = \frac{\partial u_r}{\partial r} + \frac{2u_r}{r} \quad (\text{A-18})$$

Conservation of Momentum

The relation expressing momentum conservation is the equation of motion. The terms of this equation are vector quantities. The components of the viscous force vector which appear in this equation are now given.

$$F^i = \frac{\partial \pi^{ij}}{\partial x^j} \quad (\text{A-19})$$

$$F^x = \frac{\partial \pi^{11}}{\partial x} + \frac{\partial \pi^{12}}{\partial y} + \frac{\partial \pi^{13}}{\partial z} \quad (\text{A-20})$$

$$F^y = \frac{\partial \pi^{21}}{\partial x} + \frac{\partial \pi^{22}}{\partial y} + \frac{\partial \pi^{23}}{\partial z} \quad (\text{A-21})$$

$$F^z = \frac{\partial \pi^{31}}{\partial x} + \frac{\partial \pi^{32}}{\partial y} + \frac{\partial \pi^{33}}{\partial z} \quad (\text{A-22})$$

Now consider Equation (A-22). This equation expresses the z-component of the viscous force. The radial viscous force term may be rewritten in the following form.

$$F^z = F^r \cos \theta \quad (\text{A-23})$$

With the appropriate differentiation, Equation (A-22) is written in terms of the radial flow velocity.

$$F^z = \mu \left\{ 2 \left[\frac{1}{r^2} \frac{\partial}{\partial r} \left(r^2 \frac{\partial u_r}{\partial r} \right) - \frac{2u_r}{r^2} \right] - \frac{2}{3} \nabla_r (\nabla_r \cdot u) \right\} \cos \theta \quad (\text{A-24})$$

Then from Equation (A-23),

$$F^r = 2\mu \left[\frac{\partial^2 u_r}{\partial r^2} + \frac{2}{r} \frac{\partial u_r}{\partial r} - \frac{2u_r}{r^2} \right] - \frac{2}{3} \mu \left[\nabla_r \left(\frac{\partial u_r}{\partial r} + \frac{2u_r}{r} \right) \right] \quad (\text{A-25})$$

The second bracket term of Equation (A-25) is expanded to the following form.

$$- \frac{2}{3} \mu \left[\frac{\partial^2 u_r}{\partial r^2} + \frac{2}{r} \frac{\partial u_r}{\partial r} - \frac{2u_r}{r^2} \right] \quad (\text{A-26})$$

The radial viscous force term is then given.

$$F^r = \frac{4}{3} \mu \left[\frac{\partial^2 u_r}{\partial r^2} + \frac{2}{r} \frac{\partial u_r}{\partial r} - 2 \frac{u_r}{r^2} \right] \quad (\text{A-27})$$

Energy Equation

The viscous term which appears in the energy equation is a scalar quantity and may be written in the following form.

$$\frac{\partial u^i \pi^{ij}}{\partial x^j} = u^i F^i + \pi^{ij} \frac{\partial u^i}{\partial x^j} \quad (\text{A-28})$$

where $F^i = \frac{\partial \pi^{ij}}{\partial x^j}$ (A-29)

Equation (A-29) and the other terms which appear in Equation (A-28) were derived in the previous section.

Therefore,

$$\frac{\partial u^i \pi^{ij}}{\partial x^j} = u_r F^r + \pi^{ij} \frac{\partial u^i}{\partial x^j} \quad (\text{A-30})$$

$$\pi^{ij} \frac{\partial u^i}{\partial x^j} = \mu \left(\frac{\partial u^i}{\partial x^j} \right) \left(\frac{\partial u^i}{\partial x^j} + \frac{\partial u^j}{\partial x^i} \right) - \frac{2}{3} \mu \frac{\partial u^k}{\partial x^k} \delta^{ij} \quad (\text{A-31})$$

or

$$\pi^{ij} \frac{\partial u^i}{\partial x^j} = \frac{4}{3} \mu \left\{ \left(\frac{\partial u_r}{\partial r} \right)^2 + \left(\frac{u_r}{r} \right)^2 \right\} \quad (\text{A-32})$$

APPENDIX B

PLASMA OSCILLATIONS

In the discussion of the expanding plasma sphere model of Chapter VI, an expression was given for the generalized Ohm's law. This expression for the current density included a term for the pressure induced current. The purpose of this section is to show the origin of this term from a microscopic point of view.

The very large pressure gradients which exist in a sphere of plasma expanding into vacuum give rise to a charge separation of the ions and electrons. In the single fluid model a distinction is provided for ion from electron through the generalized Ohm's law. This expression may be given by the following:

$$\vec{J} = \sigma [\vec{E} + \mu_0 (\vec{u} \times \vec{H})] + \rho_q \vec{u} - \frac{\sigma}{\rho_e} \vec{\nabla} P_e + \frac{\sigma}{\rho_i} \vec{\nabla} P_i \quad (\text{B-1})$$

The terms of this equation are well known, but for emphasis the following terms are again defined.

ρ_q = total free charge density

ρ_e = electron density

ρ_i = ion density

P_e = electron pressure

P_i = ion pressure

The last two terms in the equation above describe the behavior

of the electrons and ions in a pressure gradient. The electron pressure given is determined by the law of partial pressures.

$$P_e = \frac{\alpha}{\alpha + 1} P_{TOT} \quad (B-2)$$

where: α = degree of ionization

P_{TOT} = total pressure

Consider the contribution to the current density by the ions. It must be kept in mind that to follow the individual nature of the ions and electrons directly in the single fluid model is impossible. However, these properties may be implied by the macroscopic parameters such as the degree of ionization, charge density, etc. A qualitative insight may be gained by comparing the displacement currents arising from the ions and electrons under the influence of a pressure gradient.

Let the current density contributions be defined as follows,

$$\vec{J}_{ion} \sim n_i e v_i \quad (B-3)$$

$$J_{electron} \sim - n_e e v_e \quad (B-4)$$

where: n = number density

v = velocity

e = electronic charge

Now consider the motion of the ion and electrons in the pressure gradient. A simplified diagram is given in Figure 63 showing the relative displacements of the particles under the influence of an external force. From the theory of plasma oscillations the electrons, so displaced by an external force, will experience a restoring

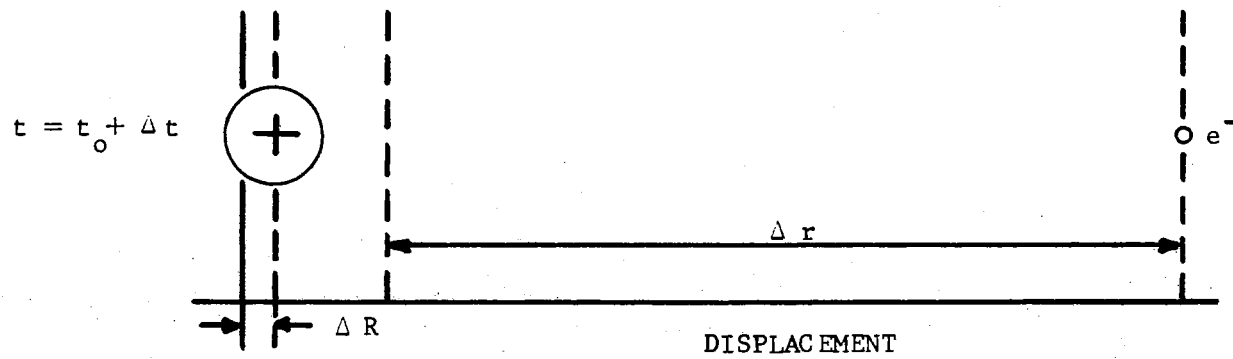
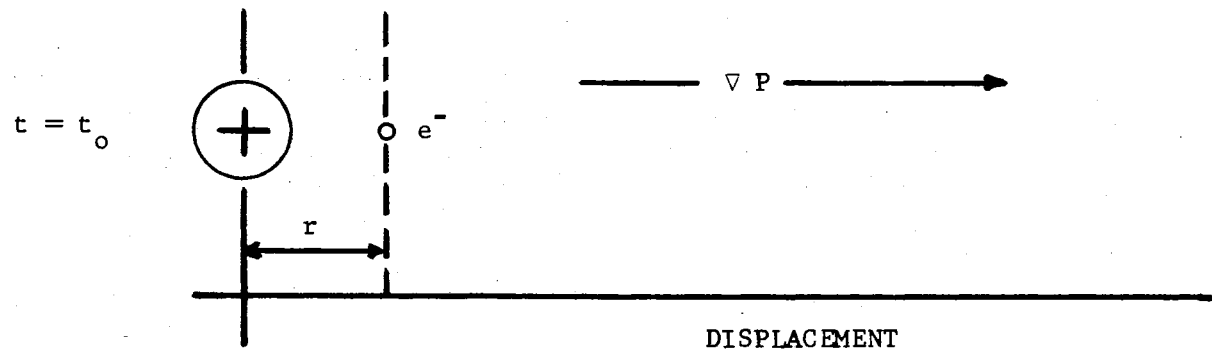


Figure 63. Relative Motion of Ion and Electron in an External Pressure Gradient

force because of the charge separation and will therefore begin to oscillate. If an arbitrary time, Δt , is defined as one-half the period of oscillation, then the displacements of the particles shown to arbitrary scale in Figure 63 will allow the qualitative determination of their relative contributions to the total current density.

For the time interval chosen, Equations (B-3) and (B-4) may be rewritten to obtain,

$$\vec{J}_{\text{ion}} \sim n_i e \frac{\Delta R}{\Delta t} \quad (\text{B-5})$$

and

$$J_{\text{electron}} \sim - n_e e \frac{\Delta r}{\Delta t} \quad (\text{B-6})$$

Now in the most general case of multi-ionized plasmas, the number density (n_i) of the ions will be less than or equal to that of the electrons (n_e).

$$n_i \leq n_e \quad (\text{B-7})$$

Also the displacement of the electrons, due to their small mass compared with the ion, will be much larger than that of the ions.

$$\Delta r \gg \Delta R \quad (\text{B-8})$$

A comparison of the magnitudes of these two current density components yields the following result.

$$\left| \vec{J}_{\text{ion}} \right| \ll \left| \vec{J}_{\text{electron}} \right| ; \quad \begin{array}{l} n_i \leq n_e \\ \Delta R \ll \Delta r \end{array} \quad (\text{B-9})$$

It should be noted that for aluminum plasmas, the relative number density of the ions and electrons is given by,

$$(n_e/n_i)_{\text{max}} = 13 \quad (\text{B-10})$$

Equation (B-9) suggests that especially for plasmas with a relatively high degree of ionization, the ionic contribution to the current density may be neglected.

For the spherical plasma model, Equation (B-1) is then reduced to the following.

$$\vec{J} = \sigma \vec{E} + \rho_q \vec{u} - \frac{\sigma}{\rho_e} \vec{\nabla} P_e \quad (\text{B-11})$$

Consider now the restoring forces which are a collective phenomena in a dense plasma, since the coulombic attraction is more complicated than that associated merely with individual ion-electron pairs. The justification for the pressure induced component of the current density will now be presented with a discussion of plasmon theory.

As was indicated by the argument above, the ions may be considered stationary, compared with the electrons, for any arbitrary time interval. This is consistent with the theory of plasmons. A plasmon may be defined as a quantized plasma oscillation. Kittel (1968) describes a plasma oscillation as a collective longitudinal excitation of an electron gas. This excitation is most simply described by considering an electron gas which undergoes a uniform displacement with respect to a stationary, positive ion background. The amplitude of this displacement which is shown in Figure 64 gives rise to an induced electric field,

$$|\vec{E}| = 4\pi n e \eta \quad (\text{B-12})$$

where: n = electron concentration

e = electronic charge

η = amplitude of electron displacement

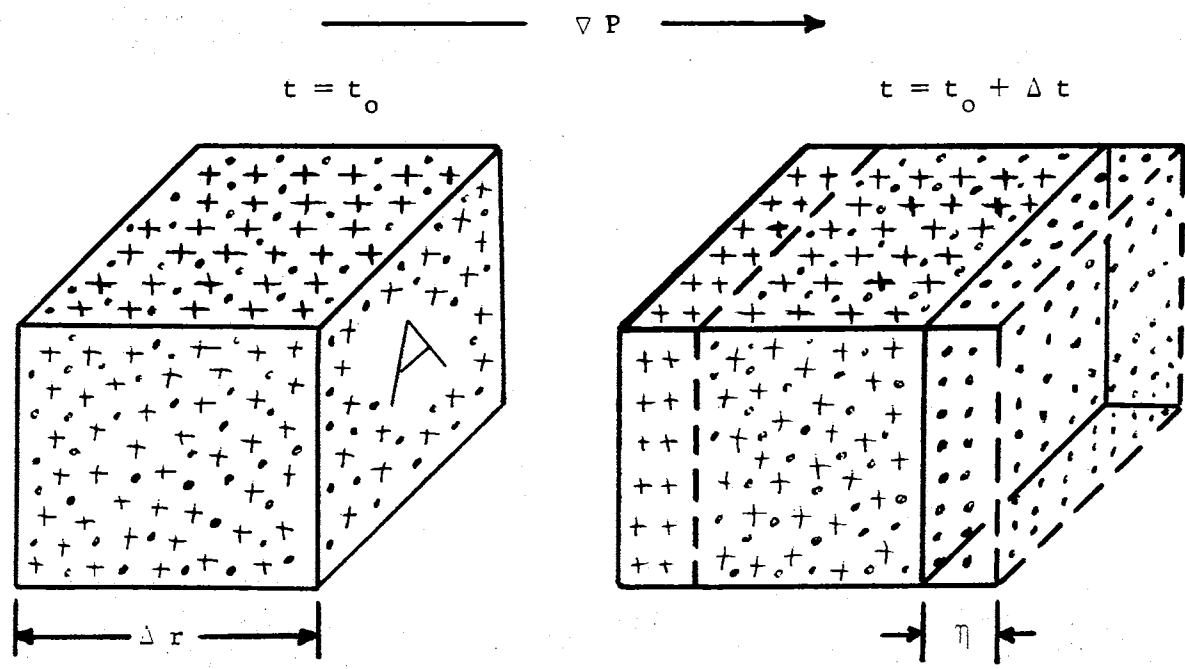


Figure 64. Displacement of Electron Gas in Ion Background

$$\sigma_s = n e \eta = \text{surface charge density}$$

The equation of motion for a unit volume of the electron gas is given.

$$n m \frac{d^2 \eta}{dt^2} = - n e E = - 4\pi n^2 e^2 \eta \quad (\text{B-13})$$

or

$$\frac{d^2 \eta}{dt^2} + \omega_p^2 \eta = 0 \quad (\text{B-14})$$

$$\text{where: } \omega_p^2 = \frac{4\pi n e^2}{m} \quad (\text{B-15})$$

ω_p = plasma frequency

m = electronic mass

Consider now the external force on the electron gas which is the consequence of the pressure gradient across the unit electron volume. The force exerted on an electron is given.

$$F_e = - \frac{1}{n} \left(\frac{\Delta P_e}{\Delta r} \right) \quad (\text{B-16})$$

where: P_e = electron pressure

Δr = dimension of electron volume

The net force on an electron in the plasma element is then given.

$$m \frac{d^2 \eta}{dt^2} = - \frac{1}{n} \left(\frac{\Delta P_e}{\Delta r} \right) - 4\pi n e^2 \eta \quad (\text{B-17})$$

The solution of this equation assumes the oscillatory form,

$$\eta = \frac{\frac{1}{n} \left(- \frac{\Delta P_e}{\Delta r} \right)}{4\pi m n e^2} - \frac{\frac{1}{n} \left(- \frac{\Delta P_e}{\Delta r} \right)}{4\pi m n e^2} \cos \omega_p t \quad (\text{B-18})$$

or

$$\eta = \eta_0 + \eta_0 \cos \omega_p t \quad (\text{B-19})$$

and

$$\eta_0 = \frac{\frac{1}{n} \left(- \frac{\Delta P_e}{\Delta r} \right)}{m \omega_p^2} \quad (\text{B-20})$$

The oscillation described by Equation (B-19) then occurs about η_0 with amplitude η_0 . The frequency of this oscillation is the characteristic plasma frequency ω_p .

Now consider the net charge which is displaced per oscillation. Let the cross-sectional area of the plasma element be given, A , so that the volume of the displaced electrons is $A\eta_0$. The net displaced charge is then given.

$$\Delta Q = n e (A\eta_0) \quad (\text{B-21})$$

The current density is then written for time interval, Δt .

$$\mathbf{J} = \frac{1}{A} \frac{\Delta Q}{\Delta t} = \frac{n e \eta_0}{\Delta t} \quad (\text{B-22})$$

Then using the expression for the displacement given by Equation (B-20), the pressure induced current term becomes.

$$\vec{\mathbf{J}} = - \frac{e \vec{\nabla} p_e}{m \omega_p^2 \Delta t} \quad (\text{B-23})$$

This term takes into account the oscillations which are known to exist in the expanding plasma. It has been used to replace the last term of Equation (B-11). The generalized Ohm's law then assumes the following form.

$$\vec{J} = \sigma \vec{E} + \rho_q \vec{u} - \frac{e \vec{\nabla} P_e}{m \omega_p^2 \Delta t} \quad (\text{B-24})$$

In deriving the pressure induced current density, the time dependent part of the solution given in Equation (B-19) was neglected because of its high frequency, in favor of the displacement component. It then becomes necessary to separately formulate the energy content of these oscillations. The oscillatory component is of such high frequency that it cannot be followed by the computer program, i.e., the period of oscillation is much smaller than any practical computer time step interval. The oscillational energy is not neglected, however.

The energy per particle of the oscillating electron gas may be written,

$$\xi_e = \frac{1}{2} (4\pi n e^2) \eta_o^2 + \frac{1}{2} m \omega_p^2 \eta_o^2 \quad (\text{B-25})$$

where the first term on the right is due to the electron gas displacement and the second term expresses the oscillational energy of the gas about the equilibrium position.

The oscillational energy per electron is then given,

$$\xi_{osc} = \frac{1}{2} m \omega_p^2 \left[\frac{\vec{\nabla} P_e \cdot \vec{\nabla} P_e}{(m \omega_p^2 n)^2} \right] \quad (\text{B-26})$$

and the oscillational energy density is written

$$\xi_{osc} = \frac{\vec{\nabla} P_e \cdot \vec{\nabla} P_e}{2 m \omega_p^2 n} \quad (\text{B-27})$$

This term was coded for the computer and has been included in the expression for the total energy given in Chapter VI.

APPENDIX C

PROGRAM CONSTRUCTION FOR SPHERICAL MODEL

The computer model for an expanding plasma sphere, which was presented in Chapter VI, represents a one-dimensional approach to the solution of the varied problems encountered in the complex study of plasma creation and evolution. The present work is a culmination of several years of research in both the experimental and theoretical areas of plasma physics. While the program to be presented here must certainly not be considered the last word in mathematical modeling, it does represent a substantial step forward in the continual research to ascertain the mechanisms attributed to plasma expansion.

The trial program listing which appears on the next several pages is only typical, since the model is in a constant state of up-dating and revision. It should, however, provide an indication of the work that has been done and the general state of the present research.

The actual computer program given here is a composite of fifteen elements, which includes a main program body, nine subprograms (or subroutines) and four statement functions. These elements are given below:

- I. MAIN PROGRAM
- II. SUBROUTINES
 1. CKOT
 2. HYDRO1

3. ICOND
4. OPTR
5. PRTOT1
6. QUAT
7. REDBL
8. REMSH
9. XOV

III. STATEMENT FUNCTIONS

1. FED
2. REEDG
3. RESET
4. XKAP

A brief description of the role of each of the program elements is now given.

- I. MAIN - The general "flow" of the program is determined by MAIN. The data is read into the computer via the main program. This data includes the tabular equation of state and states the initial mesh size for the model. Also included in MAIN are the flow equations, which include the gas dynamic equations and the Maxwell electromagnetic equations. The gas dynamic equations include the conservation laws. Other calculations which are included in the main program are for the viscous force term and the viscous energy term, the electrical conductivity, the oscillational energy and the Courant condition. Execution, program progress and termination are, for

the most part, controlled by the main program.

II. SUBROUTINES - The subprograms are called by the MAIN program to provide some specific information for calculation or to provide a check on the orderly progress of the program as a whole.

1. CKOT - The CheckOut routine was constructed to monitor all the flow variables to insure that feasible limits are not violated.
2. HYDRO1 - Higher Derivatives of certain flow variables are calculated via finite difference techniques in this subroutine. Specifically, the second partial derivatives which are encountered in the flow equations are dealt with in this routine.
3. ICOND - The Initial Conditions are specified for the program model in this routine. The initial values for all the flow variables are given for the mesh points and cell centers in the model at $t = 0$.
4. OPTR - OPTical pROPERTIES are provided for the calculations with this subroutine. The electron and ion collision times and the screening length are also calculated and conveyed to the main program.
5. PRTOT1 - PRinTOut #1 is one of several subroutines which may be used to display the program description and data in such a manner that

it may be efficiently reduced. This routine has the capability to read out the data to magnetic tape, as well as the conventional paper print out. This data tape may then be used to obtain computer-drawn graphs of the data for a more convenient analysis.

6. QUAT - The eQUATION of state subroutine provides, in matrix format, the thermodynamic variable values over the range covered by the model. This equation was developed previously in tabular form and has been incorporated into the present model. The thermodynamic range extends from several times solid density to $\sim 10^{-6}$ solid density, with the accompanying, consistent values for temperature and pressure. The general form of this equation was given in Chapter VI.
7. REDBL - The REDouBLe routine provides additional computer "space" into which the plasma may expand when the initial mesh is about to be overrun.
8. REMSH - The REMeSH routine is used each time cycle to reposition the variable values in the mesh as they evolve in time.
9. XOV - The calculation (X) Of the coefficient of Viscosity is provided in this routine.

III. STATEMENT FUNCTIONS

1. FED
2. REEDG
3. RESET
4. XKAP

} These functions provide a routine calculation that is not provided by the computer system library. For example, SIN(X) is provided for in the computer, but an arbitrary function such as RESET (c.f. Equation (6.31)) may be temporarily added to the system library of available functions, if many repeated calculations so warrant.

A machine listing of the spherical model program used for the initial trial computer runs is presented in the following tables.

TABLE VII

MACHINE LISTING OF MAIN PROGRAM

```

CFOR, IS MAIN, MAIN
  DIMENSION ATE(15)
  COMMON ALP(10,12), AOSC(51), DELT, DEN(10), DENQ1(51), DENQ2(51),
  1DENQ3(51), DELR, DR, EANDM, EDE(10,12), EGRM1(51), EGRM2(51), EGRM3(51),
  2EO, EOSC1(51), EOSC2(51), EOSC3(51), I, INTS, ITOT, ITOT1, NCYL, POSC(51),
  3PCAL1, PCAL2, PCAL3, PRES1(51), PRES2(51), PRES3(51), PRS(10,12),
  4R(51), RELC1(51), RELC2(51), RELC3(51), RHOM1(51), RHOM2(51), RHOM3(51),
  5RJDE1(51), RJDE2(51), RJDE3(51), RVEL1(51), RVEL2(51), RVEL3(51),
  6SDDEL, TCAL1, TCAL2, TCAL3, TEM(12), TEMP1(51), TEMP2(51), TEMP3(51),
  7TES1, TI, TIC, TIM, XION1(51), XION2(51), XION3(51), XO, PO
C*** DEFINITION OF VARIABLES *****
C   FV1(1) = VALUE OF FLOW VARIABLES AT MESH POINTS AT TIME T
C   FV2(1) = VALUE OF FLOW VARIABLES AT CELL CENTERS AT TIME T+DT
C   FV3(1) = TIME RATE OF CHANGE OF FLOW VARIABLES AT CELL CENTERS
C   ALAM = DEBYE LENGTH
C   ALP(10,12) = AVERAGE IONIZATION AT (RHOM,T) FOR EQUATION OF STATE TABLE
C   AOSC = AMPLITUDE OF OSCILLATIONS (CM)
C   ATE(15) = FUNCTION VALUES FOR X*EXP(X) X=0,1,...,14 (OPTK ROUTINE)
C   BH = PLANCK'S CONSTANT / 2 PI
C   CELN = CELL NUMBER WHERE THE INITIAL INTERFACE LIFS.
C   CHG = TOTAL ELECTRONIC CHARGE DENSITY
C   CLT = SPEED OF LIGHT (CGS)
C   COOK = COURANT COEFFICIENT
C   DELR = DELTA R (CM)
C   DELT = DELTA T (SEC)
C   DEN(10) = RELATIVE DENSITY FOR EQUATION OF STATE TABLE
C   DENQ = NET CHARGE DENSITY (COUL/M3) (MKSA)
C   DPER = PRESSURE GRADIENT
C   DR = INITIAL SEPARATION BETWEEN LINEAR MESH POINTS

```

TABLE VII (Continued)

C EANDM = CONTROL FOR ELECTROMAGNETIC EQUATIONS. IF EANDM<1.0, OMIT E AND M
 C CHARACTER OF THE PROBLEM (GASDYNAMIC APPROXIMATION).
 C EDE(10,12) = ENERGY DENSITY AT (RHOM,T) FOR EQUAT.OF STATE TABLE (ERG/CM3)
 C EFLOX = INTERMEDIATE ENERGY TERM
 C EFLUX = INTERMEDIATE ENERGY TERM
 C EGRM = INTERNAL ENERGY PER UNIT MASS (ERG/GM)
 C EO = INITIAL INTERNAL ENERGY PER UNIT MASS
 C EOSC = OSCILLATIONAL ENERGY PER UNIT MASS (ERG/GM)
 C EPSIV = PERMITIVITY CONSTANT (MKS)
 C EQN1 = MASS DENSITY OF ALUMINUM FOR USE IN EQUATION OF STATE
 C EQN2 = INTERNAL ENERGY FOR USE IN EQUATION OF STATE
 C FED = STATEMENT FUNCTION USED FOR CALCULATING PRESSURE GRADIENT
 C FEL = ELECTRIC FORCE TERM
 C FVIS = VISCOUS FORCE TERM
 C ITNS = NUMBER OF CELLS INSIDE OF TARGET SPHERE
 C ITOT = THE TOTAL NUMBER OF CELLS
 C ITOT1 = ITOT+1
 C KCG = CONTROL PARAMETER TO EXIT SUBROUTINE OPTR
 C NCYL = NO. COMPLETE CYCLES OF THE PROGRAM FOR A GIVEN TIME T+DT
 C PCAL1 = CALCULATES 2ND DERIVATIVES OF RVEL W.R.T. R(VISC. FORCES,MGM.CALC)
 C PCAL2 = DUMMY VARIABLE IN COMMON PACKAGE
 C PCAL3 = DUMMY VARIABLE IN COMMON PACKAGE
 C PI = 3.14
 C PO = INITIAL PRESSURE INSIDE SPHERE (DYNES/CM2)
 C POSC = PERIOD OF OSCILLATIONS (1/SEC)
 C PRES = PRESSURE (DYNE/CM2) NOTE.. 1 ATMS= 1.0E-06 DYNE/CM2
 C PRS(10,12) = PRESSURE AT (RHOM,T) FOR EQUAT. OF STATE TABLE (DYNE/CM2)
 C QE = ELECTRONIC CHARGE (4.8 E-10 ESU)
 C R(1) = RADIUS (CM)
 C RCEN = CELL CENTER RADIAL CO-ORDINATE

TABLE VII (Continued)

C RELC = RADIAL ELECTRIC FIELD (VOLT/M = NT/COUL) (MKSA)
 C REX = NON-SUBSCRIPTED VARIABLE FOR MASS DENSITY
 C RHOM = MASS DENSITY (GM/CM³)
 C RJDE = RADIAL CURRENT DENSITY (AMPS/M²) NOTE.. (MKSA)
 C ROVEL = RADIAL MOMENTUM
 C RP = RADIAL CO-ORDINATE FOR PEAK PRESSURE
 C RR = RADIAL CO-ORDINATE FOR PEAK MASS DENSITY
 C RT = RADIAL CO-ORDINATE FOR PEAK TEMPERATURE
 C RV = RADIAL CO-ORDINATE FOR PEAK RADIAL VELOCITY
 C RVEL = FLOW VELOCITY (CM/S)
 C SAT = LOWER LIMIT FOR RADIAL VELOCITY (-1.1E+09)
 C SDELTA = TIME INTERVAL FOR PREVIOUS CYCLE
 C SIG2 = ELECTRICAL CONDUCTIVITY (MKS)
 C SORJ = SOURCE TERM FOR CURRENT DENSITY
 C TAU = RELAXATION OR COLLISION TIME
 C TCAL1 = D²T/DR² (CALCULATED IN HYDR01)
 C TCAL2 = DUMMY VARIABLE IN COMMON PACKAGE
 C TCAL3 = DUMMY VARIABLE IN COMMON PACKAGE
 C TCOU = COURANT TIME INTERVAL
 C TEM(12) = TEMPERATURES FOR EQUATION OF STATE TABLE (EV)
 C TEMP = TEMPERATURE (EV)
 C TES1 = CONTROL FOR MESH - OVER-RUN
 C TEX = NON-SUBSCRIPTED VARIABLE FOR TEMPERATURE
 C TI = INITIAL TEMPERATURE
 C TIC = INITIAL VACUUM TEMPERATURE
 C TIM = TOTAL ELAPSED TIME
 C VELCK = ABSOLUTE VALUE OF THE RADIAL VELOCITY
 C WP = PLASMA ANGULAR FREQUENCY
 C WP2 = SQUARE OF PLASMA FREQUENCY
 C XA = NON-SUBSCRIPTED IONIZATION USED IN EQUATION OF STATE
 C XEX = NON-SUBSCRIPTED VARIABLE FOR IONIZATION
 C XIUN = DEGREE OF IONIZATION (NO. FREE ELECTRONS/ATOM)

TABLE VII (Continued)

C XKAP = STATEMENT FUNCTION FOR CALCULATING HEAT CAPACITY
 C XKPC = THERMAL CAPACITY TERM
 C XKP1 = THERMAL CAPACITY TERM
 C XKP2 = THERMAL CAPACITY TERM
 C XLAM = DEBYE LENGTH
 C XME = MASS OF ELECTRON (CGS)
 C XMU = VISCOSITY CO-EFFICIENT
 C XMWP2 = (MASS OF ELECTRON) * (SQUARE OF PLASMA FREQUENCY)
 C XNE = TOTAL ELECTRON NUMBER DENSITY
 C XO = INITIAL RELATIVE IONIZATION
 C XP = NON-SUBSCRIPTED PRESSURE USED IN EQUATION OF STATE
 C XPRM = PERMEABILITY CONSTANT (MKS)
 C XT = NON-SUBSCRIPTED TEMPERATURE USED IN EQUATION OF STATE
 C ZAG = CONTROL VARIABLE FOR IDENTIFICATION AND TRANSFER
 C*** FORMAT STATEMENTS ***
 5 FORMAT(8E9.3)
 6 FORMAT(10F7.1)
 7 FORMAT (50X,26HAN EXPANDING PLASMA SPHERE,///
 8 FORMAT (22X,70HTHE EQUATION OF STATE TABLES USED FOR THIS CALCULAT
 XION ARE GIVEN BELOW,///
 9 FORMAT(///<,40X,33HINTERNAL ENERGY DENSITY (ERGS/GM),///
 10 FORMAT(4X,16HRELATIVE DENSITY,3X,F10.3,2X,E10.3,2X,E10.3,2X,E10.3,
 X2X,E10.3,2X,E10.3,2X,E10.3,2X,E10.3)
 11 FORMAT (1X,16HTEMPERATURE (EV.))
 12 FORMAT(4X,E10.3,9X,E10.3,2X,E10.3,2X,F10.3,2X,E10.3,2X,E10.3,2X,
 XE10.3,2X,E10.3,2X,E10.3)
 13 FORMAT(///<,49X,20HPRESSURE (DYNES/CM2),///
 14 FORMAT(///<,49X,19HRELATIVE IONIZATION,///
 15 FORMAT(1E10.3)
 21 FORMAT (/,50X,21H*****PEAK VALUES*****)
 22 FORMAT (10X,14HCYCLE NUMBER=,14,10X,5HTIME=,E12.5,10X,36HTIME INC
 XREMENT USED FOR THIS CYCLE =,F10.3)

TABLE VII (Continued)

23 FORMAT(1X,12HMASS DENSITY,2X,8HPOSITION,10X,13HFLOW VELOCITY,2X,8H
XPOSITION,10X,8HPRESSURE,2X,8HPOSITION,10X,11HTEMPERATURE,2X,8HPOSI
XTION)

24 FORMAT(3X,E9.3,2X,E9.3,12X,E9.3,2X,E9.3,8X,E9.3,4X,E9.3,10X,E9.3,
X4X,E9.3)

25 FORMAT(5X,8H(GM/CM3),4X,4H(CM),14X,6H(CM/SEC),6X,4H(CM),10X,10H(DY
XNE/CM2),5X,4H(CM),16X,4H(EV),9X,4H(CM))

26 FORMAT (//,15X,39HCOURANT TIME INCREMENT FOR NEXT CYCLE= ,E10.3,2X
X,39HNOTE: COURANT COEFFICIENT FOR THIS RUN=,F5.1,//)

27 FORMAT (5X,110H*****
X*****)

28 FORMAT (/////5X,110H*****
X*****)

29 FORMAT (30X,71HTHIS PROGRAM CALCULATES THE EXPANSION PROPERTIES OF
X AN ALUMINUM SPHERE.)

30 FORMAT (20X,94HTHE INITIAL BOUNDARY CONDITIONS ARE CONSISTENT WITH
X THE EQUATION OF STATE AND ARE GIVEN BELOW:,//)

31 FORMAT (30X,2H1.,2X,61HTHE INITIAL SOLID SPHERE FILLS 25 RADIAL ME
XSH CELLS WHICH ARE,E10.3,2X,20HCENTIMETERS IN SIZE.//)

32 FORMAT (30X,2H2.,2X,36HTHE INITIAL VOLUME OF THE SPHERE IS,E10.3,2
XX,18HCUBIC CENTIMETERS.//)

33 FORMAT (30X,2H3.,2X,39HTHE INITIAL TOTAL MASS OF THE SPHERE IS,E10
X.3,2X,6HGRAMS.//)

34 FORMAT (30X,2H4.,2X,40HTHE INITIAL TEMPERATURE OF THE SPHERE IS,E1
X0.3,2X,3HEV.//)

35 FORMAT (30X,2H5.,2X,29HTHE INITIAL PRESSURE IS GIVEN,E10.3,2X,10HD
XYNES/CM2.//)

36 FORMAT (30X,2H6.,2X,34HTHE INITIAL RELATIVE IONIZATION IS,E10.3,2X
X,19HELECTRONS PER ATOM.//)

37 FORMAT (30X,2H7.,2X,29HTHE INITIAL ENERGY DENSITY IS,E10.3,2X,10HE
XRG/GRAM,,2X,22HWHICH IS EQUIVALENT TO,E10.3,2X,8HEV/ATOM.//)

TABLE VII (Continued)

38 FORMAT (30X,2H8.,2X,45HTHIS CORRESPONDS TO A TOTAL INITIAL ENERGY
 XOF,E10.3,2X,5HERGS.,//)
 39 FORMAT (30X,2H9.,2X,29HTHE INITIAL TIME INCREMENT IS,E10.3,2X,8HSE
 XCONDS.,/////
 40 FORMAT (22X,29HTHE ORIGINAL INTERFACE WAS AT,E10.3,2X,40HCENTIMETE
 XRS, WHICH IS NOW AT CELL NUMBER,F7.2,//)

C***DATA DEFINITION ***

PI=3.141
 ITOT=50
 ITOT1=ITOT+1
 TIM=0.0
 COT=1.0
 TIC=0.0235
 QE=4.8E-10
 XME=9.1E-28
 EPSIV=8.85E-12
 XPRM=1.256E-06
 EANDM=5.0
 SDELTA=0.0
 PCAL1=0.0
 PCAL2=0.0
 PCAL3=0.0
 TCAL1=0.0
 TCAL2=0.0
 TCAL3=0.0
 CELM = 25.0
 COCK = 0.9

ROOM T

C***TO SUPPRESS E&M, EANDM=0.0 ***

BH=1.061E-27
 CLT=3.00E+10

C*** THE FOLLOWING INITIAL VALUES ARE CONSISTENT WITH THE EQUATION OF STATE ***

C*** INITIAL ENERGY INSIDE SPHERE (HOT SPHERE) *****

TABLE VII (Continued)

```

      E0 = 1.81E+11
C*** INITIAL RELATIVE IONIZATION INSIDE SPHERE ***
      X0 = 3.0
C*** INITIAL PRESSURE INSIDE SPHERE ***
      P0 = 2.57E+12
C*** INITIAL TEMPERATURE INSIDE SPHERE ***
      TI = 2.0
      NCYL=0
C*** TIME INCREMENT DEFINITION *****
      DELT = 1.0E-10
C**** GENERATION OF N*EXP(N) FOR XOV AND OPTR *****
      DO 101 N=1,15
      Y=N-1
      ATE(N)=Y*EXP(Y)
101 CONTINUE
C*** EQUATION OF STATE INPUT ***
      READ(5,5) (DEN(K),K=1,8)
      READ(5,6) (TEM(K),K=1,11)
      DO 111 K=1,11
      READ(5,5) (EDE(J,K), J=1,8)
      DO 105 I=1,8
      EDE(I,K)=EDE(I,K)/(2.70*DEN(I))
105 CONTINUE
111 CONTINUE
      DO 121 K=1,11
      READ(5,5) (ALP(J,K),J=1,8)
121 CONTINUE
      DO 131 K=1,11
      READ(5,5) (PRS(J,K),J=1,8)
131 CONTINUE
C*** INPUT OF MESH SIZE FOR ICOND *****
      READ(5,15) DR

```

TABLE VII (Continued)

```

C*** CALCULATE INITIAL VOLUME OF SPHERE ***
      RRR = 25.0*DR
      VOL = (4.0*PI*RRR*RRR*RRR)/3.0
C*** CALCULATE TOTAL INITIAL MASS OF SPHERE ***
      XMAS = 2.7 * VOL
C*** CALCULATE EQUIVALENT ENERGY PER ATOM ***
      AVON = 6.02E+23
C      GRAM MOLECULAR WEIGHT FOR ALUMINUM = 27 GM/MOLE ***
C      THERE ARE 10 CC/MOLE FOR SOLID ALUMINUM
C      THERE ARE 2.23E+22 ATOMS/GRAM FOR SOLID ALUMINUM
C      ENERGY PER ATOM ( EPA ) IS THEN CALCULATED
      EPA = E0/2.23E+22
C      THERE ARE 1.602E-12 ERGS PER EV
      EPA = EPA/1.602E-12
C      THE TOTAL INITIAL ENERGY
      TIE = XMAS * E0
      WRITE(6,7)
      WRITE(6,29)
      WRITE(6,30)
      WRITE(6,31) DP
      WRITE(6,32) VOL
      WRITE(6,33) XMAS
      WRITE(6,34) TI
      WRITE(6,35) PC
      WRITE(6,36) XO
      WRITE(6,37) E0,EPA
      WRITE(6,38) TIE
      WRITE(6,39) DELT
C*** TO OUTPUT EQUATION OF STATE TABLES ***
      WRITE(6,8)
      WRITE(6,9)
      WRITE(6,10) (DEN(K),K=1,8)

```

TABLE VII (Continued)

```

WRITE(6,11)
DO 141 J=1,11
WRITE(6,12) TEM(J),EDE(1,J),EDE(2,J),EDE(3,J),EDE(4,J),EDE(5,J),
XEDE(6,J),EDE(7,J),EDE(8,J)
141 CONTINUE
WRITE(6,13)
WRITE(6,10) (DEN(K),K=1,8)
WRITE(6,11)
DO 151 J=1,11
WRITE(6,12) TEM(J),PRS(1,J),PRS(2,J),PRS(3,J),PRS(4,J),PRS(5,J),
XPRS(6,J),PRS(7,J),PRS(8,J)
151 CONTINUE
WRITE(6,14)
WRITE(6,10) (DEN(K),K=1,8)
WRITE(6,11)
DO 161 J=1,11
WRITE(6,12) TEM(J),ALP(1,J),ALP(2,J),ALP(3,J),ALP(4,J),ALP(5,J),
XALP(6,J),ALP(7,J),ALP(8,J)
161 CONTINUE
C*** INITIAL CONDITIONS *****
CALL ICOND
TIME=0.0
C*** BRANCH POINT FOR TIME CYCLES ***
251 ZAG=1.0
C*** SET PEAK VALUES BEFORE ENTERING TIME CYCLE *****
PRHOM=0.0
PRVEL=0.0
PTEMP=0.0
PPRES=0.0
TES1=0.0
IF(NCYL.LT.1) GO TO 271
C*** TES1 = OVERUN CONTROL. IF MESH OVERUN, TES1 = 1.0, IF NOT, =0.0 *****

```

TABLE VII (Continued)

```

C*** THE DENSITY TEST FOR OVER RUN IS MADE AT END OF REMSH ***
  CALL REMSH
  IF(TE51.LT.0.5) GO TO 271
  CALL REDBL
271 ZAG=1.0
  CALL CKOT
C***GENERATE TEMPORARY SPARE FV2 VALUE SET IN FV3 LOCATIONS*****
  DO 281 I=1,ITOT
  DENQ3(I)=DENQ2(I)
  EGKM3(I)=EGRM2(I)
  EOSC3(I)=EOSC2(I)
  PRES3(I)=PRES2(I)
  RELC3(I)=RELC2(I)
  RHOM3(I)=RHOM2(I)
  RJDE3(I)=RJDE2(I)
  RVEL3(I)=RVEL2(I)
  TEMP3(I)=TEMP2(I)
  XION3(I)=XION2(I)
281 CONTINUE
C*** FLOW EQUATIONS *****
  DO 5003 I=1,ITOT
C*** CELL CENTER CO-ORDINATES ***
  RCEN=(R(I)+R(I+1))/2.0
C*** DELTA R ***
  DELR=R(I+1)-R(I)
C*** FV3 VALUES RESERVED FOR OLD VALUES AT CELL CENTER. ARE LATER USED AS TIME
C DERIVATIVES OF CELL CENTERS *****
C*** CONSERVATION OF MASS ***
  RHOM2(I)=-1.0*DELT*((0.5*RVEL3(I)*RHOM3(I)/RCEN)+((RHOM1(I+1)*RVEL
  X1(I+1)-RHOM1(I)*RVEL1(I))/DELR)) + RHOM2(I)
  IF(RHOM2(I).LE.0.0) RHOM2(I)=RHOM3(I)
C*** CONSERVATION OF RADIAL MOMENTUM ***

```

TABLE VII (Continued)

```

C*** VISCOUS TERM ***
C*** CALL HYDRO1 TO RETURN D2V/DR2=PCAL1 ***
      CALL HYDRO1
C*** CALL XOY TO RETURN MU ***
      KCO=9
      REX=KHOM3(I)
      TEX=TEMP3(I)
      XEX=XION3(I)
      IF(XEX.LE.0.1) GO TO 1001
      CALL OPTR (REX,XME,BH,TEX,XEX,PI,QE,ATE,KCO,CLT,TAU,XLAM)
      ALAM=XLAM
      CALL XOY(QE,XEX,ALAM,TEX,ATE,XMU)
      GO TO 1001
1001 XMU=0.0
1011 ROVEL=(-1.0*RHOM3(I)*RVEL3(I)*(RVEL1(I+1)-RVEL1(I))/DELR)-((PRES1(I)
      XI+1)-PRES1(I))/DELR)
C*** ELECTRIC FORCE TERM CONVERTED TO C G S ***
      FEL=DENQ3(I)*FELC3(I)*1.0E-01
C*** VISCOUS FORCE TERM ***
      FVIS=1.33*XMU*(PCAL1+2.0*((RVEL1(I+1)-RVEL1(I))/DELR)-2.0*RVEL3(I)
      X/RCEN)
C*** COMPLETION OF ROVEL ***
      ROVEL=ROVEL+FVIS+FEL
      RVEL2(I)=RVEL3(I)+DELT*(ROVEL/RHOM3(I))
C*** CHECK TO SEE RVEL.LT.0.11C ***
      IF(RVEL2(I).GT.1.1E+09) RVEL2(I)=1.1E+09
      SAT=-1.1E+09
      IF(RVEL2(I).LT.SAT) RVEL2(I)=SAT
C*** ENERGY DENSITY CALCULATION ***
C*** WITHOUT ELECTRICAL TERM (COMPUTED AFTER J-CALC) ***
      EFLUX=-1.0*(RHOM3(I)*EGRM3(I)*RVEL3(I)/RCFN)-(((RHOM1(I+1)*EGRM1
      X(I+1)*RVEL1(I+1))-((RHOM1(I)*EGRM1(I)*RVEL1(I))))/DELR)

```

TABLE VII (Continued)

```

EFLUX=EFLUX-(PRES3(I)*RVEL3(I)/RCEN)-(((PRES1(I+1)*RVEL1(I+1))
X-(PRES1(I)*RVEL1(I)))/DELR)
C*** VISCOUS TERM ***
EFLUX=EFLUX+(1.33*XMU*(RVEL2(I)/RCEN)*(RVEL2(I)/RCEN))+(1.33*XMU*
X((RVEL1(I+1)-RVEL1(I))/DELR)*((RVEL1(I+1)-RVEL1(I))/DELR))+(FVIS*
XRVEL3(I))
C*** CALLING THERMAL CONDUCTIVITIES NEEDED IN THERMAL TERM ***
KCO=3
TEX=TEMP1(I+1)
XEX=XION1(I+1)
REX=RHOM1(I+1)
CALL OPTR(PFX,XME,PH,TEX,XEX,PI,GE,ATF,KCO,CLT,TAU,XLAM)
XKP1=XKAP(TEMP1(I+1),TAU,XION1(I+1),RHOM1(I+1))
TEX=TEMP1(I)
XEX=XION1(I)
REX=RHOM1(I)
CALL OPTR(PFX,XME,PH,TEX,XEX,PI,GE,ATF,KCO,CLT,TAU,XLAM)
XKP2=XKAP(TEMP1(I),TAU,XION1(I),RHOM1(I))
TEX=TEMP3(I)
XEX=XION3(I)
REX=RHOM3(I)
CALL OPTR(PFX,XME,PH,TEX,XEX,PI,GE,ATF,KCO,CLT,TAU,XLAM)
XKPC=XKAP(TEMP3(I),TAU,XION3(I),RHOM3(I))
C*** THERMAL TERMS IN ENERGY EQUATION ***
EFLUX=EFLUX+((XKPC/RCEN)*((TEMP1(I+1)-TEMP1(I))/DELR))
EFLUX=EFLUX+(((XKP1-XKP2)/DELR)*((TEMP1(I+1)-TEMP1(I))/DELR))
C*** TCAL1 = D2T/DF2 (CALCULATED PREVIOUSLY BY HYDRO1) ***
EFLUX=EFLUX+(XKPC*TCAL1)
C*** CONSERVATION OF CHARGE ***
DENG2(I)=DENG3(I)-((CLT*((RJD3(I)/RCEN)+((RJD1(I+1)-RJD1(I))/DE
XLR)))
C*** CHECK FREE CHARGE DENSITY .LT. 0.2 TOTAL ELECTRON CHARGE ***

```

TABLE VII (Continued)

```

CHG=1.6E-19*6.0E+22*XION3(I)*RHOM3(I)/2.70
CHG=CHG*1.0E+06*0.2
IF(DENQ2(I).GT.CHG) DENQ2(I)=CHG
CHG=-CHG
IF(DENQ2(I).LT.CHG) DENQ2(I)=CHG
C*** ELECTRICAL TERM ***
EFLUX=EFLUX+(RELC3(I)*RJDE3(I)*10.0)
EFLOX=EFLUX-(EGRM3(I)*(RHOM2(I)-RHOM3(I))/DELT)
C*** NEW ENERGY TERM ***
EGRM2(I)=EGRM3(I)+(DELT*EFLOX/RHOM2(I))
C*** ELECTRIC FIELD ***
RELC2(I)=RELC3(I)+((DELT*RJDE3(I))/EPSIV)
C*** CURRENT DENSITY CALCULATION ***
C*** ELECTRICAL CONDUCTIVITY - M K S -USING WIEDERMANN-FRANZ RATIO ***
C*** CONDUCTIVITY - CGS ***
SIG2=(XKPC*2.75E+04/TEMP3(I))
C*** CONDUCTIVITY - MKS - ***
SIG2=SIG2/9.0E+09
C*** CALCULATION OF SOURCE TERM ***
C11=FED(XION3(I+1),PRES3(I+1))
C12=FED(XION3(I),PRES3(I))
DPER=(C11-C12)/DELP
C*** CALCULATION OF TOTAL ELECTRON NUMBER DENSITY ***
XNE=RHOM3(I)*6.02E+22*XION3(I)/2.70
IF(XNE.LE.0.0) GO TO 1500
WP2=4.0*PI*XNE*GE*GE
WP2=WP2/XME
C*** VECTOR DISPLACEMENT ***
WP=WP2**0.5
XMWP2=XME*WP2
AOSC(I)=DPER/(XNE*XMWP2)
C*** PERIOD OF OSCILLATION ***

```


TABLE VII (Continued)

```

      POSC(I)=2.0*PI/WP
C*** SOURCE TERM ***
      SORJ=AOSC(I)*1.6E-19*XNE/DELT
C*** AMPLITUDE OF OSCILLATION ***
      AOSC(I)=ABS(AOSC(I))
C*** CURRENT DENSITY ***
      RJDE2(I)=(SIG2*RELC3(I))+(DENQ3(I)*RVEL3(I)*1.0E-02)+
      X(SORJ*1.0E-04)
C*** OSCILLATIONAL ENERGY (ERG/GM) ***
      EOSC2(I)=0.5*AOSC(I)*AOSC(I)*WP2
      EOSC2(I)=EOSC2(I)*XME*XNE/RHOM3(I)
      GO TO 1600
1500 AOSC(I)=0.0
      POSC(I)=0.0
      SORJ=0.0
      RJDE2(I)=(SIG2*RELC3(I))+(DENQ3(I)*RVEL3(I)*1.0E-02)
      EOSC2(I)=0.0
C*** CALCULATION OF PRESSURE, IONIZATION AND TEMPERATURE ***
1600 EQN1 = RHOM2(I)
      EQN2=EGRM2(I)-(0.5*(RVEL2(I)*PVEL2(I)))-EOSC2(I)
C*** CALL EQUATION OF STATE ROUTINE *****
      CALL QUAT(EQN1,EQN2,XP,XT,XA)
      EGRM2(I)=EQN2
      RHOM2(I)=EQN1*2.70
      XION2(I)=XA
      PRES2(I)=XP
      TEMP2(I)=XT
      IF(RHOM2(I).LE.PRHOM) GO TO 2001
      PRHOM=RHOM2(I)
      RR=RCEN
2001 VELCK=ABS(RVEL2(I))
      IF(VELCK.LE.PVEL) GO TO 2010

```

TABLE VII (Continued)

```

PRVEL=VELCK
RV=RCEN
2010 IF(PRES2(I).LE.PPRES) GO TO 2020
PPRES=PRES2(I)
RP=RCEN
2020 IF(TEMP2(I).LE.PTEMP) GO TO 5003
PTEMP=TEMP2(I)
RT=RCEN
5003 CONTINUE
C*** SET FV3'S TO DERIVATIVES *****
DO 5050 J=1,ITOT
DENG3(J)=(DENG2(J)-DENG3(J))/DELT
EGRM3(J)=(EGRM2(J)-EGRM3(J))/DELT
EOSC3(J)=(EOSC2(J)-EOSC3(J))/DELT
PRES3(J)=(PRES2(J)-PRES3(J))/DELT
RELC3(J)=(RELC2(J)-RELC3(J))/DELT
RHOM3(J)=(RHOM2(J)-RHOM3(J))/DELT
RJDE3(J)=(RJDE2(J)-RJDE3(J))/DELT
RVEL3(J)=(RVEL2(J)-RVEL3(J))/DELT
TEMP3(J)=(TEMP2(J)-TEMP3(J))/DELT
XION3(J)=(XION2(J)-XION3(J))/DELT
5050 CONTINUE
TIM=TIM+DELT
C*** THE FOLLOWING CARD LIMITS THE OUTPUT BY NUMBER OF CYCLES*****
IF(NCYL.GE.100) GO TO 6001
NCYL=NCYL+1
WRITE(6,28)
WRITE(6,22) NCYL,TIM,DELT
WRITE(6,27)
WRITE(6,21)

```

TABLE VII (Continued)

```

WRITE(6,23)
WRITE(6,24) PPHOM,PR,PRVEL,RV,PPRES,KP,PTEMP,RT
WRITE(6,25)
C*** COURANT CONDITION *****
C*** LINEAR MESH ONLY ***
TCOU=0.0
IF(PRVEL.LE.0.0) GO TO 5070
TCOU=DELR/PRVEL
C*** CHOICE OF TIME INCREMENT FOR NEXT CYCLE *****
5070 SDELT=DELT
DELT = COUK * TCOU
C*** NOTE COURANT COEFFICIENT = 0.9 *****
IF(DELT.GT.1.0E-09) DELT = 1.0E-09
WRITE(6,26) TCOU,COUK
IF(TES1.GT.0.5) CELN = CELN/2.0
WRITE(6,40) RRR,CELN
C*** CONDITIONS FOR CALLING PRTOT CAN BE ADDED HERE LATER ***
CALL PRTOT1
C*** ADDITIONAL CONDITIONS FOR TERMINATION CAN BE ADDED HERE LATER *****
IF(TIM.GT.1.0E-06) GO TO 6001
GO TO 251
6001 ZAG=1.0
STOP
END

```

TABLE VIII

SUBROUTINE CKOT

GFOR, IS CKOT, CKOT

SUBROUTINE CKOT

DIMENSION MC(15), NC(15)

COMMON ALP(10,12), AOSC(51), DELT, DEN(10), DENQ1(51), DENQ2(51),
 1DENQ3(51), DELR, DR, EANDM, EDE(10,12), EGRM1(51), EGRM2(51), EGRM3(51),
 2EO, EUSC1(51), EOSC2(51), EOSC3(51), I, INTS, ITOT, ITOT1, NCYL, POSC(51),
 3PCAL1, PCAL2, PCAL3, PRES1(51), PRES2(51), PRES3(51), PRS(10,12),
 4R(51), RELC1(51), RELC2(51), RELC3(51), RHOM1(51), RHOM2(51), RHOM3(51),
 5RJDE1(51), RJDE2(51), RJDE3(51), RVEL1(51), RVEL2(51), RVEL3(51),
 6SDDEL1, TCAL1, TCAL2, TCAL3, TEM(12), TEMP1(51), TEMP2(51), TEMP3(51),
 7TES1, TI, TIC, TIM, XION1(51), XION2(51), XION3(51), XO, PO

C*** ISN 10 - 67 ***

- 1 FORMAT (30X,1H1,10X,41HMASS DENSITY IS LESS THAN 2.7 E-07 GM/CM3)
- 2 FORMAT (30X,1H2,10X,40HMASS DENSITY IS GREATER THAN 5.40 GM/CM3)
- 3 FORMAT (30X,1H3,10X,30HOSCILLATION ENERGY IS NEGATIVE)
- 4 FORMAT (30X,1H4,10X,54HINTERNAL ENERGY IS INCONSISTENT WITH EQUATI
 XUN OF STATE)
- 5 FORMAT (30X,1H5,10X,31HPRESSURE LESS THAN 2.25E-04 BAR)
- 6 FORMAT (30X,1H6,10X,33HPRESSURE GREATER THAN 10 MEGABARS)
- 7 FORMAT (30X,1H7,10X,35HRELATIVE IONIZATION GREATER THAN 13)
- 8 FORMAT (30X,1H8,10X,31HRELATIVE IONIZATION IS NEGATIVE)
- 9 FORMAT (30X,1H9,10X,35HTEMPERATURE F IS LESS THAN 0.0235 EV.)
- 10 FORMAT(29X,2H10,10X,33HTEMPERATURE IS GREATER THAN 5 KEV)
- 11 FORMAT(29X,2H11,10X,43HPADIAL FLOW VELOCITY EXCEEDS 1.0E+09 CM/SEC
 X)
- 13 FORMAT (10X,57HOPERATIONAL CORRECTIONS HAVE BEEN MADE BECAUSE OF P
 XREASON ,12,4H AT ,I4,17H MESH POINTS AND ,I4,13H CFLL CENTERS)
- 14 FORMAT (///,10X,108HDURING THE COURSE OF THE PROBLEM IT MAY BE NEC
 XCESSARY TO PERFORM THE OPERATIONAL CORRECTIONS ENUMERATED BELOW)
- 15 FORMAT (/ ,23X,13HREASON NUMBER)

TABLE VIII (Continued)

```

16 FORMAT (29X,2H13,10X,64HFREE CHARGE DENSITY EXCEEDS 10% OF TOTAL F
    ELECTRON CHARGE DENSITY)
17 FORMAT (29X,2H14,10X,69HRADIAL CURRENT DENSITY EXCEEDS (10% RHO TO
    XIAL ELECTRON)*(10% C-LIGHT))
    IF(NCYL.GT.0) GO TO 19
    WRITE(6,14)
    WRITE(6,15)
    WRITE(6,1)
    WRITE(6,2)
    WRITE(6,3)
    WRITE(6,4)
    WRITE(6,5)
    WRITE(6,6)
    WRITE(6,7)
    WRITE(6,8)
    WRITE(6,9)
    WRITE(6,10)
    WRITE(6,11)
    WRITE(6,16)
    WRITE(6,17)
19 DO 26 I=1,15
    MC(I)=0
    NC(I)=0
26 CONTINUE
    SAT=1.0E+09
    SIT=-1.0*SAT
    DO 1001 J=1,ITOT1
    IF(RHOM1(J).GT.2.67E-07) GO TO 290
    MC(1)=MC(1)+1

```

TABLE VIII (Continued)

```
      RHOM1(J)=2.70E-07
290  IF(RHOM1(J).LE.5.4) GO TO 300
      MC(2)=MC(2)+1
      RHOM1(J)=5.4
300  IF(EOSC1(J).GE.0.0) GO TO 310
      MC(3)=MC(3)+1
      EOSC1(J)=0.0
310  EQN1=RHOM1(J)
      EQN2=EGRM1(J)
      CALL QUAT(EQN1,EQN2,XP,XT,XA)
      SK=0.1*EQN2
      IF(SK.LT.0.0) SK=-1.0*SK
      TISK=EQN2+SK
      TASK=EQN2-SK
      IF(EGRM1(J).LT.TASK) GO TO 340
      IF(EGRM1(J).GT.TISK) GO TO 340
      GO TO 350
340  MC(4)=MC(4)+1
      EGRM1(J)=EQN2
350  PRES1(J)=XP
      IF(XP.GT.2.24E+02) GO TO 360
      MC(5)=MC(5)+1
      PRES1(J)=2.25E+02
360  FPZ=2.5E+15*RHOM1(J)
      IF(XP.LE.FPZ) GO TO 370
      MC(6)=MC(6)+1
      PRES1(J)=FPZ
370  XION1(J)=XA
      IF(XA.LE.13.0) GO TO 380
      MC(7)=MC(7)+1
      XION1(J)=13.0
380  IF(XA.GE.0.0) GO TO 390
```

TABLE VIII (Continued)

```
MC(8)=MC(8)+1
XION1(J)=0.0
390 TEMP1(J)=XT
   IF(XT.GT.0.0234) GO TO 400
MC(9)=MC(9)+1
TEMP1(J)=0.0235
400 IF(XT.LE.5.0E+03) GO TO 410
MC(10)=MC(10)+1
TEMP1(J)=5.0E+03
410 CHIG=XION1(J)*RHOM1(J)*6.02E+22/2.70
CHIG=1.6E-19*CHIG*1.0E+06*0.1
CHAG=-1.0*CHIG
   IF(DENQ1(J).LE.CHIG) GO TO 420
MC(11)=MC(11)+1
DENQ1(J)=CHIG
GO TO 430
420 IF(DENQ1(J).GE.CHAG) GO TO 430
MC(12)=MC(12)+1
DENQ1(J)=CHAG
430 CUR=CHAG*3.0E+07
CAR=-CUR
   IF(RJDE1(J).LE.CAR) GO TO 440
MC(13)=MC(13)+1
RJDE1(J)=CUR
GO TO 450
440 IF(RJDE1(J).GE.CUR) GO TO 450
MC(14)=MC(14)+1
RJDE1(J)=CAR
450 IF(RVEL1(J).LE.SAT) GO TO 460
MC(15)=MC(15)+1
RVEL1(J)=SAT
GO TO 470
```

TABLE VIII (Continued)

```
460 IF(RVEL1(J).GE.SIT) GO TO 470
    MC(11)=MC(11)+1
    RVEL1(J)=SIT
470 IF(J.GT.ITOT) GO TO 1001
    IF(RHOM2(J).GT.2.67E-07) GO TO 490
    NC(1)=NC(1)+1
    RHOM2(J)=2.70E-07
490 IF(RHOM2(J).LE.5.4) GO TO 600
    NC(2)=NC(2)+1
    RHOM2(J)=5.4
600 IF(EOSC2(J).GE.0.0) GO TO 610
    NC(3)=NC(3)+1
    EOSC2(J)=0.0
610 EQN1=RHOM2(J)
    EQN2=EGRM2(J)
    CALL QUAT(EQN1,EQN2,XP,XT,XA)
    SK=0.1*EQN2
    IF(SK.LT.0.0) SK=-1.0*SK
    TISK=EQN2+SK
    TASK=EQN2-SK
    IF(EGRM2(J).LT.TASK) GO TO 640
    IF(EGRM2(J).GT.TISK) GO TO 640
    GO TO 650
640 NC(4)=NC(4)+1
    EGRM2(J)=EQN2
650 PRES2(J)=XP
    IF(XP.GT.2.24E+02) GO TO 660
    NC(5)=NC(5)+1
    PRES2(J)=2.25E+02
660 FPZ=2.5E+15*RHOM2(J)
    IF(XP.LE.FPZ) GO TO 670
    NC(6)=NC(6)+1
```


TABLE VIII (Continued)

```
      PRES2(J)=FPZ
670  XION2(J)=XA
      IF(XA.LE.13.0) GO TO 680
      NC(7)=NC(7)+1
      XION2(J)=13.0
680  IF(XA.GE.0.0) GO TO 690
      NC(8)=NC(8)+1
      XION2(J)=0.0
690  TEMP2(J)=XT
      IF(XT.GT.0.0234) GO TO 800
      NC(9)=NC(9)+1
      TEMP2(J)=0.0235
800  IF(XT.LE.5.0E+03) GO TO 810
      NC(10)=NC(10)+1
      TEMP2(J)=5.0E+03
810  CHIG=XION2(J)*RHOM2(J)*6.02E+22/2.7U
      CHIG=1.6E-19*CHIG*1.0E+06*U.1
      CHAG=-1.0*CHIG
      IF(DENQ2(J).LE.CHIG) GO TO 820
      NC(13)=NC(13)+1
      DENQ2(J)=CHIG
      GO TO 830
820  IF(DENQ2(J).GE.CHAG) GO TO 830
      NC(13)=NC(13)+1
      DENQ2(J)=CHAG
830  CUR=CHAG*3.0E+07
      CAR=-CUR
      IF(RJDE2(J).LE.CAR) GO TO 840
      NC(14)=NC(14)+1
      RJDE2(J)=CUR
      GO TO 850
840  IF(RJDE2(J).GE.CUR) GO TO 850
```

TABLE VIII (Continued)

```
NC(14)=NC(14)+1
RUEZ(J)=CAP
850 IF(RVEL2(J).LE.SAT) GO TO 860
NC(11)=NC(11)+1
RVEL2(J)=SAT
860 IF(RVEL2(J).GE.SIT) GO TO 870
NC(11)=NC(11)+1
RVEL2(J)=SIT
870 ZAG=1.0
1001 CONTINUE
DO 1011 I=1,15
IF(MC(I).GE.1) GO TO 1009
IF(NC(I).GE.1) GO TO 1009
GO TO 1011
1009 WRITE(6,13) I,MC(I),NC(I)
1011 CONTINUE
RETURN
END
```

TABLE IX

SUBROUTINE HYDRO1

```

C FOR IS HYDRO1, HYDRO1
  SUBROUTINE HYDRO1
    COMMON ALP(10,12), AOSC(51), DELT, DEN(10), DENQ1(51), DENQ2(51),
    1DENQ3(51), DELR, DR, EANDM, EDE(10,12), EGRM1(51), EGRM2(51), EGRM3(51),
    2EO, EOSC1(51), EOSC2(51), EOSC3(51), I, INTS, ITOT, ITOT1, NCYL, POSC(51),
    3PCAL1, PCAL2, PCAL3, PRES1(51), PRES2(51), PRES3(51), PRS(10,12),
    4R(51), RELC1(51), RELC2(51), RELC3(51), RHOM1(51), RHOM2(51), RHOM3(51),
    5RJDE1(51), RJDE2(51), RJDE3(51), RVEL1(51), RVEL2(51), RVEL3(51),
    6SDELT, TCAL1, TCAL2, TCAL3, TEM(12), TEMP1(51), TEMP2(51), TEMP3(51),
    7TES1, TI, TIC, TIM, XION1(51), XION2(51), XION3(51), XO, PO
C*** THIS SUBROUTINE CALCULATES D2V/DR2 AND D2T/DR2 FOR VISCOUS AND THERMAL
C CONDUCTION TERMS IN ENERGY AND MOMENTUM EQUATIONS *****
    IF(I.GE.ITOT) GO TO 501
    IF(I.LT.2) GO TO 301
C*** CALCULATION FOR INTERIOR CELLS *****
    DIF1=(R(I+2)-R(I))/2.0
    DIF2=(R(I+1)-R(I-1))/2.0
    TERM1=(RVEL3(I+1)-RVEL3(I))/(DELR*DIF1)
    TERM2=(RVEL3(I)-RVEL3(I-1))/(DELR*DIF2)
    PCAL1=TERM1-TERM2
    TERM1=(TEMP3(I+1)-TEMP3(I))/(DELR*DIF1)
    TERM2=(TEMP3(I)-TEMP3(I-1))/(DELR*DIF2)
    TCAL1=TERM1-TERM2
    GO TO 510
C*** CALCULATION FOR THE FIRST CELL *****
301 DIF1=(R(5)-R(3))/2.0
    DIF2=(R(4)-R(2))/2.0
    TERM10=(RVEL3(4)-RVEL3(3))/(DELR*DIF1)
    TERM20=(TEMP3(4)-TEMP3(3))/(DELR*DIF2)

```

TABLE IX (Continued)

```

TERM11=(RVEL3(3)-RVEL3(2))/(DELX*DIF2)
TERM21=(TEMP3(3)-TEMP3(2))/(DELX*DIF2)
C*** 2ND DERIVATIVES AT CENTER OF CELL NO. 3 *****
TERM15= TERM10-TERM11
TERM25=TERM20-TERM21
DIF1=(R(4)-R(2))/2.0
DIF2=(R(3)-R(1))/2.0
TERM10=(RVEL3(3)-RVEL3(2))/(DELX*DIF1)
TERM20=(TEMP3(3)-TEMP3(2))/(DELX*DIF1)
TERM11=(RVEL3(2)-RVEL3(1))/(DELX*DIF2)
TERM21=(TEMP3(2)-TEMP3(1))/(DELX*DIF2)
C*** 2ND DERIVATIVES AT CENTER OF CELL NO. 2 *****
TERM16= TERM10-TERM11
TERM26= TERM20-TERM21
C*** USING 2ND DERIVATIVES FROM 2ND AND 3RD CELLS TO CALCULATE VALUE IN 1ST CELL
DEF=(R(4)-R(3))/2.0
DIF=(R(3)-R(1))/2.0
RAT=DIF/DEF
PCAL1=TERM16-(RAT*(TERM15-TERM16))
GO TO 510
C*** CALCULATION FOR FINAL CELL *****
501 DIF1=(R(ITOT+1)-R(ITOT-1))/2.0
DIF2=(R(ITOT)-R(ITOT-2))/2.0
TERM10=(RVEL3(ITOT)-RVEL3(ITOT-1))/(DELX*DIF1)
TERM20=(TEMP3(ITOT)-TEMP3(ITOT-1))/(DELX*DIF1)
TERM11=(RVEL3(ITOT-1)-RVEL3(ITOT-2))/(DELX*DIF2)
TERM21=(TEMP3(ITOT-1)-TEMP3(ITOT-2))/(DELX*DIF2)
C*** 2ND DERIVATIVES AT CELL ITOT-1 *****
TERM15=TERM10-TERM11
TERM25=TERM20-TERM21
DIF1=(R(ITOT)-R(ITOT-2))/2.0
DIF2=(R(ITOT-1)-R(ITOT-3))/2.0

```

TABLE IX (Continued)

```

TERM10=(RVFL3(ITOT-1)-RVFL3(ITOT-2))/(DELR*DIF1)
TERM20=(TEMP3(ITOT-1)-TEMP3(ITOT-2))/(DELR*DIF1)
TERM11=(RVFL3(ITOT-2)-RVFL3(ITOT-3))/(DELR*DIF2)
TERM21=(TEMP3(ITOT-2)-TEMP3(ITOT-3))/(DELR*DIF2)
C*** 2ND DERIVATIVES AT CENTER OF CELL ITOT-2 *****
TERM16=TERM10-TERM11
TERM26=TERM20-TERM21
C*** USING 2ND DERIVATIVES AT CELLS ITOT-2 AND ITOT-1 TO FIND 2ND DERIV. AT ITOT
DEF=(R(ITOT)-R(ITOT-1))/2.0 CHECK
DIF=(R(ITOT+1)-R(ITOT-1))/2.0
RAT=DIF/DEF
PCAL1=TERM15+ RAT*(TERM15-TERM16)
TCAL1=TERM25+RAT*(TERM25-TERM26)
510 ZAG=1.0
RETURN
END

```

TABLE X

SUBROUTINE ICOND

```

GFOR, IS ICOND, ICOND
  SUBROUTINE ICOND
C*** THIS ROUTINE PROVIDES THE INITIAL CONDITIONS FOR THE PROBLEM *****
  COMMON ALP(10,12), AOSC(51), DELT, DEN(10), DENQ1(51), DENQ2(51),
  1DENQ3(51), DELR, DR, EANDM, EDE(10,12), EGRM1(51), EGRM2(51), EGRM3(51),
  2EO, EOSC1(51), EOSC2(51), EOSC3(51), I, INTS, ITOT, ITOT1, NCYL, POSC(51),
  3PCAL1, PCAL2, PCAL3, PRES1(51), PRES2(51), PRES3(51), PPS(10,12),
  4R(51), RELC1(51), RELC2(51), RELC3(51), RHOM1(51), RHOM2(51), RHOM3(51),
  5RJDE1(51), RJDE2(51), RJDE3(51), RVEL1(51), RVEL2(51), RVEL3(51),
  6SDELT, TCAL1, TCAL2, TCAL3, TEM(12), TEMP1(51), TEMP2(51), TEMP3(51),
  7TES1, TI, TIC, TIM, XION1(51), XION2(51), XION3(51), XO, PO
C     FOR THE INITIAL PHASE OF THIS PROBLEM THERE ARE 50 CELLS, ITOT = 50.
C     THERE ARE 25 CELLS INITIALLY FILLED WITH SOLID MATERIAL AND 25 CELLS WHICH
C     ARE EMPTY (FILLED WITH MATERIAL OF ARBITRARILY LOW DENSITY, VACUUM VALUES).
C     THERE ARE ITOT+1 OR 51 MESH POINTS. INTERFACE IS AT MESH POINT # 26.
C*** GENERATE MESH ***
  R(1) = 0.0
  DO 5 I=1, ITOT
    R(I+1)=R(I)+DR
  5 CONTINUE
C*** FILL MESH POINTS WITH FLOVAR INITIAL VALUES ***
  DO 27 I=1, ITOT1
    IF(I.GT.26) GO TO 26
C     INITIAL CONDITIONS INSIDE TARGET SPHERE
    DENQ1(I)=0.0
    EGRM1(I)=EO
    EOSC1(I)=0.0
    PRES1(I) = PO
    RELC1(I)=0.0
    RHOM1(I)=2.70

```

TABLE X (Continued)

```

RIDE1(I)=0.0
RVEL1(I)=0.0
TEMP1(I)=TI
XION1(I)=XO
GO TO 27
C INITIAL CONDITIONS OUTSIDE OF TARGET SPHERE, VACUUM
26 DENO1(I)=0.0
EGRM1(I)=1.37E+09
EOSC1(I)=0.0
PRES1(I)=2.25E+02
RELC1(I)=0.0
RHOM1(I)=2.7E-07
RIDE1(I)=0.0
RVEL1(I)=0.0
TEMP1(I)=TIC
XION1(I)=0.0
27 CONTINUE
C***FILL CELL CENTERS ***
DO 30 I=1,ITOT
IF(I.GT.25) GO TO 28
C INITIAL CONDITIONS AT CELL CENTERS IN SPHERE
DENO2(I)=0.0
EGRM2(I)=EO
EOSC2(I)=0.0
PRES2(I) = PO
RELC2(I)=0.0
RHOM2(I)=2.70
RIDE2(I)=0.0
RVEL2(I)=0.0
TEMP2(I)=TI
XION2(I)=XO
GO TO 30

```

TABLE X (Continued)

```

C      INITIAL CONDITIONS AT CELL CENTERS OUTSIDE OF SPHERE
28  DENG1(I)=0.0
      EGRM2(I)=1.37E+09
      EOSC2(I)=0.0
      PRES2(I)=2.25E+02
      RELC2(I)=0.0
      RHOM2(I)=2.70E-07
      RJD2(I)=0.0
      KVEL2(I)=0.0
      TEMP2(I)=TIC
      XION2(I)=0.0
30  CONTINUE
C*** SPECIFY INITIAL TIME RATE OF CHANGE OF THE FLOW VARIABLES ***
      DO 31 I=1,ITOT
      DENG3(I)=0.0
      EGRM3(I)=0.0
      EOSC3(I)=0.0
      PRES3(I)=0.0
      RELC3(I)=0.0
      RHOM3(I)=0.0
      RJD3(I)=0.0
      KVEL3(I)=0.0
      TEMP3(I)=0.0
      XION3(I)=0.0
31  CONTINUE
      RETURN
      END

```


TABLE XI

SUBROUTINE OPTR

```

C FOR, IS OPTR, OPTR
  SUBROUTINE OPTR(BRHO, XME, BH, TEE, ZR, PI, QE, ATE, KCO, CLT, TAU, XLAM)
  DIMENSION ATE(15)
  WLAS=2.72E+15
  UNUS=0.0
  IF(UNUS.GT.0.0)GO TO 198
  IF(BRHO.LT.1.0E-09)GO TO 96
45  EFR=BH/(2.0*XME)
  EFR=BH*EFR
  XNEL=ZR*BRHO*6.023E+22/2.70
  WET1=(XNEL*3.0*PI*PI)**0.667
  EFR=EFR*WET1
  XT1=TEE*1.602E-12
  W6=4.0*XNEL*PI*QE*QE/XME
  IF(XNEL.LE.0.0) GO TO 96
  WP=W6**0.50
  XNA=BRHO*6.023E+22
  XNA=XNA/2.7
  IF(XT1.LT.EFR) GO TO 65
C  CALCULATION OF THE DEBYE LENGTH KT.GT.EFR
  N1=0
  DO 49 N=1,13
  IF(N1.GT.1)GO TO 47
  QEZ=N
  IF(ZB.LE.QEZ)N1=2
47  CIL=0.0
49  CONTINUE
  Q3=QEZ-1.0
  RN2=ZR-Q3
  RN1=1.0-RN2

```

TABLE XI (Continued)

```

w2=4.0*PI*QE*QE*XNA*(ZB+(RN1*Q3*Q3)+(RN2*QEZ*QE7))
XLAM=(XT1/W2)**0.5
GO TO 69
C CALCULATION OF THE DEBYE LENGTH KT.LT.EFR
65 w2=XT1*EFR
w3=4.0*PI*GF*GE*XNEL
w3=w3*((ZB*XT1)+EFR)
ARM=w2/W3
IF(ARM.LE.0.0)GO TO 66
XLAM=(W2/W3)**0.5
GO TO 67
66 XLAM=1.0E-08
67 ZAG=1.0
C RELAXATION TIME
B12=ZB*QE*QE
B13=2.0*XLAM*EFR
B14=B12/B13
B15=0.0
GO TO 71
69 B12=ZB*QE*QE
70 B13=3.0*XT1*XLAM
B14=B12/B13
71 ZAG=0.0
IF(KCO.LT.7)GO TO 72
RETURN
72 M3=0
B15=0.0
DO 73 N=1,14
IF(B14.GT.ATE(N))M3=N+1
B15=M3
73 CONTINUE
IF(B15.LT.0.5)GO TO 197

```

TABLE XI (Continued)

```

      IF(B15.GT.14.1)GO TO 203
74  M4=M3-1
      IF(M3.GT.2)GO TO 77
      B17=1.0+(B14*4.0)
      B17=B17**0.5
      XT3=(B17/2.0)-0.50
      GO TO 79
77  B16=B14/ATE(M4)
      B17=ALOG(B16)
      B18=ATE(M3)/ATE(M4)
      B19=ALOG(B18)
      XT3=B15-2.0+(B17/B19)
79  XT4=1.0/XT3
      IF(XT1.GT.EFR)GO TO 88
      B10=2.0*XME*EFR
      B10=B10**0.5
      B11=PI*XNA*ZB*ZB*QE*QE
      B12=1.0+XT4
      B11=B11*ALOG(B12)
      B10=B10*EXP(2.0*XT3)
      BAO1=B10/B11
      B10=QE*QE
      BAO1=BAO1/B10
      BAO8=0.66*EFR
      TAU=BAO1
      IF(XT1.LT.BAO8)GO TO 95
88  B10=XME*XT1
      B10=B10**0.5
      B10=B10*4.0*EXP(2.0*XT3)
      PE=(2.0*PI)**0.5
      B11=PI*XNA*ZB*ZB*QE*QE*PE
      B12=1.0+XT4

```

TABLE XI (Continued)

```

IF(B12.LE.0.0)GO TO 196
89 B11=B11*ALOG(P12)
   BAU2=R10/E11
   B10=QE*QE/XT1
   BAU2=BAU2/P10
   IF(XT1.GT.EFR)GO TO 93
   IF(BAU2.GT.BAU1)TAU=BAU2
   GO TO 95
93 TAU=BAU2
   GO TO 95
96 TAU=0.0
95 ZAG=1.0
   GO TO 210
196 B12=1.1
   GO TO 89
197 B14=0.5
   M3=2
   GO TO 74
198 TAU=0.0
   XLAM=0.0
203 B14=12.8*EXP(12.8)
   GO TO 74
210 ZAG=1.0
   RETURN
   END

```

TABLE XII

SUBROUTINE PRTOT1

```

C FOR, IS PRTOT1, PRTOT1
  SUBROUTINE PRTOT1
  DATA IPLT/11/
  DIMENSION PCEN(50)
  COMMON ALP(10,12), AOSC(51), DELT, DEN(10), DENQ1(51), DENQ2(51),
  1DENQ3(51), DELR, DR, EANDM, EDE(10,12), EGRM1(51), EGRM2(51), EGRM3(51),
  2EO, EOSC1(51), EOSC2(51), EOSC3(51), I, INTS, ITOT, ITOT1, NCYL, POSC(51),
  3PCAL1, PCAL2, PCAL3, PRES1(51), PRES2(51), PRES3(51), PRS(10,12),
  4R(51), RELC1(51), RELC2(51), RELC3(51), RHOM1(51), RHOM2(51), RHOM3(51),
  5RJDE1(51), RJDE2(51), RJDE3(51), RVEL1(51), RVEL2(51), RVEL3(51),
  6SDEL1, TCAL1, TCAL2, TCAL3, TEM(12), TEMP1(51), TEMP2(51), TEMP3(51),
  7TES1, TI, TIC, TIM, XION1(51), XION2(51), XION3(51), XO, PO
C*** THIS SUBROUTINE PRINTS OUT VALUES OF THE FLOW VARIABLES *****
1 FORMAT (20X,52H THE FLOW VARIABLES HAVE THE FOLLOWING VALUES WHEN T
X=,E10.3,2X,15H AT CELL CENTERS)
2 FORMAT(4X,4H CELL,4X,6H RADIUS,5X,12H MASS DENSITY,3X,15H INTERNAL FNF
XRGY,3X,8H PRESSURE,2X,19H RELATIVE IONIZATION,1X,11H TEMPERATURE,2X,
X13H FLOW VELOCITY)
3 FORMAT(5X,3H NO.,5X,4H(CM),8X,8H(GM/CM3),9X,8H(ERG/GM),5X,10H(DYNE/
XCM2),3X,15H(ELECTRON/ATOM),7X,4H(EV),7X,8H(CM/SEC),/)
4 FORMAT (/,12X,6H RADIUS,5X,14H CHARGE DENSITY,1X,14H ELECTRIC FIELD,1
XX,15H CURRENT DENSITY,4X,6H PERIOD,9X,6H ENERGY,7X,9H AMPLITUDE)
7 FORMAT(5X,12,3X,E10.3,5X,E10.3,5X,E10.3,5X,E10.3,5X,E10.3,5X,E10.3
X,5X,E10.3)
8 FORMAT (//,73X,35H PLASMON OSCILLATION CHARACTERISTICS)
9 FORMAT (13X,4H(CM),9X,9H(COUL/M3),8X,8H(VOLT/M),6X,8H(AMP/M2),8X,
X5H(SEC),9X,8H(ERG/GM),10X,4H(CM),//)
  WRITE(6,1) TIM
  WRITE(6,2)
  WRITE(6,3)

```

TABLE XII (Continued)

```

DO 101 J=1,ITOT
  RCEN(J)=(R(J)+R(J+1))/2.0
  WRITE(6,7) J,RCEN(J),RHOM2(J),EGRM2(J),PRES2(J),XION2(J),TEMP2(J),
  XRVEL2(J)
101 CONTINUE
  WRITE(6,8)
  WRITE(6,7)
  WRITE(6,4)
  WRITE(6,9)
  DO 151 J=1,ITOT
    WRITE(6,7) J,RCEN(J),DENQ2(J),RELC2(J),RJDE2(J),POSC(J),FCSC2(J),
    XACSC(J)
151 CONTINUE
C*** TO MAKE DATA TAPE, REMOVE COMMENT ON NEXT THREE WRITE CARDS*****
  WRITE(IPLT) TIM,NCYL,(RCEN(J),RHOM2(J),EGRM2(J),PRES2(J),XION2(J),
  XTEMP2(J),RVFL2(J),DENQ2(J),RELC2(J),RJDE2(J),POSC(J),FCSC2(J),ACSC
  X(J), J = 1,ITOT)
  ZAG=1.0
  RETURN
  END

```

TABLE XIII

SUBROUTINE QUAT

FOR, IS QUAT, QUAT

SUBROUTINE QUAT(EQN1, EQN2, XP, XT, XA)

DIMENSION RKT(12)

COMMON ALP(10,12), AOSC(51), DELT, DEN(10), DENQ1(51), DENQ2(51),
 1DENQ3(51), DELR, DR, EANDM, EDE(10,12), EGRM1(51), EGRM2(51), EGRM3(51),
 2EO, EOSC1(51), EOSC2(51), EOSC3(51), I, INTS, ITOT, ITOT1, NCYL, POSC(51),
 3PCAL1, PCAL2, PCAL3, PRES1(51), PRES2(51), PRES3(51), PRS(10,12),
 4R(51), RELC1(51), RELC2(51), RELC3(51), RHOM1(51), RHOM2(51), RHOM3(51),
 5RJDE1(51), RJDE2(51), RJDE3(51), RVEL1(51), RVEL2(51), RVEL3(51),
 6SDELT, TCAL1, TCAL2, TCAL3, TEM(12), TEMP1(51), TEMP2(51), TEMP3(51),
 7TES1, TI, TIC, TIM, XION1(51), XION2(51), XION3(51), XO, PO

EQN1=EQN1/2.70

PI=3.141

IF(EQN1.LE.2.0) GO TO 210

EQN1=2.0

GO TO 230

210 IF(EQN1.GT.1.00E-06)GO TO 230

EQN1=1.0E-07

EQN2=1.37E+09

XT=0.0235

XP=2.25E+02

XA=0.0

GO TO 290

230 IF(EQN2.LT.3.73E+15) GO TO 231

EQN2=3.73E+15

XP=EQN1*6.75E+15

XT=5.0E+03

XA=15.0

GO TO 290

10-23-70

10-23-70

10-23-70

10-23-70

10-23-70

10-23-70

TABLE XIII (Continued)

231 KAD=0
 DO 235 K=2,8
 IF(KAD.GT.2) GO TO 233
 IF(DEN(K).GT.EQN1) KAD=K
 233 BARF=0.0
 235 CONTINUE
 JAD=KAD-1
 B16=DEN(KAD)/DEN(JAD)
 B17=EQN1/DEN(JAD)
 B18=ALOG(B17)/ALOG(B16)
 IF(EQN1.LT.6.0E-01)GO TO 237
 C CALCULATION OF E GROUND STATE (Z=3)
 XNA=6.0E+22
 XNA=XNA*EQN1
 RS=4.0*PI*XNA/3.0
 B21=1.0/3.0
 RS=RS**B21
 RS=1.0/(RS*5.28E-09)
 B22=3.0**B21
 EG=3.915+(((1.98*1.96/(RS*RS*RS))- (3.0/RS))*9.0)
 EG=EG+((2.21*3.0*B22*B22)/(RS*RS))+ (1.2*3.0*3.0/RS)
 EG=EG-((0.916*3.0*B22/RS))
 B23=RS/B22
 B24=0.115-(0.0313*ALOG(B23))+0.0005*B23
 EG=(EG-(3.0*B24))*13.58
 EG=EG*3.55E+10
 IF(EQN1.GT.1.0) GO TO 241
 IF(EG.GT.0.0)EG=0.0
 GO TO 241
 237 ZAG=0.0
 IF(EQN1.LT.1.0E-01)GO TO 239
 C CALCULATION OF E GRAND STATE (Z=1)

10-23-70

3/6/70

TABLE XIII (Continued)

```

XNA=6.0E+22
XNA=XNA*EQN1
RS=4.0*PI*XNA/3.0
B21=1.0/3.0
RS=RS**B21
RS=1.0/(RS*5.28E-09)
EG=0.440+((1.98*1.98)/(RS*RS*RS))-(3.0/RS)
EG=EG+(2.21/(RS*RS))+(1.2/RS)-(0.916/RS)
B24=0.115-(0.0313*ALOG(RS))+0.0005*RS
EG=(EG-B24)*13.58*3.55E+10
IF(EG.GT.0.0)EG=0.0
GO TO 241
239 EG=0.0
241 ZAG=1.0
IF(EQN2.LT.EG)EQN2=EG+1.0
EDIF=EQN2-EG
KBE=0
DO 247 K=2,11
IF(KBE.GT.1)GO TO 245
B25=EDE(KAD,K)/EDE(JAD,K)
RKT(K)=ALOG(EDE(JAD,K))+(B18*ALOG(B25))
RKI(K)=EXP(RKT(K))
RKT(K)=RKT(K)-EG
IF(RKT(K).GT.EDIF)KBE=K
245 BAKF=0.0
247 CONTINUE
IF(KBE.LT.1)GO TO 252
JBE=KBE-1
IF(KBE.LT.3)RKT(JBE)=0.0
B21=EDIF-RKT(JBE)
B22=RKT(KBE)-RKT(JBE)

```

TABLE XIII (Continued)

```

b23=b21/b22
XT=TEM(JBE)+(B23*(TEM(KBE)-TEM(JBE)))-0.0006
IF(XT.LT.0.0235)XT=0.0235
b24=ALP(JAD,JBE)+B18*(ALP(KAD,JBE)-ALP(JAD,JBE))
b25=ALP(JAD,KBE)+B18*(ALP(KAD,KBE)-ALP(JAD,KBE))
XA=B24+(B23*(B25-B24))
b25=PRS(KAD,JBE)/PRS(JAD,JBE)
b26=PRS(KAD,KBE)/PRS(JAD,KBE)
b27=ALOG(PRS(JAD,KBE))+(B18*ALOG(B26))
b26=ALOG(PRS(JAD,JBE))+(B18*ALOG(B25))
IF(KBE.GT.2)GO TO 250
b26=TEM(KBE)-TEM(JBE)
b28=(XT-TEM(JBE))/B26
b29=EXP(B27)
b30=EXP(B26)
XP=B30+(B28*(B29-B30))
IF(EQN1.GT.0.60)XP=XP-4.20E+07
IF(XP.LT.2.25E+02)XP=2.25E+02
GO TO 290
250 ZAG=1.0
b28=ALOG(XT/TEM(JBE))
b25=TEM(KBE)/TEM(JBE)
b28=b28/ALOG(B25)
b29=b26+(B28*(B27-B26))
XP=EXP(B29)
GO TO 290
252 b21=CDIF-RKT(11)
b22=RKT(11)-RKT(10)
b23=b21/B22
XT=TEM(11)+(B23*(TEM(11)-TEM(10)))
b24=ALP(JAD,10)+(B18*((ALP(KAD,10)-ALP(JAD,10))))
b25=ALP(JAD,11)+(B18*((ALP(KAD,11)-ALP(JAD,11))))

```

TABLE XIII (Continued)

```
XA=B25+(B23*(B25-B24))
B26=XT/TEM(11)
B26=ALOG(B26)
B25=TEM(11)/TEM(10)
B25=ALOG(B25)
B26=B26/B25
B22=PRS(KAD,10)/PRS(JAD,10)
B22=ALOG(B22)
B27=ALOG(PRS(JAD,10))+(B18*B22)
B22=PRS(KAD,11)/PRS(JAD,11)
B22=ALOG(B22)
B28=ALOG(PRS(JAD,11))+(B18*B22)
B29=B28+(B26*(B28-B27))
XP=EXP(B29)
290 BARF=0.0
IF(XT.LT.0.0235)XT=0.0235
IF(XA.LT.0.0)XA=0.0
IF(XP.LT.2.25E+02)XP=2.25E+02
IF(XA.GT.13.0)XA=13.0
RETURN
END
```

TABLE XIV

SUBROUTINE REDBL

```

C FOR IS REDRL,REDPL
SUBROUTINE REDRL
COMMON ALP(10,12),AOSC(51),DELT,DFN(10),DFN01(51),DEN02(51),
1DEN03(51),DELR,DR,EANDM,EDE(10,12),EGRM1(51),EGRM2(51),EGRM3(51),
2EO,EOSC1(51),EOSC2(51),EOSC3(51),I,INTS,ITOT,ITOT1,NCYL,POSC(51),
3PCAL1,PCAL2,PCAL3,PRES1(51),PRES2(51),PRES3(51),PRS(10,12),
4R(51),RELC1(51),RELC2(51),RELC3(51),RHOM1(51),RHOM2(51),RHOM3(51),
5RJDE1(51),RJDE2(51),RJDE3(51),RVEL1(51),RVEL2(51),RVEL3(51),
6SDELT,TCAL1,TCAL2,TCAL3,TEM(12),TEMP1(51),TEMP2(51),TEMP3(51),
7TES1,TI,TIC,TIM,XION1(51),XION2(51),XION3(51),XO,PO
C*** GENERATION OF NEW CO-ORDINATES FOR GRID *****
C*****THIS ROUTINE PROVIDES ADDITIONAL SPACE INTO WHICH THE PLASMA MAY
C EXPAND AFTER ALL EXISTING CELLS HAVE BEEN FILLED *****
C*** DOUBLES LINEAR MESH ONLY ***
DR=2.0*DR
R(1)=0.0
DO 5 I=1,ITOT
R(I+1)=R(I)+DR
5 CONTINUE
C*** ASSIGN FV1 VALUES IN THE NEW EXPANDED MESH ***
DO 15 I=1,ITOT1
IK=2*I-1
IF(IK.GT.ITOT+1) GO TO 13
DEN01(I)=DEN01(IK)
EGRM1(I)=EGRM1(IK)
EOSC1(I)=EOSC1(IK)
PRES1(I)=PRES1(IK)
RELC1(I)=RELC1(IK)
RHOM1(I)=RHOM1(IK)

```

TABLE XIV (Continued)

```

RJDE1(I)=RJDE1(IK)
RVEL1(I)=RVEL1(IK)
TEMP1(I)=TEMP1(IK)
XION1(I)=XION1(IK)
IF(IK.GT.ITOT) GO TO 14
DENG2(I)=DENG1(IK+1)
EGRM2(I)=EGRM1(IK+1)
EOSC2(I)=EOSC1(IK+1)
PRES2(I)=PRES1(IK+1)
RELC2(I)=RELC1(IK+1)
RHOM2(I)=RHOM1(IK+1)
RJDE2(I)=RJDE1(IK+1)
RVEL2(I)=RVEL1(IK+1)
TEMP2(I)=TEMP1(IK+1)
XION2(I)=XION1(IK+1)
GO TO 15

```

C*** FLOW VARIABLE FREE SPACE VALUES *** (MESH POINT VALUES) ***

```

13 DENG1(I)=0.0
EGRM1(I)=1.37E+09
EOSC1(I)=0.0
PRES1(I)=2.25E+02
RELC1(I)=0.0
RHOM1(I)=2.70E-07
RJDE1(I)=0.0
RVEL1(I)=0.0
TEMP1(I)=TIC
XION1(I)=0.0
IF(I.GT.ITOT) GO TO 15

```

C*** FLOW VARIABLE FREE SPACE VALUES *** (CELL CENTER VALUES) ***

```

14 DENG2(I)=0.0
EGRM2(I)=1.37E+09

```

TABLE XIV (Continued)

```
EOSC2(I)=0.0  
PRES2(I)=2.25E+02  
RELC2(I)=0.0  
RHOM2(I)=2.70E-07  
RUDE2(I)=0.0  
RVEL2(I)=0.0  
TEMP2(I)=TIC  
XION2(I)=0.0  
15 CONTINUE  
RETURN  
END
```

TABLE XV

SUBROUTINE REMESH

```

@FOR, IS REMSH, REMSH
  SUBROUTINE REMSH
    COMMON ALP(10,12), AOSC(51), DELT, DEN(10), DENQ1(51), DENQ2(51),
    1DENQ3(51), DELR, DR, EANDM, EDE(10,12), EGRM1(51), EGRM2(51), EGRM3(51),
    2EO, EOSC1(51), EOSC2(51), EOSC3(51), I, INTS, ITOT, ITOT1, NCYL, POSC(51),
    3PCAL1, PCAL2, PCAL3, PRES1(51), PRES2(51), PRES3(51), PRS(10,12),
    4R(51), RELC1(51), RELC2(51), RELC3(51), RHOM1(51), RHOM2(51), RHOM3(51),
    5RJDE1(51), RJDE2(51), RJDE3(51), RVEL1(51), RVEL2(51), RVEL3(51),
    6SDELT, TCAL1, TCAL2, TCAL3, TEM(12), TEMP1(51), TEMP2(51), TEMP3(51),
    7TES1, TI, TIC, TIM, XION1(51), XION2(51), XION3(51), XO, PO
  C***REMSH THE INTERIOR MESH POINTS ***
  C*** IMPORTANT NOTE....THE ARGUMENTS MUST BE IN IDENTICAL ORDER WITH THE
  C STATEMENT FUNCTION RESET ***
  C*** BECAUSE I SCREWED UP ( DELT SHOULD BE SDELT) *****
    DIRT=DELT
    DELT=SDELT
    DO 7 I=2,50
      DEL=(R(I)-R(I-1))/2.0
      DEL1=(R(I+1)-R(I-1))/2.0
      DENG1(I)=RESET(DENG1(I),DELT,DENG3(I-1),DFL,DEL1,DENG3(I))
      EGRM1(I)=RESET(EGRM1(I),DELT,EGRM3(I-1),DEL,DEL1,EGRM3(I))
      EOSC1(I)=RESET(EOSC1(I),DELT,EOSC3(I-1),DFL,DEL1,EOSC3(I))
      PRES1(I)=RESET(PRES1(I),DELT,PRES3(I-1),DEL,DEL1,PRES3(I))
      RELC1(I)=RESET(RELC1(I),DELT,RELC3(I-1),DFL,DEL1,RELC3(I))
      RHOM1(I)=RESET(RHOM1(I),DELT,RHOM3(I-1),DEL,DEL1,RHOM3(I))
      RJDE1(I)=RESET(RJDE1(I),DELT,RJDE3(I-1),DEL,DEL1,RJDE3(I))
      RVEL1(I)=RESET(RVEL1(I),DELT,RVEL3(I-1),DFL,DEL1,RVEL3(I))
      TEMP1(I)=RESET(TEMP1(I),DELT,TEMP3(I-1),DFL,DEL1,TEMP3(I))
      XION1(I)=RESET(XION1(I),DELT,XION3(I-1),DFL,DEL1,XION3(I))

```

TABLE XV (Continued)

```

7 CONTINUE
C*** REMESH THE FIRST MESH POINT *** NOTE...(NO DO LOOP)
C*** NOTE THE DEFINITION OF DEL ***
DEL=(R(1)-R(2))/2.0
DEL1=(R(3)-R(1))/2.0
DENQ1(1)=REEDG(DENQ1(1),DELT,DENQ3(1),DEL,DEL1,DENQ3(2))
EGRM1(1)=REEDG(EGRM1(1),DELT,EGRM3(1),DEL,DEL1,EGRM3(2))
EOSC1(1)=REEDG(EOSC1(1),DELT,EOSC3(1),DEL,DEL1,EOSC3(2))
PRES1(1)=REEDG(PRES1(1),DELT,PRES3(1),DEL,DEL1,PRES3(2))
RELC1(1)=REEDG(RELC1(1),DELT,RELC3(1),DEL,DEL1,RELC3(2))
RHOM1(1)=REEDG(RHOM1(1),DELT,RHOM3(1),DEL,DEL1,RHOM3(2))
RUDE1(1)=REEDG(RUDE1(1),DELT,RUDE3(1),DEL,DEL1,RUDE3(2))
RVEL1(1)=REEDG(RVEL1(1),DELT,RVEL3(1),DEL,DEL1,RVEL3(2))
TEMP1(1)=REEDG(TEMP1(1),DELT,TEMP3(1),DEL,DEL1,TEMP3(2))
XION1(1)=REEDG(XION1(1),DELT,XION3(1),DEL,DEL1,TEMP3(2))
C*** REMESH THE LAST MESH POINT *** NOTE...(NO DO LOOP)
DEL=(R(ITOT+1)-R(ITOT))/2.0
DEL1=(R(ITOT+1)-R(ITOT-1))/2.0
DENQ1(ITOT+1)=REEDG(DENQ1(ITOT+1),DELT,DENQ3(ITOT),DEL,DEL1,
XDENQ3(ITOT-1))
EGRM1(ITOT+1)=REEDG(EGRM1(ITOT+1),DELT,EGRM3(ITOT),DEL,DEL1,
XEGRM3(ITOT-1))
EOSC1(ITOT+1)=REEDG(EOSC1(ITOT+1),DELT,EOSC3(ITOT),DEL,DEL1,
XEOSC3(ITOT-1))
PRES1(ITOT+1)=REEDG(PRES1(ITOT+1),DELT,PRES3(ITOT),DEL,DEL1,
XPRES3(ITOT-1))
RELC1(ITOT+1)=REEDG(RELC1(ITOT+1),DELT,RELC3(ITOT),DEL,DEL1,
XRELC3(ITOT-1))
RHOM1(ITOT+1)=REEDG(RHOM1(ITOT+1),DELT,RHOM3(ITOT),DEL,DEL1,
XRHOM3(ITOT-1))
RUDE1(ITOT+1)=REEDG(RUDE1(ITOT+1),DELT,RUDE3(ITOT),DEL,DEL1,

```


TABLE XV (Continued)

```
XRUDE3(ITOT-1)
RVEL1(ITOT+1)=REEDG(RVEL1(ITOT+1),DELT,RVEL3(ITOT),DEL,DEL1,
XRVEL3(ITOT-1))
TEMP1(ITOT+1)=REEDG(TEMP1(ITOT+1),DELT,TEMP3(ITOT),DEL,DEL1,
XTEMP3(ITOT-1))
XION1(ITOT+1)=REEDG(XION1(ITOT+1),DELT,XION3(ITOT),DEL,DEL1,
XXION3(ITOT-1))
C*** CHECK FOR MESH OVERUN *****
IF(RHOM1(45).GT.1.0E-06) TES1=2.0
DELT=DIRT
RETURN
END
```

TABLE XVI

SUBROUTINE XOY

```

C FOR, IS XOY, XOY
  SUBROUTINE XOY(QE, ZB, ALAM, TEE, ATE, XMU)
  DIMENSION ATE(15)
C   GUTS TO VISCOSITY
  IF(ALAM.LE.0.0)GO TO 199
  IF(UNUS.GT.1.0)GO TO 199
  B12=ZB*QE
  B12=B12*B12
  B13=5.0*ALAM*TEE*1.6E-12
  B14=B12/B13
71  ZAG=1.0
  M3=0
  B15=0.0
  DO 73 N=1,14
  IF(B14.GT.ATE(N))M3=N+1
  B15=M3
73  CONTINUE
  M4=M3-1
  IF(B15.GT.14.1)GO TO 197
  IF(B15.LT.0.5)GO TO 199
  IF(M3.GT.2)GO TO 77
  B17=1.0+(B14*4.0)
  B17=B17**0.5
  XT3=(B17/2.0)-0.50
  GO TO 79
77  B16=B14/ATE(M4)
  B17=ALOG(B16)
  B18=ATE(M3)/ATE(M4)
  B19=ALOG(B18)

```

TABLE XVI (Continued)

```

      XT3=B15-2.0+(B17/B19)
79  XT4=1.0/XT3
      B12=XT3*ALAN
      B12=B12*B12
      XT4=1.0+(1.0/XT3)
      B13=B12*ALOG(XT4)
      B14=5.625E-20/B13
      XMU=TEE**0.5
      XMU=B14*XMU
      GO TO 201
197  B14=12.8*EXP(12.8)
      B15=14.0
      M4=13
      M3=14
      GO TO 77
199  UNUS=0.0
      XMU=0.0
201  ZAG=1.0
      RETURN
      END

```

TABLE XVII
STATEMENT FUNCTIONS

GFOR, IS FED, FED

FUNCTION FED(C1,C2)

TZ=1.0+C1

FED=C1*C2/TZ

RETURN

END

GFOR, IS RESET, RESET

FUNCTION RESET(A1,A2,A3,A4,A5,A6)

RESET=A1+A2*(A3+((A4/A5)*(A6-A3)))

RETURN

END

GFOR, IS REEDG, REEDG

FUNCTION REEDG(A1,A2,A3,A4,A5,A6)

REEDG=A1+A2*(A3+((A4/A5)*(A3-A6)))

RETURN

END

GFOR, IS XKAP, XKAP

FUNCTION XKAP(TAR,TAU,ZR,BRHU)

XNEL=BRHU/2.70

XNEL=XNEL*ZR*6.02E+22

XKAP=XNEL*TAR*TAU*2.815E+03

RETURN

END

TABLE XVIII

PROGRAM DATA

```

C*** DATA *****
+.100E-05+.100E-04+.100E-03+.100E-02+.100E-01+.100E+00+.100F+01+.100E+02
0.02350  1.0    2.0    5.0   10.0   20.0   50.0  100.0  200.0  500.0
 1000.0
+.000E+00+.000E+00+.000E+00+.000E+00+.000E+00+.000E+00-.321E+12+.154E+15
+.866E+06+.732E+07+.532E+08+.480E+09+.535E+10+.497E+11+.265E+11+.154E+15
+.311E+07+.235E+08+.172E+09+.144E+10+.125E+11+.112E+12+.488F+12+.154E+15
+.796E+07+.779E+08+.710E+09+.586E+10+.387E+11+.345E+12+.318F+13+.154E+15
+.252E+08+.189E+09+.130E+10+.109E+11+.997E+11+.902E+12+.799E+13+.171E+15
+.104E+09+.779E+09+.571E+10+.425E+11+.303E+12+.264E+13+.192F+14+.242E+15
+.299E+09+.304E+10+.254E+11+.204E+12+.151E+13+.110E+14+.838F+14+.539E+15
+.391E+09+.389E+10+.386E+11+.386E+12+.320E+13+.216E+14+.185F+15+.128E+16
+.117E+10+.114E+11+.982E+11+.609E+12+.700E+13+.520E+14+.460E+15+.310E+16
+.178E+10+.178E+11+.178E+12+.178E+13+.155E+14+.140E+15+.130F+16+.970E+16
+.280E+10+.278E+11+.304E+12+.280E+13+.263E+14+.260E+15+.260F+16+.220E+17
+.000E+00+.000E+00+.000E+00+.000E+00+.000E+00+.000E+00+.300E+01+.400E+01
+.940E+00+.754E+00+.472E+00+.300E+00+.250E+00+.145E+01+.300E+01+.400E+01
+.188E+01+.147E+01+.110E+01+.930E+00+.100E+01+.165E+01+.300E+01+.400E+01
+.295E+01+.287E+01+.261E+01+.215E+01+.225E+01+.205E+01+.300E+01+.400E+01
+.403E+01+.357E+01+.308E+01+.295E+01+.271E+01+.255E+01+.310E+01+.400E+01
+.699E+01+.617E+01+.528E+01+.450E+01+.365E+01+.400E+01+.381F+01+.400E+01
+.109E+02+.106E+02+.994E+01+.879E+01+.736E+01+.607E+01+.530E+01+.400E+01
+.111E+02+.110E+02+.110E+02+.112E+02+.108E+02+.970E+01+.683F+01+.500E+01
+.130E+02+.129E+02+.125E+02+.117E+02+.112E+02+.110E+02+.104F+02+.700E+01
+.130E+02+.130E+02+.130E+02+.130E+02+.130E+02+.129E+02+.121F+02+.100E+02
+.130E+02+.130E+02+.130E+02+.130E+02+.130E+02+.129E+02+.121F+02+.120E+02
+.226E+03+.226E+04+.226E+05+.226E+06+.226E+07+.226E+08+.100F-19+.224E+15
+.186E+06+.169E+07+.146E+08+.153E+09+.209E+10+.459E+11+.165F+13+.224E+15
+.552E+06+.477E+07+.414E+08+.401E+09+.491E+10+.877E+11+.257F+13+.224E+15
    
```

TABLE XVIII (Continued)

+.191E+07+.187E+08+.180E+09+.168E+10+.163E+11+.212E+12+.391E+13+.224E+15
 +.495E+07+.441E+08+.397E+09+.385E+10+.395E+11+.436E+12+.626E+13+.224E+15
 +.172E+08+.141E+09+.123E+10+.111E+11+.993E+11+.111E+13+.143E+14+.224E+15
 +.579E+08+.633E+09+.542E+10+.492E+11+.439E+12+.400E+13+.300E+14+.525E+15
 +.116E+09+.116E+10+.116E+11+.115E+12+.104E+13+.940E+13+.730E+14+.800E+15
 +.270E+09+.268E+10+.260E+11+.245E+12+.243E+13+.230E+14+.195E+15+.165E+16
 +.675E+09+.675E+10+.675E+11+.675E+12+.710E+13+.680E+14+.630E+15+.540E+16
 +.135E+10+.135E+11+.135E+12+.135E+13+.140E+14+.142E+15+.135E+16+.120E+17
 1.0E-04

VITA ^W

Harold Wayne Willis

Candidate for the Degree of

Doctor of Philosophy

Thesis: ANALYTICAL AND EXPERIMENTAL INVESTIGATIONS OF THE TRANSIENT PROPERTIES OF DENSE ALUMINUM PLASMAS

Major Field: Physics

Biographical:

Personal Data: Born in Beaumont, Texas, October 1, 1942, the eldest of three sons of Harold West and Mary McDonald Willis. Married Eva Gerard Bomer on August 11, 1968.

Education: Attended grade school in Olympia, Washington, Silsbee, Texas and Kountze, Texas; graduate from Kountze High School, Kountze, Texas in May, 1960; received the Bachelor of Science degree with a major in Physics from the Lamar State College of Technology in Beaumont, Texas in May, 1966; received the Master of Science degree from Oklahoma State University in August, 1969; completed requirements for the Doctor of Philosophy degree in May, 1971.

Professional Experience: Laboratory technician and operator assistant for the South Hampton Company of Houston, Texas prior to completion of the requirements for the B. S. degree; teaching assistant for the Department of Physics, Lamar State College of Technology; President, Lamar chapter of the American Institute of Physics, Beaumont, Texas; Laboratory Assistant for the 1965 National Science Foundation Summer Science Institute, Lamar Tech; recipient of the National Science Foundation Summer Science Institute appointment in Physical Science at the Howard Payne College, Brownwood, Texas, 1959; Field Salesman for the Periodical Publishing Company, Houston, Texas; Rodman for the Geophysical Section of the Texaco Company, Inc., Gravity Part No. 105, Houston, Texas; Floorman for the Carl Martin Oil Service Company, Houston, Texas; Teaching Assistant for the Physics Department, Oklahoma State University; Research Assistant for the Oklahoma State University

Research Foundation; Salutatorian of High School graduating class; Member of the Lamar Freshman Honor Society; Associate Member of Sigma Pi Sigma, Lamar Chapter; Member of Sigma Pi Sigma, Oklahoma State University; Member of the Oklahoma State University Flying Aggies; Member of the American Association of Physics Teachers; Member of the Oklahoma Academy of Science; Member of the South Eastern Section of the American Physical Society; Member of the American Institute of Aeronautics and Astronautics; Deputy Principal investigator for Dense Plasma, NASA Contract NAS8-25055 during summer of 1970; Member of Board of Directors and Assistant Secretary for Pleasant Leasing and Investing Corporation, a Texas Corporation; technical consultant for the South Hampton Company; Senior Research Assistant for the Research Institute, division of Graduate Studies and Research, The University of Alabama in Huntsville.